Faster Convergence in Seismic History Matching by Dividing and Conquering the Unknowns

Farzaneh Sedighi

A thesis Submitted for the
Degree of **Doctor of Philosophy**

Institute of Petroleum Engineering
Heriot-Watt University
Edinburgh-Scotland, UK
December 2011

Abstract

The aim in reservoir management is to control field operations to maximize both the short and long term recovery of hydrocarbons. This often comprises continuous optimization based on reservoir simulation models when the significant unknown parameters have been updated by history matching where they are conditioned to all available data. However, history matching of what is usually a high dimensional problem requires expensive computer and commercial software resources. Many models are generated, particularly if there are interactions between the properties that update and their effects on the misfit that measures the difference between model predictions to observed data.

In this work, a novel 'divide and conquer' approach is developed to the seismic history matching method which efficiently searches for the best values of uncertain parameters such as barrier transmissibilities, net:gross, and permeability by matching well and 4D seismic predictions to observed data. The ‘divide’ is carried by applying a second order polynomial regression analysis to identify independent sub-volumes of the parameters hyperspace. These are then ‘conquered’ by searching separately but simultaneously with an adapted version of the quasi-global stochastic neighbourhood algorithm.

This 'divide and conquer' approach is applied to the seismic history matching of the Schiehallion field, located on the UK continental shelf. The field model, supplied by the operator, contained a large number of barriers that affect flow at different times during production, and their transmissibilities were largely unknown. There was also some uncertainty in the petrophysical parameters that controlled permeability and net:gross. Application of the method was accomplished because it is found that the misfit function could be successfully represented as sub-misfits each dependent on changes in a smaller number of parameters which then could be searched separately but simultaneously. Ultimately, the number of models required to find a good match reduced by an order of magnitude. Experimental design was used to contribute to the efficiency and the ‘divide and conquer’ approach was also able to separate the misfit on a spatial basis by using time-lapse seismic data in the misfit. The method has effectively gained a greater insight into the reservoir behaviour and has been able to predict flow more accurately with a very efficient 'divide and conquer' approach.

Dedication

This thesis is dedicated to my family

Acknowledgements

I would like to express my sincere appreciation to my supervisor, Dr. Karl D. Stephen, for his precious guidance and supervision. His comments provided valuable encouragement for me to explore this new area of study at Heriot-Watt. His support provided me the excellence to present my research work.

I also wish to thank the examiners, Dr. Olwijn Leeuwenburgh from TNO and Dr. Mahmoud Jamiolahmady from the Institute of Petroleum Engineering of Heriot Watt University, for examining this thesis.

I would like to thank the people of the SHM and ETLP groups, the Institute of Petroleum Engineering staff, and my friends specially Dr. Panteha Ghahri for their support.

I would like to thank the Schiehallion field partners: BP, Shell, Amerada Hess, Statoilhydro, Murphy Oil and OMV, for providing the data and permission to publish the results of this work. BP, ConocoPhilips, Shell and StatoilHydro are also thanked for funding of this research. Schlumberger Geoquest is thanked for use of the software. Malcolm Sambridge is thanked for use of the Neighbourhood Algorithm.

ACADEMIC REGISTRY
Research Thesis Submission

Name*:*	Farzaneh Sedighi		
School/PGI:	Institute of Petroleum Engineering (IPE)		
Version: *(i.e. First, Resubmission, Final)*	Final	Degree Sought (Award **and** Subject area)	PhD Petroleum Engineering

Declaration

In accordance with the appropriate regulations I hereby submit my thesis and I declare that:

1) the thesis embodies the results of my own work and has been composed by myself
2) where appropriate, I have made acknowledgement of the work of others and have made reference to work carried out in collaboration with other persons
3) the thesis is the correct version of the thesis for submission and is the same version as any electronic versions submitted*.
4) my thesis for the award referred to, deposited in the Heriot-Watt University Library, should be made available for loan or photocopying and be available via the Institutional Repository, subject to such conditions as the Librarian may require
5) I understand that as a student of the University I am required to abide by the Regulations of the University and to conform to its discipline.

* *Please note that it is the responsibility of the candidate to ensure that the correct version of the thesis is submitted.*

Signature of Candidate*:*	Sedighi	Date:	09/12/2011

Submission

Submitted By *(name in capitals):*	Farzaneh Sedighi
Signature of Individual Submitting:	Sedighi
Date Submitted:	09/12/2011

For Completion in the Student Service Centre (SSC)

Received in the SSC by *(name in capitals):*			
Method of Submission *(Handed in to SSC; posted through internal/external mail):*			
*E-thesis Submitted (**mandatory for final theses)***			
Signature:		Date:	

Publications

Sedighi, F., and Stephen, K. D., 2009. Faster Convergence in Seismic History Matching by Efficient Parameter Searching. SPE-121210-MS, SPE Europec/EAGE Annual Conference and Exhibition, Amsterdam, 9-11 June 2009.

Sedighi, F., and Stephen, K.D., 2010. Improved Convergence in Seismic History Matching Combining Experimental Design with a Divide and Conquer Approach. 72nd EAGE Conference and Exhibition incorporating SPE EUROPEC held in Barcelona, 14-17 June, 2010.

Table of Content

List of Figures

List of Tables

Nomenclature

$\boldsymbol{A}$ = Raw attribute at time t, observed or predicted, prior to normalisation

$\boldsymbol{a}$ = Normalised attribute at time t, observed or predicted.

$\boldsymbol{C_i}$ = Covariance matrix of the i^{th} variable

$\boldsymbol{E_\kappa^r}$ = Excess compliance of the bulk modulus (r = sand or shale), m/Lt^2, Pa

$\boldsymbol{E_\mu^r}$ = Excess compliance of the shear modulus (r = sand or shale), m/Lt^2, Pa

$\boldsymbol{I}$ = Impedance, m/L^2t, $kgm^{-2}s^{-1}$

$\boldsymbol{I_{ij}}$ = Impedance on the seismic grid, m/L^2t, $kgm^{-2}s^{-1}$

$\boldsymbol{I_{IJ}}$ = Impedance on the simulation grid, m/L^2t, $kgm^{-2}s^{-1}$

$\boldsymbol{I_{ij}^{interp}}$ = Interpolated Impedance, m/L^2t, $kgm^{-2}s^{-1}$

$\boldsymbol{J_i}$ = Misfit of the i^{th} variable

$\boldsymbol{k}$ = Permeabiliy, L^2, mD

$\boldsymbol{M_m}$ = P-wave modulus, m/Lt^2, Pa

$\boldsymbol{M^{cell}}$ = P-wave modulus for a cell, m/Lt^2, Pa

$\boldsymbol{M^r}$ = P-wave modulus of lithofacies within a cell (r = sand or shale), m/Lt^2, Pa

$\boldsymbol{N}$ = Number of bins (observed data) in the sector

$\boldsymbol{n_i}$ = number of initial models resampled by the NA

$\boldsymbol{n_r}$ = number of best models resampled by the NA

$\boldsymbol{n_s}$ = number of models per iteration

$\boldsymbol{NTG}$ = Net:Gross

$\boldsymbol{P}$ = Pressure, m/Lt^2, Pa

$\boldsymbol{P_{eff}}$ = Effective (overburden – pore) pressure, m/Lt^2, Pa

$\boldsymbol{P_\kappa^r}$ = Stress sensitivity of the bulk modulus (r = sand or shale), m/Lt^2, Pa

$\boldsymbol{r}$ = position vector of a cell centre, L, m

$\boldsymbol{RMS}$ = Root Mean Square

$\boldsymbol{S_g}$ = gas saturation

$\boldsymbol{S_o}$ = oil saturation

$\boldsymbol{S_w}$ = water saturation

$\boldsymbol{\alpha}$ = $(1-\kappa^r_{dry}/\kappa_{gr})$

$\boldsymbol{\gamma Ao}$ = areal mean of seismic attribute, A, calculated for the pre-production survey.

$\boldsymbol{m}$ = model error for the i^{th} variable

$\boldsymbol{W}$ = weighting factor

$\boldsymbol{\varphi}$ = porosity

$\boldsymbol{\kappa}$ = bulk modulus, m/Lt^2, Pa

$\boldsymbol{\kappa_f}$ = fluid bulk modulus, m/Lt^2, Pa

$\boldsymbol{\kappa_g}$ = gas bulk modulus, m/Lt^2, Pa

κ_{gr} = grain bulk modulus, m/Lt^2, Pa

κ^r_{inf} = bulk modulus at STP (r = sand or shale), m/Lt^2, Pa

κ_o = oil bulk modulus, m/Lt^2, Pa

κ^r_{dry} = dry bulk modulus (r = sand or shale), m/Lt^2, Pa

κ^r_{sat} = saturated bulk modulus (r = sand or shale), m/Lt^2,Pa

κ_w = water bulk modulus, m/Lt^2, Pa

μ^r = shear modulus (r = sand or shale), m/Lt^2, Pa

ρ = density, m/L^3, $kg.m^3$

d^{obs} = observed variable

s^{sim} = predicted variable

σ_A^o = areal standard deviation of the attribute, A, calculated for the pre-production survey

Subscripts

cell = cell average

d = data

dry = dry rock

eff = Effective pressure, overburden - pore

fl = fluid modulus

g = gas

gr = grain

i = i^{th} variable

Inf = at infinite effective pressure

m = model

o = oil

sat = saturated rock

w = water

x = x direction

y = y direction

z = z direction

Superscripts

error = error component

sim = simulated (predicted)

obs = observed

r = rock type (sand or shale)

CHAPTER 1 An Introduction to 'Divide and Conquer' of Unknowns for Faster Convergence in Seismic History Matching

1.1 Introduction

Despite a weak global economy, in a time when energy demand was down by about two percent on recent years, the world still appears to be consuming all the oil and gas that can be produced. The quest for oil and gas continues worldwide, but based on the most depletion analysis, the peak supply is likely to be passed within 10 years (ASPO international 2011). The age of easy energy is over and oil and gas reservoirs are harder and more expensive to exploit than ever before. These realities drive the increase in oil price and encourage more effort to make new discoveries and enhanced production to recover more reserves from known reservoirs.

Further, the conditions in which oil and gas fields are now being discovered are much more unconventional, complex, and challenging. Also, currently developed fields are becoming depleted and therefore more marginal and less manageable. Unless there is a way to continuously monitor and take correct decisions on an optimal basis, it is hard to justify continuing to produce fields for economically, even with the continued soaring price of oil.

In many oil and gas assets, model based predictions are used to help with field management and can provide a large number of feasible production profiles. Then computer assisted methods should be used to analyse the possibilities and optimise the planning faster and more effectively than more traditional methods. Real time (closed-loop) reservoir management is a means to meet the business objectives by regularly optimising the performance of oil and gas fields. It is an integrated approach in all aspects including reserves, production, net present value (NPV), rate of return (ROR), capital and operation and maintenance costs, and health and safety and environment.

The entire approach is a long-term and focused on the overall life periods of the assets as shown in Figure 1.1

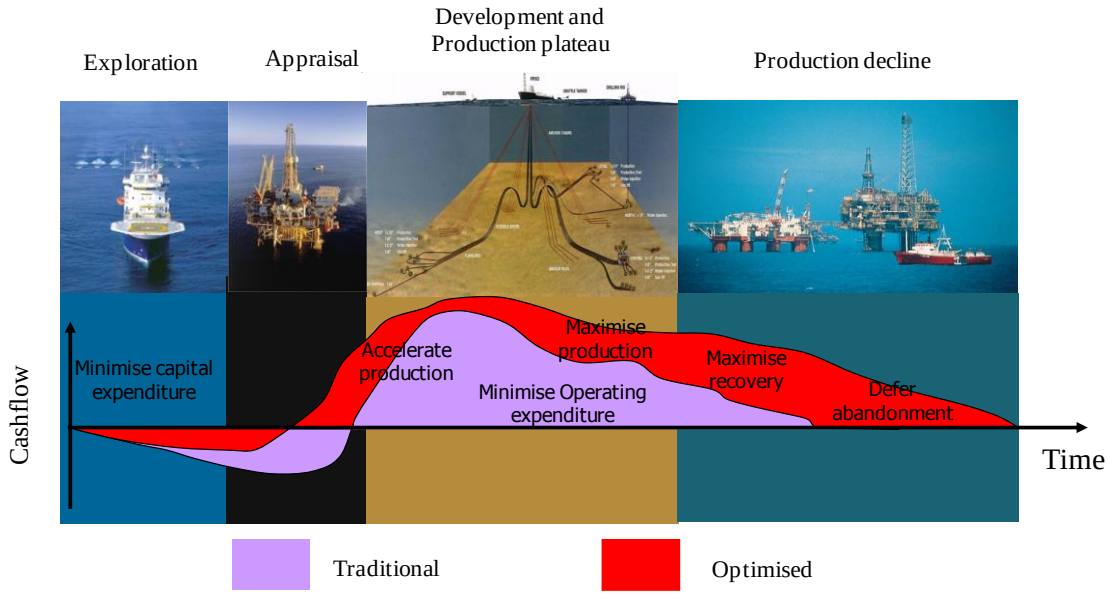

Figure 1.1: Reservoir optimization focuses on the overall life of the assets. Through time, oil and gas fields go through four basis stages: Exploration, Appraisal, Development and production. Objectives change as fields mature impacting expenditures, development and production strategies. Innovation in reservoir management techniques can help optimize production, enhancing the value of assets at every stage (after Eide et al. 2002).

The core of closed-loop reservoir management (see Figure 1.2) begins with modelling the physics via a mathematical representation of the reservoir system. Then, continuous data gathering, data assimilation, and updating of the reservoir simulation model are essential components. The data are gathered during the exploration and appraisal phase; and also by monitoring when the field goes on production. The elements of closed-loop control are:

i) history-matching reservoir models with production data,
ii) optimization of the production strategy for next couple of years,
iii) implementation of the production strategy,
iv) collection of output data, and
v) re-optimization production strategy in short time intervals.

Consequently, 'history matching' is a crucial stage in the reservoir management which entails building the comprehensives static reservoir model and calibrating the model using dynamic data.

A major challenge of this thesis is focused on this stage and in particular to improve the process of reservoir history matching while the valuable information obtained from well and time-lapse seismic data is integrated. This study explores enhanced techniques that are needed to accelerate the routine field application of 4D seismic history matching.

Manual history matching is a conventional option, but it is a trial-and-error task that can be time consuming and difficult because reservoir models are complex, with many unknown parameters which may be highly interlinked. Automatic history matching, however, potentially saves significant amounts of man power, although it does not eliminate the complexity of the process regarding the number of unknowns and requirement for reservoir engineering skills. History matching is an inversion technique and its application is well developed and may be accomplished by coupling a reservoir simulator with an optimization routine. In such circumstances an objective function that quantifies numerical differences between observed data and simulation responses are evaluated. The minimum of the objective function is found and the optimal reservoir models are estimated. These models should give more reliable forecasts for reservoir behaviour and thus are used for a range of decision makings regarding optimal operational decisions and control conditions. Consequently, increased oil recovery and revenue should be achieved (Figure 1.2).

Time-lapse (4D) seismic technology is now mature in the field of reservoir geophysics and engineering. 4D seismic maps are derived from repeated acquisition of 3D seismic data over time intervals and facilitate fluid movement monitoring in the reservoir. Seismic data are sensitive to static properties such as net:gross and porosity as well as dynamic properties such as fluid saturation and pore pressure. 4D seismic data may be used qualitatively to identify the time varying position of fluid fronts and to implicitly infer the reservoir characteristics that control the flow of fluids in the subsurface. Also, 4D seismic data may be used as a quantitative tool in 'seismic history matching' through the use of a petro-elastic modelling linked to a reservoir simulation. Thus it is a fundamental element of reservoir management.

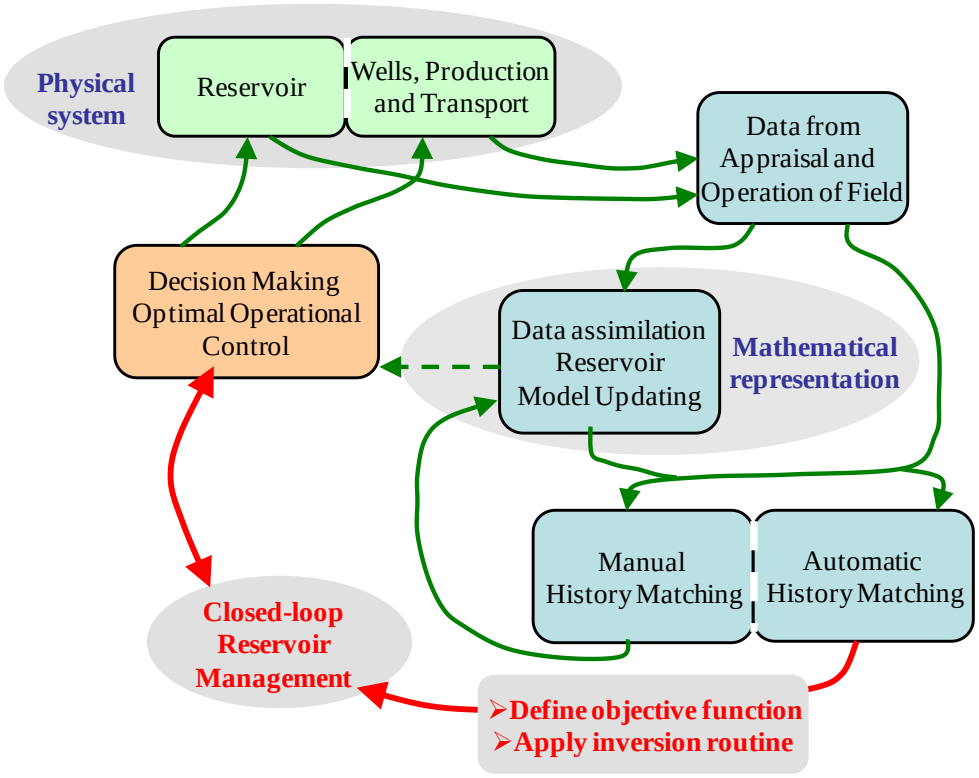

Figure 1.2: Reservoir data assimilation, model updating, manual and automatic history matching. The inversion process of history matching helps provided the closed-loop reservoir management scheme with better models with which decisions about optimal operational scenarios can be made.

The reservoir simulator uses a spatial grid, and the history matching process then adjusts the reservoir model properties such as permeability and porosity in grid cells of the simulation model to best fit the production and seismic data. Conventionally a large number of reservoir parameters have to be retrieved, and in particular for large scale models, there may be more than hundreds of such unknown parameter. Optimization methods, which are used in as a tool in history matching, are based on sampling algorithms that explore/exploit the parameter space to find models that fit the observed data. They require a large numbers of samplings, and thus simulation runs, to converge to the best fitting model or models. This is not only time consuming but software license costs are considerable. The number of simulations required increases if we do not know the link between the unknown parameters that are adjusted. There is a significant demand for efficient and fast approaches that can reduce the order of the required modelling and thus accelerate the process of such high dimensional history matching problems.

In this thesis we aim to use a technique which converts a full order high dimensional history matching problem into a set of low-dimensional subspaces, thus reducing the number of parameters samples that are required to be evaluated by the optimisation procedures. We propose an approach which is based on a proper orthogonal decomposition and identification of the unknowns that are not coupled. We call this 'divide and conquer' approach. This is an efficient technique and consists of following major phases:

- Breaking the problem into several sub-problems that are similar to the original problem but smaller in size.
- Solve the sub-problem recursively (successively or in parallel but independently).
- Combine these solutions of the sub-problems to create a solution to the original problem.

The research of this thesis is thus devoted to develop such an approach. The key contribution of 'divide and conquer' is to establish a speed up in the convergence rate of history matching while at the same time delivering high quality results. Here, this has been implemented in the context of Seismic History Matching (SHM).

In this chapter we start with an overview for reservoir simulation and history matching and several related aspects. Then the objective and the motivation of this thesis are expanded. After that an idea for 'divide and conquer' approach is presented. We finish with an outline of the content of the following chapters of thesis.

1.2 Reservoir Simulation and History Matching

The reservoir simulator is an essential tool in closed-loop management of oil and gas reservoirs. By using a simulator, history and forecasting of reservoirs can be analysed. The reservoir simulation formulation is based on several fundamentals, including:

- The physical fundamentals of conservation of mass in a control volume
- Darcy's law of fluid flow through porous media and Equations of state for prediction the thermodynamic behaviour of fluids
- Capillary pressure and relative permeability relationships

- Multiple fluid phases that may exist in the porous rocks

By applying these fundamentals a set of partial differential diffusivity equations governing the fluid flow of various phases of oil, gas, and water in the porous media are then derived. These equations are difficult to solve analytically, so the finite-difference approximate form both in time and space are used (e.g. Aziz and Settari 1979). Accordingly, the reservoir volume is discretised to a great number of grid cells in space, which is called a reservoir model. Grid cells should capture the interpreted heterogeneity in the reservoir by being populated with reservoir rock petro-physical properties such as porosity and permeability, and so on. Hence, the reservoir models are built based on the geological setting and the properties that are acquired through core, wireline logging, and well measurements. These properties are sparsely sampled in the reservoir (i.e. at the well locations only) and reflect the quality of the rock in a small region such as the well drainage area and the connected regions. Thus they are very sparse relative to the great number of grid blocks that constitute a geo-model or simulation model (e.g.10^6-10^8 cells).

One of the real challenges therefore is that insufficient information is obtainable from the reservoir between the wells. Fortunately, 3D seismic imaging can play at important role in understanding of the reservoir characteristics, volumetrically. The 3D signature interpretations assist in mapping petro-physical properties (i.e. lithology, pore volume, and net:gross) of the subsurface and enhance the reservoir descriptions. These data provide useful information when building the reservoir model nevertheless they do not delineate the fluids dynamics in a reservoir.

As a result of production activities, pressure in the reservoir changes and at the same time the fluid saturation changes in the pores of the rocks. From one single seismic survey, one is not able to differentiate between features caused by static properties and those caused by dynamic behaviour. Contrasting seismic surveys acquired at different times, however, may eliminate the impact of static details, and enable extraction of information about the changes in the reservoir dynamic properties induced by production. 4D seismic monitoring can capture oil depletion by various phenomena through the life cycles of the field, i.e. from development to plateau and finally up to secondary and tertiary recovery scenarios, that is:

- In primary production, mainly the effect of change in pore pressure due to pressure draw down, gas evolution and compaction of geomechanically active fields can be understood.

- In a field under water flooding and in mature fields when secondary recovery schemes are implemented, water saturation and pore pressure changes can be detected.

- In tertiary recovery practice in more mature fields often the results of the thermal and saturation changes due to steam injection, in-situ combustion, hot water injection, compaction etc. can be inferred.

All these changes in pore pressure, pore volume and fluid saturation have an impact on geophysical properties such as rock and fluid and rock compressibility. For example in the Nelson field a trough/peak 4D signature was observed in the far offset of conventional differences (Redondo-Lopez et al. 2002, MacBeth et al. 2002), Figure 1.3 shows such a 4D signature difference map over six years of production (1990-2000). 4D seismic maps can enhance the understanding of saturation patterns and general flow, thus we are able to determine critical areas that need more attention and adjustment in reservoir models. If time-lapse (4D) seismic data are available, they are utilized in conditioning of the reservoir properties of models through history matching.

In Figure 1.3, the trough corresponds to the moved Oil-Water Contact (OWC) and the peak corresponds with the original OWC (Redondo-Lopez et al. 2002). The trough/peak signature was mapped for use in the prediction of moved oil-water contact in the reservoir simulation history matching. The result facilitated identification of sweep, along with visualisation of areas of unswept oil, highlighting infill opportunities. Early outcomes from infill drilling validated the method and indicated the potential economic benefits of 4D seismic technologies (McInally et.al. 2003).

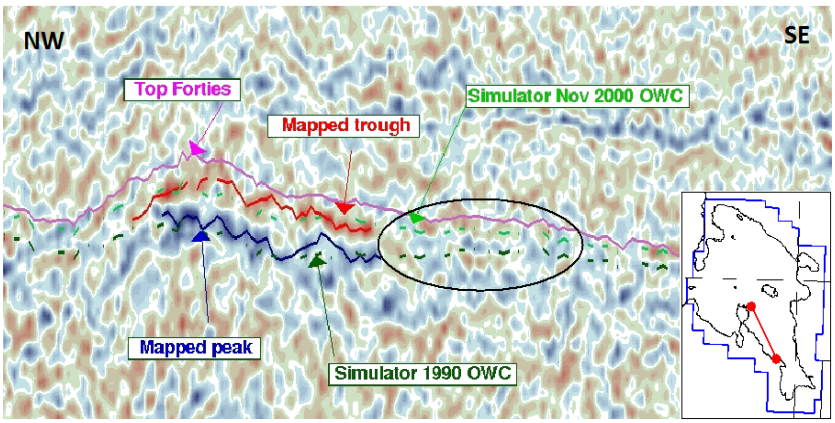

Figure 1.3: A conventional far-offset difference map (1990-2000) that shows the typical trough (red)-peak (blue) 4D signature in the Nelson field (after McInally et al. 2003).

Direct measurements of reservoir properties are limited (i.e. petro-physical data are only measured at well locations), contamination with noise (i.e. 3D seismic data), and are measured at different scales. Therefore reservoir properties such as porosity and permeability are usually unknown or poorly defined in the static geo-cellular fine scale model. A model that is only conditioned to such data is less likely to replicate the reservoir production history and thus is less reliable when used for forecasting purposes. The reservoir parameters could be better estimated using indirect measurement, such as well production and 4D seismic data. A more geologically sound and accurately characterized model which reproduces the past reservoir performance more precisely, will make more reliable prediction. History matching as further conditioning, constraints the reservoir model through assimilation of all available static and dynamic data, and is essential to forecast a confident and optimal production scenario.

Production and seismic datasets are often used separately in history matching with the supposition that since the data are of different spatial and temporal scales, each is suitable for calibrating a particular set of parameters. Nevertheless, the models updated using well production data, often could not reasonably predict the seismic dataset, and vice versa. However, combined use of production and seismic data put more constraints on the reservoir model and result in more realistic estimates of model parameters. Various case studies have illustrated the success of integration of 4D seismic monitoring and production data in estimation of the reservoir properties mostly permeability, net:gross and particularly flow barriers (Huang et al. 1997, Landrø 2001, Meadows 2001, Gosselin et al. 2003, Mezghani et al. 2004, Dong and Oliver 2005,

Stephen et al. 2006, Roggero et al. 2007, Jakobsen et al. 2007, Walker and Lane 2007, Dong and Oliver 2008, and Castro et al. 2009).

4D reservoir history matching studies have derived more reliable models that could assess the path of fluids movements and the phase-front progress, identify bypassed volumes in the un-swept reservoir compartments, evaluate drilling risks that are evolved over the life of fields, and estimate remaining reserves with fewer associated uncertainties. Ultimately, they have optimised the recoverable oil and gas from reservoirs yielding more profits. Although it is not easy to quantify exactly, the economic impact of such methods appears to have been considerable. As an example, the estimated savings for Gullfaks are more than $1billion (Helland et al. 2008). Overall there has been a 6% reduction in drilling costs and additional reserves have increased by 5%. An extrapolated assessment by BP towards the end of 2022 has concluded that the use of 4D imaging across their fields would result in an additional sum of 66 MM stb reserves, taking the total to 95 MMstb of reserves (Figure 1.4). These statistics are dominated by 4D activity carried out in the North Sea only, and such rewards are consistently and substantially in excess of the produced volumes originally anticipated (Marsh 2004). Currently, the North Sea accounts for more than 80% of the global 4D market in terms of survey expenditures, however, because of such economical benefits further 4D practice may take up continuously (Evans 2008).

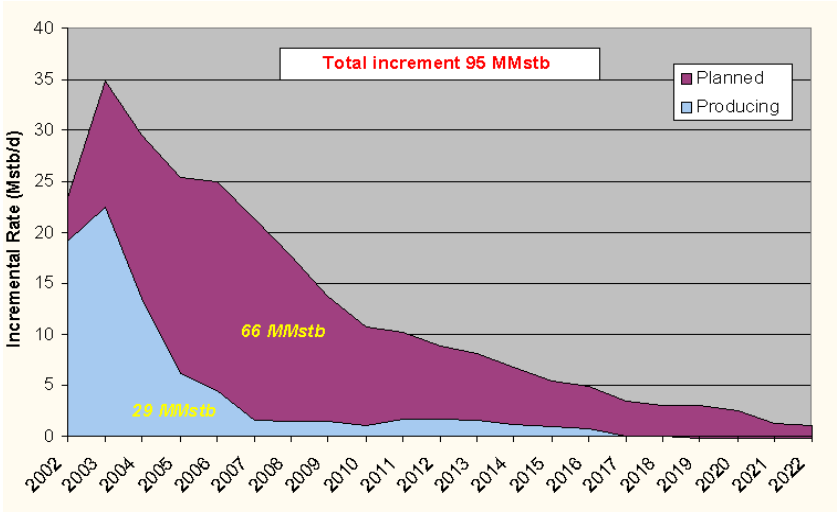

Figure 1.4: Production increment assigned to the use of 4D seismic practice in North Sea fields (after Marsh 2004).

Developments in 4D technology have stimulated the advances in the seismic acquisition capabilities in recent years, which have led to improved 4D data quality (Figure 1.5), and a reduction in the time period between surveys. In return, there is continued desire for the development of more efficient quantitative 4D seismic interpretations to identify the fine-scale information content of the 4D signatures, than is currently available in the reservoir seismic history matching practices.

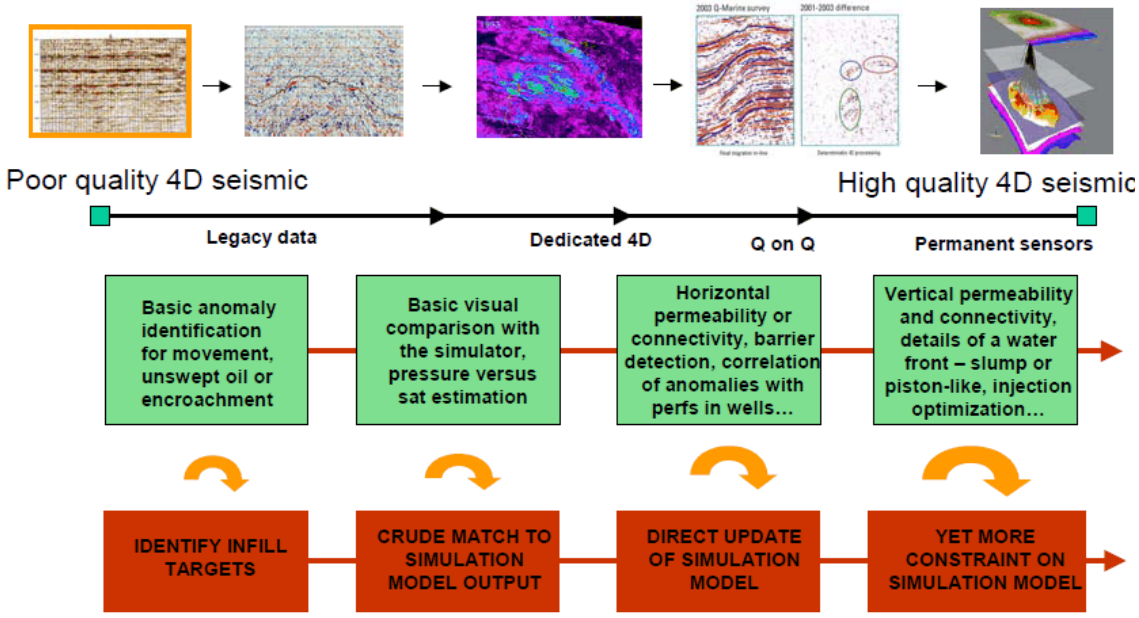

Figure 1.5: Quality of 4D seismic data is improving, this leads to an ever increasing ability to extract reservoir fine-scale details that can then used to improve the simulation model via integrated seismic history matching process (after MacBeth et al. 2008).

1.3 Requirements for History Matching

The requirements for carrying out the process of history matching include consolidation of the various sources of data into a reservoir mode which are divided into several types as described in following paragraphs.

Static Data: typically, the reservoir fine scale geo-cellular models are created with static data from various sources (see Figure 1.6). A pre-production static model is built based on the geological setting of the reservoir and by integration of 3D seismic data, core lab data, well log measurements, and sedimentary models using appropriate geostatistical techniques. These static data are measured at different scales. 3D seismic

acquisitions offer high resolution areally with low vertical resolution, while well logs are often extremely sparse spatially but may have some high resolutions measurements, usually vertically. In geophysical measurements the data are grouped in bins which typically measure about 25 metres, while in the geo-modelling cell dimensions may be between 25 to 100 metres, and typically for the upscaled numerical simulation, the grid size suits around 100 to 200 metres horizontally, and several metres vertically.

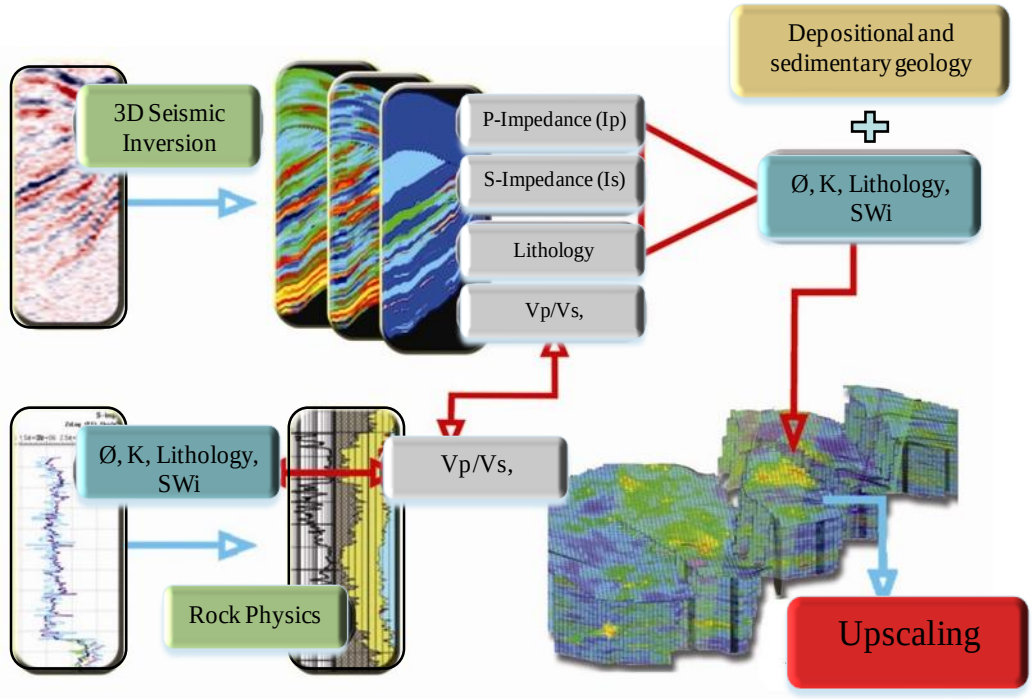

Figure 1.6: A static model is constructed based on geological settings and several sources of data. Then it is upscaled for simulation purposes (after Eastwood 2009).

Upscaling of the Static Model: this is a common practice to reduce the computational time of simulation runs. However, this process introduces approximation and extra uncertainties in the model properties which propagate to the simulation predictions. Upscaling increases in the cell dimension (and reductions the number of cells) and results in a loss of resolution of geological information. Upscaling procedure is complex because the upscaled cells should represent the flow (rate and pressure) effects enforced by the finer scale cells.

Unknown parameters: there are numerous unknown rock properties in the static reservoir model that are candidates to be updated in history matching. The three main

properties that have considerable spatial variability consist of: net:gross, porosity and permeability. These properties are typically correlated. There is also a large number of other uncertain parameters that are not necessarily directly related to the spatial grid cells. Examples include fault transmissibility multipliers, fluid properties (e.g. viscosities and densities), rock-fluid parameters (e.g. relative permeability and capillary pressure), aquifer size and strength, rock compressibility, water-oil contact, gas-oil contact and etc. However, the degrees of uncertainty in these data are different. For example for the lab data such as fluid properties, rock compressibility, elastic moduli of rock, relative permeability, and capillary pressure, the uncertainty is usually less than other data though there are issues of representivity.

Dynamic Data: in general this includes those data that are related to fluid displacement and the field production activity. They include well and repeat surveys of seismic data. Although the well data are limited to a few spatial locations, they provide information continuous in time that is more useful for short-term characterization of regions near the wells. Seismic surveys, conversely, are spatially spread over entire reservoir but are infrequent in time. They present better information about changes in the saturation and pressure maps in later time.

Well production data include oil, water and gas production rates, water-oil ratio (WOR), gas-oil ratios (GOR), water-gas ratios (WGR), bottom hole static and flowing pressure (BHP and FBHP). These types of well data are typically acquired with accuracy between 1-20%. Also, water and gas arrival times and fluid saturations from core data and RFT and transient well test measurements can be used in history matching (Mattax and Dalton 1990). As a practice sometimes the simulation model draws an initial part of well history data leaving the remaining portion of well production information to test the history matching methods during subsequent forecasting.

4D seismic data include various seismic acquisitions that measure P-wave velocity, reflectivity, amplitude, two-way-travel time in the time domain; and impedance or pseudo impedance which is in the depth domain. The use of time lapse data in history matching assumes that there is a practical basis for comparison of observed and simulated seismic data. However, geophysicists and reservoir engineer draw various attributes of the reservoir, i.e. they work in different domains of time or depth. Simulation models predict the reservoir pressure and fluid saturations (or impedance) in

the depth domain. However, the changes in pore pressure and saturation (and also temperature) due to production result in changes in seismic velocities and impedance, which is measured by seismic amplitude in the two-way time domain. There are other domains in which we can compare observed and simulated data including seismic impedance (or pseudo impedance) and pressure/saturation domains (see Figure 1.7).

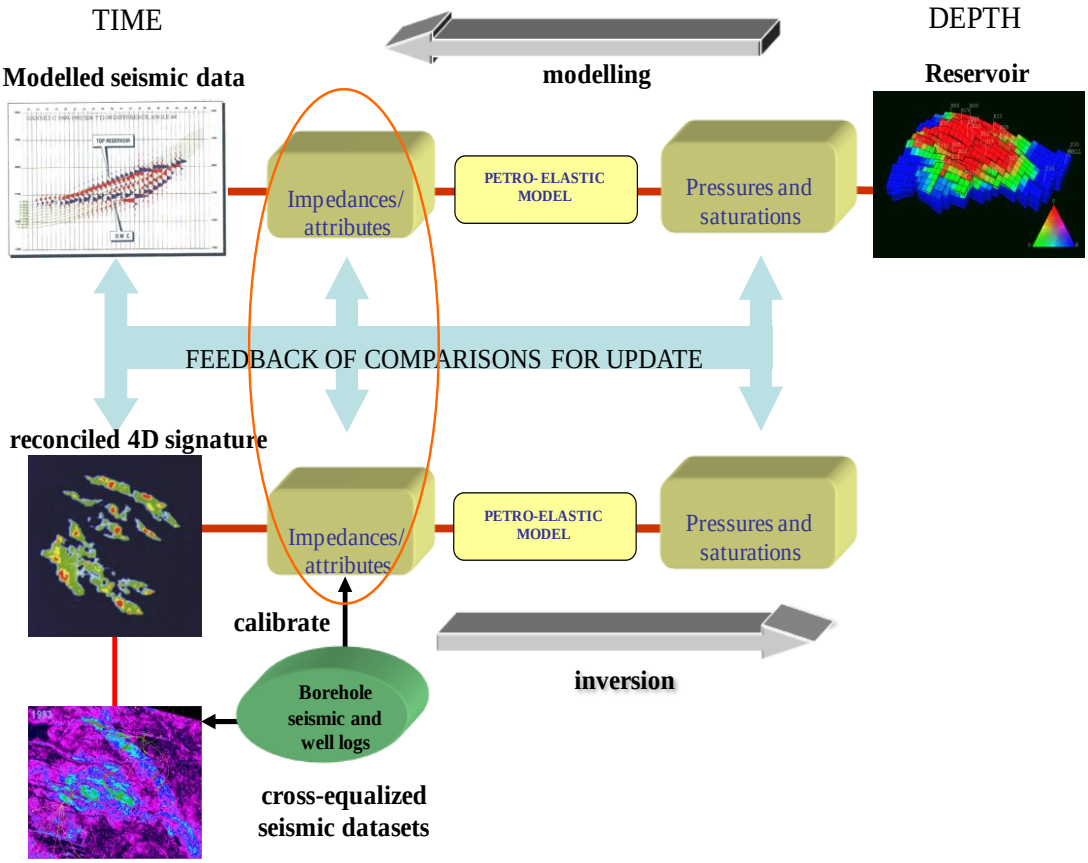

Figure 1.7: The various domains for comparison of measured and simulated seismic data Red circle identify the domain that has been used in this work (after MacBeth 2007).

Reservoir rock-physics properties link seismic and reservoir properties, and seismic properties can be estimated from simulated pressure and saturation using a petro-elastic modelling. Since rock property data is always limited, this calculation carries uncertainties which come from petro-elastic and seismic modelling. This approach is moderately time intensive for convolution methods approximately equivalent to the simulation time, but too time consuming and with more accurate full wave simulation. Likewise, seismic data can be converted to impedance and then by an inversion the changes in pressure and saturation may be quantified albeit with more uncertainty.

There are uncertainties which come from the seismic inversion utilized to estimate the pressure and saturation attributes either from the petro-elastic model or else from calibration issues via empirical inversion. Therefore, complications exist in comparing in each domain. All methods for this purpose rely on the accuracy of an underlying velocity model which requires fine-tuning.

Identifying the best domain for the seismic comparison is an active research area. We sought to avoid both the forward modelling to generate synthetic seismic traces and also the seismic inversion to estimate the pressure and saturation, since both may add uncertainty. To reach a balance between time and accuracy we considered the impedance domain as the best place for comparing real and simulated data (Stephen et al. 2006). In this study, impedance data are simulated, and we therefore required observed impedance data or an equivalent attribute. Coloured inversion seismic data was used to get observed pseudo impedance for 4D seismic history matching of the Schiehallion field in this work. Previously, pseudo impedance data were also used (Stephen et al. 2005, Stephen 2006, Stephen and Macbeth 2006, and Stephen and Macbeth 2008).

Many studies in seismic history matching have chosen the impedance domain since simulation of impedance is reasonably straightforward and is not very time consuming relatively (Bentley 1998, Gosselin et al. 2001, Waggoner et al. 2002, Gosselin et al. 2003, Mezghani et al. 2004, Dong and Oliver 2005, Emerick et al. 2007, Skjervheim et al. 2007, Roggero et al. 2007). Other domains have also have been studied, for example, saturation and pressure domain (Risso 2007, Machado 2009, De Souza et al. 2010), full amplitude time and seismic attribute domain (Huang et al. 1999, Parr et al. 2000, Aggio and Burns 2001, Lygren et al. 2003, Dadashpour et al. 2007, Leeuwenburgh 2008) and phase shifted amplitude (pseudo impedance) (Stephen et al. 2007, Edris 2008, Kazemi et al. 2010).

Seismic history matching has been applied in a number of field studies (Ditzhuijzen 2001, Litvak 2004, Stephen et al. 2007, Evensen et al. 2007, Roggero et al. 2007, Rwechungura 2010). It has also been performed using synthetic reservoirs cases (Castro et al. 2005, Stephen 2007, Jin et al. 2008, Echeverría 2009, Fahimuddin 2010, Leeuwenburgh et al. 2010, Trani et al. 2011). The benefit in synthetic studies is that the effect of 4D seismic signal/noise ratio in the final results could be investigated and the degree of success of 4D history matching could be evaluated. Additionally, in such

cases the size of the simulation model is usually small making it easier to parameterize the reservoir.

SHM Synopsis: the general approach for automatic seismic history matching is outlined in Figure 1.8. At each iteration simulation predict well behaviour and grid cell pressures and saturations. These dynamic attributes are used to calculate synthetic impedance of each grid block of the simulator using a petro-elastic model (PEM) based on the Gassmann (1951) equation and using MacBeth (2004) correlation for stress sensitivity. The simulated seismic properties are calculated at times corresponding to the 4D monitor surveys and are then upscaled vertically and downscaled horizontally at the geophysical model scale (seismic bin size) to estimate acoustic impedance. Observed and synthetic data are compared by computing a misfit function which includes both production and 4D seismic data. An optimization routine is used to minimize the misfit objective function and update the reservoir parameters to find the best matched model.

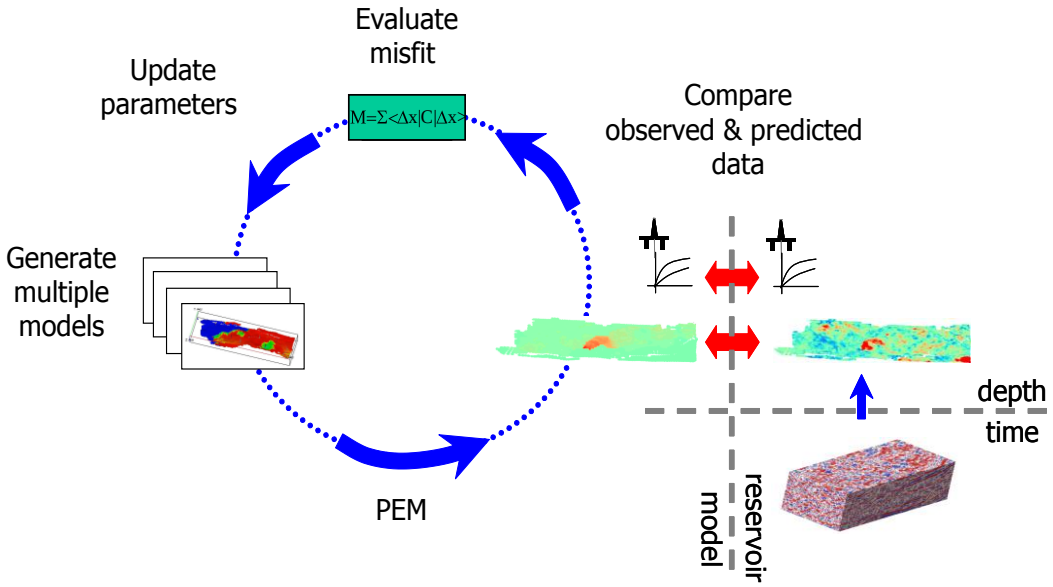

Figure 1.8: Depiction of the Seismic History Matching (SHM) process (Stephen et al. 2006).

Updating Algorithms: are an essential element of the automatic (computer aided) history matching methods. We refer to routines which seek to minimize or maximise some function that depends on some controlling parameters. We exclude details of the function. Gradient-based optimization methods such as Gauss-Newton, Levenberg-Marquardt, steepest descent, and others are usually quite efficient in converging to a local minimum of the

objective function. In general, the objective function is likely to have many minima. Only those minima that give a sufficiently good match to the data are of interest. The aim of global optimisation methods is to track down the global minimum of the objective function and find multiple matching models instead of one single model.

Well-known stochastic global methods are simulated annealing, neighbourhood algorithm and genetic algorithms. In such derivative-free optimisation methods only the rank of the models with respect to the objective function are used to drive the searches. Thus the CPU intensive mathematical calculation of the sensitivities and second derivative of the objective function are avoided. However they require many simulations to converge. The Neighbourhood Algorithm (NA) (Sambridge 1999) is a direct search quasi-global algorithm and is used in this thesis to sample the parameter space in the SHM workflow. The NA performance, like all stochastic optimisation methods, relies on generating an ensemble of models to be generated initially and also many models are produced during the search. The advantage is that the routine is amenable to parallel processing.

1.4 Objective of this thesis

It is a fact that oil and gas reservoir systems are too complex to be modelled accurately because: i) that we do not know all the parameters that are involved in affecting flow behaviour in the reservoir, and ii) even if we know the parameters the relationship between these parameters may be very complex. As a result history matching is usually a high dimensional and non-linear inverse problem. It is classified as being a problem that is ill-posed and underdetermined and one which suffers from a large number of unknowns, also known as the 'curse of dimensionality'. The number of unknowns is enormous particularly relative to the available data. The unknowns usually include the various properties of a large number of reservoir model grid blocks (such as permeability, net:gross, etc. Currently, research efforts are focused on dealing with the complexity of the history matching process in many academic and industrial centres. It remains the case that further developments are needed especially for the purposes of:

i) Providing a means for reducing the number of the unknown.

ii) Identifying the link between the reservoir parameter unknowns.

iii) Simplifying the history matching problem.

One response to these demands is the employment of the 'divide and conquer' approach which is a new initiative that is proposed in this thesis. The incentives associated with developing this approach is fast convergence time, low computation cost and a capability to acquire qualified results at the same time, in the seismic history matching analysis. It is a development of the existing Seismic History Matching (SHM) procedure (Stephen et al. 2006) which is used here and has also been successfully applied to both synthetic and realistic field studies previously.

Tackling the limitation caused by the great number of unknown parameters is very much necessary when using any type of optimisation routine, particularly when using stochastic methods. It is also important when using gradient-base algorithms. Overcoming this limitation reduces the iterations in history matching applications and thus the number of simulation runs required to obtain a solution. Thus an obvious saving in computational (CPU) time can be made which is important given the cost of using commercial simulators, e.g. Eclipse100 software (Eclipse Manual 2007). Commonly, the rough cost of using such simulators is £50-100K for the price of a license, and about £1K per day for fee of running and maintenance, which would be around £30K for one month (http://www.egpet.net, vbulletin 2011).

From qualitative analyses of applications of history matching procedures it is recognizable that individual well performance and time-lapsed (4D) seismic predictions are directly linked to the changes in particular localities in the reservoir, e.g. the area around an injector well. Indeed in many similar cases, especially when there are many updated parameters (i.e. high dimensional cases) it may be the case that groups of parameters may be changed independently to improve the history matching results. In such cases history matching can be split into a number of more simplified problems that could be handled more efficiently.

The method developed in this research initially seeks to determine whether we can ignore the interaction between the parameters that we wish to update in order to divide the entire parameter space of the problem into several sub-volumes of lower dimensions. Then, the sub-volumes of parameters are searched independently but

simultaneously, i.e. in parallel, more efficiently and in a shorter time. We therefore get an improvement in the convergence of SHM. We call this approach 'Divide and Conquer' and it is a novel initiative.

1.5 Motivation of the thesis

The number of models required to find an optimal solution (or several if there are multiple minima) using stochastic search routines, e.g. Neighbourhood Algorithm (NA) increases exponential as the parameter space of the problem grows in dimension, i.e. $\mathbf{2}^{nd}$ where n_d is the number of parameters. This is particularly the case if we assume that there are interactions between the parameters to be updated. When the interactions between various parameters are negligible, however, and the parameter space is searched as if it is fully coupled, over-sampling may occur. In fact many wasted models will be generated in the course of inversion processes which bring no new information.

In Figure 1.9 we illustrate the concern of oversampling with a simple two dimensional (2D) model (used as an example). When the response surface is non-orthogonal (Figure 1.9a), the function cannot be split into sub-functions and so the parameters have to be sampled all-together during the each search. However, if the function is orthogonal, it can be represented as a summation of two separate functions, each independent of the other (Figure 1.9b); then the problem of finding the global minimum of the surface is much simpler. We can sample along each parameter space of each sub-function independently but simultaneously, i.e. in parallel. We can also sample along the path of constant values for one parameter, and find the minimum of the other parameter and vice versa, i.e. in serial.

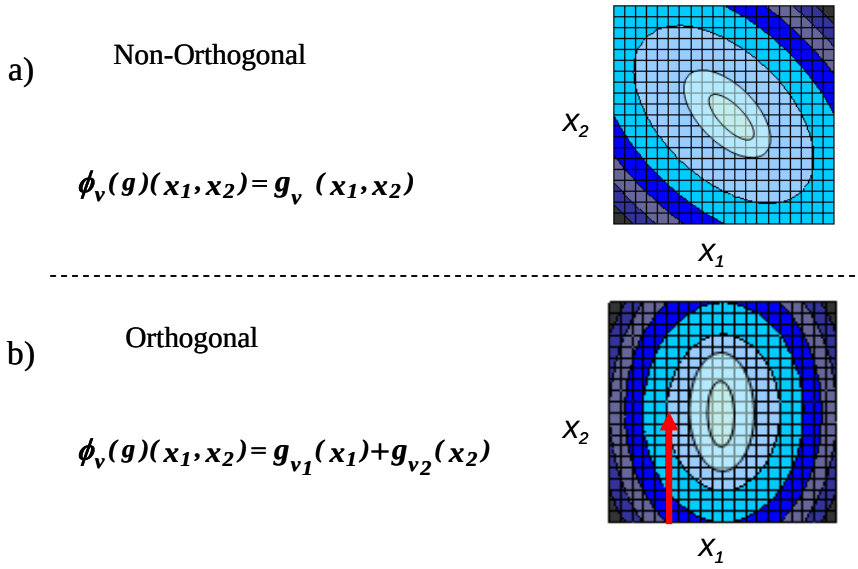

Figure 1.9: Schematic of misfit surfaces that are a) non-orthogonal and b) orthogonal. When searching for a global minimum of a non-orthogonal function, parameters need to be sampled all-together. In the case of an orthogonal function parameters can be searched individually in parallel.

We now illustrate the problem further with a high dimensional example. We consider a fourteen-dimensional (14D) quadratic response function in the form of:

$$g(x)=\sum_{i=1}^{7}(x_{2i-1}^2+x_{2i}^2+2x_{2i-1}x_{2i}) \tag{1.1}$$

In reality the function consists of seven pairs of mutually interacting parameters and could be split into seven two-dimensional (7×2D) sub-functions, as below:

$$g_i(x)=(x_{2i-1}+x_{2i})^2 \tag{1.2}$$

So:

$$g(x)=\sum_{i=1}^{7}g_i(x) \tag{1.3}$$

We consider solving the problem by splitting up the search in different components of the sub-volumes using NA (see x-axis of Figure 1.10 for these cases). First the entire 14D parameter space is searched using the NA. A parallelized version of NA is used to search the decoupled parameter sub-volumes individually but simultaneously. For example we consider a (12D +2D) problem so that only one 2D sub-function is used and the remainder is regarded as one 12D sub-function. As the degree of function decomposition increases from the first case up to last case (7x2D) the number of function evaluations decreases exponentially, see Figure 1.10. The results illustrate the driving initiative behind dividing the parameter space to several non-interacting sub-domains and shows the degree to which we may speed up convergence.

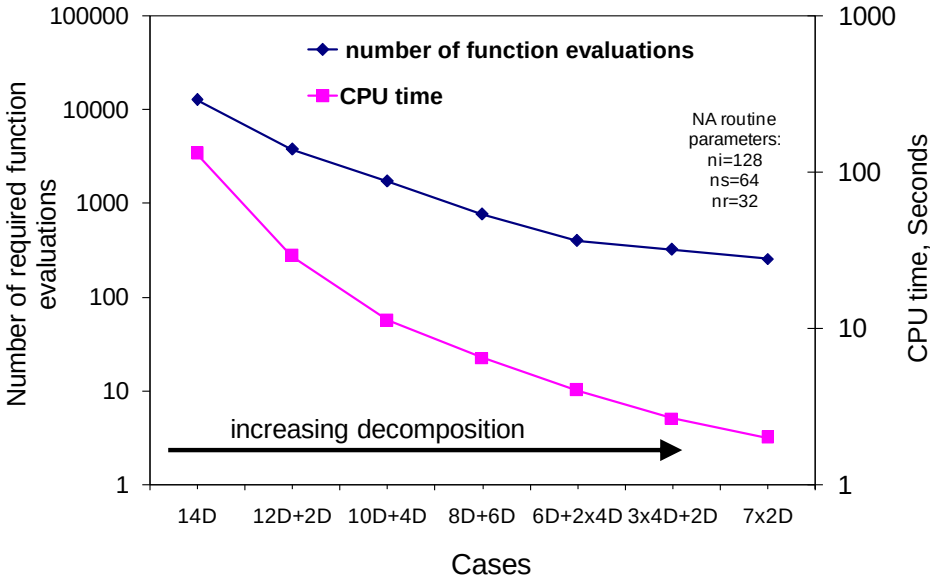

Figure 1.10: The number of required function evolutions to converge to a minimum declines exponentially by increasing the function decomposition.

1.6 Overview of 'Divide and Conquer' the unknowns

To perform the 'divide and conquer' approach (Figure 1.11) we take advantage of a numerical or analytical representation of the misfit function. To begin with, for a sufficient number of parameter combinations and the misfit values are evaluated. Then Response Surface Modelling (RSM), also known as proxy models, is used. A proxy model is used to assign and fit the misfit values of the set of initial models to a multi-dimensional second order polynomial including full parameter interaction. By interrogating the interaction terms that appear in the polynomial, the interdependency

between parameters and therefore the state of orthogonality in parameter space is identified. Then the misfit objective function is decomposed to sub-misfits along with its sub-volume.

An adapted version of the NA routine searches these sub-domains in parallel in order to modify the parameters. Alternatively the decoupled sub-domains could be searched in series. The results of individual searches are integrated and passed to the next iteration of the SHM loop. In Figure 1.8 the decoupling process is shown relative to the main SHM loop. We can carry out this step with every iteration but so far once is enough following the run of the initial models (for more description on the method see Chapter 3, and for applications of the method see Chapter 4, 5,6 and Sedighi and Stephen 2009 and 2010).

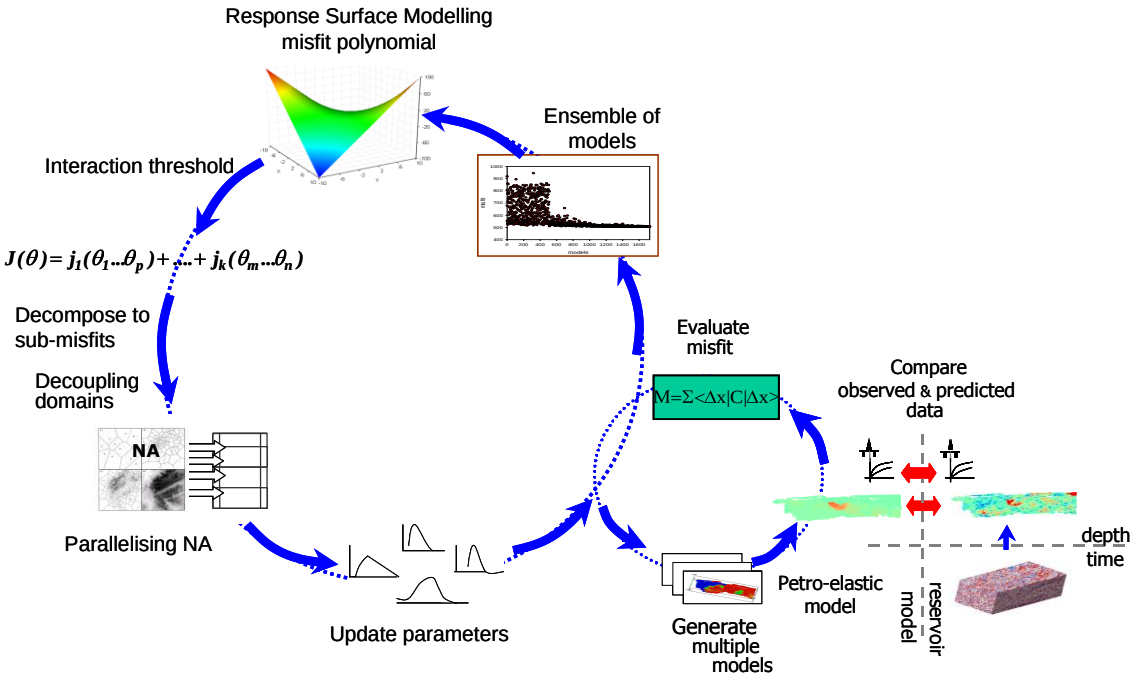

Figure 1.11: Analysis used in decomposition of the misfit and subsequent parallel searching of the sub-domains. The larger loop indicates the steps involved in analysis of the results of the first pass of the smaller loop of original SHM workflow.

Stochastic inversion routines such as NA usually require a large number of initial models to effectively sample the parameter space to start with, particularly since quasi-random sampling is used. In order to reduce the number of initial models, an approach

of integrating Experimental Design (ED) techniques with the 'divide and conquer' method is implemented. These designs play an important role in complicated design problems, because in addition to the main effect and interaction, they can be used to determine the second order non-linear effects.

Here, experimental design techniques are enabled to sample the parameter space more efficiently to build the proxy to the objective function with sufficient accuracy. The number of initial simulation runs is also reduced significantly compared to a typical full inversion using NA. When this innovative step is combined with the 'divide and conquer' approach, we obtained dramatic speed up in the total convergence rate. The approach has been successfully applied to several high dimensional seismic history matching studies of the Schiehallion field. In these studies, the transmissibilities of various barriers are the dominant parameters and for a number of cases, the local properties of permeability and net:gross are also updated. The number of models required to reach a corresponding solution by performing the 'divide and conquer' method combined with experimental designs is ten times smaller compared to the many models involved in the full inversion using NA.

1.7 Closing Review and Content of the thesis

This chapter comprised a brief overview to the topic of close-loop reservoir management and the major role of the history matching in reservoir optimisation. Then, we presented an introduction to the 'divide and conquer' approach which has been developed during this research. A brief explanation on how this method is developed and an example of how it may improve the convergence rate of seismic history matching was provided. The rest of the chapters of this thesis are as follows.

Chapter 2: Time-lapsed seismic (4D) methods and the main challenges of 4D seismic practices are discussed. The basics concepts supporting this research work are given. A description of inversion theory and history matching in reservoir management is specified. The definition of the objective function and the non-linearity, ill-posedness non-uniqueness, and curse of dimensionality are discussed. The importance of analysis and identifying model errors in the final residuals as well as errors in data are presented. Various parameterization techniques, inversion algorithms, and probabilistic approaches using Bayes theorem for handling uncertainty of reservoir outcomes are defined. The

essence of petroelastic modelling and the Gassmann equation are described. The proposed method of this research is based on utilizing two techniques of Response Surface Modelling (RSM) and Experimental Design (ED), they are discussed.

Chapter 3: The integration of well production data and 4D seismic data for the purpose of better reservoir model characterization are outlined. A description of the Seismic History Matching (SHM) approach used in this thesis is provided. The approach of 'divide and conquer' of the parameter space in the SHM work flow is established. Methods of Parallel-SHM and Serial-SHM are explained. The approach of combining experimental designs and 'divide and conquer' is presented.

Chapter 4: The aim of this chapter is to show the application of the method of 'divide and conquer'. The method is applied to a seismic history matching case study of the Schiehallion field where the uncertain reservoir model parameters include the transmissibility of 10 barriers. The results acquired by the 'divide and conquer' method are then compared against the results obtained by full inversion seismic history matching application to the same problem.

Chapter 5: The application of the approach of integrating experimental design techniques with the 'divide and conquer' method is presented. This method has faster convergence and is applied to the same 10-dimensional seismic history matching of the Schiehallion field (example of Chapter 4). Also the method is applied to an 18-dimensional case study where the parameters to be updated include transmissibility multiplier of barriers, and net:gross, horizontal permeability, and vertical permeability multiplier of two groups of pilot points.

Chapter 6: The approach of the spatial decomposition of misfit objective functions by 'divide and conquer' of the seismic territories is demonstrated. This method identifies the spatial components of the misfit function which depend only on a smaller number of the elements of total updating parameters. Again the method is applied to the same 10-dimensional case study of Chapter 4 and 5.

Chapter 7: The thesis closing phase includes a summary, recommendations for further work and conclusion.

CHAPTER 2 Basic Concepts and Supporting Materials

Introduction

In this chapter the fundamental concepts and background material are presented upon which the research in this thesis is built. First, a description of the principles of time-lapse seismic analysis and challenges are presented. Then, beginning with an overview on inversion theory, history matching in the context of reservoir characterization is described. The mathematical expression of the objective function which is the mismatch between simulated and observed data is discussed. The circumstances in history matching that lead to nonlinearity, high degree of freedom, ill-posedness, non-uniqueness are all explained. The existence of errors in models and in the data, the curse of dimensionality, and the requisite for reservoir parameterization are also discussed.

Subsequently, a brief review of gradient-based and non-derivative inversion routines is provided. Application of Bayesian theory and the likelihood function are reviewed. A description of petro-elastic modelling is given. The method of 'divide and conquer' of the unknowns makes use of Response Surface Modelling (RSM) and Experimental Design (ED) techniques which they are discussed in the last section.

2.1 Time-lapse (4D) Seismic

Time-lapse (4D) seismic imaging plays an important role in subsurface monitoring of petroleum reservoirs (e.g. Harris et al. 1995, Rickett and Lumley 2001). This is primarily due to the flow induced seismic changes that occur in the reservoir by production (Wynn 2003). The 4D seismic difference signals are obtained from repeated 3D seismic surveys over the time of reservoir production, and now analysis of such data is a well developed and understood field (Yilmaz 2001).

Normally, the subsurface seismic attribute map could be represented as $\boldsymbol{A(x,y,z)}$, where $\boldsymbol{(x,y,z)}$ is a co-ordinate and A is a derived seismic attribute such as amplitude,

compression and shear wave reflectivity and impedance. These attributes are estimated from acquiring and processing a single 3D seismic survey which is comprised of the coupled effects from the background geology along with the fluids and the pressure of the reservoir rock. The estimation and interpretation of this information at location ***(x,y,z)*** of a single survey can be inferred as seismic reservoir characterization which depends on properties such as net thickness ($\boldsymbol{\tau}$), lithology ($\boldsymbol{L}$), porosity ($\boldsymbol{\varphi}$), pressure ($\boldsymbol{P}$) and fluid saturations ($\boldsymbol{S}$) (Nur 1989, Wang et al. 1991, Batzle and Wang 1992):

$$\boldsymbol{A = A(x, y, z, \tau, L, \varphi, P, S) = A(X)} \qquad (2.1)$$

Where: $\underline{\boldsymbol{X}}$ is a vector representing reservoir properties. The net thickness ($\boldsymbol{\tau}$), the lithology ($\boldsymbol{L}$), and the porosity ($\boldsymbol{\varphi}$) remain the same after a certain period of production and injection. Of course the reservoir pressure and fluid saturations change. By differencing a series of seismic attributes, it is often assumed that $\boldsymbol{A(\underline{X})}$ removes the static geologic contribution, and isolates time varying seismic characterization.

The gradient of $\boldsymbol{A}$ with respect to $\boldsymbol{S}$ and $\boldsymbol{P}$ depends mainly on the change in petro-elastic properties of the rock due to the change of fluid distribution and the pressure change around the production or injection wells. Implicitly, therefore, the gradient of $\boldsymbol{A}$ with respect to $\boldsymbol{S}$ and $\boldsymbol{P}$ is principally linked to the reservoir characteristics such as porosity, net:gross, permeability and transmissibility. It is deemed that 4D seismic data is potentially a much less ambiguous task than reservoir characterization using 3D seismic data then because the effects of geology and fluid flow may be decoupled by comparing time varying seismic sets.

At present, time-lapse seismic data is applied with the objectives of monitoring saturation and pressure changes, reservoir compaction detection, and moreover fine-tuning of the reservoir model through seismic history matching. For example, 4D seismic surveys from the North Sea Gullfaks field (Figure 2.1) were used to monitor the replacement of oil by water in the reservoir which is understandable when the baseline survey 1985 (Figure 2.1a) and the monitor survey 1995 (Figure 2.1a) are compared.

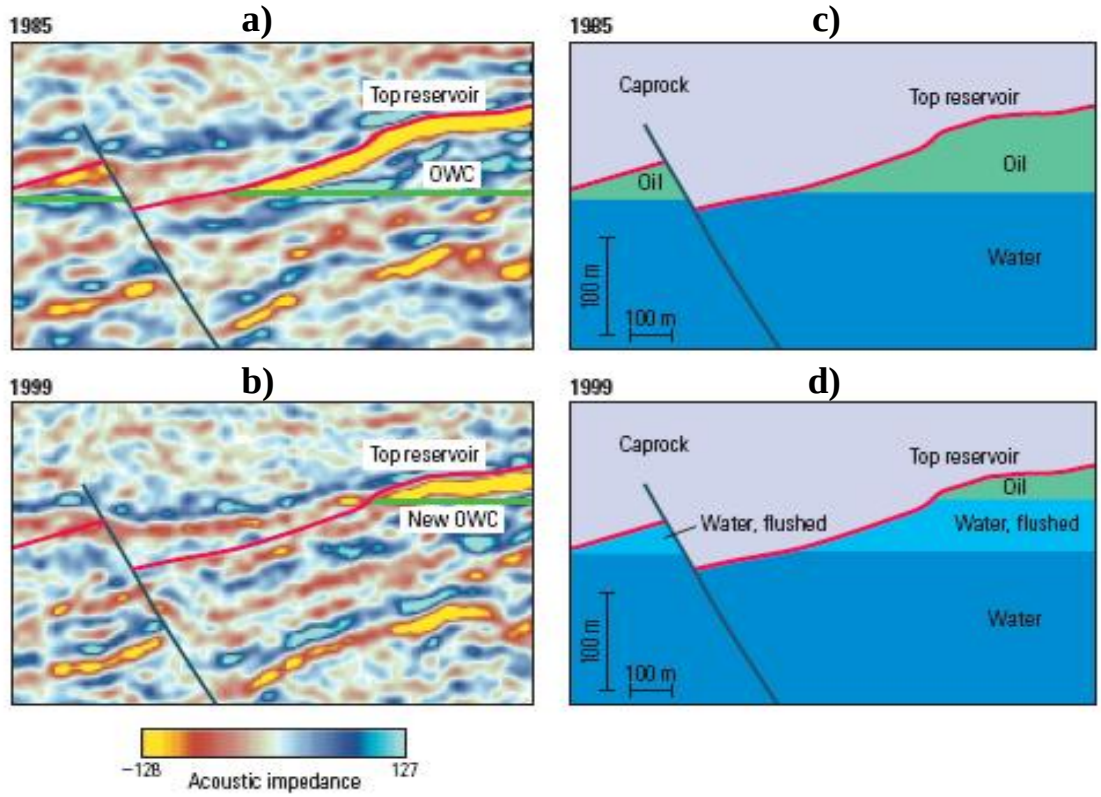

Figure 2.1: The changes in seismic reflection amplitude between the two surveys in a) 1985, and b) 1999 due to production, and also the interpretation of the reservoir condition in c) 1985, and d) 1999. The difference in the signal strength at the top of the reservoir is related to a decrease in oil saturation and change of the oil-water-contact (OWC). The strong seismic response from the oil-water-contact in 1985 has also been dimmed by oil production. In the seismic maps disappearance of red and yellow colours from 1985 to 1999 represent a reduction in acoustic impedance (after Traine 2002).

One of the first 4D seismic acquisition applications consisted of seismic surveys before and after a steam injection at the Athabasca tar sands reservoir (Pullin et al. 1987). By comparing time shift and amplitude attenuation difference of the two surveys, swept and un-swept zones were mapped. After that, the 4D seismic technique was assessed for monitoring of small-scales fluid flow local to the wells in the Duri field (Jenkins et al. 1997, Lumley 2001). The primary objectives for the time-lapse seismic acquired on the Foinaven field (Cooper et al. 1999) were to map fluid movements to identify by-passed oil areas. The results qualitatively agreed with the later performance of the reservoir. 4D seismic surveys on the Meren field (Lumley et al. 1999) were used to identify pathways of injected water, sealing faults, and compartments that may have by-passed oil. For the Bay Marchand field (Behrens et al. 2002) time-lapse seismic surveys were

used to monitor water influx, identify the by-passed oil, and provide a qualitative comparison of the quality of data before and after cross equalization, which is important in 4D data processing. There are other references that have discussed the success of time-lapse seismic in monitoring of hydrocarbon movement in reservoirs during production in the literature (e.g. Ross et al. 1996, Hughes 1998, Burkhart et al. 2000, Rickett and Lumley 2001, Waggoner et al. 2002, Gouveia et al. 2004, Lumley 2004, Dong and Oliver 2005, Leeuwenburgh et al. 2008). These analyses have helped in well planning, injection and production strategies revised drainage strategy; and thus has added extra value to hydrocarbon assets.

4D seismic interpretation is best applied when the acquisition geometry, the collecting technology, and processing do not change from survey to survey (Lumley et al. 1994), thus we can effectively disregard the source of seismic noise. Also 4D practices can be executed in fields where rock is compressible and porous and there is a sufficient compressibility contrast and large saturation and pore pressure changes between monitor surveys (Lumley et al. 1997). There remain numerous challenges in 4D seismic activities which are reviewed in the following section.

2.1.1 Time-laps Seismic Challenges

Feasibility: while 4D seismic studies have been very successful, they have been feasible when the sensitivity of seismic signal to changes in reservoir condition was adequate. Large reliable 4D seismic contrasts can occur where there are free-gas saturation changes, injected steam, and gas or CO_2 injection (Shyeh et al. 1999). Oil-water systems are harder to monitor if the reservoirs are under-saturated and are of very stiff, cemented and low porosity rock compared to the more easily tracked volatile oils in soft and high porous sands. In general when the rock matrix is compressible (e.g. unconsolidated sand) and there is a large compressibility contrast between the fluids (e.g. water and gas), there would be a large 4D seismic signal that could be detectable, (see Figure 2.2). Conversely, stiff rocks and/or similarly compressible fluids produce a weak 4D signal. Highly compressible rock and very large fluid compressibility contrasts produce strong but complex nonlinear signals which could not be interpreted easily for 4D seismic response (Fanchi 1999, Lumley 2001).

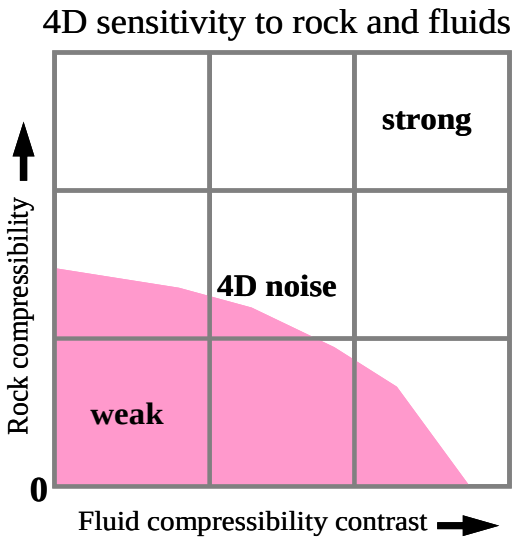

Figure 2.2: Schematic of 4D seismic sensitivity to porous rock frame compressibility and fluid compressibility contrast. The 4D seismic non-repeatable noise envelope is shown in pink, i.e. when the noise in dominant relative to signal. Stiff rocks and fluids of similar compressibility produce weak 4D signals (lower left quadrant), that are masked with noise in measurements and are not detectable. Soft rocks and large fluid compressibility contrasts produce strong but complex nonlinear 4D seismic responses (top right quadrant), which are most easily interpretable. Moderate combinations of rock and fluid compressibility produce a sweet spot of both good 4D seismic delectability and interpretability in the center of the matrix with controllable amount of noise (after Lumley 2009).

Non-repeatability in 4D seismic images: the challenges in seismic acquisitions, as with any measurement, are that they are always contaminated with errors or noise. The ability to detect a 4D signal depends both on the magnitude of the signal and on the noise level in the data. In practice, 4D seismic data record time shifts (amplitude vs. time changes) in reservoir properties due to production, as well as non-repeatable noise from external variables. External variables include a) uncontrolled ground motion noise interference with seismic signals, b) ambient noise such as tide, temperature for marine and weathered zones for land, and whether it is coherent or random, c) electrical recording noise due to use of different equipment between surveys, d) inconsistency in source-receivers geometry, and e) incorrect geophone and hydrophone positioning. The changes in external variables are what lead to the 'non-repeatability noise' of 4D seismic acquisitions.

Then the aim of seismic processing is to alter the seismic data in order to suppress the noise and enhance signal and migrate seismic events to the appropriate location in the subsurface space. Seismic processing facilitates better interpretation because subsurface structures and reflection geometries become more apparent. Processing of raw seismic data involves several steps typically including analysis of velocities and frequencies, static corrections, deconvolution, normal moveout, dip moveout, stacking, and migration, which can be performed before or after stacking (for more on seismic processing details see Yilmaz 1991).

There may be differences due to previous survey processing that may mask the changes in the dynamic reservoir properties or may convey discrepancies in the sections, including differences in the velocity model and processing parameters and algorithms, which induce uncertainty in identifying the dip move-outs and should be minimized and removed as well. Also, incorrect binning occurs when the stacked data bins are not of the same offset ranges, and when the number of seismic trace contributions to each offset bin is not consistent between surveys. There are effects of diffracted energy by sea state conditions and inter-beds (multiple reflections). Multiples are seismic energy that has been reflected more than once. Multiples are considered noise on seismic records and are attenuated to improve signal to noise ratio by determining a set of filter functions, however they are difficult to remove and therefore may lead to a major source of poor time-lapse data quality.

There are a number of manifestations of non-repeatable noise when seismic data are processed, which commonly comprise variable amplitude gain, frequency content, static shifts, and waveform phase changes, and also event positioning between the multiple vintages of data sets. Despite efforts to circumvent non-repeatability and retain exact acquisition conditions (installing permanent receiver sensor e.g. in Foinaven and Vahall field), discrepancies still remain in the sections of the survey profiles that should not experience any change in geological and dynamic conditions and hence no change in seismic reflectivity. These types of subsurface ambiguities that could not easily be interpreted are called geological noise (Waal and Calvert 2003, Calvert 2005, Lacombe et al. 2011, Helgerud et al. 2011).

A common way to quantify non-repeatable noise is to compute the energy (e.g. amplitude) of the difference data compared to the energy of each individual data series

with the Normalized Root-Mean-Square (NRMS) differences. The metric is defined so that in a perfectly repeatable condition NRMS=0, if the two data sets consist of random uncorrelated noise NRMS=1.41, and if the data sets were identical but polarity-reversed NRMS=2. With current 4D seismic acquisition and processing NRMS of 0.4-0.6 are considered good quality and NRMS less than 0.2 are considered excellent (Lumley 2009). Generally 'cross-equalization' studies are aimed to tackle these non-repeatable noise sources.

Cross-equalization of 4D seismic images: the aforementioned effects lead the need for the post-acquisition issue of 'cross-equalization' processing which transforms one seismic section to be comparable with the others (Ross et al. 1996). The content of the different surveys are scaled through analysing repeated signals (trace by trace) in sub-cubes located away from the reservoir area that are not affected by depletion. Cross-equalization of post-stack seismic datasets typically includes the following generic elements (for more details see Rickett and Lumley 2001):

- survey realignment to a common grid (re-binning), including spatial and temporal re-registration to correct the effects of geometry errors, differential statics time shifts, or different velocity functions used.
- bandwidth and phase equalization to compensate for different source wavelets, for example.
- amplitude balancing to scale the data to the same amplitude (or energy) level.

A common approach in processing of 4D seismic data sets is suppression of the noise due to non-repeatability through application of a variety of filters to the data sets, in pre-stack or post-stack volumes. Unfortunately, in some instances filters are unstable and are a strong function of the filter design criteria. It is very easy to unconsciously overmatch the data sets both within and outside the design window, thus overlook important time-lapse signals, or to under-match the data or drive the filter to instability and hence lead to artificial time-lapse signals in the data. Different cross-equalization techniques have been successfully applied in recent years to estimate and remove time shifts between time-lapse images (Bertrand et al. 2005, Aarre 2006). Most of these cross-equalization procedures are based on conventional Wiener Filter methods.

Wiener Filter: this filter minimizes the energy of the differences between traces of successive 4D surveys in a least-squares sense. These traces are from a region within the reservoir volume in which production effects are minimal. In the time domain, filtering could be carried out using a convolution operator (*). In that case the filtered signal, $\hat{s}[t]$, can be represented as the convolution that amounts to passing measured signal, $x[t]$, through a filter whose impulse response is, $h[t]$, as below:

$$h[t] * x[t] = \hat{s}[t] \tag{2.2}$$

To solve Equation 2.2 in practice the seismic recorded signals are broken down into their different frequency components by Fourier transform. This allows the frequency filter design to be performed more concisely to remove spurious noise (for more details see Recipes, Press et al. 2007).

Frequency of 4D Survey Repetitions: another aspect that influences whether times-lapse signals can be detected relies on the frequency of the repetition of surveys are repeated, which is related to the rate of fluids produced from the reservoir (Landrø et al. 1999, Arts et al. 2004). Typically, the time intervals between successive acquisitions are in the order of one or two years. Such a strategy works well for some time-lapse projects but not for all applications. For instance, in fields with many years of production left, or those with complicated reservoir characteristics it is more effective to carry out frequent surveys, typically at intervals of less than one year. For some reservoirs even earlier detection of the changes in the reservoir condition is very important (Kristiansen et al 2009). Then, the seismic surveys could be taken from intervals of a few months. Examples of such cases are:

- in high-pressure reservoirs where production is associated with compaction (Hawkins 2007), that can result in the subsidence at the seabed such as in chalk reservoirs of Central Graben in North Sea, e.g. Ekofisk field, and Elgin field with 500 bar pressure drop over its production life.

- in sequestered CO_2 reservoirs (Benson 2006) where continuous site monitoring is necessary for both tracking the migration of CO_2, and for environmental

licensing required for the purpose of the early possible leakage detection, e.g. in the Sleipner, Weyburn, and Salah geological sequestration projects.

Recently, permanently installed Ocean Bottom Seismic (OBS) is a cost efficient alternative to conventional repeated survey in such reservoirs. For example, success with Life of Field Seismic (LoFS) systems have been demonstrated on the Valhall field of a highly porous but low permeability chalk (Van Gestel et al. 2009), and the Clair field and the Chirag-Azeri fields (Foster et al. 2008). These technologies have not been widely adopted on a larger scale however mostly due to cost and environmental complications.

Discrimination of Saturation and Pressure Effects: Quantitative estimates of saturation and pressure changes is required in accurate rock physic modelling in order to derive and calibrate attributes such as impedance and reflectivity. Changes in additional dynamic reservoir properties, such as temperature, fluid viscosity, stress-induced porosity, fractures, etc., complicate this analysis of discrimination of saturation and pressure changes further (Watts et al. 1996). In some fields, the seismic sensitivity to stress changes is much greater than the sensitivity to saturation changes, while it is conversely true for some other fields. Most importantly there is always some coupled outcome of changes (Landrø et al. 2001). For example, in an aquifer-drive reservoir, the pressure drops due to production and an increase in the net effective pressure will result while the oil saturation decreases. Both effects will increase the P-wave velocities and impedances so that the two effects strengthen each other. In a water-flood reservoir, the oil saturation decreases but the pressure may increase near the injector and there would be a decrease in the net effective pressure. In this case, saturation and pressure compete with each other, partially, or even totally and may cancel the effects of each other on seismic properties (Wang 1997), this phenomenon is shown in Figure 2.3.

Techniques for the separation of saturation and pressure effects are conventionally dependent to angle-dependent reflectivity and amplitude variation with offset (AVO) attributes. AVO quantities are calculated from seismic amplitude versus source-receiver separation. Using offset data, the relative strength of saturation and pressure effects are understood from a semi-empirical approach (Tura and Lumley 1999) or using rock physic models (Landrø 2001). For example, Lumley at al. (2003) presented a 4D seismic inversion method while two seismic attributes: i) near and far offset/angle

amplitudes, and ii) pre-stack-inverted P- and S- impedance data were cross-plotted against each other. Leeuwenburgh et al. (2008) used two-way seismic travel time surveys to invert and provided (depth-averaged) estimates of pressure and saturation. Trani et al. (2011) proposed a method using different combinations of 4D attributes based on four correlations: two expressing changes in pre-stack AVO attributes (zero-offset and gradient reflectivities), and two expressing post-stack time-shifts of P- and S-waves. Rocks saturated with compressible fluids show higher P-wave velocities (V_P) and impedances; however S-wave velocities (V_S) and impedances are much less affected by pore fluids because fluids have no rigidity (resistance to shear stress). Such V_P and V_p/V_S dependencies on pore fluid are the basis for saturation effect discrimination. These approaches work well when physical properties, i.e. shale volume and porosity, within the reservoir are relatively uniform.

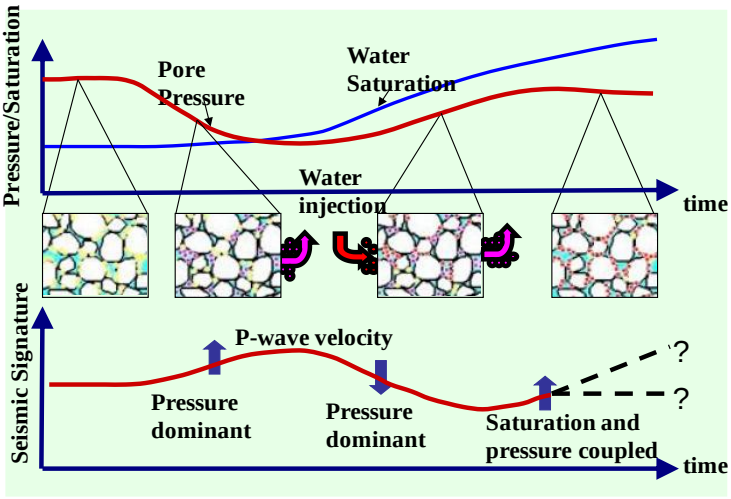

Figure 2.3: Change in acoustic velocity following changes in pressure and saturation due to production and injection in the reservoir close to a injector well. P-wave velocity increases primarily due to pressure drop in the reservoir (depletion). Then by water injection acoustic velocity decreases since there is a lift in pressure. When the water saturation increases due to arrival of the water front, initially the effect of pressure is cancelled, there is a coupled effect of saturation and pressure changes on acoustic velocity.

2.2 Overview of Inversion Theory

Most petroleum engineering applications deal with a subsurface that is not easily accessible and the properties controlling theses physical behaviours are numerous. For example some properties such as permeability require fine resolution in space, and

others such as fluid saturation and pressure change in time. In such conditions inversion is the only practical approach to integrate all available information (Figure 2.4).

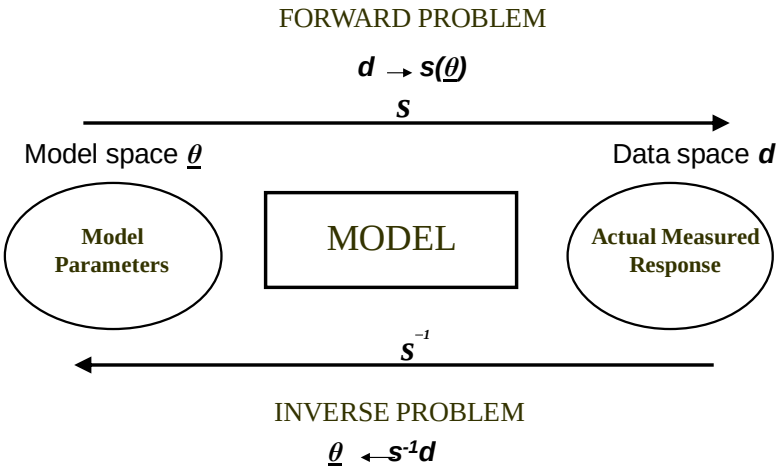

Figure 2.4: Forward problem versus inverse problem. Forward problem estimates observed data, d, using simulation model, s, that depends on model parameters, $\underline{\theta}$, however, in the inverse problem the focus is on finding model parameters, $\underline{\theta}$, given observed data d.

According to Jackson (1972) inversion is the 'interpretation of inaccurate, insufficient and inconsistent data'. For given data the inversion procedure seeks to define a model for a physical system which agrees most with the observation (e.g. Line and Treitel 1984). Seismologists initially extended the formulation of inverse problems for data processing and interpretation (Mosegaard and Tarantola 2002). The practical principle of inverse problems relies on the objective function, which measures the difference between modelled and observed data, and identification its minimum value. This was of prime concern to earth scientists. Tarantola and Valette (1982) generalized this concept for non-linear inversion in two influential papers introducing the idea of a Gaussian approach for parameter estimation.

Applications of inverse theory in the petroleum industry are in two major areas. In geophysics, 'inversion of seismic data in oil and gas fields' is carried out, while in reservoir engineering 'inversion of reservoir history data' is performed. The purpose of inversion of seismic data is to recover the subsurface elastic properties (e.g. velocity and acoustic impedance). Many algorithms for this purpose have been developed (Tarantola 1984, Russell 1988). For example, Oldenburg et al. (1983) discussed the deterministic

inversion for impedance, while Cao et al. (1989) illustrated an inversion method to estimate velocity and impedance simultaneously. Landrø (2001) proposed a method to express the changes in amplitude as a function of variation of reservoir pressure and saturation. Ouair and Strønen (2006) proposed a global inversion method where all 4D vintages are inverted simultaneously.

Figure 2.5, illustrates the application of forward and inverse formulations to seismic modelling, with the convolution and deconvolution methods. Each layer in the earth model is characterized by its acoustic velocity or impedance, which can be computed at wells from logs of P-wave and S-wave velocity along with bulk density. The normal incidence reflectivity, R, of a layer interface is a function of the impedance contrast between the layers on each side. Convolutional forward modelling combines the sequence of reflectivity coefficients with a seismic pulse represented by the wavelet to generate synthetic traces. The problem is often that there is not a good model of either the earth or the seismic source wavelet. Surface seismic data may be available, though, and they are used to infer each thickness of layers and impedance or velocity. The inverse approach then extracts the signature of the pulse from seismic traces through deconvolution to deliver the inverted normal incidence reflectivity series, R, from which the acoustic impedances of each layer can be computed. The synthetic traces are usually inverted to fit the real traces.

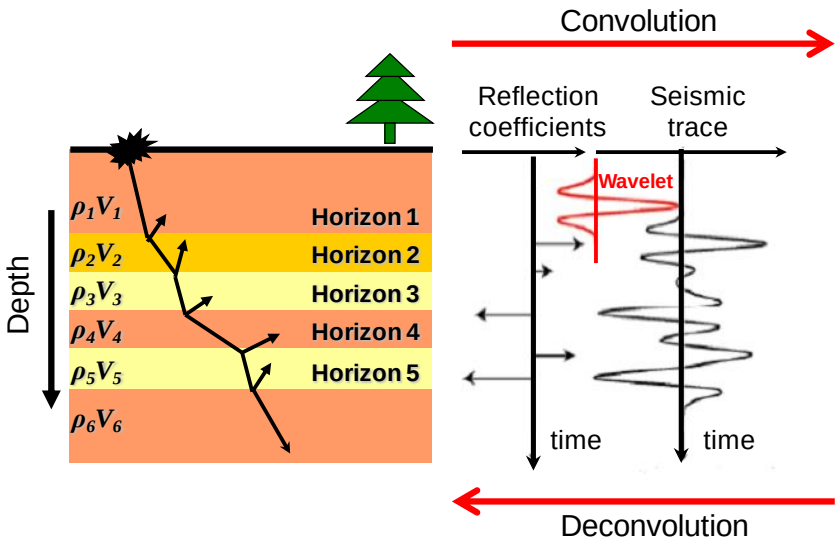

Figure 2.5: A schematic that depicts the application of forward (convolution) and inverse problems (deconvolution) in seismic modeling of the impedances (ρV) of reservoir layers.

2.2.1 Inversion Process of History Matching

A more geologically defined and accurately characterised reservoir simulation model can reproduce the reservoir performance more precisely. Such a model would utilize a tool to forecast the performance of a reservoir as accurately as possible. More reliable predictions are then obtainable for decision making in the reservoir management to optimise the recovery from the oil and gas accumulations.

The classical manual history matching approach is a trial and error method based on the experiences and skills of reservoir engineer. The reservoir simulator is run many times with different values of model parameters until a satisfactory match to history data is achieved. This process is time consuming and inefficient. In contrast, automatic history matching is usually an efficient process. Using an optimization algorithm the uncertain reservoir parameters are perturbed in order to minimize an 'objective function' that measures the mismatch between simulated and observed data (Figure 2.6).

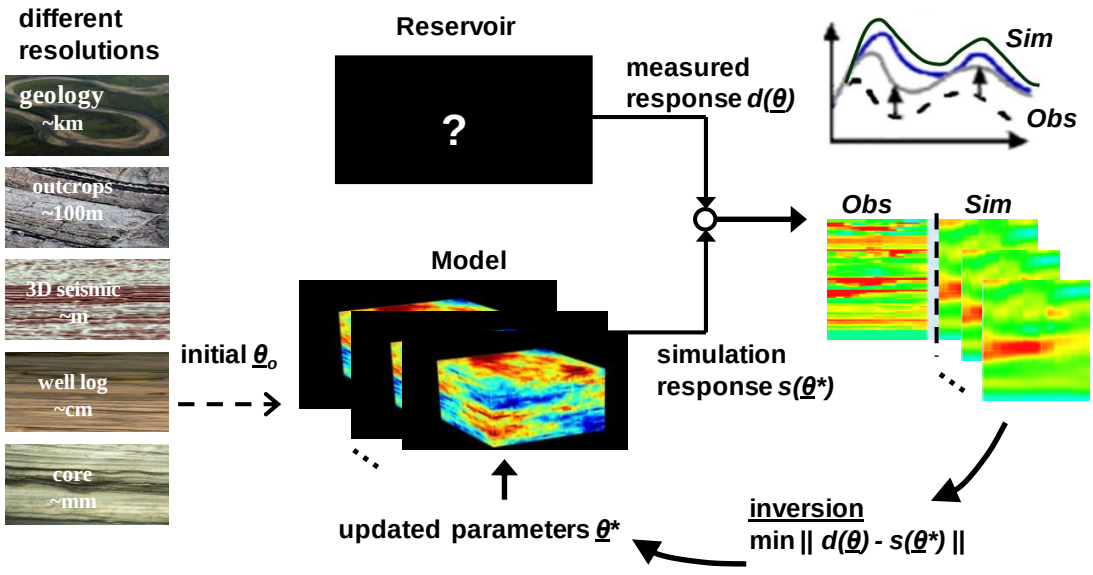

Figure 2.6: Automatic history matching process which minimize differences between observed data, d, and the simulation model responses, s, by updating the model parameters, $\underline{\theta}^*$. Initially, model parameters $\underline{\theta}_o$ are characterised based on sparse and inconsistent data, the anticipation is to find the true reservoir model $\underline{\theta}$.

Automatic history matching processes were first used fifty years ago (Jahns 1966, Jacquard and Jain 1965, Chen et al. 1974), and has mostly progressed in the nineties (e.g. Deutsch and Journel 1992, Bissell et al. 1994, Datta-Gupta et al. 1995, Sen et al. 1995, Reynolds et al. 1996, Oliver 1996, Landa and Horne 1997, Roggero and Hu 1998). In spite of numerous improvements in optimization routines and their applications, history matching demands intensive computation. Automatic history matching can be formulated in the framework of statistics, which provides a probabilistic justification for using a specific estimator such as least squares as the best misfit. Then through calculation of maximum likelihood and Bayesian theory, the uncertainty in prediction of the reservoir performance could be estimated (Romero et al. 2000, Arenas et al. 2001, Christie et al. 2002, Caers 2003, Li et al. 2003, Gao and Reynolds 2004, Gu and Oliver 2005, Stephen et al. 2006, Roggero et al. 2007, Ballester and Carter 2007, Leeuwenburgh 2008; 2010).

2.2.2 Time-lapse Seismic Incorporated in History Matching

Nowadays, time-lapse seismic are used as additional data in history matching leading to improved simulation models and then better reservoir prediction and management are achieved (e.g. Stephen et al. 2006). An objective function is defined to quantify the differences between simulated production and 4D seismic attributes (provided by a petro-elastic model) and real production and seismic data using appropriate weighting factors. An iterative optimisation algorithm is usually used to minimize this objective function by updating the reservoir model parameters.

Several studies have used different approaches to integrating time-lapse seismic and production data in updating the reservoir model. Huang et al. (1997) and Waggoner (2002) used time-lapse seismic amplitude data and the finite perturbation method to calculate required derivatives in the inversion process and updating simulation model. Tura and Lumley (1999), Landrø (2001), Meadows (2001) Arenas et al. (2001), and Waggoner et al. (2002) estimated the changes in reservoir model saturation and pressure directly from time-lapse seismic data and used P-wave velocity differences. Ditzhuijzen et al. (2001) matched production and seismic data when parameterized geometrical objects (size, orientation and transmissibility of faults and baffles). Phan and Horne (2002) used water saturation changes interpreted from time-lapse seismic to adjust channel orientation and deviation of the centre line from maximum continuity. Bogan

et al. (2003) used multiple time-lapse attributes, including velocity, impedance, and amplitude in a GOM (Gulf of Mexico) field to estimate fluid flow barriers, facies parameters, and variogram structures. Gosselin et al. (2003) deduced pressure and saturation changes from production and time-lapse seismic data and used Gradzones (a gradient based optimization) in reservoir parameterization.

Mezghani et al. (2004) used time-lapse acoustic impedance derived from pre-stack data to predict petrophysical properties using non-linear optimization based on derivatives with respect to the parameterization. Similarly Dong and Oliver (2005) related seismic impedance and production data to porosity and permeability and matched them using the adjoint and the LBFGS method. Dong et al. (2006) used the ensemble Kalman filter (EnKF) to match of production and time-lapse seismic impedance data and to improve estimation of porosity field. Walker (2006) used seismic data integration in characterising reservoir models using Genetic Algorithm. Leeuwenburgh et al. (2008) used two-way seismic travel times to the top and bottom of the reservoir.

Roggero et al. (2007) interpreted seismic data to constrain the reservoir model and update the fine scale geo-statistical parameters using the gradual deformation method. Dadashpour et al. (2008) calibrated porosity and permeability properties to estimate pressure and saturation changes from time-lapse seismic data by formulation of a nonlinear Gauss–Newton inversion scheme. Leeuwenburgh et al. (2010) showed the distribution of reservoir fluids and rock properties (porosity and permeability) can be better extracted from seismic amplitude data by combination of two inversion steps of both 3D and 4D data using two ensemble-based methods of the Kalman Filter and the randomized maximum. Trani et al. (2011) found the importance of the porosity in inversion of the changes in saturation and pressure from 4D seismic AVO and time-shift of compressional and shear waves.

As a rule, history matching is a challenging task, finding a minimum of a misfit function does not necessarily denote the true values of the reservoir parameters. One model that fits the observations best may not be the best one for the prediction forecasts. Sometimes a model with parameters close to the base case might lead to a good forecast for the true case although the production match to history is bad (Tavassoli et al. 2004). This situation arises because there may be a number of different (multiple) solutions to the history matching problem due to the fact that there is very limited information about

the actual details of the reservoir properties. Geological information may be highly conceptual and non-specific which may not describe the reservoir at all possible scales. Measured data at core, well logs, 3D/4D seismic surveys, well test and production records, however are specific. These data measure the properties at different scales. For example, well data are in centimetre to metre scale at high vertical resolution but only at a few well locations, while seismic data provide larger-scale stratigraphic and structural information and have higher coverage area (see Figure 2.7).

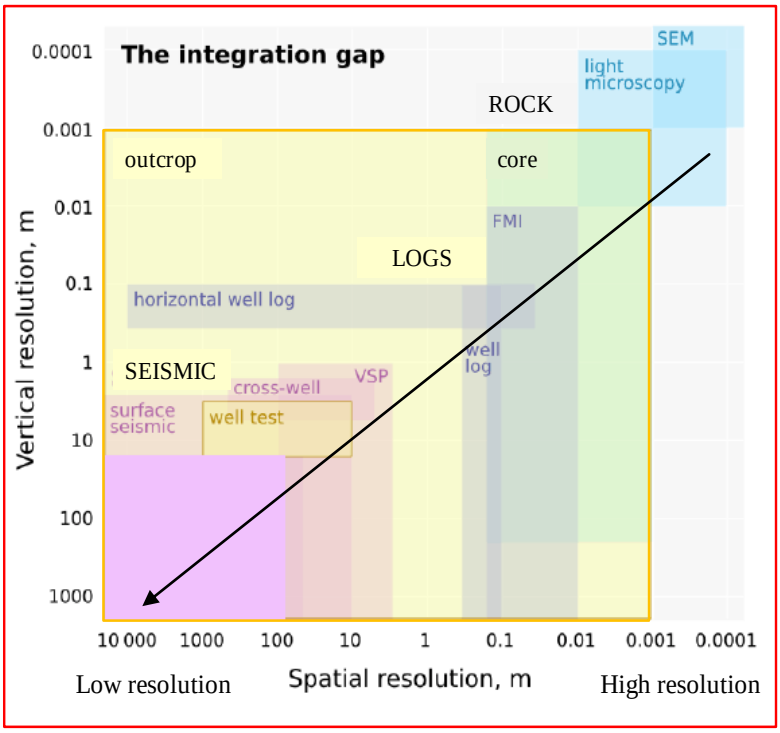

Figure 2.7: Resolution of common data used in reservoir characterisation. They are from core and well log measurements, borehole production and seismic records, and 3D/4D seismic images. The low areal resolution of well data is complemented by the larger areal sampling of the seismic data (after CSEG 2011).

By integration all these measurements in characterising the reservoir model, the variability and the spatial correlation of the actual heterogeneities in the reservoir properties may not be represented. That means there are a high number of unknowns in history matching problems. Another challenge in data integration is that most current approaches are hierarchical. Fine scale models are used for integrating well-log/core and seismic data (geostatistical models) while coarse models are used to integrate

mostly production data (simulation models) and once the scale is changed, data conditioning, maintained in the previous scale, may be lost. Therefore, the sufficiency of data, the ability to identify the model parameters, and the efficiency of the inversion process must be evaluated systematically. A description of the components and challenges involved in inversion formulation of the history matching process is illustrated in the following sections.

2.3 Objective Function in History Matching Process

A typical measure of the "objective function" also called "error function", "cost function", and more frequently just "misfit", is the squared difference between simulated and observed historical data known as the L2 or Euclidean norm. Moreover, a weighting covariance matrix is assigned to data which results in the fit of accurate data to be improved most, and then the general form or covariance-related norm of the objective function (Tarantola 1987) may be expressed as:

$$J(\underline{\theta}) = \sum_{i=1}^{n} (\underline{d}^{obs} - \underline{s}^{sim}(\underline{\theta}))^T \underline{C}_m^{-1} (\underline{d}^{obs} - \underline{s}^{sim}(\underline{\theta})) \qquad i = 1,...,n \qquad (2.3)$$

Where: n is the dimension of simulated and data vector, $\underline{d}^{obs}$ is the observed data of 4D seismic and production/injection (i.e. oil and water rate, and pressure), $\underline{s}^{sim}$ is their corresponding simulated response, and $\underline{\theta}$ is the vector of uncertain model parameters to be updated. $\underline{C}_m$ is the covariance matrix, and stands for correlated random error which is calculated for the model and observed data. It also provides weighting factors to scale the data of different type, magnitude and accuracy.

Generally, the objective function is a hyper-surface in a multi-dimensional parameter space with a global minimum that occurs for the best estimation of the parameter values. For complex physical systems such as reservoir simulation with non-linear mathematical formulation, the topography of the objective function away from the minimum may exhibit multiple local minima, inflection points, and stationary points where the gradient of the function is zero and/or the gradient turns from a positive to a negative value or vice versa. Such topology makes it obscure for an optimization algorithm to converge towards a global minimum. Figure 2.8 is an example

visualization of the objective function for a 2-Dimensional (2D) parameter space. The main characteristics of misfit function are discussed in the following paragraphs.

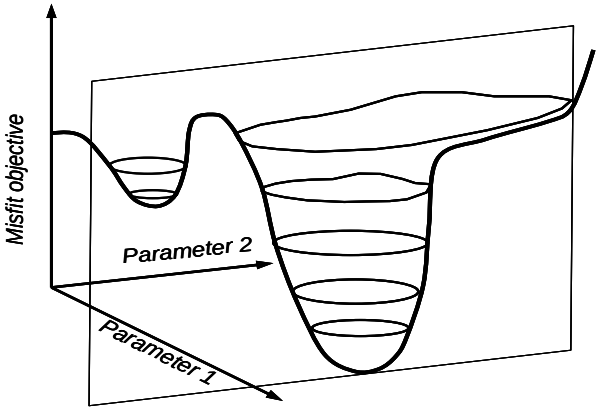

Figure 2.8: Objective function in two-dimensional parameter space.

Degrees of Freedom, Ill-posedness and non-uniqueness: properties such as permeability are not fully known, they may vary over the reservoir space in a small scale (~1 millimetre), much smaller than simulation grid blocks (~100 metres). Thus the actual number of parameters describing this resolution may be infinite, and the number of reservoir parameters to be updated is much greater than observed data; making the problem under-determined. For practical applications a finite set of parameters is used to reduce the number of parameters such as a box of grid blocks, zones, etc. (see section 2.6). However, still a large number of such unknown leads to a high degree of freedom. Forward reservoir modelling is well-conditioned. However, the inverse process of history matching is ill-posed (Tarantola 1987, Omre and Tjelmeland 1996). For a well-posed problem: i) the solution exists, and ii) it is unique, and iii) it depends continuously on data (stability) (Hadamard 1902). In inversion via history matching, multiple parameter combinations with misfit close to the minimum of the objective function define non-uniqueness. Uncertainty analysis is appropriate and is a common practice which tackles both non-uniqueness and helps reservoirs management (see section 2.8).

Curse of Dimensionality: the enormous number of large unknowns characterises the 'cures of dimensionality' in history matching and normally leads to high computation time even for problems of moderate dimensions. This computational time reflects the

many misfit evaluations that are needed and increases exponentially with the dimension of the problem. Moreover, in such cases there would be even fewer possibilities to find the optimal set of unknown parameters.

Prior information as regularization for the objective function: for the parameters to be updated there is usually prior information derived from remote measurements which can be included in the formulation of the objective function as a means of regularizing the inversion process for further constraint of parameter estimates (Carrera and Neuma 1986a, Chavent 1991, Neumaier 1998). Then the formulation of objective function would be:

$$J(\underline{\theta}) = \sum_{i=1}^{n} (\underline{d}^{obs} - \underline{s}^{sim}(\underline{\theta}))^T \underline{C}_m^{-1} (\underline{d}^{obs} - \underline{s}^{sim}(\underline{\theta})) + (\underline{\theta} - \underline{\theta}_o)^T \underline{C}_\theta^{-1} (\underline{\theta} - \underline{\theta}_o) \quad (2.4)$$

where $\underline{\boldsymbol{\theta}}_o$ is the vector of initial parameter information, $\underline{\boldsymbol{C}}_\theta$ is the covariance matrix of random error in the prior information measurements. Inclusion of such 'regularization' may reduce the ill-posed inverse problem by posing constrain to acceptable solutions. However, the prior parameter information must be conceptually consistent with the observations of the reservoir response to avoid biased estimation. For example, if the permeability measured at core scale is used as prior information in an inversion of a regional flow model the difference in scale (modelling error) may compromise the solution (refer to Section 2.5.2).

2.3.1 Differentiating Residual Errors in the Objective Function

Simulation models are simplified numerical representations of reservoirs. They are also imprecise since the input data are measured inaccurate (of incorrect scale) or are sparse (insufficient). In general there is a need to focus on all sources of errors including representative numerical errors, particularly when the prior parameter information is used in the objective function. Generally there are several sources contributing to the residual error vector $\underline{\boldsymbol{J}}$ which can be represented in the form of:

$$J_i = \underline{d}_i^{obs} - \underline{s}_i^{sim} \quad (2.5)$$

We can split the observed and modelled variables into (e.g. Glimm et al. 2004):

$$\underline{d}_i^{obs} = \underline{x}_i^t + \underline{\varepsilon}^{obs} \tag{2.6}$$

$$\underline{s}_i^{sim} = \underline{x}_i^t + \underline{\varepsilon}_i^{sim} + \underline{\varepsilon}_i^p \tag{2.7}$$

So that

$$J_i = \underline{\varepsilon}_i^{obs} - (\underline{\varepsilon}_i^{sim} + \underline{\varepsilon}_i^p) \tag{2.8}$$

where $\underline{x}_i^t$ is the true value of the variable (reservoir response), and ε_i is the error with superscripts ***o***, ***m*** and ***p*** corresponding to the measurement error of the observed data (often assumed as a random component in the data), the model error (i.e. due to inaccuracies of the model that can not be removed), and the parameter error (due to incorrectness of the parameter values and deficiency in model characterisation).

According to this definition, the total residual in the misfit function is the total 'error due to deficiency in parameter characterization', $\underline{\varepsilon}_i^p$, and 'error in the modelling', $\underline{\varepsilon}_i^{sim}$, and the apparently random component 'error in the data', $\underline{\varepsilon}_i^{obs}$, (Figure 2.9). We aim to reduce the parameter error to zero by history matching. It is important to appreciate however that it is very difficult to identify the difference between model and data error. The inversion procedure will try to reduce the error due to parameter deficiency. If the error in observed data is large the estimated parameter vector may be a biased relative to the true parameter value, and the model prediction will not closely reproduce the true behaviour. The systematic simulation model errors also need to be accounted for in the objective function, so that the final residuals contain random components that can be described by posterior error analysis and the uncertainty estimates.

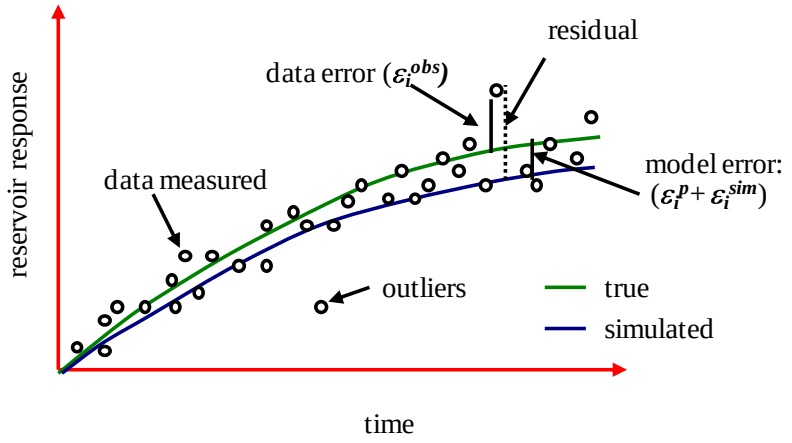

Figure 2.9: True, measured, and simulated reservoir output response and definition of measurement error, model error and residual in misfit function.

2.3.2 Data Error

Errors in observed data can occur both in time-lapsed seismic and wells measurements.

Noise in 4D Seismic Data: 4D seismic difference data are often contaminated by several sources of non-repeatable noise (for more details refer to Section 2.1), those errors need to be suppressed before any time-lapse anomalies linked to production can be included in the objective function.

Upscaling of 4D Seismic Data: in comparing simulated and observed seismic data, lateral downscaling of simulated impedance is often carried out. An alternative could be to upscale the observed seismic data. Here the problem is that there is no cleverly defined process. Flow simulation upscaling is based on relationships derived for fine scale model behaviour, i.e. obtaining the same pressure drop and flow rate for the coarse and the fine scale simulations. However, it is not apparent what an upscaled seismic trace would be. Simple averaging is a first approximation but may be incorrect. Seismic data upscaling requires excellent information on seismic processing.

Seismic inversion methods are used to estimate impedance at a geological fine scale (laterally and vertically) nowadays. The process can be applied before history matching, but due to non-uniqueness it is likely that we end up with an erroneous impedance distribution since no constraints from flow are included. Avansi (2010) assumed a low vertical resolution of 4D impedance data and derived pressure and saturation

distribution from 4D seismic data at a fine grid seismic scale and then upscaled these to a coarse grid simulation model through simple averaging. It was highlighted that the upscaling procedure hampered the history matching in some regions due to the information lost in the upscaling technique.

Then Avansi and Schiozer (2011) proposed an upscaling procedure for acoustic impedance based on an arithmetic average from a fine geophysical scale to a coarser flow simulation scale. The information lost due to the upscaling procedure was evaluated through comparison between flux model properties and seismic attributes, at each respective scale. They concluded that the technique improved the parameter estimation, but the method did not check the other scale issues such as difference in seismic measurements and representation in geo-model. Where typical seismic signals are obtained from the 25 m cube, we could use a larger bin (50 or 100 m) (re-binning), but there are issues linked to sensible processing.

Errors in Well Data: the observed production data have an error component due to the constraints of instrumental measuring of pressures and rates; and allotting accurate well completion intervals. For example wellhead-sampling can introduce large uncertainty in water-cut data and the method breaks down when excessive GOR (gas-oil ratio) production is encountered, such as after gas breakthrough and during gas lift operation (Kabir and Young 2004).

2.3.3 Errors in the Modelling

Induced errors in the modelling downweights the value of the predictions in history matching. When the errors in the simulation are considered in inversion of history data the updated parameters of flow simulation models would be more accurate. The mean model error significantly reduces the bias effects while the covariance gives a realistic spread from the mean prediction (O'Sullivan and Christie 2006).

Reservoir Simulation Errors

Numerical dispersion and simulation upscaling: reservoir simulations are discretised in time and in rock volume inevitably introduces some errors. Although the errors normally reduce when the simulation grid is finer, most simulations are based on upscaled models of a fine grid geo-model to circumvent requirements for large

computational memory and processing time. When relative permeability and capillary pressure curves used in the simulation model are measured at the wrong scale (core scale but not simulation scale), numerical dispersion can induce spreading of the simulated flood front (Kyte and Berry 1975), i.e. when water enters one face of a grid block, it is instantaneously dispersed throughout and the water saturation at the far end of the grid block will be the same as at the inlet (see Figure 2.10). As a result, the water front is smeared, causing early breakthrough in the coarse grid model. One remedy to tackle this is to upscale from the core plug scale using the data from the SCAL (Special Core Analysis) (Barker and Dupouy 1999). Steady-state (Pickup et al. 2000) and dynamic (Barker and Dupouy 1999, King et al. 1993) two phase upscaling techniques are considered to be more appropriate. Most of the time upscaling of permeability, relative permeability, and capillary pressure is difficult, however.

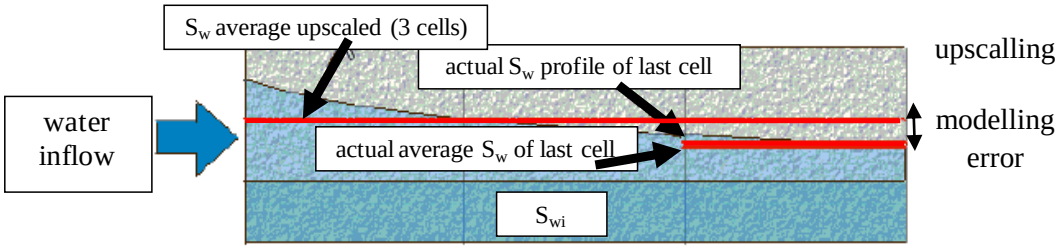

Figure 2.10: The 1D effect of numerical dispersion explains front flow behaviour for different grid scales. For three fine grid cells the front is close to the actual (analytical solution), but for the case of one coarse grid (upscaled of 3 cells) there is a resolution error in the front prediction.

When there is a strong heterogeneity in the reservoir, the relative permeability and capillary pressure curves measured at the core scale could be used to represent the effects of sub-simulation scale heterogeneities. Due to the larger upscaled grid block sizes, the simulators cannot account for small distances of physical dispersion, and it is very difficult to simulate such variations. Consequently, such physical dispersions may be captured by numerical dispersions (described above).

Sablok and Aziz (2005) investigated the effect of upscaling and discretisation errors and showed that the reservoir predictions obtained from highly upscaled models can be significantly errorus. The variability in the results was due to upscaling errors and was

not induced by the variability in the ensemble of the geological models alone. Several similar publications in literature are those by Higdon et al. (2002), Omre and Lodoen (2004), Chen and Durlofsky (2006). Aanonsen and Eydinov (2006) proposed a multi-scale method for parameter estimation with application to reservoir history. They applied large-scale corrections for using fast upscaled models which combined with a downscaling procedure and attained better final adjustment of the coarse models to the fine-scale model match. The study of Carter (2004) disclosed that in history matching; it is important to include a modelling error in the objective function when using numerical model with significant modelling error.

Streamline approximation introduces model errors also. Stephen at al. (2007), Kazemi and Stephen (2008) determined the model errors for production rates and time-lapse seismic predictions by running random ensembles (50 models) using both finite difference and streamline simulators. The mean and standard deviations of all production rate errors and the seismic errors were then used in objective function to account for modelling error and this improved the history matching results.

Rock Physics Modelling Errors

Difference in scale: another source of model error arises in seismic attribute simulation using petro-elastic modelling (see Section 2.9). Rock physics transforms are based on data generated in the laboratory at the scale of centimetres or in the well at the scale of metres. However, they are used at the seismic scale in tens of metres. The substantial discrepancy between these scales may lead to error. Stephen et al. (2007) calibrated the scale dependence of the model errors to reduce this effect. They showed that the error due to scale dependent simulation and subsequent petro-elastic transformation are of equal size and produce a non-zero minimum misfit which affects the ability to history match to a degree that is equivalent to errors in the observed seismic data.

Scale dependence of phase moduli: Domenico (1976) and Knight et al. (1996) have pointed to the scale dependence of the uniform relationship (saturated harmonic average) used in calculation of the phase moduli required for petro-elastic modelling. This relationship is valid when the pore volume for the reservoir region is completely connected hydraulically and freely permits fluid pressure communication into and out of adjoining pore spaces. If this relationship is applied to large scales (i.e. large grid cells) then the seismic induced pressure wave is not fully equilibrated over the sample

volume. To avoid this difficulty the maximum cell size can be estimated using the relationship for critical grid length (e.g. Mavko 1998). This critical length is typically of the order of a metre (Knight et al. 1996) at low seismic frequencies. The fine grid cells are usually in this range but coarse cells are not (~100 m). The 'patchy' relationship for phase moduli (volumetric weighted arithmetic average) is suggested as an upper limit for the fluid modulus. It is used for situations where laminae or beds are separated by thin shale barriers or impermeable inter-connected sand bodies and derived by applying uniform relationship separately to each region or layer (of thickness less than or equal to critical length). The relationship is applicable independent of the shape, size and distribution of each discrete, isolated region of rock, but it requires that fluids are segregated in discrete volumetric regions which may not be fully applicable for coarse model. Sengupta and Mavko (1998) showed that seismic velocities upscaled from small scale simulations are closer to the uniform saturation case than the patchy saturation.

MacBeth and Stephen (2008) also found that the estimates of fluid-bulk moduli extracted from seismic data do not correspond to the true (pore-volume weighted) average value of saturation used for flow simulations. This discrepancy arises because the seismic waves sample the reservoir geological and saturation heterogeneity differently from the fluid flow. They also developed a relationship for turbidite reservoirs that connects the true saturation to the effective fluid modulus from seismic data via statistical measures of the porosity and saturation variations in the reservoir. Saturation variation at the fine vertical scale in reservoir below seismic resolution can affect the seismic response; and that the saturation outputs from flow simulators may be too smooth vertically to create reasonable synthetic 4D seismic representative of the observed seismic response (Doyen 2007).

Sengupta et al. (2007) also showed that the sub-resolution lateral distribution of fluids, not captured by flow simulators, can have impact on seismic responses. Despite the good qualitative match between the fluid changes output from the flow simulator and the fluid changes estimated from seismic data, the simulator yields smooth saturation profiles (so does 4D seismic predictions), which does not quantitatively match the observed time-lapse seismic changes. This is because a proper petro-elastic transform of fluid changes to time-lapse seismic prediction requires estimates of fluid changes at scales much smaller than the reservoir simulation blocks.

Scale dependence of dry rock moduli: Stephen and MacBeth (2006) also identified that the core based bulk stress sensitivity, as measured in the laboratory, may over predict the 4D seismic behavior in the reservoir for large pore pressure increases unless the shale content are accounted. This result is in agreement with the observation that stress sensitivity measurements on sandstone core plugs experience the larger stress responses in situ caused by internal damage of the rocks during unloading from in situ conditions (Nes et al. 2000).

Downscaling simulated seismic properties: the areal interpolation of predicted impedances at the simulation scale (~ 100 m × 100 m) down to the seismic scale bins (25 m × 25 m) adds to the model error. Sharp transitions of the fine grid impedances, which may be due to saturation changes at the waterfront or at geological variation such as at faults, cannot be captured accurately. However if faults or other permeability transitions are absent, a pressure dominated seismic response has negligible model error (Stephen and MacBeth 2006). In the literature a proposition to remedy scale dependent errors consists of pressure and saturation downscaling from simulation grids in order to predict seismic properties at the observed seismic scale. The downscaling of saturations was initially envisaged as a simple mapping. The fine grid blocks included in a given coarse reservoir grid block are attributed the same saturation and pressure values as the coarse grid block. This scheme allows a petro-elastic model to be applied at the seismic scale and per facies which is considered to be much more rigorous than per reservoir unit in the simulation scale (Fornel et al. 2007). However this approach still ignores some degree of fine scale geological heterogeneity that are not included in reservoir simulations. Practically, such an approach should respect some additional constraints: i) the downscaling process must be consistent with the upscaling method in terms of conservation of volumes, ii) non-reservoir facies as well as dead cells in the fine grid must be excluded from the saturation effects, and iii) saturation end points assigned to facies at the fine scale should be represented to avoid saturation effects under the irreducible water saturation, for example (Roggero et al. 2007).

Although downscaling the saturation and pressure is an active research topic, it is a complex and ill-posed problem. The average pressure and saturation values of each coarse grid block should be re-distributed properly in the underlying fine grid blocks. These kinds of techniques are not yet very practical for complex multiphase simulation. They lead to a significant increase of computation time in the history matching process.

According to Flacone et al. (2004) the downscaling of dynamic properties such as transmissibility between cells of a simulation model is not straightforward. In flow-based downscaling for more complicated flow patterns, the difficulty ties in selecting the coarse grid blocks following a suitable order of downscaling to handle boundary conditions. Castro et al. (2006) and Enchery et al. (2007) proposed a more thorough flow-based downscaling to reproduce fine-scale saturation and pressure distributions from coarse scale simulations. For each coarse grid block, considering the fine grid blocks included in it, they first solve the pressure equation implicitly and then the saturation equation explicitly. The boundary conditions are derived from the flow simulation performed for the coarse reservoir model to ensure mass conservation for each coarse grid block.

Mezghani el al. (2004) deployed the geological scale as the domain to seismic predictions. The simulated saturation and pressure with the coarse scale fluid flow simulator were downscaled to the fine scale geo-model. They then applied the petro-elastic modeling at this scale and computed the elastic properties. However, the method added extra uncertainty by downscaling of simulated properties to the uncertainty already embedded in the petrophysics to observed seismic scale calibrations (upscaling), because well logs are on the centimetres to decimetres scale but seismic data are on scale of metres. Menezes et al. (2006) proposed that the most convenient scale to apply petro-elastic modelling is the flow simulation grid, suggesting that methods working at the fine scale only reverts the problem from one of upscaling of observed seismic data to that more difficult downscaling (and upscaling as well). Other authors (Annonsen et al. 2002, Gosselin et al. 2003) had also proposed to upscale the seismic data and incorporate them in the reservoir history matching at the coarse scale.

Vertical upscaling simulated seismic properties: Backus (1962) presents a well-known method of producing the effective seismic properties for a thinly layered medium composed of either isotropic or and anisotropic elastic layers. This method applies either to spatially periodic layering or to random layering, and the layer thicknesses may also be random. This method is frequently used to calculate the average value of p-wave impedance for a column of simulation grid cells as well. This approach is valid (MacBeth 1995) for reservoir beds that are less than one tenth of the seismic wavelength thick and reservoirs of around one quarter seismic wavelength thick (a typical wavelength is 50 to 100 m) or greater, otherwise there would be model errors

relating to upscaling Roggero et al. 2007). In general, the key idea behind any upscaling process should keep the saturation and pressure differences (flow responses) equivalent in both resolutions. Well logs are also scaled up by averaging the properties over a defined wavelength; they shall always be scaled to the seismic bandwidth through a proper averaging method.

In this thesis the focus was on developing new method to improve the convergence of the history matching process and study the effect of the modelling errors were considered beyond this research work, thus they are ignored and are not included in the misfit objective function.

2.4 Parameterization in the History Matching Process

The reduction of the number of parameters from infinity (for a continuous system) to a finite number is called parameterization (e.g. Yeh 1986). The process presents the choice of the parameters and preference of modification representative for the spatial distribution of reservoir properties, such as net:gross, and permeability, in the model. The success in history matching depends on suitable choice of parameterization and the range of parameter values. An inadequate set of parameters would result in inaccurate uncertainty estimations, and introduce bias errors. A large number of parameters with a wide range requires a large computational time, increases the variance errors and decrease the stability of the solution. Usually the reservoir parameterization stage is subjective. The type, number, and range of parameters are determined based on petro-physics, well test, and seismic and geological interpretations and experiences. Common parameterization approaches are demonstrated in the following paragraphs.

Individual Grid Cells: this technique considers the value of properties, such as permeability in every grid block to be independent parameters. The limitations of this approach are that it may not keep the knowledge of geological deposition. There are a large number of unknowns and results in a lack of spatial continuity in the reservoir model (Floris et al. 2001). A recent application of this method on a synthetic case was studied by Dadashpour et al. (2007) however this method is not suitable for real reservoir cases.

Zonation or Regions: this technique is a common practice in model construction and involves the assumption that reservoirs can be divided into several regions of uniform properties, distinguished by a Flow Zone Indicator (FZI) (see Figure 2.11). The benefits of using this method is to reduce the number of parameters (Gavalas et al. 1976, Makhlouf et al. 1993, Abacioglu et al. 2001, Huang et al. 2001), and it also incorporates in some degree the geological knowledge of the reservoir (Le Ravalec-Dupin et al. 2001, Aanonsen 2005). Appropriate zones account for layers, genetic or hydraulic units within layers, impermeable and permeable streaks, and drainage areas of wells. The drawback of the method is that it may not be sufficient for describing the actual heterogeneities of the properties, and may generate abrupt changes at the borders of regions, also some preconceived idea about the regions are not exact.

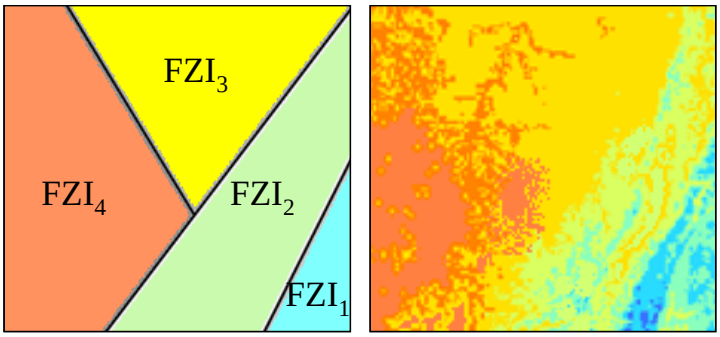

Figure 2.11: Zonation method principal.

Pilot Points Method: the pilot point method with kriging (de Marseily G. 1984) was developed to modify underground properties to enable continuous spatial variation in heterogeneous properties such as permeability between the prefixed locations or groups of locations called 'pilot points'. The method consists of three stages. First, the initial value for the property at pilot points are obtained by prior geo-statistical realizations conditioned to a variogram and the observed fix point values. Then, the property at pilot points is perturbed by the inversion routine. The third stage is to propagate the perturbation induced by pilot points to the nearby grid cells in the reservoir model using a spatial interpolation scheme such as kriging.

In fact such approaches (Landa and Horne 1997, Bissell et al. 1997, Roggero 1997, Arenas et al. 2001, Wen et al. 2002) consist of calibrating an initial kriged reservoir

generated from the measurement of that property and create a set of synthetic conditional simulation realizations at selected unmeasured locations with pilot points at centre (see Figure 2.12), preserving statistical mean, standard deviation, and the spatial correlation of the properties. Generally, the pilot points are selected at locations with large uncertainties in properties, and the method solves most of the troubles encountered by zonation approach. The technique provides a practical tool to be incorporated in history matching (Ravalec-Dupin 2007).

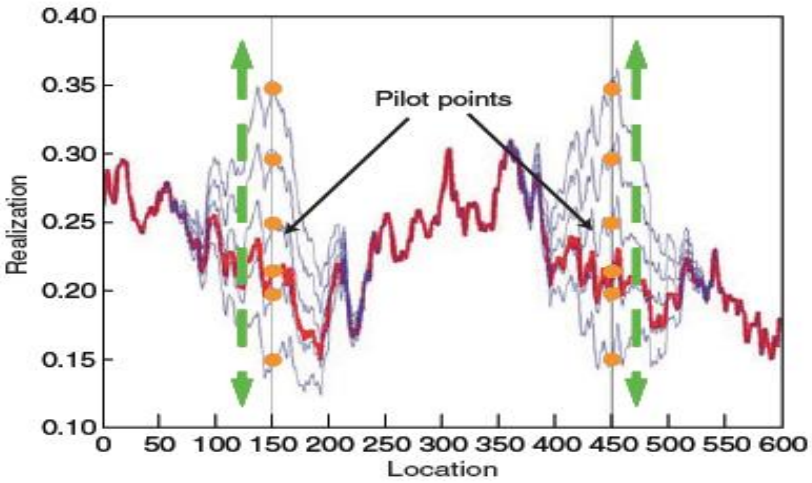

Figure 2.12: Simulation of one a dimensional case when modifying the initial realization (thin curve) using two Pilot Points at locations 150 and 450. The perturbations induced by Pilot Points are local. The modified regions for different realizations (thin curves), cantered at Pilot Point locations, have radius equal to the correlation length (Ravalec-Dupin and Hu 2007).

Object Based Parameterization: in this approach the permeability or net:gross at each simulation grid is a function of a set of implied parameters related to geological features of the reservoir, referring to each as an object, such as channels, channel margins, facies and etc. The purpose in object modeling is to preserve the large scale geological entities to reduce the dimension of the problem. For example a channelized reservoir can be parameterized with only a few parameters per channel (such as d_0, d_1 and d_2 in Figure 2.13), which are smaller than the number of grid cells that define the channel size, spacing and shape. An example of this approach is the Boolean methods (Haldorsen and Damsleth 1988, Deutsch and Wang 1996, Lantuéjoul 1997). The advantage of this

method is that the shape of objects resembles actual channels. The drawback of the method is that objects are notoriously difficult to condition simply since there are many parameters and it requires a realistic geological and statistical interpretation of the characteristics of the size and shape distribution of the objects (Vargas-Guzmán and Al-Qassab 2006).

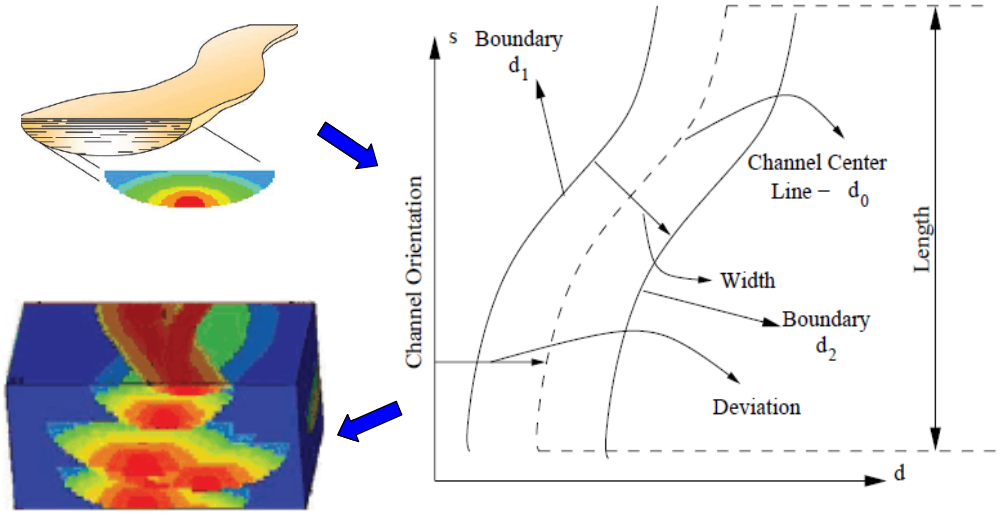

Figure 2.13: Principal of object base modeling. Channelized reservoir can be parameterized with few independent parameters, such as d0, d1 and d2 defining channel sizes, spacing and shape.

Structural Faults and Barriers or Baffles: the existence of barriers significantly influence the depletion performance of reservoirs by inducing flow and pressure discontinuities, particularly in compartmentalized and channelized reservoirs (Yielding et al. 1999a). The flow barriers can be horizontal, such as shales, impermeable streaks, and vertical, such as faults or sub-vertical such as shale drapes. The barrier's distribution, location, thickness and transmissibility are hard to identify correctly from well test and log data. Although, barriers represent the borders of channels or faults may be identified in 3D/4D seismic maps. Properties of barriers are a source of uncertainty for reserve estimation (Lia et al. 1997) and are often picked as the parameters for calibrating reservoir models in history matching (kruijsdijk 2001, Stephen 2006, and Edris 2009).

Gradual Deformation: this method developed by Hu et al. (2000) and makes possible the gradual global transformation of the initial reservoir geo-statistical realization with a set of parameters which act as weights (Figure 2.14). For any value of this parameter the process provides a new property distribution. The simplest gradual deformation scheme consists of combining two independent Gaussian random functions Y_1 and Y_2 with mean y_o and identical covariance:

$$[Y(t) - y_o] = [Y_1 - y_0]\cos(t) + [Y_2 - y_0]\sin(t) \qquad (2.9)$$

where t is a deformation parameter between $[0,\pi/2]$, $\cos(t)$ and $\sin(t)$ are the combination coefficients making the method depend on only one parameter, t. Such combinations provide continuous chains of realizations ensuring that $Y(t)$ is also a random Gaussian function with the same mean and the same covariance as Y_1 and Y_2. Instead of using two, it is possible combining several independent realizations which provides more flexibility for deforming realizations in history matching (Roggero and Hu 1998). Then the number of deformation parameters equals the number of complementary realizations added to the starting one.

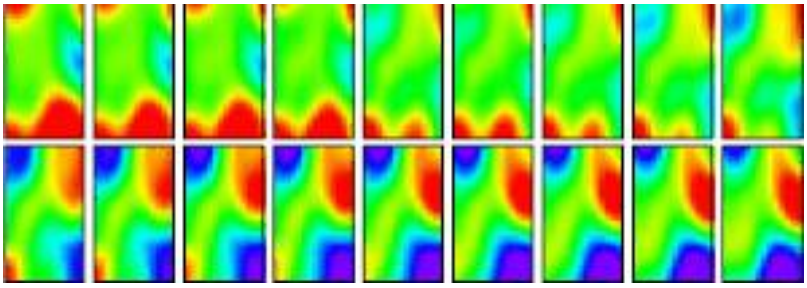

Figure 2.14: An example of a continuous train of realizations for a 2-dimensional continuous Gaussian Random Function by gradually deformation, here two realizations at top right and bottom left are combined (after Roggero et al. 2005).

The advantages of gradual deformation are that the key statistic (i.e. variogram and variance) identify the target statistics and the scheme allows for reduction of the number of the parameters and thus it is computationally efficient. Its drawback is that it is mostly efficient in multi-Gaussian random fields (Le Ravalec-Dupin 2005).

The Probability Perturbation Method: this method shares some of the ideas behind gradual deformation (Strebelle 2000, Caers 2003 and 2004) and works with Gaussian fields and more geologically complex reservoirs where multiple-point statistics are required to describe the geology sufficiently. The method exploits the structure of sequential simulation algorithms which make use of local conditional probability functions. Where gradual deformation perturbs properties at the grid block scale directly, this technique perturbs probabilities at the grid block scale. Then a sequential simulation results in a perturbation of the desired field properties. The method does not rely on any assumptions and is suitable therefore, for any kind of geology that can be realized by sequential simulation. Examples of application of this method can be found on reservoir flow model calibration studies by Hoffman and Cares (2003), Berrera and Srinivasan (2009), and Li and Reynolds (2009).

2.5 Classification of Optimization Algorithms

The inversion procedure of history matching requires an optimization algorithm to guide the selection of the best possible updated parameters in order to minimize the objective. The optimization routines need to be robust and efficient. They should converge to a minimum (providing a reasonable initial guess for reservoir parameters), and with a reasonable amount of time and efforts. The optimization algorithms are classified according to whether they are gradient-based or gradient-free. If the optimization methods are non-random, they are called deterministic, i.e. their outcome is 'pre-determined'. A deterministic algorithm, for instance, if given the same input information will always produce the same output. In this context, the gradient-based routines are deterministic while non-derivative methods may be deterministic, stochastic or probabilistic. All categories are iterative. A comparison of such optimization algorithms can be found in a study by Finsterle (2007).

2.5.1 Gradient-Based Methods

These methods update the parameter values in small steps along the search direction determined by the gradient of the objective function with respect to the parameter vector (Figure 2.15). Various modifications to the basic scheme of these methods are different in the choice of the length of step in the search. Examples of such methods include: Steepest Descent (Press et al. 1992), Quasi-Newton, and Fletcher-Powell-Davidon

(Fletcher 1987). Also, several other approaches are based on second derivatives and the Hessian matrix and perform well for nearly linear least-squares problems. In such methods the computational cost for calculating the second derivatives is usually compensated by an efficient stepping length. Examples of them are Gauss-Newton, Levenberg-Marquardt (Levenberg 1944, Marquardt 1963), and Adjoint Method (Chavent et al. 1975).

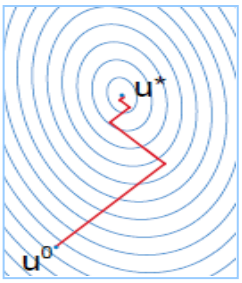

Figure 2.15: Illustration of gradient-based optimization procedure.

Several gradient-based methods used in history matching are based on adjoints to calculate the sensitivity coefficients (Anterion et al. 1989, Bissel 1994, Landa and Horne 1996, Wu et al. 1999, Li and Petzold 2004), Steepest Descent (Roggero et al. 2007), Gauss-Newton (Gosselin et al. 2001), and Levenberg-Marquardt (Arenas et al. 2001) algorithms. The use of all the gradient-based algorithms is efficient if the objective function is symmetrically convex, with one global minimum, and continuous. In many cases however these assumptions are violated mainly due to the complicated topology of the objective function. Also, these methods are inefficient when there is a large number of observed data (e.g. the time-lapse seismic data), then the gradient/Hessian matrix of objective function is difficult to calculate, particularly when the number of reservoir simulation parameters is large.

These methods result in one solution (model), which may be a local minimum of the function, as a result they are also considered as local optimisation algorithms. In such local optimization methods, the solution is usually strongly dependent on the initial model. They are capable of handling a certain amount of noise in data as long as large steps can be taken to calculate the gradient. Near the solution, the increments to calculate the gradients must be small, and the algorithm is then affected by the noise.

2.5.2 Non-Derivative Methods

In such methods the model is evaluated for different parameter combinations, mapping out the objective function in the multi-dimensional parameter space, which is explored by generated trajectories, until a satisfactory minimum is reached. Because no derivatives need to be calculated, they perform well where there is no assumption about the topology of objective function. Three types of gradient-free algorithms can be categorized as deterministic, stochastic and probabilistic.

Deterministic Methods

In such methods, the result of optimization is entirely determined by its initial state and inputs which is not random or stochastic.

Generalized Pattern Search (GPS): these direct search methods (e.g. Torczon 1997, Audet and Dennis 2003) use successive exploration and linear search descent directions in a multi-dimensional parameter space. The method is illustrated by application of a Coordinate Search algorithm to a simple example composed of a two parameters (x and y) in Figure 2.16. The algorithm starts at the initial point "0", that is the combination of x3 with y10 and it performs the first exploratory search, points labeled "1". The point with the best value of objective function indicates the direction for the search. Points labeled "2" are the first linear search. With this best point, the algorithm performs a new exploratory search. The process is repeated until a minimum point labeled as "4" is reached (Maschio et al. 2008).

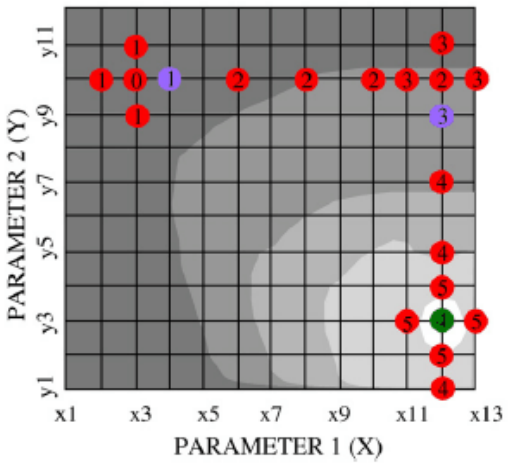

Figure 2.16: Schematic of application of the Generalized Pattern Search (GPS) algorithm in finding the minimum of a 2-dimensional objective function (after Maschio et al. 2008).

Each GPS algorithm has a rule to select the initial point, the mesh coordinates and a finite number of points on a mesh and step size (in present example is defined by $x+\Delta x$). It is this rule that distinguishes the various GPS algorithms such as the Generalized Hooke-Jeeves (GJH) (1961) (Figure 2.17) and the Generalized Coordinate Search (GCS) (Figure 2.16). The drawbacks of the GPS methods are: i) they are inherently serial because of its search strategy, and cannot benefit from parallel distributed computing and thus they are slow, and ii) they have difficulty in finding a global minimum, principally for complex objective functions of large amount of data such as in 4D seismic surveys if they are contaminated with noise. Schiozer (1999) and Leitão and Schiozer (1999) developed a type of JH direct search method suitable for distributing computing applied to the history matching problem. Since then several applications of various alternatives of this method can be found in the literature (Maschio and Schiozer 2005, Maschio et al. 2008, and Dadashpour et al. 2011).

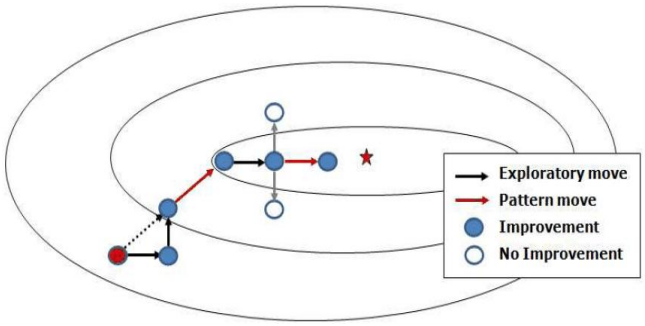

Figure 2.17: Schematic representation of exploratory and pattern searches in Hooke-Jeeves direct search method (after Iseber 2009).

Downhill Simplex: this is a method (Nelder and Mead 1965, McKinnon 1999, Press et al. 2002) for minimization of a function of ***n*** variables and depends on the comparison of misfit values at (***n + 1***) vertices of a general simplex, followed by the replacement of the vertex with the worst point, with a point reflected through the centroid of the remaining ***n*** points. If this point is better than the best current point, then the simplex stretches exponentially out along this line; but if this new point is not better than the previous; then it is steps across a valley. The simplex shrinks towards a better point. Thus the simplex adapts itself to the local landscape, and contracts onto the final minimum. This evaluation-only method does not require any gradient calculations and is therefore simpler but can be extremely slow and inefficient. The method was applied

to history matching (Zabalza et al. 2000) and has been combined with stochastic methods for well placement problems (Badru and Kabir 2003, Guyaguler et al. 2002, Bittencourt and Horne 1997).

Stochastic Methods

Stochastic methods are considered as global optimizers, although this is not always the case. They require numerous simulations and considerable amounts of computational power, compared to deterministic algorithms. However, due to the rapid advances in computation speed and memory, stochastic algorithms have received more attention recently. They have the advantage of generating a range of different probable models that can then be used to quantify the uncertainty in the reservoir forecasts. Therefore, they are more suitable for non-unique history matching problems.

Simulated Annealing (SA): this method (Kirkpatrick et al. 1983, Mosegaard and Vestergaard 1991, Sen and Stoffa 1991) replicates the annealing procedure in metallurgy, which involves the heating and controlled cooling of a material to increase the size of its crystals. The atoms move from their initial positions and wander randomly through the states of higher energy by heat. Then, they obtain more chance of finding configurations with lower internal energy than their initial state by slow cooling. SA has the advantage that there is a chance of escaping local minima, but it requires many forward models and therefore is computationally prohibitive. SA has been employed a number of the history matching studies (Sen et al. 1992, Portellaand and Prais 1999). Jin et al. (2009) proposed the combination of very fast Simulated Annealing method with pilot-point parameterization for solving the 4D seismic history of a synthetic case, however when they compared that with Particle Swarm and Neighbourhood Algorithm (Jin et al. 2011), they found that the method requires comparatively more iterations to converge due to the sequential nature of the method.

Particle Swarm Optimization (PSO): the idea of this algorithm was originally derived from modelling social behaviour, in particular modelling the flight of a flock of birds (Kennedy and Eberhart 2001). Here the "particles" which make up the population, move in the search direction with a velocity that is determined relating to the experience (of the objective function) of each individual particle and the population. In essence each individual particle memorizes the best position it has encountered and uses this together with the memory of the best position of its population. Hence changes in the particles

trajectory are made from these influences in each iteration. Position updates are then made from the new calculated velocity. The resulting effect of these interactions is that particles move towards a solution while still searching the surrounding localities.

Ideally, the PSO optimizer has good exploration ability while still being able to refine searches and has the ability to escape from local minima (Kathrada 2009). Fernández et al. (2009) showed the application of PSO to seismic history matching to update the geological facies model to match production and 4D seismic data. The results show that PSO performed much better than other global methods and was as fast as other local optimization techniques used. PSO allows estimation uncertainty for the model parameters like all stochastic methods and it requires reasonably fast forward modelling. As a more recently developed global optimization technique, it has been examined in a number of history matching cases (Mohamed et al. 2010, Abdollahzadeh et al. 2011, Reynolds et al. 2011).

Evolutionary Algorithm (EA): is a term for all optimization routines that are inspired by evolutionary mechanisms. They are similar in their basic principles but have differences. The main concept in Evolutionary Algorithms is the use of ensembles in generating parent-to-child sequences (Goldberg 1989). Various examples of such algorithms are Genetic Programming, Evolutionary Programming, Evolution Strategy and Neuro-evolution. These algorithms are especially useful in cases where gradient of the objective function is difficult to evaluate or when other algorithms fail because of significant non-linearity or discontinuities in search space. They are also amenable to parallel computing. The most popular type of EA is the Genetic Algorithm (GA).

Genetic Algorithm (GA): the initial insight of the GA algorithms developed by Holland in the early 1970s (Fogel et al. 1966, Holland 1975, Sambridge and Drijkoningen 1992, Sen and Stoffa 1995). The algorithm is based on biological principles of evolution, or "survival of the fittest". GA is a population search method and starts with an initial population whose members are called "chromosomes". The chromosome consists of a fixed number of variables (binary or real codes) which are called genes. In order to evaluate and rank chromosomes in a population, a fitness function is defined. The probability survival of a chromosome (individual) is related to the fitness of the individual divided by the sum of the fitness of all individuals in the

population. Three operators are used in the GA: selection, crossover and mutation (see Figure 2.18).

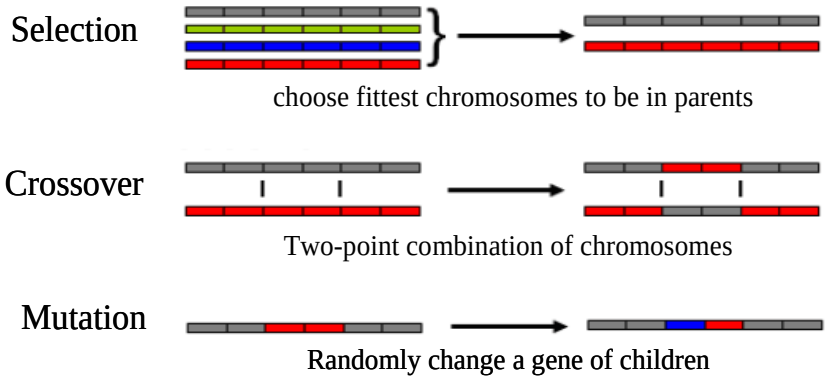

Figure 2.18: Schematic representation of the main Genetic Algorithm operators.

The selection operator chooses an intermediate population from the current one with the highest fitness to be used by crossover and mutation operators. Crossover combines two or more chromosomes (parents) by randomly picking a gene value from parents (with some pre-defined probability) to reproduce new off-spring, with the hope that one of them collect all good features that exist in the parents. Mutation randomly alters one (or more) gene to a new value in a chromosome based on a Gaussian distribution around the original value (with some small pre-defined probability). Mutation aims to achieve some stochastic variability of chromosomes in order to get a quicker convergence but also to escape local minima. The initial population size, crossover and mutation rates play major roles in the performance of GA. They control the premature convergence of GA by two effects of lack of diversity in the population and disproportionate exploitation/exploration (Herrera et al. 1995).

Many investigations of various parameter choices for optimal selection, crossover and mutation of chromosomes via various string structures have been carried out and used (for more details see Pott el al. 1994). In order to accelerate the inversion process of history matching, various Genetic Algorithms have been applied to such studies (Carter and Ballester 2004, Walker et al. 2006, Erbas and Christie 2007, Maschio et al. 2008). Genetic Algorithms have been also used in the Top-Down Reservoir Modelling

(TDRM) approach developed by BP in tuning many parameters together while history matching to the well and 4D seismic data (TDRM is an integrated workflow and its philosophy is "to start investigations with the simplest possible model and simulator appropriate for the business decision") (Williams et al. 2004).

Neighbourhood Algorithm (NA): is a quasi-stochastic search routine originally developed to solve geophysical inversion problems (see Sambridge 1999; 2002). The algorithm makes use of geometrical constructs known as voronoi polygons to direct the search and sampling of the parameter space. The voronoi polygons (i.e. the neighbourhoods) represent the volumes closest to the points that define models in a high dimensional parameter space. Sampling for new parameter values is carried out by assuming that better models may be found somewhere in the neighbourhoods of the best models found so far. An example of utilizing the voronoi cells within NA to find the minimum of a 2D synthetic misfit surface (Figure 2.19a) is depicted in Figure 2.19. The NA workflow is outlined in Figure 2.19b, and the steps of the routine are:

a) Firstly an initial ensemble of n_i models is usually generated randomly in the search space. For each model the forward problem (the flow and seismic simulation) is solved, the relevant misfit value, $\boldsymbol{M}$, is obtained and the voronoi polygons are established, see Figure 2.19c.

b) In the second step, the n_r models having the lowest misfit values among the previously generated models are determined, see Figure 2.19d.

c) Then, n_s new models are placed throughout the n_r voronoi cells selected at the previous step by sampling from a uniform probability across each of the cells. That means that n_s/n_r models are placed in each voronoi cell in the set of n_r models that were selected and the misfits for the new models are obtained, see Figure 2.19e.

d) The algorithm returns to step (b) and the process is repeated. In each iteration the voronoi cells are more refined and progressively concentrated in the regions where the fit is high, see Figure 2.19f.

e) The process continues until it reaches the user-defined number of total iterations. Thus a total of $N=n_i+(n_s \times \text{iteration no.})$ models is generated by the algorithm.

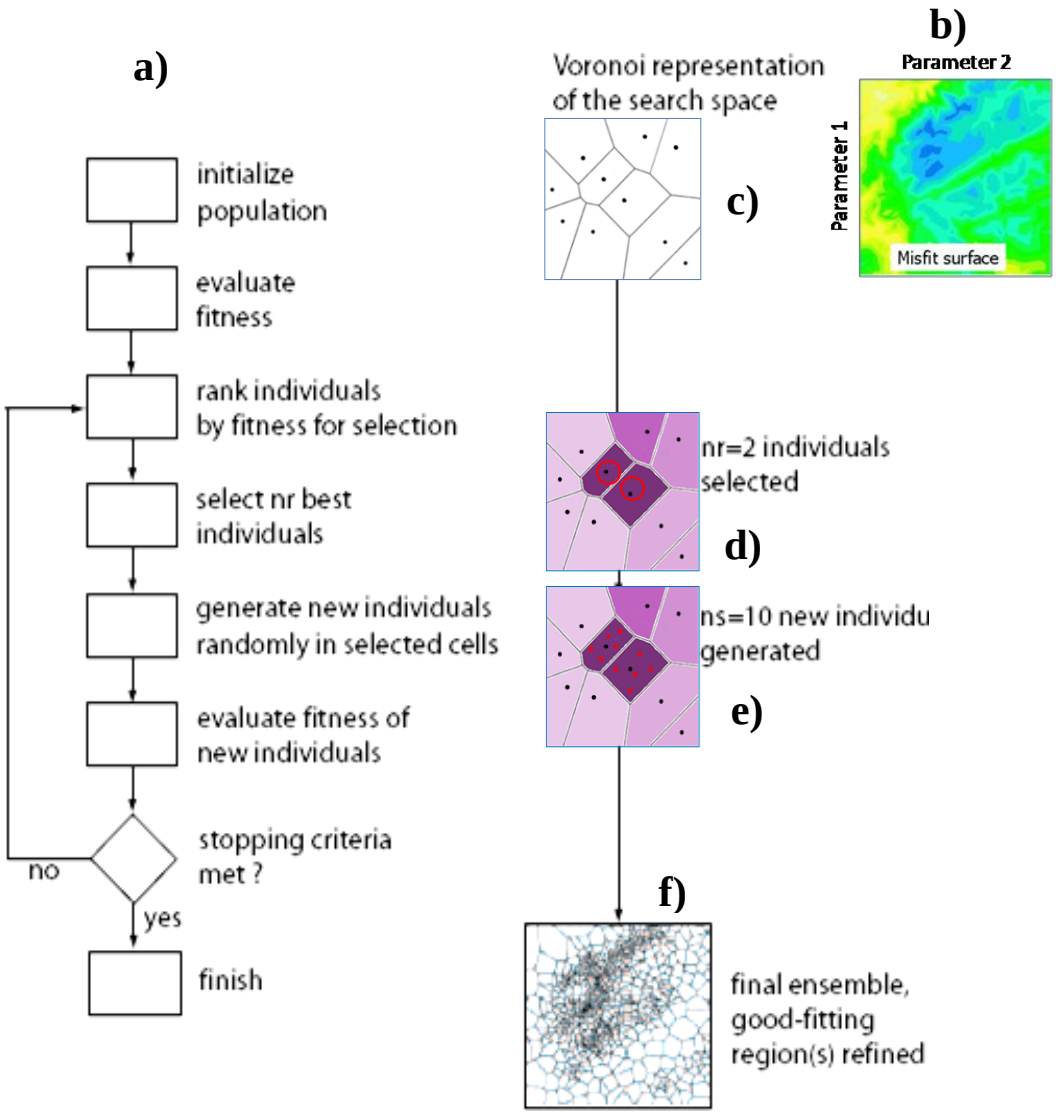

Figure 2.19: a) Neighbourhood Algorithm workflow for searching the parameter space, b) a synthetic 2D misfit surface with blue indicating small misfit values and yellow high misfit values, c) a number (ten) of initial models are sampled in the parameter space of the problem and their voronoi cells are constructed to indicate the neighbourhoods, d) the two best models with smallest misfit are identified, dark purple indicate highest probability cells, e) new models are distributed randomly in the neighbourhoods of these two best models, e.g. five per voronoi cell, and the new misfits are calculated, f) the process is repeated a number of times, each time the voronoi cells are more refined and concentrated in the regions of low misfit, and eventually the misfit is reduced (modified after Sambridge 1999 and Erbas 2006).

For the NA to have a good initial sample, Sambridge (2001) recommends that the initial models n_i should be equal to $\mathbf{2}^{\boldsymbol{nd}}$, where $\boldsymbol{n_d}$ is the number of unknown parameters in the optimization problem. The required number of initial models is therefore large, particularly in high-dimensional problems. The convergence performance of the algorithm depends on n_s, n_r, and the ratio of n_s/n_r as tuning parameters. They control the explorative and exploitative behaviours of the algorithm respectively. Exploration is a feature by which an algorithm searches in the parameter space without considering what it has 'learned' from previous sampling. Conversely, exploitation makes use of previous sampling. Setting NA parameters for greater exploration, i.e. small n_s to n_r ratio, increases the chance of finding the global minimum compared with less explorative NA runs. Setting NA parameters for greater exploitation, i.e. high n_s to n_r ratio could result in trapping in a local minimum although convergence is faster. At each stage of the exploitation and the sampling procedure, selective sampling of the good data-fit regions is achieved by exploiting information about all the previously generated models. Figure 2.20 shows the result of searching for the minima of a synthetic 2D misfit surface (Nicotra et al. 2006). In this example there are five minima (indicated by the green crosses) and the equation representing the misfit is the Branin function. The voronoi cells are coloured by the associated model objective function value. Figure 2.20 compares a case of strong exploitative behaviour to an explorative one under the same number of models generated per iteration (n_s = 60). When NA is set for strong exploitation (n_s/n_r = 15), it concentrates the search only around 2 over 5 minima (Figure 2.20a) by thickening the same voronoi cells, when set for exploration (n_s/n_r = 1), it is able to locate all global minima (Figure 2.20b).

From the standpoint of optimization, the rule of thumb is that the more explorative an algorithm is, the less likely it will fall into local minima, but the less efficient it will be at converging to a solution. Examples of other methods that lie at the extremes would be a uniform random search, which is completely explorative, and a Newton-type descent algorithm which is purely exploitative. Clearly, the most appropriate technique will depend on the nature of the problem and any pre-knowledge of the shape of the misfit function. For smoothly varying, near quadratic-like objective functions we would prefer an exploitative approach, such as a gradient method which allows rapid convergence. For highly nonlinear problems with multiple minima/maxima in the objective function a combination of exploration and exploitation would probably suit

best. However, controlling the trade-off between the two properties is often quite difficult, as is deciding in advance which approach is best suited to a particular problem where the shape of the misfit surface is unknown.

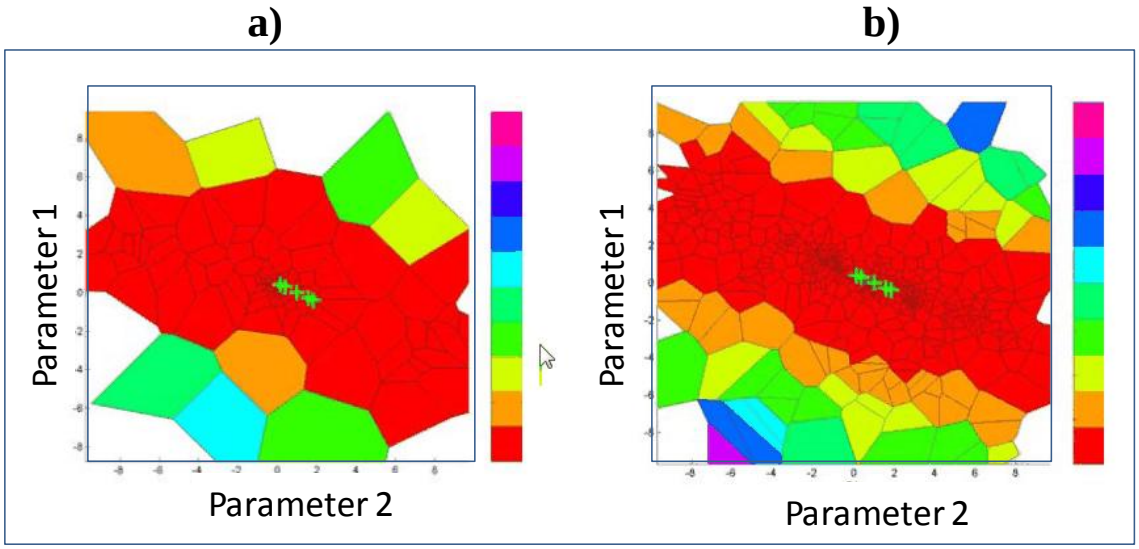

Figure 2.20: 2D voronoi cells coloured by the associated model objective function value obtained for a search of the 2D Branin Equation. From a) case (n_s = 60 and n_r = 4) to b) case (n_s = 60 and n_r = 60), they show shift of NA from exploitative to explorative behaviour (n_s/n_r = 15 to 1). Green crosses indicate global minima positions (after Nicotra et al. 2006).

Nicotra et al. (2006) observed that for problems with high dimensional parameter space and a complicated misfit surface, generation of quite a large number of initial models, n_i = $\mathbf{2}^{nd}$, and then the use of exploitative tuning with n_s/n_r = 2 or 4 and resulted in a good performance of the NA, i.e. this strategy would make it possible to reduce considerably the total number of models generated to reach a threshold convergence. For problems with a simpler response surface, the number of models can be reduced further.

The advantages of the NA are: i) the simplicity of its two-parameter tuning scheme in contrast to the more complicated tuning mechanisms of other methods, such as Simulated Annealing and Genetic Algorithms, and ii) in NA, similar to evolutionary algorithms, the selective sampling of good data-fit regions is achieved by exploiting information about all previously generated models thus enabling convergence to solution (Sambridge 1999a). NA has been used for reservoir history matching (Subbey

et al. 2002, Christie, et al. 2002; 2006, Suzuki and Caers 2006, Erbas 2006, Stephen et al. 2006, Kazemi and Stephen 2008; 2009, Edris and Stephen 2008; 2009, Sedighi and Stephen 2009; 2010). Wathelet (2008) proposed that the NA tuning parameters (ns and nr) be tuned on the road to the convergence to improve the exploitation. The key point is that one can increase convergence by decreasing n_r compared to n_s to target the voronoi cells whose misfits are lowest but inevitably this surrenders exploration. Arwini and Stephen (2010 and 2011) on the other hand showed that by combining the NA and response surface modelling during exploitation, the NA convergence rate could significantly be improved by replacing uniform sampling in each voronoi cell with a biased sample based on a proxy model. This approach obtained better exploitation without sacrificing exploration. NA is used in this thesis as the optimization routine for minimization of the misfit function in the seismic history matching and updating the reservoir model parameters. Here, the random samples within a voronoi cell follow the original one as the procedure described by Sambridge (1999).

General applicability of the NA to history matching methods: the neighbourhood algorithm has been applied to several field history matching problems using a variety of parameterization approaches and has performed well with various complexities in the reservoirs. It has also been used with several data types (seismic and production data). For example Edris et al. (2008; 2009) performed synthetic seismic history matching case studies using the NA routine and pilot points with kriging as the parameterization scheme to update the field permeability distributions and obtained a good representation of the true model even though the starting model consisted of a different realization. In field applications, however, it is generally hard to identify whether or not a poor match at the end of history matching is due to the poor performance of the optimization routine, incompleteness of the parameterization scheme, poorly estimated uncertainty in the observed data or strong modelling errors in particular.

However there are many examples of successful applications of NA in real reservoir history matching problems of different degrees of complexity. An example of such a history matching case is the Nelson field where NA routine was integrated with streamline simulation and parameterization via pilot points and kriging to identify update three reservoir properties including: net:gross, horizontal, and vertical permeability of various geo-bodies in the model (Stephen et al. 2007, Kazemi and Stephen 2010; 2011). Also in history matching studies on the Schiehallion field, NA

was used to update reservoir parameters such as permeability, barrier transmissibilities and net:gross and good matches to the 4D seismic data (Stephen 2006, Edris 2009) were obtained along with production data. Another example is Teal South in the Gulf of Mexico where BP's Top Down Reservoir Modelling (TDRM) was applied based on using NA, and the method was very successful (Subbey et al. 2002, Skinner et.al. 2004). In several case studies on this field the key unknowns were the geostatistical simulation parameters (channel directions, channel dimensions, variagram ranges). Additionally, end points of relative permeability curves, dependencies of compressibility factors and permeability on effective stress, transmissibility multipliers across faults, water-oil contact, and porosity multiplier of the aquifer were considered as uncertain parameters and updated in other history matching case studies of the field (Litval et al. 2004). NA was used in a case study of the Rigel field where flowing bottom-hole pressures and water cut history data were matched while varying the fault transmissibilities (Nicotra et al. 2005).

Typically a large number of models are required by NA both for the initial ensemble and in the search for minima of the misfit function. It has been claimed that in cases where multiple minima exist, each initial random population may lead to convergence to distinct solutions (Erbas 2007) if the ensemble is too small. This effect is more severe in high dimensional problems (e.g. updated grid cells properties) and also in a wide range of model parameters. One way to tackle this is to apply NA several times, each time with a different initialisation within the predefined bounds of each parameter or, alternatively, use different bounds of each parameter and thus different initialisation models. The identification of these multiple solutions is essential to reveal the different minima of the objective function landscape, which in turn is important in the reservoir uncertainty assessments (for more details on identifying different optimal regions of the parameter space from an ensemble of acceptable models see Sambridge 2001; 2003).

NA algorithms may also be unsuitable where the reservoir properties are defined in a strongly stochastic manner, e.g. through Sequential Gaussian Simulation (SGS). In general, the NA is more suitable where the user correctly makes assumptions that the dependence of the misfit on the parameters is not very erratic or random. That is, there are not too many minima and the misfit is smoothly varying with parameter changes. However, if these assumptions are not valid, the impact will be that the convergence rate will be very slow. An example of this is the study carried out by Carter et al.

(2003) and Carter (2004) using a synthetic reservoir model and a Genetic Algorithm as an optimization routine. Only three parameters were changed during history matching including the throw of a fault and permeability of two facies which made up layers in the model. The resulting misfit was deterministic but very complex.

Similar degrees of suitability of NA are expected for the 'divide and conquer' approach proposed in this thesis including Parallel-SHM and Serial-SHM applications as long as we are able to resolve the independent parameter sub-volumes. However properties such as relative permeability may not be straightforward. In such cases it is difficult to decouple the effect of a global property (relative permeability) and more local parameter effects (e.g. barriers) that may exist. Regional relative permeability could be used more effectively using spatial decomposition method, however.

Stopping criteria of optimization routine: a general stopping criteria may follow the following process at the end of calculating misfits:

1. We first check if the misfit value has dropped below some threshold below which would consider that we are over-fitting to the noise, i.e. $\boldsymbol{M<M^{noise}\ (1+\delta)}$ (where $\boldsymbol{M}$ is the misfit and $\boldsymbol{\delta}$ is some small number much less than unity and indicates that we do not wish $\boldsymbol{M^{noise}}$ exactly). For example, the misfit for a perfect model would be (Equation 2.3), $\boldsymbol{M=N}$, where $\boldsymbol{N}$ is number of data in the misfit function. Here we ignore the model error, and the data contain uncorrelated Gaussian errors (for more details see Appendix B). If this is the case it means that we obtain an acceptable match. Then either:
    a) We may check if there could be alternative solutions for the problem by:
        i. Restarting the search elsewhere in parameter domain to find new solutions or
        ii. Restarting by selecting new parameterization to find alternative solutions
    b) Else stop

2. Otherwise we may check that no further reduction in the misfit value would be obtained by continuing, e.g. $\Delta\boldsymbol{M/M<}$ a threshold (indicating convergence). If this is the case then:

a) If we do not accept this solution, we consider searching for alternative solutions in the parameter space where we:
    i. Restart with new misfit weights for various data types (e.g. observed seismic or production data) thus varying the importance of the data or
    ii. Restart with a search restricted elsewhere in the parameter space or
    iii. Restart with new parameterization
b) Else stop

3. Else if we cannot afford more iterations (considering limitations of a deadline for completion of the job, or limitations on CPU time and software license costs) then stop

4. Else continue another iteration

Such stopping criteria fulfil the need to terminate the history matching loop perhaps trading a reasonable history matching result against avoiding using unnecessary computing time. For many field cases, the data are difficult to match and there is usually a deadline for completion of history matching and limitation for simulation licenses and CPU cost. Normally, when the optimization process has reached convergence (hopefully to a good solution), we should terminate the process because further optimization steps may lead to over-sampling, perhaps over-fitting to noise in the data, and wastes resources. The matching criteria often become "as good as one can get it in the time that one has". The real question is then whether or not we have converged to the best model or not. Then if we have it is there another better model out there. If we have not converged, what should we do? Should we revise the importance of the misfits, consider alternative parameters or use a different parameterization? As such we can then think of history matching as a set of nested iterative loops and the key question is when we terminate one loop when we should complete all. These questions are still a topic of research and are recommended as future work.

We may consider some straightforward comparisons (of misfits) that offer appropriate stopping criteria. These include using the rate of change of the reduction in the minimum misfit over the iteration, or one may consider that a misfit threshold may be used as stopping criteria. However, more importantly, even though a mismatch is calculated, it is usually inappropriate to specify some misfit tolerance when we are not

acquainted with the contribution of the model and data errors and appropriate weights of different data types. This is usually explored by engineers changing the weights of various data types used in the misfit function in an 'ad hoc' way when they do not achieved the desired outcomes in the history matching. It happens particularly if the match to one observed dataset (e.g. seismic data) is acceptable but the other (e.g. production data) is not. Often a moderate match to various types of data is deemed to be more acceptable.

In this thesis, we by set a termination criterion using a predefined number of iteration (models); this is takes into account the limited availability of computational resources and in the absence of an overall convergence towards the minimum misfit. The Neighbourhood Algorithm (NA) usually exhibits rapid progress at the beginning and flattens out at the end indicating convergence to a minimum misfit. If we reach a point where we consider that the quality of match will not improve we do not continue with further iterations. In this work we do not consider alternative parameters or parameterization schemes or variations to the misfit weighting as we are mainly interested in the performance of the inner most history matching loop.

Quasi-Random samples used in NA: the initial ensemble of n_i models generated in NA are part of a Sobol sequence (Sobol 1967), a common quasi-random sequence. Other quasi-random sequences include the Halton sequence and the Hammersley sequence (Niederreitere 1988). Mathematically, these sequences are defined as having low-discrepancy. Discrepancy refers to the difference between the actual number of samples in a given volume (of multidimensional space) and the number of samples that should be there assuming a uniform distribution.

Quasi-random sequences should not be confused with pseudo-random sequences which are entirely different. Pseudo-random sequences are computer-generated sequences that behave as if they were truly random, even though produced by deterministic algorithms. An early computer-based Pseudo-random generator suggested by Neumann (1951). In Figure 2.21 comparison of the visual uniformity of the sequences is shown. The pseudo-random sequence exhibits clustering of points and there are regions with no points at all, but the Sobol quasi-random sequence appear to cover the area more uniformly.

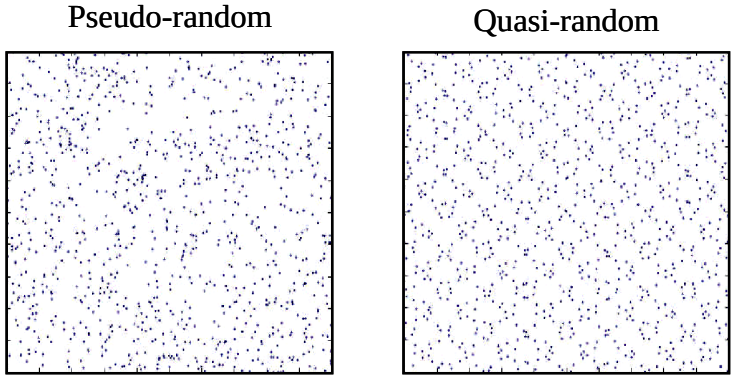

Figure 2.21: Pseudo-random compared to Sobol Quasi-random sequence. They were created by generating 1000 samples in a 16-dimensional space, and then plotting the 4^{th} dimensional component of each point against its 5^{th} dimensional component (after Levy 2002).

Probabilistic Methods

Two famous algorithms in this category are Ensemble Kalman Filter algorithms and Monte Carlo method.

Ensemble Kalman Filter (EnKF): is an extension of the traditional Kalman filter (Kalman 1960) and was first introduced by Evensen 1994 as a sequential data assimilation approach for history matching studies; i.e. new data are accounted for when they arrive (Burgers et al. 1998). The algorithm begins with the generation of an ensemble of initial models, typically 50 to 100, consistent with prior knowledge of the initial state (pressure and saturation and other input data such as well production history) and probability distribution. These models are advanced to the time of the next observation or some time period using a simulator. The covariance of the model variables (such as permeability, net:gross, etc) is estimated directly from the ensemble of states. The model updating step of EnKF follows within a probabilistic Bayesian framework. Property distributions are sampled using the so called Kalman gain to modify the grid cell properties including the dynamic state (e.g. saturation and pressure). This process is then continued for the next period of history. The formulation of EnKF involves the minimisation of an objective function and statistical minimisation in the ensemble space. It provides an approximate solution while sequentially updating multiple models to capture the probability densities in the parameter map. It is necessary for ensuring that adjustments to the current model parameters do not destroy the match at the previous step.

Recently EnKF has been widely applied to history matching studies (Neavdal et al. 2003, Liu and Oliver 2005, Dong et al. 2006, Evensen et al. 2007, Leeuwenburgh et al. 2008; 2010). EnKF supposed to allows for simultaneous estimation of a large number of poorly known parameters for each grid cell since it utilizes cross-covariances between measurements and model parameters estimated from the ensemble. Skjervheim et al. (2005) examined EnKF for handling of large amount of 4D seismic data together to well data and found the method recursive with little additional cost.

For practical field applications, however, the ensemble size needs to be small for computational efficiency. This leads to poor approximations of the cross-covariance matrix, resulting in a loss of geological realism. Specifically, the updated parameters tend to become scattered with a loss of connectivities of extreme values such as high permeability channels and low permeability barriers. This is one of the limitations of EnKF, which could lead to the loss of ensemble variability, referred to as "ensemble collapse" (Gu and Oliver 2005, Lorenc 2009, Zhang and Oliver 2010).

Another limitation of the EnKF is that its computations are based on first- and second-order moments (mean and variance), and there are difficult problems to handle, for example when representing a bimodal channel facies distribution (Wang et al. 2009) and property fields associated with non-Gaussian permeability distribution (Haugen et al. 2008). Unfortunately, using EnKF the geostatistical correlations between model parameters are not maintained (Sarma et al. 2006), i.e. it tends to transform multi-modal permeability distributions to a more normal distribution over a sequence of many updates. These transformations lead to a loss of structure in the permeability field. The effect of filter divergence is such that the distribution produced by the filter drifts away from the truth. Filter divergence normally occurs because the posterior probability distribution becomes too narrow and the observations have gradually diminishing impact on the Kalman gain. It then tends to find local rather than global minima.

Aanonsen et al. (2009) stated that EnKF is more suitable when there is a small amount of observed data and thus not suitable for use in 4D seismic history matching. When there is a weak match between prediction and observed data, the problem could be due to the state of the reservoir at the current time or from the time of the first survey. It is not straightforward then to go back in time in order to carry out "Kalman smoothing"

which is the process where new changes to the model are propagated backwards in time to older seismic survey predictions.

Monte Carlo (MC): is a purely probabilistic workflow for solving inverse problems. MC methods consist of two parts, the sampling method and the optimization method. The sampling scheme of MC is based on generating a population reservoir models with reasonable statistical characteristics of a random variable. The random models will be generated from a specific probability distribution. Thousands of possible outcomes of models will be generated then. The optimization routine of MC is based on random walks. This means that the algorithm will move around a marker in multi-dimensional space in order to find the lower misfit (Mosegaard and Sambridge 2002).

Probabilistic Approach of History Matching and Uncertainty Analysis

These approaches incorporate all quantifiable sources of uncertainties that arise in reservoirs from static and dynamic data as well as the simulation model when seeking solution of the inverse problem. All models generated during inversion iterations are used for further analysis to identify the most probable parameter values. In so doing, the probability distribution of the updated parameters is continuously extended by new information using Bayes formulation and the principle of estimating the maximum likelihood. They are then re-sampled as part of uncertainty analysis using Markov Chain Monte Carlo (MCMC) methods to determine probability distributions of the reservoir outcomes, i.e. saturation and pressure, well data, and also for uncertainty analysis of reservoir performance predictions (Sambridge 1999b, Oliver et. al. 1996). If a sufficient number of models are generated, this MCMC re-sampling can continue without further reservoir simulation in uncertainty analysis of history matching results. The models generated equivalent to running an order of magnitude or more additional models.

Bayes Theorem: is used for combining the probabilistic prior information with the information contained in the misfit to observed data in order to update the prior distribution which is then the posterior probability distribution given the data. The posterior distribution of parameters, $p(\underline{\theta}^{posterior} / d^{obs})$, thus is just the conditional Probability Density Function (PDF) of d^{obs} for given estimated parameters $\underline{\theta}$ posterior:

$$p(\underline{\theta}^{posterior} \left| d^{obs} \right.) = p(d^{obs} \left| \underline{\theta}^{prior} \right.).p(\underline{\theta}^{prior}) / p(d^{obs}) \quad (2.10)$$

$p(d^{obs})$ is difficult to establish and is most often to be assumed Gaussian and effectively as a normalisation factor.

$$p(d^{obs}) = \sum_{i=1}^{n} p(d^{obs} \left| \underline{\theta}^{prior} \right.).p(\underline{\theta}^{prior}) \quad (2.11)$$

For a uniform probability distribution of parameters given by upper and lower bounds, the prior distribution, $p(\underline{\theta}^{prior})$, also can be expressed as a constant value normalized to one. Then the posterior distribution is simplified:

$$p(\underline{\theta}^{posterior} \left| d^{obs} \right.) \propto p(d^{obs} \left| \underline{\theta}^{prior} \right.) \quad (2.12)$$

Gaussian Maximum Likelihood: is defined theoretically for a normal Gaussian distribution with zero mean, constant variance, and values from zero to infinity. The probability function of observed data (given the vector of prior parameter) can be expressed as the likelihood function of the objective function. Typically it is assumed, that the model error is negligible in the residuals of misfit function and the error of observed data has normal Gaussian distribution. As a result, $p(d^{obs} / \underline{\theta}^{prior})$ is also commonly labeled as the Gaussian likelihood function which is exponential and is given by:

$$p(\underline{\theta}^{posterior} \left| d^{obs} \right.) = p(d^{obs} \left| \underline{\theta}^{prior} \right.) \propto L(\underline{\theta}) \propto exp(-\frac{1}{2} J(\underline{\theta})) \quad (2.13)$$

with $J(\underline{\theta})$ being the misfit or objective function (Equation 2.3 or 2.4). The likelihood of a model, $L(\underline{\theta})$ is a measure of how likely a parameter vector $\underline{\theta}$ reproduces the observed data, d^{obs}, in other words, it quantifies the degree to which the observed data support a given hypothesis regarding the model parameters.

2.6 Petro-Elastic Modelling

Petro-Elastic models for fluid and stress dependency in rocks are necessary for quantifying and analysing time-lapse seismic signatures during reservoir depletion and injection. Qualitatively, seismic impedance is the ability of passage of an acoustic wave. High impedance indicates the reservoir rock is hard to compress and low impedance shows that rock is soft. Amplitude is another seismic attribute depending on reflectivities at layer boundaries and is also used in seismic history matching. However, since it hinges on interfaces rather than layers which relate to impedance, it is preferred in 3D seismic interpretation of geological structure, while impedance is more favored in 4D seismic simulation calculation using the reservoir simulator pressure and saturation output which requires rock-physics properties at each grid block to be obtained (Dong and Oliver 2003). The acoustic impedance, I_p, is a function of two porosity-dependent properties and is given by:

$$I_p = \rho_b V_p \tag{2.14}$$

Where ρ_b is bulk density and V_p is compression (P-wave) velocity. The P-wave velocity and S-wave velocity, V_S, are given by:

$$V_p = \sqrt{\frac{\left(\kappa + \frac{4}{3}\mu\right)}{\rho_b}} \tag{2.15}$$

$$V_S = \sqrt{\mu / \rho_b} \tag{2.16}$$

where κ is the bulk modulus and is of large value for stiff rocks. The shear modulus, μ, is the coefficient between shear strain and shear stress of elastic rock. The velocity of acoustic waves in fluid filled porous rock is mainly sensitive to pressure, and depends on pore volume. It varies with heterogeneity in mineral composition, rock matrix texture and cementation, fluids types and saturations in the pores (Vernik 1994, Avseth 2000), and exhibits frequency and scale dependent dispersion (Mukerji 1995, Rio et al. 1996). Pore shape also significantly influences seismic velocity (Tsuji and Iturrino

2008b), and existence of thin cracks or voids with small pore volume can considerably decrease the velocities (Kuster and Toksoz 1974).

Compression (P-wave) and Shear (S-wave) velocities in porous rock are replicated through models that are either theoretical or determined empirically from laboratory and field observations (Hertz-Mindlin 1949, Han 1986, Wang and Nur 1992; 2000, Mavko et al. 1998, Shapiro and Troyan 2002, Macbeth 2004).

Early Empirical Models: were used to estimate the velocity in dry pore rock, these models (Han et al. 1986, Krief at al. 1990) follow the assumption that the first derivatives of the velocity with respect to porosity and/or pressure exists. They fulfill the requirements of gradient-based techniques to solve the seismic inverse problems, but imply in practice that the reservoir volume/layer consists of the uniform rock type and the mineral, textural, and pore geometry effects are not important. They are not accurate models and generally as an alternative, empirical models are now often derived for estimation of the bulk modulus of the dry porous rock.

Substitution of fluids (i.e. water, oil, and gas) by change in fluid saturation changes the acoustic properties of rock frame. Figure 2.22a shows the variation in acoustic velocity with effective pressure for different fluids measured in a Berea sandstone core sample. There is an apparent decrease in velocity as the fluid changes from water, to oil and gas, particularly for effective pressures below ~700 bars (~10300 psi). This is because water is less compressible than air so that substitution of water by air increases the bulk modulus of the system. For oil-saturated rock this effect is similar but smaller since oil is more compressible and has lower density than water.

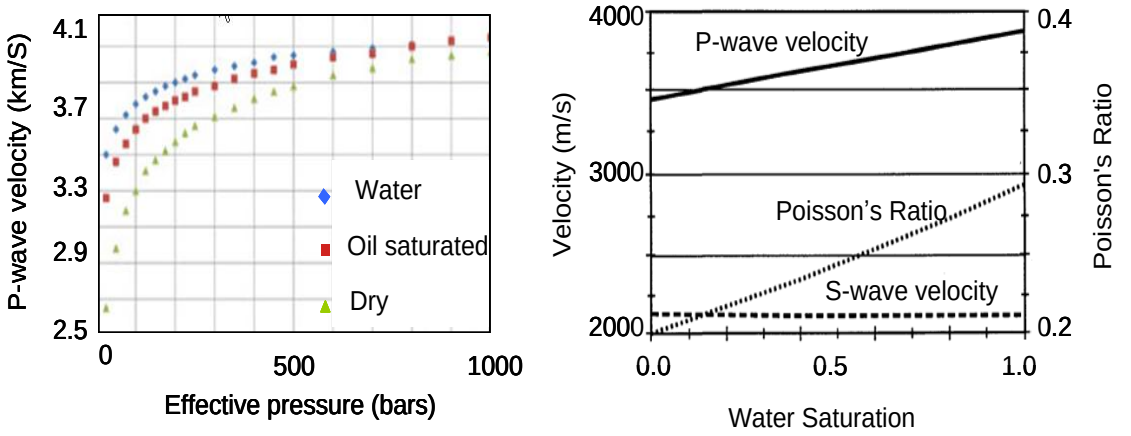

Figure 2.22: a) change in P-wave velocity with effective pressure as a function of different fluid types (after Cheng 2009), and b) the change in P- and S-velocities and Poisson's ratio as function of water saturation (after Skopec and Ross 1994).

The bulk-volume deformation produced by a passing seismic wave results in a pore-volume change and causes a pressure increase in pores filling with water or oil that are less compressible than air. This pressure increase stiffens the rock frame and causes an increase in bulk modulus. Shear deformation, however, does not produce a significant pore-volume change, and consequently different fluids show negligible if any affect on shear modulus. Fluid-saturation effect mainly correlates to a change in bulk modulus.

Figure 2.22b shows the increase in the P-velocity and Poisson's ratio and Shear-wave velocity as a function of water saturation measured on a sandstone core with minor clay. Poisson's ratio is the ratio of transverse contraction to longitudinal extension strain in the direction of the stretching force and demonstrates greater change with respect to increase in water saturation. Poisson's ratio depends on the P-wave to S-wave velocity ratio. Generally, increasing water saturation in a rock increases Poisson's ratio, and also increase $\boldsymbol{V_p/V_s}$ and thus $\boldsymbol{V_p}$ (see Figure 2.22b).

We require a need for a petro-elastic model to account for the changes in both fluid saturations and pressure in estimating the velocity and thus simulation of seismic impedances. In this thesis, the Gassmann equation (1951) captures the saturation effects and stress dependency of the rock is captured in an empirical relationship (MacBeth 2004).

Stress dependency

Bulk and Shear modulus of dry rock frame properties, κ_{dry} and μ_{dry}: will vary significantly with stress, and also stress history and stress path. It is usually assumed that the stress-dependence of the elastic moduli is the result of the compression of grain contacts, and the closure of microcracks that may present in the rock frame. Estimation of the bulk and shear muduli of the dry frame of rocks is usually deficient. They are obtained by combination of core measurement, well logs or empirical equations (Guerin 2000, Wang 2001, Smith et al. 2003, and MacBeth 2004). Core measurements are expensive and samples are sparse, nevertheless dense core sampling usually shows there is a lot of variability in the elastic properties even in a seemingly homogeneous reservoir. Consolidated rocks often break up during coring, and hence the stress sensitivity is likely to be over-predicted in the lab relative to the in-situ conditions (Furre et al. 2009).

Besides, for unconsolidated sands, acquisition of friable core samples is not often feasible. Core measurements are typically done at ultrasonic frequencies and require the cores to be completely dry to avoid dispersion effects. Well measurements may originate in the hydrocarbon saturated interval of the reservoir where the sonic and density logs are affected by invasion of mud filtrate resulting in inaccurate in-situ log data. Well measurements may be taken from the brine-saturated interval; the advantage is that the mud invasion is largely avoided, although the rock matrix may be different from the oil-saturated section in terms of porosity, clay content, or cementation. Therefore, no matter how V_P, and V_S are collected, errors are introduced and propagate to fluid replacement modelling (Engelmark 2002).

Hertz-Mindlin's theory: in the literature physical models for predicting pressure sensitivity in unconsolidated dry sediments are based on granular contact models of Hertz-Mindlin (Mindlin 1949). The porosity at which a granular composite ends to be a suspension and becomes grain-supported is called the critical porosity. Dvorkin and Nur (1996) supposed that at critical porosity, the effective elastic moduli of the dry-mineral frame can be calculated using Hertz-Mindlin's contact theory, for porosities smaller than the critical porosity, the modified Hashin and Shtrikman (1963) lower bound, and for porosities larger than the critical porosity the modified Hashin and Shtrikman upper bound can be used.

A comparison of the empirical results to theoretical Hertz-Mindlin effective-medium models demonstrates that the theoretical models predict a lower pressure exponent for the bulk modulus and velocities (e.g. $V \propto p^{\sim 1/6}$) than is generally observed (e.g. $V \propto p^{\sim 1/4}$) in the data. This discrepancy is attributed to the inability of the models to account for decreases in the amount of slip or grain rotation occurring at grain-to-grain contacts with increasing pressure (Zimmer et al. 2007). Therefore in this thesis, using empirical relationships are proffered where it is needed. Section 3.2.2 of Chapter 3 depicts the stress sensitivity correlation used in the SHM workflow of this thesis which is based on calculating the rock dry bulk modulus using MacBeth (2004).

Saturation Dependency

Gassmann model for bulk moduli of saturated rock: is a porosity dependent, well known, and frequently used relationship (Gassmann 1959). This theoretical model derives the bulk modulus of a fluid saturated porous rock via the modulus of three elements: i) the bulk of the dry frame, ii) the mineral constituents in the rock matrix, and iii) the fluids in the pores (Figure 2.23) as below:

$$\kappa_{sat}^{r} = \kappa_{dry}^{r} + \frac{(1-\alpha)^2}{\frac{\varphi}{\kappa_{fl}} + \frac{\alpha-\varphi}{\kappa_{m}}} \qquad (2.17)$$

where $\alpha = (1 - \kappa_{dry}^{r} / \kappa_{m})$, φ is porosity, κ is the bulk modulus, and subscripts ***fl***, ***dry*** and ***m*** stand for fluid, dry-rock frame and mineral, respectively, and ***r*** refers to sand or shale.

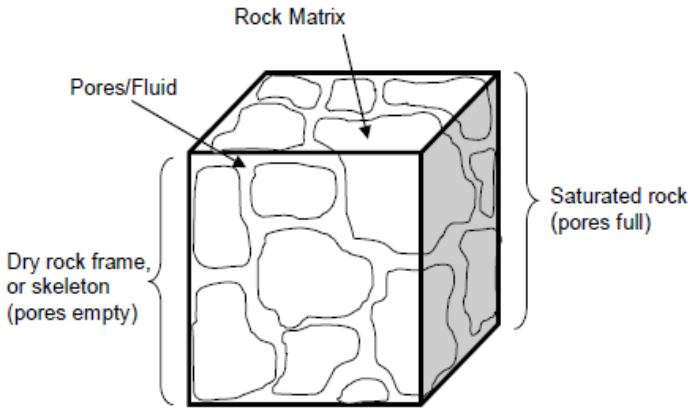

Figure 2.23: In the Gassmann equation (Equation 2.21) a cube of saturated porous rock is characterized by three components: the rock matrix, the pore fluids, and the dry rock frame.

The Gassmann formulation is based on several assumptions: i) rocks properties are homogeneous and isotropic, ii) pores in rocks are well connected, iii) wave frequency is low enough to achieve equilibrium, iv) viscosities of the fluids are negligible, and v) no chemical effects is between fluids and rock (Smith et al. 2003, Wang 2001). Most of these assumptions are generally satisfied for low frequency conditions, which is usually true in seismic exploration due to the attenuation of high-frequency wave components. However, reduction in the accuracy of predictions by the Gassmann equation are expected if the rocks consist of different minerals with strong contrasts in their elastic properties or there are noticeable mineral heterogeneous alignments, the pores are anisotropic in their shapes, or the rock has very low porosity. Up to here, we know how we could obtain κ_{dry}, else we need to know how to calculate κ_{fl} and κ_m.

Bulk modulus of rock matrix or grain, κ_m: the presence of various clays in reservoir rocks can s affect the evaluation bulk modulus of rock matrix. If there are considerable clays in reservoir formation then bulk modulus of rock matrix is usually calculated by averaging the modulli of different mineral constituents and their fraction in rocks. Voigt (1929) proposed an arithmetic average resulting from applying iso-strain boundary conditions. Reuss (1928) suggested the harmonic average resulting from iso-stress boundary conditions. For instances when the reservoir rocks mainly consist of sand and clay, it can be calculated using the mean of arithmetic and harmonic averages of moduli of constituents (Mavko et al. 1998):

$$\kappa_m = \frac{1}{2}\left[f\kappa_c + (1-f\kappa_s) + \frac{\kappa_c \kappa_s}{\kappa_s f + \kappa_c (1-f)} \right] \quad (2.18)$$

where ***s*** and ***c*** stand for sand and clay, and ***f*** is the shaliness or fraction of clay. P- and S-wave muduli for common pure minerals are available in the literature. Variations in the bulk moduli of sand, clay and shaliness do not cause substantial deviations in prediction of seismic impedance change compared to changes caused by fluid saturation variation according to a study carried out by Dong and Oliver (2002). In this study also we considered that there is negligible clay in the rock matrix.

Bulk modulus of fluids, κ_{fl}: Batzle and Wang (1992) proposed empirical relations to compute the velocity and by extension the bulk and shear moduli of common fluids in petroleum reservoirs. The bulk modulus of the fluid mixture depends on the details of the small-scale fluid distribution (Mavko and Mukerji 1998). If the fluids are mixed uniformly, which happens usually at a very fine scale, then harmonic average (Domenico 1976) based on Reuss' model or iso-stress condition is used. If the fluids are "patchy", at a scale smaller than the seismic wave length but larger than the scale at which the pore scale fluids can equilibrate pressures through local flow, then the effective fluid bulk modulus is larger. This upper limit is the saturation weighted arithmetic average based on Voigt's model or iso-strain condition. Therefore, the bulk modulus of the fluid is a saturation-weighted average of the bulk modulus of the individual components (Mavko and Nolen-Hoeksema 1994, Marion et al. 1995) and is calculated through one of the following relationships:

$$\frac{1}{\kappa_{fl}} = \frac{S_w}{\kappa_w} + \frac{S_o}{\kappa_o} + \frac{S_g}{\kappa_g} \quad \text{harmonic average} \quad (2.19)$$

$$\kappa_{fl} = S_w.\kappa_w + S_o.\kappa_o + S_g.\kappa_g \quad \text{arithmetic average} \quad (2.20)$$

where ***S*** is saturation and ***w***, ***o***, ***g*** refer to water, oil and gas, respectively, and $S_w + S_o + S_g = 1.0$.

The choice of averaging method makes a non-trivial difference in the application of the Gassmann equation. Using the harmonic average leads to smaller bulk modulus values

are of more influence. Then any small amount of gas causes the estimation of the fluid bulk modulus to be small (usually the magnitude of κ_g is two orders of magnitude smaller than κ_o and κ_w). The arithmetic average is influenced by the larger bulk modulus and an increase in water saturation results in the fluid bulk modulus estimates to be large. The selection of averaging method depends on the fluid distribution and the frequency of the seismic waves under consideration. For seismic data obtained over undisturbed reservoirs the assumption of the uniform fluid distribution is usually deployed and the harmonic average is used.

When fluid displacement has taken place through water flooding or when ex-solution of gas has occurred, some patchiness of fluid distributions is expected. Then the arithmetic average is used. In fact the bed and intra-bed heterogeneity at the geological scale provides the fluid fluctuation and initial water saturation is probably non-uniform. For example, it is known that connate water saturation varies with rock pore-scale properties and hence, lithofacies (Morrow and Melrose 1991). Indeed, initial water saturation can typically vary from about 0.70 down to 0.05, depending on the heterogeneity of rocks. Moreover, water saturation evolution over production time also depends on the initial saturation distribution and the pore-scale attributes. Then appropriate bulk modulus of the fluid mixture falls between the iso-stress and iso-strain bounds.

Shear modulus, μ: an empirical equation for estimating the shear modulus of pure sand as a function of porosity initially was derived by Murphy et al. (1993), and then modified by Ramammorthy et al. (1995) to account for the percentage of shaliness of the rock. Usually it is assumed that the shear modulus is unaffected by fluid saturations.

Bulk density, ρ_b: the bulk density of a saturated rock is related to the rock porosity and fluid saturations and is the volumetric average of the constituent densities:

$$\rho_b = (\rho_o S_o + \rho_g S_g + \rho_w S_w)\varphi + (1-\varphi)\rho_{dry} \qquad (2.21)$$

Where S is saturation, ρ is density, φ is porosity, and w, o, g and dry refer to water, oil, gas and dry rock, respectively. Dry bulk density, ρ_{dry}, usually measured on core samples (dried at 230 °F) is the weight of the reservoir dry rock per unit volume (lb/cuft). Variation in bulk density is attributable to the relative proportion and specific gravity of

minerals, the porosity of the rock, and the degree of in situ compaction condition. Such data are necessary and are needed to be accurate and correct (i.e. for the amount of clay content and in situ compaction). Otherwise they introduce uncertainty in the modelling results.

2.7 Response Surface Modelling

The basic reason for applying response surface modelling (also referred to as approximation, surrogate, proxy, and metamodel) is to construct a simplified approximation of the complex and computationally expensive simulation to facilitate design optimization, design space exploration and reliability analysis (Sacks et al. 1989, Kleijnen et al. 1995, Anderson and Whitcomb 2005). Response surface modelling has been used in history matching studies in the past to simplify problem mainly: i) through identifying parameters which are not significant and reduce the dimension of problem, ii) by finding interaction between parameters, and ultimately, and iii) when it is used to optimize production and investigation of the p10–p50–p90 uncertainty envelopes in the reservoir performance forecasts (see Figure 2.24).

In such approaches first an initial of sample of reservoir models is obtained to determine the sensitivity of parameters to simulator outputs and to identify the significant parameters. Next, the proxy models of numerical simulator responses, e.g. initial oil in place and oil recovery, are constructed as a function of significant parameters. The proxies may then be used many times as an input in a Monte Carlo-Bayes practice for estimating the probability distribution of the responses and uncertainty analysis (Fishman 1996, Guyaguler and Horne 2000, White and Royer 2003, Badru and Kabir 2003, Peng and Gupta 2004, Li and Fridmann 2005, Yeten et al. 2007, Yu et al. 2008, Scheidt and Caers 2009). Due to the high computational efficiency of proxy-models extensive sampling then can be achieved.

Sample Validation Plotting	Interpretation: • Parameter significance • Parameter interactions • Correlation analysis	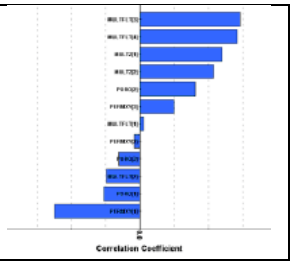
Response Surface Modelling of simulation outputs	Regression method $y = \beta_o + \beta_1 x_1 + \beta_2 x_2 + \beta_{12} x_1 x_2 + \beta_{11} x_1^2 + \beta_{22} x_2^2 + \varepsilon$ $\hat{Z}(x_0) = \sum_{i=1}^{n} w_i(x_0) Z(x_i)$ Neural Network	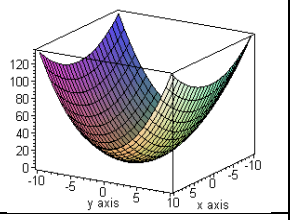
Uncertainty of: reservoir recovery	Monte Carlo simulation on proxy of response: 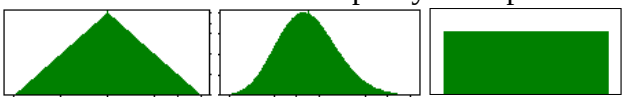	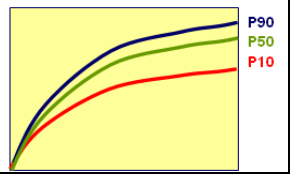

Figure 2.24: Application of response surface modelling in the sensitivity analysis of parameters and uncertainty analysis of reservoir model predictions.

There are several reported applications of proxy response surfaces to the misfit function. For example, Zabalza et al. (2000) used a second order polynomial. Then the minimization of this response surface was performed by applying the simplex method and the best parameter domain was identified. Yemen et al. (2005) used response surfaces based on kriging interpolation as a proxy to the misfit function to rank and screen the parameters, and then accelerated the convergence while applying a Genetic Algorithm on the misfit proxy. Roggero et al. (2007) proposed a global adaptive learning method based on building a proxy model of the objective function using kriging, and also improving the approximation model in the process of searching for the minimum using a Steepest Descent routine. Slottle and Smørgøv (2009) constructed individual polynomial proxy models for the outputs of the simulator that were then entered into a global objective function while each was influenced only by a limited subset of total parameters. For each simulator response one set of the optimal kriging correlation lengths of the parameters was determined at each iteration and then a genetic algorithm searched them for a global minimum of the objective function.

In all circumstances, the proxy models need to be adequately representative of the simulator key outputs. In the method of this thesis, i.e. 'divide and conquer', we also

get use of polynomial response surface modelling in the seismic history matching. However, the aim is to use them just for identifying the independent groups of interacting parameters, thus more of the variability of the systems are preserved while are considerably simplifying the inversion problem of history matching.

In the literature various response surface models have been used (e.g. polynomials, kriging, radial basis functions and neural networks). They should be used for different optimization roles. Therefore, criteria must be established for distinguishing goodness or weakness of each according to their applications (Barton 2006). More important criteria to identify performance of response surface models in optimization are: i) approximation fidelity, ii) computational cost, and iii) globality. Fundamentally, in order to increase the fidelity of the proxy model, more complicated templates of models must be used. This in turn requires that the number of experimental simulation runs, and therefore computation cost be increased. Globality means that there is a wider variable design space with guaranteed fidelity of the proxy model. In order to increase the globality, computational cost increases. When approximation fidelity is taken as a constraint, there is a trade-off relationship between globality and computational cost as shown in Figure 2.25.

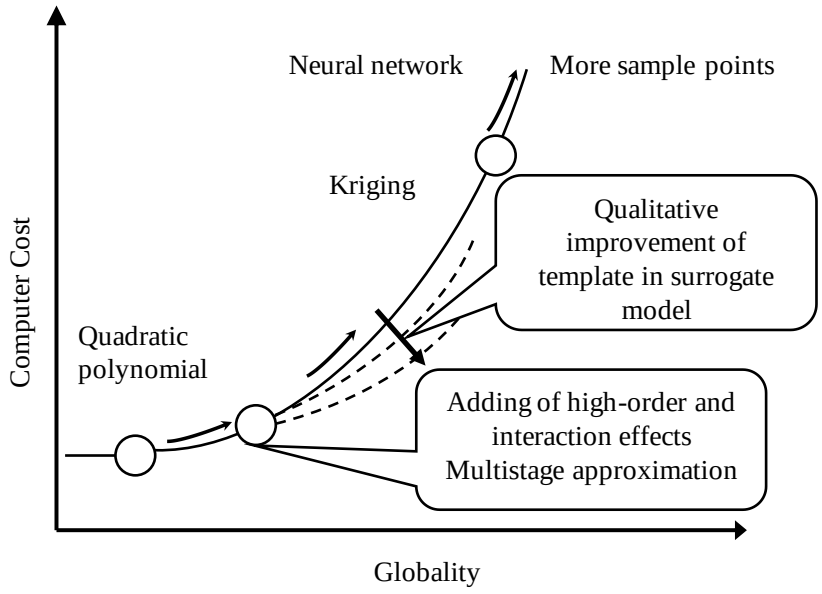

Figure 2.25: Computational cost against globality in response surface modelling (after Fujita and Kounoe 2005).

Various response surface models have distinctive features. For instance, quadratic polynomials are typical surfaces with low computation cost but with less globality. The kriging method typically can approximate nonlinear systems with higher fidelity, but is only suitable for less noisy physical systems. In non-noisy computer simulation, kriging has the advantage of giving predicted values exactly equal to the simulated output values (Sacks et al. 1989, Simpson et al. 2001). However to have the same fidelity as polynomials, they need many simulation runs. Other sophisticated response surfaces that are superior in globality and are of good fidelity include neural network, Radial Basis Function (RBF), and the Cubic Splines. They are based on piecewise local approximation and require a relatively large number of sample points. Good modeling practice implies we aim to find the simplest metamodel that captures the essential characteristics of the system in minimum computational cost (Myers 1999, Montgomery 2000).

Several types of response surface models have been used in history matching studies, for example Cullick et al. (2006) utilized an Artificial Neural Network (ANN) as a proxy. They found the results of history matching with proxy model are acceptable if an initial dataset of sufficient size can be used. Osterloh (2008) used a kriging model. Peng and Gupta (2004) compared kriging and polynomial for predicting uncertainty in Hydrocarbons Initially in Place (HCIP) and found no significant difference between results in each case. Li et al. (2005) proposed thin plate splines as proxy.

Simpler metamodels are easier to justify when they only require a small number of models to be constructed, yet interpreting the results may be tricky because several system characteristics are overlooked. Some systems exhibit highly nonlinear output requiring a more complicated template or may be impossible to predict by most proxy techniques, and may lead to a conclusion that a large stochastic component is required. In many instances, polynomial response surfaces show high fidelity with less computational cost, especially quadratic polynomials that are the simplest and mostly used in optimization and inversion fields. Higher-order polynomials of third and fourth order may result in higher quality models but need too many simulation experiments compared to other methods. Fortunately, engineering processes that require a third-order model are very rare. The quadratic RSM is advantageous since is very flexible and can take on a wide variety of functional forms, it is easy to estimate the coefficients of the

polynomial using the least squares regressions, and there is considerable practical experience of them (Narayanan 1999).

2.8 Experimental Design (ED)

The workflow proposed in this thesis is also combined with Experimental Design. Experimental designs have been used in history matching by several studies (White et al. 2003, Castellini et al. 2004, Peake et al. 2005, Sedighi and Stephen 2009; 2010, Arwini and Stephen 2010; 2011, Wolff 2010). They are techniques usually used to determine the optimum number and combination of experiments that will yield the most information from system behaviour (Box et al. 1978, Myers et al. 2000, Montgomery 2000).

In ED each factor or input variable is set to two or more levels. Then the term design denotes a matrix with a column of samples of factors, usually in coded levels, and each row represents a particular combination of levels for all factors used in the experiment. Converting the original factor levels to normalized coded values (-1, 0, and +1, i.e. minimum, middle, and maximum, respectively) avoids distortion of effects meaning that after normalization of the factors, the coefficients of the polynomial directly indicate the significance of effects and thus provide insight into the system. A design may be orthogonal in the coded factor but not in the original factor (Bettonvil and Kleijnen 1990).

There is no a unique plan for using the design experiments in engineering problems (see Kleijnen 2005). Then, because the same problem may be addressed through different designs, several quality attributes should be identified, including i) the number of experiment runs, ii) the efficiency of having minimal standard errors for the estimated metamodel coefficients for a limited number of design points, and iii) bias protection by sampling not only at the edges of the hypercube that defines the factors region, but also in the interior, and iv) orthogonality to allow each effect in the response model to be evaluated independently of all the others, especially in screening and decoupling of effects.

The selection of designs depend on the metamodel that the user tentatively assumes, and the restricting fact that complicated metamodels require more simulation runs.

Generally in response surface modeling, the user is prone to make simplifying assumptions and starting from left of the plan shown in Figure 2.26, which is likely to reduce the initial data collection effort. Alternatively, one can start from complex response surfaces at the upper right of this figure if little is known about the nature of the response **(**Kleijnen et al. 2005).

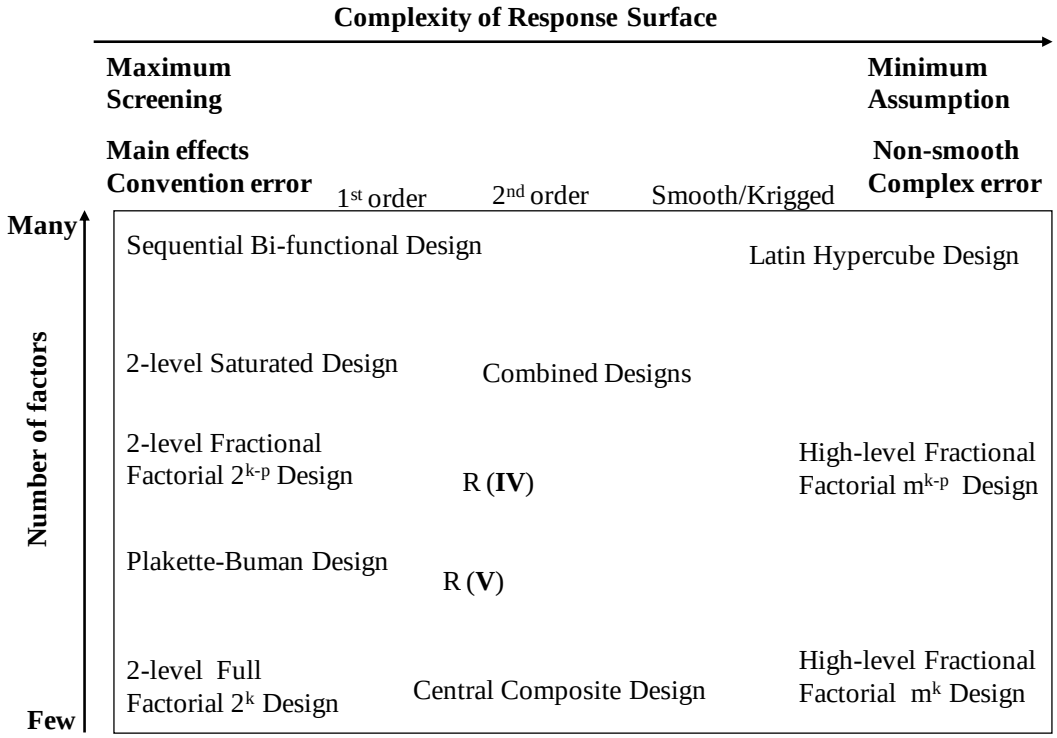

Figure 2.26: General guides for experimental design selection for response surface modelling based on the number of factors and the complexity of proxy models (after Kleijnen et al. 2005). For more details on the various experimental designs and resolutions (R) presented in this figure, see Montgomery (2000).

Proxy models combined with design of experiment are widely used for sensitivity analysis in history matching. One-parameter-at-a-time scenarios are used for linear sensitivity analyses and quadratic experimental designs are used to determine correlation and higher order effects. Yeten et al. (2005) studied different experimental designs and found that polynomial, kriging and splines proxies along with space filling designs are proficient to predict uncertainties in the field performance. The study by Peng and Gupta (2004) on different experimental designs in conjunction with kriging

and polynomial models concluded that no significant difference in utilizing kriging over polynomial and in using Latin hypercube design over conventional designs.

There are always challenges for creating proxy models of a high fidelity which to a certain extent may be related to the sampling strategies. In reservoir simulation we are dealing with highly non-linear output. Therefore, the design experiments uniformly distributed over the uncertainty domain may not be sufficient for construction of an adequate proxy. To overcome this limitation several techniques have been proposed. Li and Friedman (2005) proposed an iterative improvement of thin-plate splines proxy quality. Wang (2003) used an iterative reduction of the design space to improve the minimization procedure with a proxy model. In this method, part of the design space with high values of the objective function was discarded at every iteration and new sampling points were proposed on the reduced design space. Jones et al. (1998) proposed an approach of proxy improvement. For a kriging proxy, the error of the prediction was included into a an objective function so that the uncertainty of the proxy estimate was taken into account and used in an optimization algorithm to improve the fidelity of the proxy model. Queipo et al. (2000) modified this approach by integrating an artificial neural network as a proxy model. Slotte and Smorgrav (2008) also included the kriging variance into an objective function. These approaches lead to iterative improvement of proxy models but through extra sampling points.

2.9 Closing Review

Time-lapse (4D) seismic technology has been introduced to monitor the reservoir during production at different times, since changes in the reservoir pressure and saturation can be detected via changes in compressibility of porous rocks. Incorporating the 4D seismic in the reservoir history matching procedure is based on the integration of a reliable petro-elastic model (PEM) with a dynamic flow simulator along with an iterative optimisation method to adjust the reservoir parameters. Ultimately we acquire a more reliable model for forecasts of reservoir performance. The essential elements and the challenges involved this integrated process were address in this chapter.

Inverse theory is commonly formulated to find a model for a physical system that agrees most with a given observation dataset. Reservoir history matching is a non-linear optimization problem which involves the minimization of an objective function that

measures misfit between observed and simulated data. Because of a large amount of unknowns in the simulation model, the minimization of the objective function is of high degree of freedom and is without unique solution, and thus suffers 'curse of dimensionality'. One remedy for this is reservoir parameterization. Also, prior parameter information can be included as regularization in the misfit function to make the problem well-posed.

There are several sources of errors in a 4D workflow comprising simulation errors, errors due to insufficient model characterization, and measurement errors. The numerical model errors are a result of model approximation or due to upscaling. Also, there are errors due to the different scales at which petro-elastic modeling is applied compared to observations. The parameter deficiency errors are the result of not capturing the reservoir heterogeneity or due to incomplete and incorrect choice of geological features description. The aim is to reduce the effect of such errors by finding the best solution of history matching.

Manual history matching is time consuming. However, by application of optimisation algorithms the process may be completed in a reasonable time. Optimization routines are either gradient-based or gradient-free. Stochastic gradient-free methods are more likely to find a global minimum while the gradient-based methods may be trapped to a local minimum. Minimization of the objective function leads to maximum likelihood estimates. Then using Bayesian theory the posterior probability distribution of parameters can be evaluated for use in reservoir uncertainty studies.

A petro-elastic model links the elastic parameters which govern wave propagation in the rock and the reservoir saturation and pressure changes governed by fluid flow in the reservoir. Gassmann's equation is usually takes account of fluid substitution in pore rocks. Bulk of dry rock moduli may vary significantly with stress. Typically, prediction of pressure effects of unconsolidated dry sediments is based on granular contact models of Hertz-Mindlin theory.

Response Surface Modelling and Experimental Design techniques play a very important role in parameter space exploration, problem simplification, and are capable of bridging the gap between slower inversion algorithms and make real time reservoir optimization possible. Second order polynomial proxy models show high fidelity with less

computational cost, which are the simplest and mostly used in combination to the optimization routines.

Up to now we have looked into the general backgrounds, in next chapter the concepts entailed to the Seismic History Matching (SHM) method and the approach of 'divide and conquer' which have been developed in this research work are expanded.

CHAPTER 3 The Method of 'Divide and Conquer' Unknowns in Seismic History Matching (SHM) Workflow

Introduction

The procedure of incorporating time-lapse data in history matching and the particular workflow of Seismic History Matching (SHM) used in this thesis are introduced. In recent times, there have been innovations in many aspects in the SHM procedure. Several of them include: a) minimizing model errors due to differences between seismic scale resolution and simulation grid size, b) reducing noise levels in the seismic data when it is notable relative to the magnitude of the seismic signal, c) investigation of the impact of successively updating parameters by adding new data to observed dataset, d) investigating various ways to optimally identify the areas in the reservoir that need to be updated, e) speeds up of the rate of convergence by using sensitivities so that we bias sampling towards better models and improve the exploitation phase in the optimization routine used for parameter sampling, i.e. Neighbourhood Algorithm, f) normalisation of observed time-lapse seismic data with associated variants to be prepared for using in mismatch computation. They are described in the next sections of this chapter.

The basic concepts supporting the development of the approach of 'divide and conquer', which is based on dividing the parameter space to sub-volumes and decomposition of the misfit function, are then extended. The core of the 'divide and conquer' approach uses a proxy model to understand how updated parameters interact in the objective function. This approach is an improvement to the usual SHM practice which effectively increases the convergence rate through two search methods. We called them Parallel-SHM and Serial-SHM. In the Parallel-SHM, we use a parallel version of NA to search all of the sub-volumes simultaneously and find the minimum of related sub-misfits of each sub-volume. In the Serial-SHM, one sub-volume is searched for the minimum misfit at a time and the associated parameters are updated with each application of the NA.

The 'divide and conquer' approach would be more attractive if we could find a more efficient means of sampling the parameter space for the purposes of: i) constructing the proxy model, and ii) identifying the ensemble of models needed to start a stochastic search routine (i.e. NA). Experimental Design (ED) is an obvious candidate for this aim. The approach of the 'divide and conquer' is combined with several ED techniques and is set up for the Parallel-SHM method.

3.1The Seismic History Matching (SHM) Method applied in this Thesis

The Seismic History Matching (SHM) method used in this thesis follows an iterative process and could be classified as a multi-dimensional quasi-global inversion approach. The basic objectives of this procedure are: i) to improve the reservoir characterisation by adding additional constraints given by the 4D seismic data, ii) to identify the fluid flow directional patterns in the reservoir, and iii) to quantify the model predictions and uncertainties using updated statistics (i.e. mean and standard deviation) of the reservoir parameters obtained after inversion. Each iteration in the SHM workflow involves the following elements (see Figure 3.1 for illustration):

- **Parameterization schemes:** for adjusting model properties, we may use i) multipliers to update the flow barrier transmissibilities, ii) multipliers to rock-physic parameters, and iii) pilot points with kriging to update net:gross and permeability, and iv) a zonal approach (Stephen et al. 2006).

- **Petro Elastic Modelling (PEM)**: which converts the reservoir simulation model outputs including pressure and saturation to seismic response, i.e. impedance, based on Gassmann (1959) fluid substitution relationship along with an empirical representation of the stress (MacBeth 2004) dependency of the pore rock.

- **An objective function**: following the idea of Tarantola (1987) we use a global misfit function using a L2 norm expression. It measures the closeness of observed reservoir production and seismic data to the equivalent outputs by reservoir flow simulation. Since both observed and simulated data deviate from the true responses by errors, the objective function includes the relevant variances to capture the noise in the data and model.

- **Parameter Space Exploration:** carried out through application of a quasi-global search routine of Neighbourhood Algorithm (NA) to minimize objective function. NA can be tuned either for more 'model exploitation' or more 'model exploration' promptly (Sambridge 1999). Therefore it makes sensible use of all information obtained in every iterative of sampling parameter space.

- **Uncertainty Analysis:** in a complete Bayesian framework, the misfits provide the conditional likelihood of each model for the given data, which are then used to update prior model probabilities and to estimate the posterior probability density of model parameters.

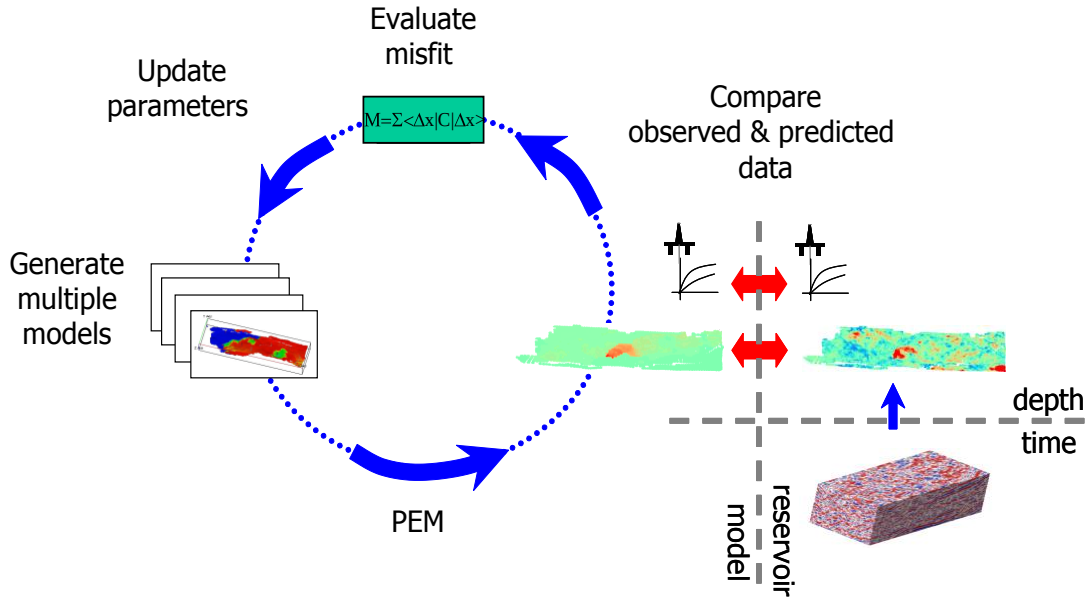

Figure 3.1: Schematic of the iterative automatic Seismic History Matching (SHM) process (Stephen et al. 2006). In this loop, a reasonable set of parameters in the reservoir model are chosen to be updated. Then forward reservoir simulation and Petrol-Elastic Modelling (PEM) are run to calculate the production and seismic responses of the reservoir model. The value of the objective function is computed and an optimization routine (e.g. Neighbourhood Algorithm) is applied to decide a perturbation to the set of parameters that hopefully results in a smaller misfit in the next iteration.

Starting with the prior Probability Density Function (PDF) of model parameters, the maximum the posterior PDF estimate of the model parameters is sought (such as porosity, permeability, fault transmissibility) by minimizing the objective function. The

prior (PDF) of models are usually estimated. Then for all models, we can calculate an updated probability in proportion to the degree they honour the history data. The history data include available production and 4D seismic data on the reservoir. Once a sufficient number of such models is available, these probabilities may be re-sampled using Markov Chain Monte Carlo methods (proposed by Sambridge 1999b) to draw conclusions about the posterior statistics of the model parameters. The posterior probabilities may be re-sampled and used as weights to determine the distribution statistics of saturation or pressure in each cell of reservoir model. Moreover, the variability in long term well and field flow predictions may be determined, instead of predicting only one future performance.

3.1.1 Petro-Elastic Modeling in SHM

The elastic moduli are calculated to reflect the changes of the fluid and the effective pressure in the rock pores, along with temperature. Due to the change in elastic moduli, the rock becomes more or less resistant to wave-induced deformations. Therefore, seismic velocities and impedances experience an increase or decrease in magnitude. In SHM, a Petro-Elastic Model (PEM) converts changes in fluid saturations and pressures from the simulations into predicted acoustic impedances for each column of simulation grid cells. The approach deployed here uses the Gassmann (1959) equation for fluid substitution (refer to Section 2.9 of Chapter 2), and calculates the rock dry bulk modulus using the MacBeth (2004) empirical correlation for the stress sensitivity:

$$\kappa_{dry}^{r} = \frac{\kappa_{inf}^{r}}{1 + E_{\kappa}^{r} \exp(-P_{eff} / P_{\kappa}^{r})} \tag{3.1}$$

Where, the superscript r identifies rock type (sand or shale), κ_{inf} represent the dry bulk modulus at Standard Temperature and Pressure, E_k is the excess compliance present in the rock as a result of geological or mechanical processes, and P_{κ} is the stress sensitivity, respectively. These parameters are determined from lab measurements or by history matching (Stephen and MacBeth 2006b). P_{eff} *is* the difference between the overburden pressure and the pore pressure. Here, we assume that the effective stress equals the differential. The shear modulus, μ^{r}, has the same form of Equation 3.1 with

equivalent parameters. It is assumed for shale to consists of dry frame only and the shear modulus is unaffected by saturation.

The value of P-wave velocity for each cell is obtained from the harmonic average of the sand and shale values, weighted by their relevant fractional volumes (net:gross). This is a valid practice for vertical wave propagation in a layered model (Backus 1962). Using this, the acoustic impedance, $\boldsymbol{I}$, for a column of cells in the simulation model is calculated as below:

$$\boldsymbol{I} = \sqrt{\langle \boldsymbol{\rho} \rangle . \left\langle \frac{\boldsymbol{1}}{\boldsymbol{M_m}} \right\rangle^{-1}} \tag{3.2}$$

$$\frac{\boldsymbol{1}}{\boldsymbol{M_m}} = \frac{\boldsymbol{(1 - V_{shale})}}{\boldsymbol{M^{sand}}} + \frac{\boldsymbol{V_{shale}}}{\boldsymbol{M^{shale}}} \tag{3.3}$$

$$\boldsymbol{M_{sand}} = \boldsymbol{\kappa_{dry}^{sand}} + \frac{\boldsymbol{4}}{\boldsymbol{3}} \boldsymbol{\mu_{dry}^{sand}} \tag{3.4}$$

$$\boldsymbol{M_{shale}} = \boldsymbol{\kappa_{dry}^{shale}} + \frac{\boldsymbol{4}}{\boldsymbol{3}} \boldsymbol{\mu_{dry}^{shale}} \tag{3.5}$$

Where: $\boldsymbol{\rho}$ is the bulk density of the cell obtained by averaging the densities of the rock frame and the fluid densities (see Equation 2.26 of Chapter 2). The brackets, < >, indicate a vertical volume weighted average over the reservoir interval, $\boldsymbol{M_m}$, $\boldsymbol{M_{sand}}$ and $\boldsymbol{M_{shale}}$ are p-wave moduli for sand-shale mixture, sand, and shale, respectively. This approach is suitable for reservoir beds that are less than one tenth of the seismic wavelength thick, and to reservoir units of around one quarter wavelength thick, a typical wavelength is 50 to 100 m (MacBeth 1995). For the case study in this thesis (Schiehallion field), the reservoir units are around 25 m thick, equivalent to one quarter of a wavelength in many places, and the predicted impedance typically represents a cell of approximately 100 m × 100 m × 6 m.

3.1.2 Scale Dependence in SHM

For the calculation of the misfit we require that the observed and predicted seismic data represent the same volume. The observed seismic data are usually obtained on a set of points on the bins defined by the acquisition inline and crossline areal coordinates with a separation of 25 m, while the wavelet samples 25 m vertically. The predicted seismic properties grids are typically coarser horizontally but they are finer vertically. The predicted seismic impedance is calculated on a grid that is typically of the size 100 m × 100 m × 6 m, which is the scale of reservoir simulation model (for our case study). Vertical upscaling and horizontal downscaling is usually needed (see Figure 3.2). Using the upscaling method (see previous section) of Backus (1962), the predicted seismic grids are calculated at the vertical scale of the observed seismic data (25 m). At this point, the thickness is equivalent but the areas are different and needed to be amended.

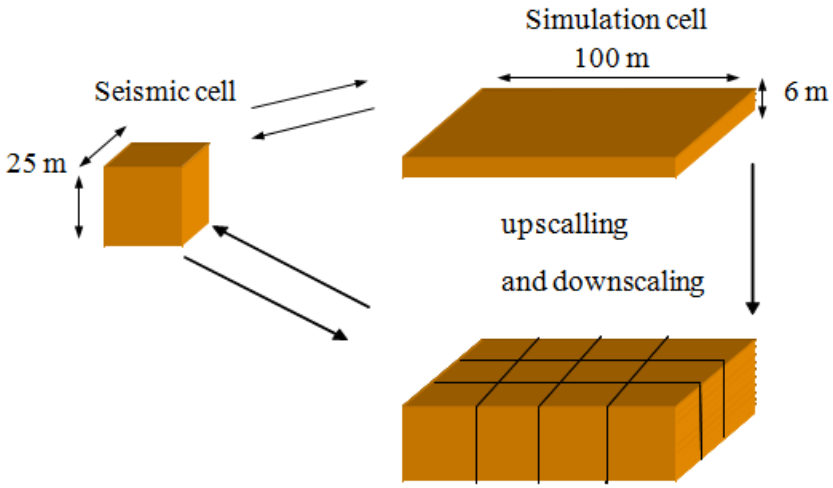

Figure 3.2: Illustration of how we convert the simulation to seismic scale. In SHM, we start upscaling by simulated seismic properties vertically during the PEM calculation, and then downscale predicted seismic to observed seismic bin horizontally.

The seismic and model grids are independent and the latter is aligned at approximately 45 degrees to the former (see Figure 3.3). The predicted seismic impedance, are downscaled horizontally onto the observed seismic bins in order to maximize the spatial information about the spatial correlation of the observed dataset and to be able to compute seismic misfits appropriately. This process is accomplished through inverse distance weighted interpolation using the Barnes (1964) method. The interpolated impedance, I^{int} is calculated as below:

$$I_{ij}^{int} = \frac{\sum_{IJ} w_{ijIJ} I_{IJ}}{\sum_{IJ} w_{ijIJ}} \quad (3.6)$$

Where:

$$w_{ijIJ} = exp(-\beta |\underline{r}_{IJ} - \underline{r}_{ij}|) \quad (3.7)$$

I and J are x and y indices for the simulation grid, i and j are the equivalent for the finer seismic grid cell, I_{IJ} are obtained from Equation 3.2. Vector 'r' is the position of a simulation cell centre, and $ß$=0.05 (m^{-1}) gives the best result, minimizing the representative error.

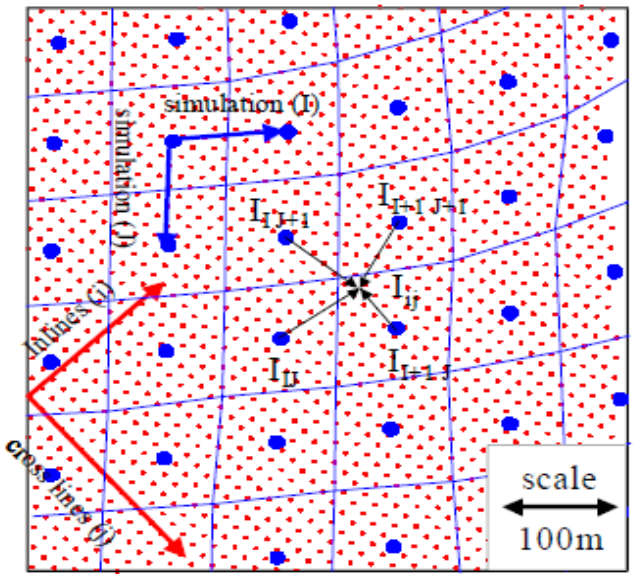

Figure 3.3: Comparison of the seismic and simulation grids SHM. Blue lines indicate the simulation cells and large blue symbols the location at which the impedances are predicted. Equation 3.6 and 3.7 are used to interpolate the impedances to obtain values at the small red symbols, i.e. where the observed seismic is measured. Solid blue and red arrows indicate the principal directions of the simulation axes and seismic grids respectively (after Stephen et al. 2006).

There are other options that can be used to make the simulated and observed seismic impedance data of the same resolution with the intention of comparing them against each other, which are not preferred choices in the SHM workflow. They may be outlined as following:

- Building the simulation model at the seismic scale where we can compare real and simulated seismic impedance. The drawback for this choice is that geo-models do not usually get built according to the seismic grid and simulations in this scale would be very slow.

- Simulate on the geo-model scale may be an alternative, however it would be very slow process despite some speed up compared to simulation on a the seismic scale. Also, there is a high degree of uncertainty introduced when mapping (upscaling or cross-scaling) simulated seismic predictions at the geo-model scale to the observed seismic scale for misfit calculation (e.g. Roggero et al. 2007).

- Downscaling properties of the simulation model scale to the seismic impedance scale can be considered. Then various properties can be downscaled and also various downscaling techniques may be used, for example:
    - Downscaling saturation and pressure to the seismic impedance scale may be attempted, but it is not straight forward. A simulator based inversion process is needed. The advantage though is that the fine scale representation of the static properties is captured (see Castro 2007).
    - Interpolating saturation and pressure output of the simulation model (scale) and producing maps in the seismic impedance scale, then the fluid properties are not properly conditioned to the flow but in some conditions may be no less accurate.

- Kriging may be an option in interpolating of simulation seismic data (i.e. downscaling to observed seismic scale), however this is a complex technique. kriging requires defining some relationships between the unknown data at various locations and some known data nearby which in reality are estimated from the coarse scale simulation.

3.1.3 Observed Seismic Data in SHM

The seismic data set used in this thesis consisted of two P-wave seismic volumes: migrated stack and coloured inversion stack from the Schiehallion field. For example, the former (Phase I) dataset were cross-equalised and calibrated then transformed by a combination of phase rotation and filtering to give the coloured inversion stack (for a definition see Lancaster and Whitcombe 2000). Time to depth conversion was implemented and the location of the reservoir horizon was provided. Then a map of Root Mean Square (RMS) amplitudes was generated from the Migrated Stack by integrating the signal over a suitable time window (Leach et al. 1999). Then a second attribute, the 'Sum of Negative Values', was obtained by summing the negative amplitude in the coloured inversion stack from the picked reservoir horizon over a suitable time window. Figure 3.4 and Figure 3.5 shows examples of such attribute data from the Schiehallion field. Following the recommendations and information provided by the operator, this attribute has been used as a pseudo-impedance to detect pressure and saturation effects via the time-lapse maps to be compared to simulated 4D seismic predictions. For more details on the latter time (Phase II) 4D seismic attributes used in this thesis see Chapter 5.

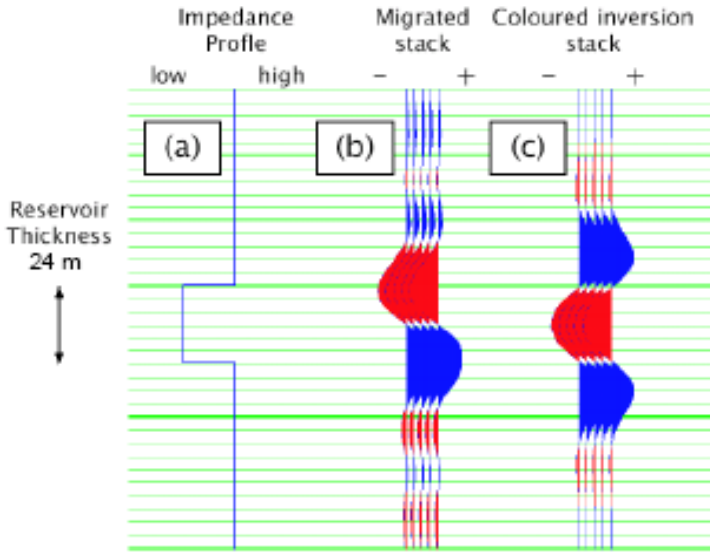

Figure 3.4: Coloured inversion schematic is showing (a) a P-wave impedance profile with a thickness of 24 m (Schiehallion field), (b) the zero angle seismic stacks, and (c) the coloured inversion stack. The reservoir is located between the two zero crossings for the case of the coloured inversion stack and the shape of the wavelet is similar to that of the impedance profile (Soldo 2005).

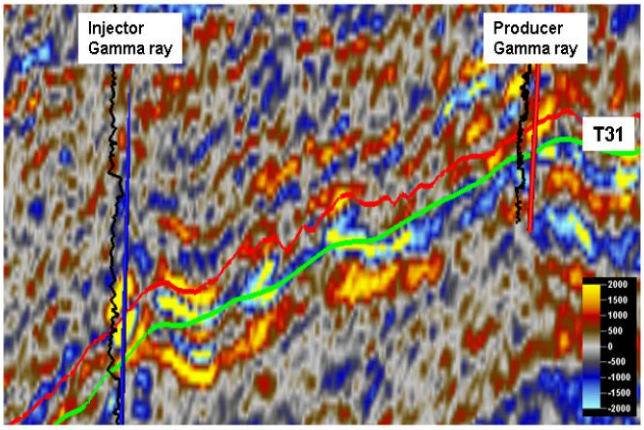

Figure 3.5: Coloured inversion product for the full offset migrated stack (from the Schiehallion field). The green and red lines indicate top and bottom of the reservoir sand (Edris et al. 2008).

The seismic property predictions consist of acoustic impedances while observed data are relative measures. Thus the observed data sets are normalised prior to comparison. This normalization step is based on the assumption that the effect of changing pressure and saturation induces an equivalent relative change in the reflectivities and impedance throughout the reservoir. For each domain, the surveys are normalised by subtracting the mean of the baseline survey, γ^0 and dividing by the standard deviation, σ^0, respectively, and thereby scaling to the range induced by varying static rock properties, as below:

$$a(t,x,y) = \frac{A(t,x,y) - \gamma_A^0}{\sigma_A^0} \tag{3.8}$$

Where: A and a are the raw and normalized attributes at monitor time t. Predicted impedances can now be compared quantitatively against the observed equivalent seismic attribute without the need for a full inversion.

3.1.4 Challenges Investigated in the SHM Workflow

So far in this thesis many aspects of the SHM process have been discussed. An ad hoc process of temporal decomposition of the misfit function was carried out (Edris et al. 2008; 2009; Edris 2009). The appropriate seismic data assimilation was identified by

investigating the impact of successively updating the model parameters (such as the transmissibility of faults). The observed seismic data were added in incremental stages so that short simulations were run initially in the history matching process. For the next stage the model and the span of the parameters were modified based on the initial results. The approach was compared to a single history match where all data was used. The best results were found when early data were used in short time simulations first as the optimum parameter values were learned. Later data were added for fine tuning and reducing the forecasting uncertainty or to explore new parameters. This incremental approach may be compared to the Ensemble Kalman Filter where the latest production data can be assimilated without re-running the simulator from the initial conditions.

Production measurements and seismograms contain data errors from a number of sources (see Chapter 2). Although it is not an easy task, to capture the impact of errors in observed data we need to assess them and include a data covariance matrix in the misfit objective function (Equation 2.6 of Chapter 2). For identifying the noise in the observation data, band-pass filtering was used for both seismic and production data which was then used to determine the data covariances (Stephen et al. 2006). The seismic data covariance was calculated for spatial correlation in the direction of the inlines and crosslines to give two matrices to the misfit. The behaviour of the covariance as a function of lag was previously observed by Gosselin et al. (2003). In practice, random sampling of a subset of inlines and crosslines can speed up the calculation of covariance matrix (for full details see Soldo 2005). Otherwise, calculation of the seismic misfit could take as long as the flow simulation. Then either the numerical representation of the matrices or a fitted exponential model (e.g. Deutsch 1992) could be used. Alternatively if the correlation is low, a diagonal matrix of the standard deviation of the noise can be assumed (Stephen et al. 2006).

Initially a least square filter (i.e. Yilmaz 1987) was used (Soldo 2005) to measure the data error in the production data and to calculate the covariance for each data component. The problem was that this method could not detect the low frequency signal properly and there was no indication for the right frequency level to stop the filtering. Then the continuous wavelet transform (Daubechies 1988, Walnut 2003) was used (Edris et al. 2008; 2009). This method was originally based on multi-resolution filtration (decomposition) by time-scaling and time-shifting often called the mother wavelet through visual assessment and the experience of the analyst. However, once again excessive

filtering or decomposition may tend to smear valuable information. In SHM, the available pressure data was related to the changes in the production profile, such as oil rate for the wells and key points where the changes in pressure appeared unnatural were identified to define the truth signal from the noise. This was then used as reference to define the right noise level. Aggrey (2007) has also presented a similar approach in high density data to filter out the non-signal components from the observed data for pressure measurements recorded from some smart wells in the North Sea.

In addition to data errors, model errors arise because of simplifications made in the simulation process (e.g. Christie et al. 2005), mainly by reservoir model discretisation and upscaling. This applies to both flow simulation and the conversion of simulation results into predicted seismic data (e.g. Stephen et al. 2005). Simulation model errors may be evaluated and determined by fine scale simulation of representative models and subsequent interpolation for other models as described by O'Sullivan (2004) and Christie et al. (2005). Also, seismic scale model errors were assessed through fine to coarse model comparison (Stephen 2007, Edris and Stephen 2008). Initially history matching to coarse scale seismic data was carried out using coarse scale simulation models as the base model. Then, history matching to the fine scale seismic data was considered. This time, when a coarse model was used as the base case, the model error dominates and comparison of the results showed that the residual error is much smaller if there are no scale errors. The scale dependent errors dominate history matching however and can prevent a good model being found in some cases. Aanonsen and Eydinov (2006) also utilized large-scale corrections combined with a downscaling procedure and provided a better initial model for the final adjustment on the fine scale. They showed that there was an improvement in the quality of the solution when compared to history matching directly on the fine scale.

History matching is an iterative time consuming task involving many simulation runs. While upscaling (e.g. Christie and Blunt 2001) was used to coarsen and speed up simulation model runs, an additional (factor 10) speed up can be obtained by using the streamline method in place of finite difference methods. Streamlines are fast because the pressure is assumed to be constant over several months, but they suffer from one major limitation. The streamline theory assumes tracer-like flow through fixed lines in the reservoir over time thus leading to increased numerical effects and approximations which thus introduce model errors. This theory is very physically powerful for matching

history of periods of primary production where compressibility is unimportant and also for estimating advanced water breakthrough at wells, i.e. viscous dominant flow (Agarwal 2003). The study of Carter (2004) disclosed that in history matching; it is important to include a modelling error term in the objective function when using numerical models with significant modelling error. The model errors for production rates and time-lapse seismic predictions were determined by running random ensembles (50 models) using both finite difference and streamline simulators. The mean and standard deviations of all production rate errors and the seismic errors were then used in the objective function account for modelling error, ignoring correlation of the model errors (Stephen et al. 2007, Kazemi and Stephen 2008).

An appropriate parameter updating schemes were examined through two proposed approaches which were regional-based and global-based. In the first, one variable (permeability or net:gross) was updated at a time albeit at separate locations using groups of pilot points. In the second, parameters were updated simultaneously but changes were restricted to a certain region each time until all selected regions were updated. The second approach resulted in a lower production misfit for most of the wells although more models were required (Kazemi and Stephen 2009). In this case there were strong dependencies within regions but not between, and the approach was valid. We consider this to be an ad hoc divide and conquer approach which reuses the analysis of this thesis approach.

To improve the convergence rate in the history matching, a method that combines a proxy model of misfit and a global stochastic search routine (i.e. NA) was developed (Arwini and Stephen 2010). The proxy model optimally directed the choice of new models during a random search by increasing the chance of finding new best models. This maximised the breadth of search offered from the stochastic approaches with rapid convergence associated with gradient type methods.The approach also used experimental design in the initial parameter search but also to derive a proxy model of the misfit and updating of the proxy model periodically during the search and thus improved the convergence rate further (Arwini and Stephen 2011). Castellini at el. (2005) used a similar idea to use high quality proxies of the objective function to accelerate the search for the solution. An efficient experimental design stage was also adopted for the selection of key parameters while an optimization routine involving a

Genetic Algorithm. The method was able to filter out a significant number of unnecessary and expensive objective function evaluations and simulations.

3.2 'Divide and Conquer' Method as a Development to SHM Workflow

In this thesis a 'divide and conquer' method is presented to improve the convergence to in seismic history matching. This method is a development to the conventional SHM workflow and is based on identifying the orthogonal sub-volumes of the parameter space by decomposing the objective function to partially separated sub-functions (Sedighi and Stephen 2009; 2010). In the method, the objective functions for each sub-domain are minimized in parallel or in turn. The details of this method are explained in the following sections. Initial numerical results show that using partial separability can dramatically reduce the number of function evaluations needed to minimize a misfit function allowing problems with very many parameters to be solved.

3.2.1 Dividing the Parameter space and Decomposition of the Misfit Function

The 'divide and conquer' approach initially provides a numerical or analytical representation of the misfit objective function (Equation 2.6 of Chapter 2) so that the parameter groups can be divided and their sub-misfit functions can be identified as shown below:

$$J(\underline{\theta}) = \sum_{i=1}^{k} j_i = j_1(\theta_1 \ldots \theta_p) + j_2(\theta_{p+1} \ldots \theta_q) + \ldots + j_k(\theta_m \ldots \theta_n) \qquad (3.9)$$

Where $\underline{\theta}$ is parameter vector, and j_i (i from **1** to k) represents the objective functions of independent parameter sub-volumes (i.e. θ_m to θ_n) of lower dimension. Indices ***p, q, m*** and ***n*** are sub-misfit parameter counters, and n could be at most equal to the total number of parameters, n_d. This decomposition is achieved with the assistance of response surface modelling which are described in the following sections.

3.2.2 Assigning a Response Surface to the Objective Function

A response surface model, also called a proxy model, is a representation of a real system or its simulation model. A proxy model becomes very useful when the direct

evaluation of the system or simulation model is either impossible or too expensive and time consuming (for more details see Section 2.10 of Chapter 2). In most engineering optimization applications, including history matching, response surface models are usually constructed with polynomial regression techniques. Interpolation methods such as kriging, thin spline and neural network are also used. Polynomial regression is straight forward to implement, and the constructed surface is accurate if the problem is not strongly non-linear and when the parameter space is not too extensive. Interpolation methods have the advantage of honouring all the training data and also handle scattered data. They tend to smooth out some changes in the response surface, however, including noise and under-fitting. More complex proxy models (e.g. artificial neural networks) may provide an accurate proxy to the data, but the required number of training and testing points is often very large and therefore, they offer limited compensation when we desire to save computing time.

The 'divide and conquer' method takes advantage of a polynomial regression in the form of a multi-dimensional second order function with linear, quadratic and interacting terms for parameters to assigned a surface to objective function. Higher order terms are assumed to be small or lost in the system noise. Mathematically this equation is represented as:

$$f(\underline{\theta}) = a_0 + \sum_{i=1}^{n_d} a_i \theta_i + \sum_{i=1}^{n_d} b_i \theta_i^2 + \sum_{i=1}^{n_d - 1} \sum_{j=i+1}^{n_d} b_{ij} \theta_i \theta_j \qquad (3.10)$$

where a_0, a_i, b_i, and b_{ij} are the coefficients of the polynomial equation and represent the constant, linear, second order, and parameter interaction terms. Indices i and j are parameter counters, and n_d is the number of parameters. In practice the above equation utilizes the normalized sampled parameters to avoid distortion effects. In the SHM workflow we also tend to sample the parameters on a $\log_{10}$ scale and hence the parameters are represented in this form. Therefore, a linear scaling transformation is applied on parameter values to map them onto the domain of [-1,1], on a $\log_{10}$.scale. This linear transform is then:

$$\theta_i' = \frac{\theta_i - \theta_i^{mid}}{\theta_i^{max} - \theta_i^{min}} \qquad (3.11)$$

$$\theta_i^{mid} = \frac{\theta_i^{min} + \theta_i^{max}}{2} \qquad i = 1, 2, ..., n_d \qquad (3.12)$$

where $\underline{\theta}'$ is the normalized parameter vector, and θ_i^{min}, θ_i^{mid}, and θ_i^{max} are the minimum, middle and maximum of the range of the i^{th} element of parameter vector $\underline{\theta}$, respectively. The singular value decomposition technique with least square regression method (Rao 1973, Paige 1985, Montgomery 2000, Press et al. 2007) is used to derive the coefficients and to construct the polynomial misfit from a number of experimental simulations where the full misfits are calculated from Equation 2.3 or 2.4 of Chapter 2

.

Typically, the coefficients of the response surface are derived using the initial ensemble of the models used in the neighbourhood algorithm run (in the full SHM inversion of the problem) but we may do so at any time during the NA execution. After the coefficients of the polynomial misfit (Equation 3.10) are computed, the negligible coefficients are identified. First the interacting coefficients are ranked from smallest to largest, then starting with the smallest, they are discarded, each in turn, from the polynomial. They are set to zero in $f(\underline{\theta})$ (i.e. Equation 3.10). As this is done, the correlation factor, R^2, between the calculated misfit values by the polynomial model and the true misfit values (calculated $J(\underline{\theta})$ by Equation 2.2) is measured.

When the R^2 drops below 0.95, the process of discarding the insignificant coefficients is stopped and a threshold is established as the smallest interacting coefficient in the polynomial. Then by interrogating the remaining interaction terms, the independent groups of the parameters that can be searched separately are characterized. Figure 3.6 illustrates the sequential steps involved in the parameter space decoupling and misfit function decomposition.

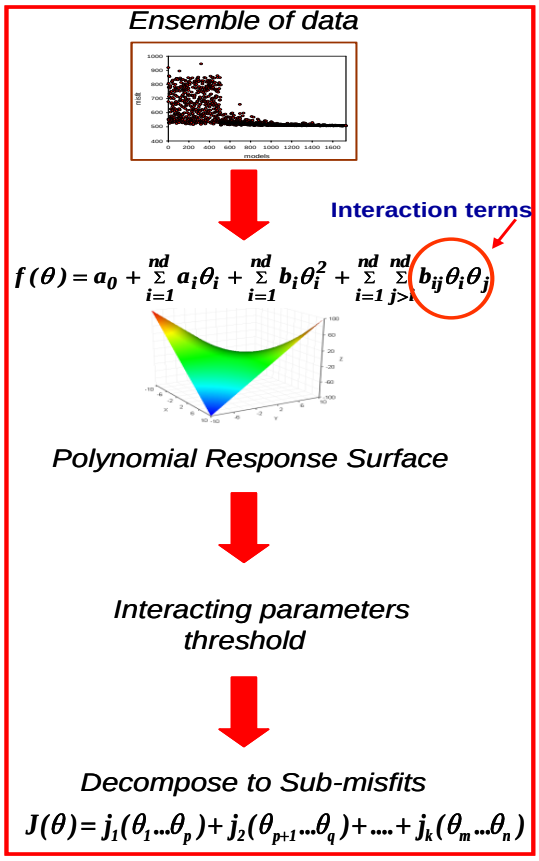

Figure 3.6: The sequential steps involved in the misfit function decomposition and decoupling the parameter space.

Separated parameter groups are defined in the following way: starting with parameter 1 as the focus (e.g. P1 in Figure 3.7), and considering it as the first element of 'Group One', then initially there are two types of parameters: i) those that do not explicitly interact with parameter 1 (with b_{1i} smaller than the threshold), and ii) those that interact directly with parameter 1 (with b_{1i} larger than the threshold), which are placed in this group, (e.g. 'Group One' consist of P1 P7 P8 in Figure 3.7). However, the interrogation of this group is not yet complete. If any element (parameter) of this group other than parameter 1, has interaction with one of the parameters outside the group, that parameter is then moved into this group (i.e. b_{1i} is small but b_{1j} and b_{ij} are large), (e.g. now P2 and P6 are added to 'Group One' in Figure 3.7). Thereby, parameters interacting implicitly with parameter 1 are captured as well, (e.g. eventually 'Group One' consists of P1 P7 P8 P2 P6 in Figure 3.7). This step finishes when all interactions are found and no more parameters could be moved into this group.

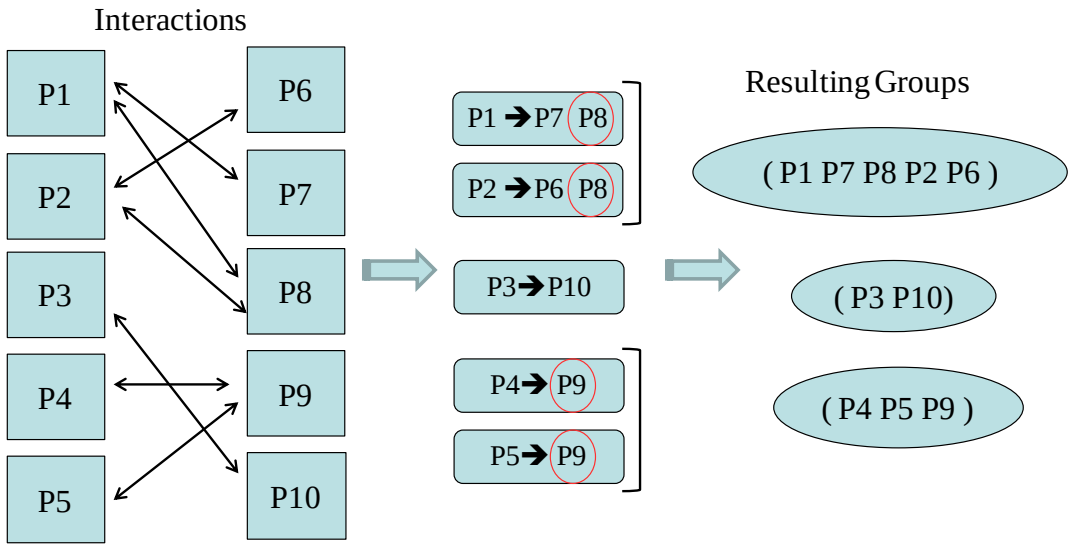

Figure 3.7: The way that interactions between parameters are found when the individual parameter groups are decoupled (as an example for 10 parameters P1 to P10). Apart from the directly interacting parameters, the parameters that interact implicitly (in red circles) are combined in one group.

The same procedure is repeated iteratively to identify additional groups but each time starting with one of the parameters that is still outside of a group. The subdivided parameter groups are thus found and are then considered to be mutually interacting within but independent of others. The resulting groups then form the sub-volumes of the problem parameter space, based on which the misfit function is then decomposed to the sub-misfits, accordingly.

3.2.3 Parallel-SHM Method

Once the independent sub-volumes of parameters are identified NA can be used to search them to find the minimum of the misfit. Here, all parameters are updated simultaneously but the sub-volumes are modified based on the misfit as it is decomposed. Because actual misfits of sub-volumes cannot be calculated, the misfits are estimated using Equation 3.9 to determine the fraction of the total calculated misfit that should be used for each sub-domain, i.e. each j_i in Equation 3.9. The Neighbourhood Algorithm was adapted appropriately to parallelise the search of sub-spaces separately but simultaneously, and thus to update the full parameter vector, $\underline{\boldsymbol{\theta}}$, during each iteration. The updated parameters are passed to the original SHM workflow for all remaining steps. Figure 3.8 summarizes the Parallel-SHM workflow. The core

loop inside the large rectangle in the schematic shows the SHM loop, the small boxes at the top show additional analyses of dividing the parameter space and decomposition of the misfit, and subsequent parallel searching of the parameter sub-spaces.

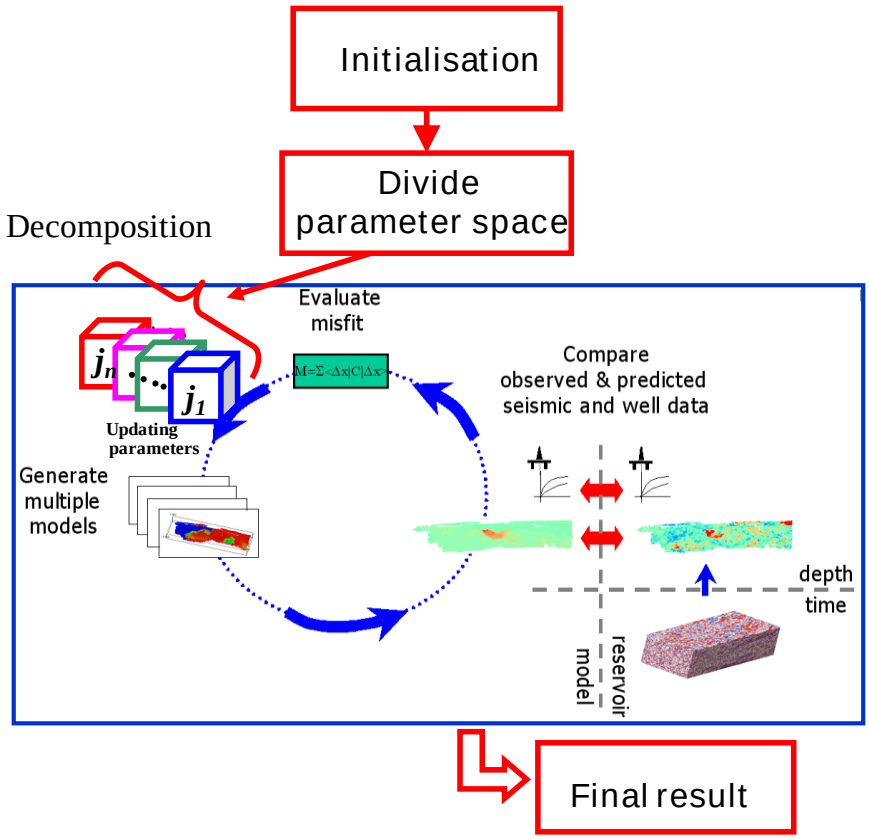

Figure 3.8: The core loop inside the large blue rectangle shows the SHM process. The red rectangles show additional analyses used in decomposition of the misfit and subsequent parallel search of the parameter sub-volumes, i.e. Parallel-SHM method.

3.2.4 Serial-SHM Method

In the Serial-SHM approach a parameter sub-volume is searched one at a time such that only part of $\underline{\boldsymbol{\theta}}$ is updated with each application of the NA while all other parameters are fixed, as demonstrated in Figure 3.9. The search is started by updating the parameters of sub-volumes in rank of the size of the dimension, i.e. higher dimensional first. Then it continues to update the parameters in rank of the importance as determined by the effects on the total misfit response, i.e. most important ones first (if sub-volumes are of identical dimensions). Parameters that are not changed are set to the base case. At the end of each sub-volume search, the best parameters obtained for that group are adjusted in the model and the search starts for the next sub-volumes. When all sub-volumes are

searched converge to a minimum misfit value is achieved with smaller number of misfit evaluations and reservoir simulation runs compared to the Full-SHM approach.

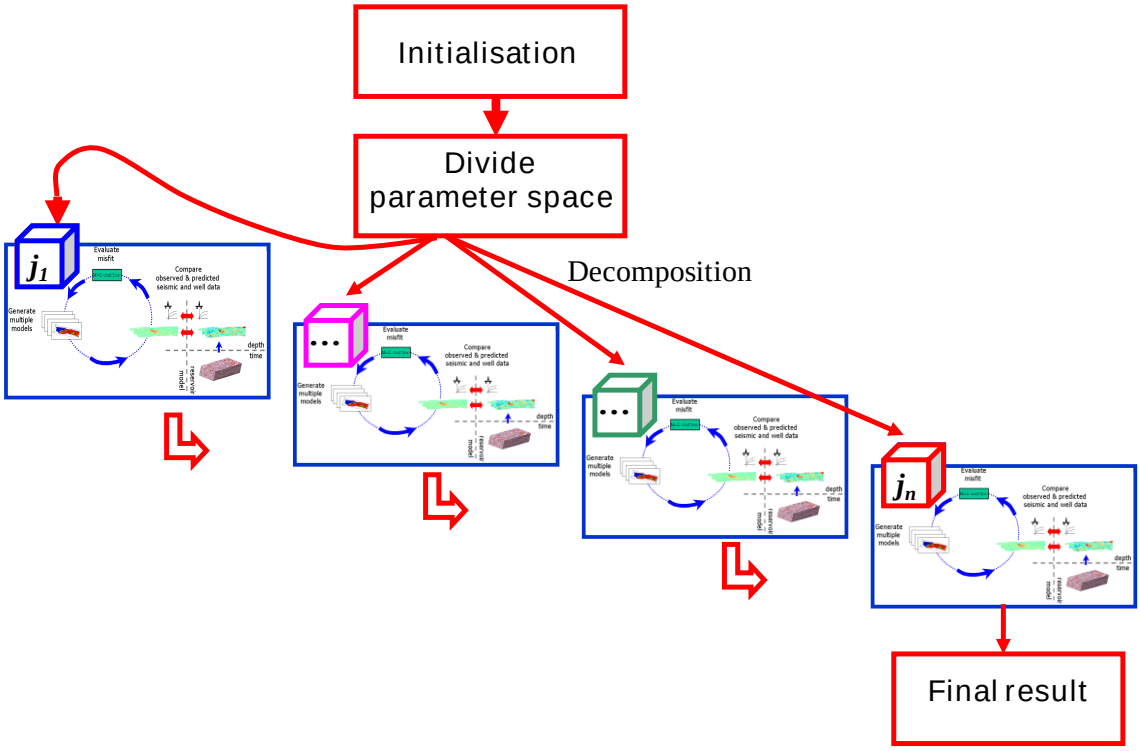

Figure 3.9: In a Serial-SHM method each parameter sub-volume is searched in turn. When one is searched the parameters of the others are fixed, initially at the base case or starting value but once updated the new values are used.

Requirement of re-initialization of the ensemble of models by Serial-SHM

The advantage of the Serial-SHM compared to the Parallel-SHM is that the component misfit of each parameter sub-volume is computed based on the exact misfit function, which is more accurate. On the other hand, the Parallel-SHM inherently involves fewer simulations because multiple parameter groups are updated simultaneously instead of in series. Each serial search step in the Serial-SHM method consists of a conventional application of the NA to a smaller dimensional history matching problem. Also, the initialization is inefficient because we need an ensemble consistent with the dimension of that particular problem. This ensemble must be different from the models used to construct the misfit proxy and then decouple the parameter sub-volumes. However, in the Parallel-SHM, the same models that are used to construct the misfit proxy are used for initialization of sub-volume searches. This is possible because the component misfits

of each orthogonal sub-volume are calculated using the misfit proxy (as happens in the following iterations). Thus the parallel search is more attractive. This property is expanded more through the following example. In a case where we have a 2D history matching problem, where we have determined orthogonality via the regression equation, then we can write the misfit, as:

_ (3.13)

Where $\boldsymbol{f}$ is misfit proxy, $\boldsymbol{j_1}$ and $\boldsymbol{j_2}$ are the misfits of parameters $\boldsymbol{\theta_1}$ and $\boldsymbol{\theta_2}$**.** The proxy model may be derived from random sampling of the quadratic-like surface in Figure 3.10, using the models indicated by the red symbols, for example. In Parallel-SHM, subsequent iterations use the proxy equation to split misfits by parameter group. Thus the initial models, whose misfits consist of $\boldsymbol{j_1}$ and $\boldsymbol{j_2}$ can be used. However, in the Serial-SHM method, each search stage consists of a usual application of the NA routine to a 1D dimensional sub-volume (i.e. $\boldsymbol{\theta_1}$ or $\boldsymbol{\theta_2}$). Since the initial models (red symbols on Figure 3.10) have the misfits $\boldsymbol{j_1}$ and $\boldsymbol{j_2}$ calculated then we either use the parallel approach of separating the misfits via the proxy, which is less accurate, or we have to choose separate models and calculate the misfits again.

In Serial-SHM, we first search the sub-volume $\boldsymbol{\theta_1}$ and begin with a set of initial models (and compute their exact misfits with $\boldsymbol{j_2}$ the same for each model in this case, e.g. yellow symbols on $\boldsymbol{\theta_1}$ axis of Figure 3.10) which are sampled only from this sub-volume. Subsequently, we search the sub-volume $\boldsymbol{\theta_2}$ (and compute their exact misfits with $\boldsymbol{j_1}$ fixed, e.g. yellow symbols on $\boldsymbol{\theta_2}$ axis of Figure 3.10) while we use the initialisation models sampled only from this sub-volume. It is the variation of $\boldsymbol{j_2}$ when sampling $\boldsymbol{\theta_1}$ in the red symbols that means these models cannot be used to initialize Serial-SHM. The above discussion can be easily extended to multiple dimensions.

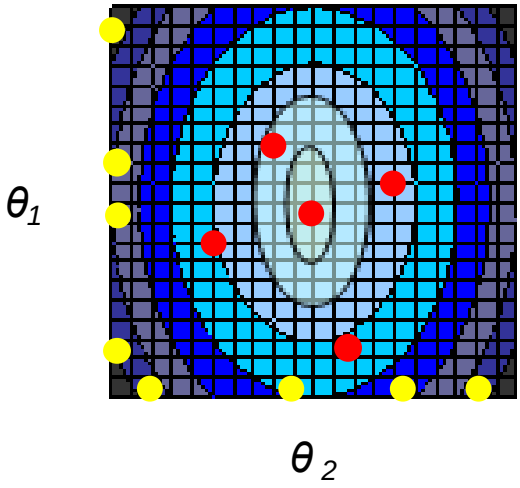

Figure 3.10: Example misfit surface of a 2D history matching case, where with orthogonality of parameters, red symbols indicate the initial models used to generate the proxy model and the subsequent Parallel-SHM search. Yellow symbols indicate the initialization of the Serial-SHM method.

The parallel approach necessitates a more accurate proxy model; otherwise, there is a possibility of not finding the minimum misfit, so the approach is not without constraint. The second order nature of the polynomial proxy can be expanded with additional, higher order terms or multiple interactions if the correlation to the true misfits is not high enough. The drawback here though is that more models are then required to determine the coefficient of the proxy model. The advantage of Serial-SHM approach over the Parallel-SHM is that it always (in each iteration) samples the parameter sub-domains based on evaluation of an exact sub-misfit. Conversely, some bias may occur as the approach is forced to start with some parameters set to the base case model and CPU time is effectively wasted as those parameters are unmodified. Therefore, this approach is used as a verification of the final results of application of the Parallel-SHM method.

Both approaches are based on 'divide and conquer' of the unknowns and are not restricted to the choice of inversion routine (i.e. NA). The strength of the approaches is that they reduce the number of models that are similar in terms of misfit response and efficiencies can be gained if other inversion methods are used. Stochastic approaches such as Genetic Algorithms or Simulated Annealing would all be made more efficient by splitting the parameter space. Similar benefits using deterministic methods could be achieved also. Gradient based methods require calculations of sensitivity coefficients, usually one per parameter is needed, and the computational requirement rises non-

linearly with the dimension of the problem. Solution of an adjoint equation or numerical calculation of gradients would be faster when sub-volumes of the parameter space are searched separately, and therefore the decoupling approach may provide some reduction in the workload.

The 'divide and conquer' approach is particularly useful for amalgamating the local effects of particular parameters on the time lapse seismic and well response. This is complimentary to the localization approaches used with the EnKF (e.g. Skjervheim et al. 2007, Chen and Oliver 2009), where more heuristic approximations are used. A similar approach could be adapted using the Parallel SHM method. The misfit of various wells and seismic data could be grouped spatially and then associated sub-volumes of the parameter space could be searched separately in parallel or in serial modes. For this purpose some knowledge of the localization is needed and appropriate spatial relationships are required. It may be more appropriate to use the method as shown here as it will find the spatial relationships implicitly.

3.2.5 Reducing the Number of Initial Models in the Parallel-SHM using Experimental Design

In the 'divide and conquer' approach, the initial ensemble of the models used in the full SHM inversion is utilized to derive the coefficients of the response surface. Initialisation of the quasi-global stochastic search routines such as the NA relies on quite a large ensemble of models. Typically the NA method requires $\mathbf{2}^{\boldsymbol{nd}}$ models, where $\boldsymbol{n_d}$ is the number of updating parameters (Sambridge 2000b). In Parallel-SHM there may be no need for so many models. However in the 'divide and conquer' approach we require an initial set of sample for constructing the proxy of the misfit function. Experimental designs samples the parameter space in a prearranged and efficient way and we need a smaller number of samples to provide information on the function dependency on the parameters (Box and Draper 1987, Myers 1999, Montgomery. 2000). We also use experimental design techniques with the 'divide and conquer' method.

The designs are conventional quadratic (second-order) in nature. Among these designs, the Central Composite design is often used. This is an embedded two level factorial or fractional factorial design with center points that are augmented with a group of 'star

points' in the centre of design space that allow estimation of curvature. The three-level full factorial design is another alternative second-order design used when the region is cuboidal, but it involves a very larger number of design points, typically $\mathbf{3}^{nd}$. When the number of parameters is high and thus is unaffordable. The Box-Behnken design is an important substitute to Central Composite design and is formed by combining two-level factorial designs with incomplete block designs. The Box-Behnken design reduces the number of required experiments by confounding higher order interactions. This reduction becomes more significant as the number of factors increases. The computer aided D-optimal design is another option and principally useful when the parameter space is irregular, i.e. when there are restrictions on the parameter space for some combinations of sample size. D-optimal designs are also more efficient than fractional factorial designs with respect to estimating model parameters for a specified number of runs. All these designs require only a few more experiments than two-level designs which involve in $\mathbf{2}^{nd}$ sampling points, and allow construction of more versatile and accurate models (see Sacks et al. 1989, Stienburg and Hunter 1984) (for more information on experimental designs refer to Section 2.11 of Chapter 2 and Appendix A).

The response surface model that is deployed in the 'divide and conquer' method is a multi-dimensional second order polynomial (see Equation 3.2). In the quadratic polynomial the number of coefficients grows with increasing number of the updated parameters or dimension of the problem. The number of coefficients is calculated using the relation of: $1+2.n_d+(n_d.(n_d-1))/2$, where n_d is the number of parameters. Similarly, in constructing the quadratic proxy model using experimental design, the required number of models increases rapidly when the number of the parameters increases as illustrated in Figure 3.11. However by using experimental design methods in high dimensional cases the required number of models is affordable, i.e. 772 models for a 20-dimensions by the Box-Behnken design. In fact the number of required models is small especially in comparison to what is required in conventional use of the NA, which is $\mathbf{2}^{nd}$ using quasi-random sampling.

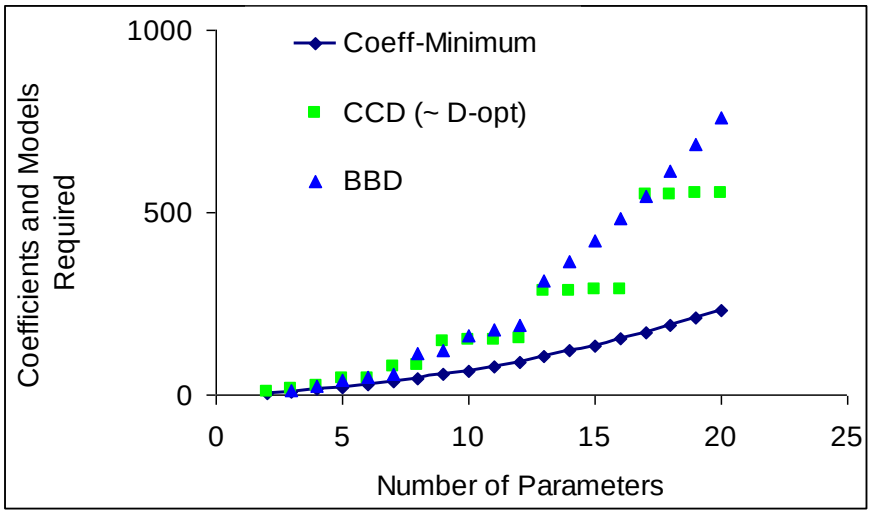

Figure 3.11: Minimum coefficients in the polynomial (Coeff-Minimum) and the number of models required as a function of increasing of the dimensionality of the problem using various experimental designs; Central Composite Design (CCD), Box-Behenken Design (BBD), and D-optima (D-opt). For depiction of the designs see Appendix A.

It is anticipated that by using conventional quadratic experimental designs, the proxy model of the misfit could be obtained with enough accuracy. Then other typical stages of 'divide and conquer' could be carried out as before giving an order of magnitude saving over random sampling. In Particular, when experimental designs are combined with the Parallel-SHM, the convergence to solution would be accomplished very quickly. The method is attractive for high dimensional problems involving many simulation runs.

3.2.6 Computer codes used to perform the various SHM methods of this thesis

In order to perform various methods of seismic history matching in this thesis that have been described in previous sections of this chapter several programs have been used. Reference of the authors of these computer codes are summarized in Table 3.1.

Table 3-1: Computer codes required to perform the various SHM methods of this thesis.

Routines	Authored by :
Neighbourihood Algorithm	Malcolm Sambridge Instructions on obtaining the latest version are available at http://rses.anu.edu.au/ malcolm/na/na.html. (for more details refer to: Sambridge, 1999a;1999b)
SHM including: parameterization, seismic and reservoir simulation control, and misfit calculation	Karl Stephen Contact: karl.stephen@pet.hw.ac.uk (for more details refer to: Stephen et al., 2006 and 'Seismic History Matching Project Code Documentation')
multidimensional regression singular value decomposition	Press et al. Numerical Recipes in FORTRAN, the Art of Scientific Computing, 2002
parameter space division and misfit decomposition	Farzaneh Sedighi Contact: farzaneh.sedighi@pet.hw.ac.uk
experimental design library	Farzaneh Sedighi Using: Matlab7.0.1 Statistical Toolbox and Design-Expert 8.0.3 softwares (for more details see Appendix A and Help Manual of Matlab program)
parallelising Neighbourihood Algorithm	Karl Stephen Contact: karl.stephen@pet.hw.ac.uk

3.2.7 Progression of the 'Divide and Conquer' Approach

Reduction of the number of simulation runs based on independent objective functions in the automatic history matching process has been examined by Maschio and Schiozer (2008) in a different way. They first defined several low dimensional independent objective functions each related to a well in the reservoir instead of a combined objective function. Then horizontal and vertical permeability parameters associated to each well were updated in a serial fashion. Sensitivity analyses showed that the parameters associated to each well influenced the misfit of other wells by less than ten per cent influence. The problem was then treated as a set of independent problems, one for each well. However, these criteria seemed to be unsuccessful in the total field production history matching. In our approach we are able to determine more effectively how the parameter sub-spaces can be identified, retaining parameter interactions where necessary.

Ding et al. (2010), and Ding and McKee (2011) proposed a similar method and have also demonstrated that in history matching, the objective function could be separated into local components related to the wells and/or the seismic zones where a local component generally depends on a smaller number of principal parameters. They explained that the partial separability of the objective function helped with computation of derivatives with a smaller number of reservoir simulations for the gradient-based optimization methods. However, we deem that the number of parameters may not be small even in regional or well level history matching. In order to simplify the problem, it is always important to investigate the possibility of separability of the parameter space.

Many reservoir engineering studies have reported the application of the response surface modelling for various purposes: i) uncertainty analysis of reservoir performance (Friedmann et al. 2003), ii) well scheme optimization (Zabalza et al. 2000, Landa et al. 2003), and iii) history matching (Edie et al. 1994, White et al. 2003). In such studies response surfaces are usually constructed with polynomial regression techniques (Chu 1990, Egeland et al. 1992, Damsleth et al. 1992, Jourdan and Zabalza-Mezghani 2004). In these circumstances, the proxy models are used as a representative of the simulator key outputs. In the methods of this thesis however the aim is identification of the individual groups of interacting parameters. In one sense we are setting our sights lower but on the other hand, we retain more of the variability of the system while still

significantly simplifying the inversion problem. In that way the method is more flexible. Besides, the set of problems where parameters can be removed from the system is probably a subset of those where a separation of groups can be found. Apart from that the approaches we use potentially allow us to remove unimportant parameters if possible.

The concept of 'divide and conquer' has been developed primarily from various industrial design problems especially where the co-evolutionary routines are applied with a great degree of success to high dimension optimization. Potter (1995) suggested that even more gain from co-evolutionary methods attained in high dimension problems which lied in the ability to apply divide-and-conquer strategies. That is, the variables in the original problem were decomposed into a number of subsets. Subsequently basis functions that handle each subset of variables independently were evolved and optimized simultaneously to locate the optima of the original problem. Since this type of evolutionary search was based on divide-and-conquer paradigm it was possible to circumvent the 'curse of dimensionality'.

Ong et al. (2002) proposed a surrogate-assisted co-evolutionary procedure using a Genetic Algorithm (GA) in a parallel mode. The method was based on dividing variables among multiple basis functions constructed using Radial Base Function (RBF) approximation. The method was conducted initially on a series of 20-variable functions having many local minima but only one global minimum and for various degrees of variable interactions. The approach converged close to the global minimum significantly quicker in comparison to the standard GA. An undesirable result was that strong interactions between the variables could lead to significant degradation of the convergence result (Potter 1997).

Egorov et al. (2002) utilized an algorithm which was based on approximation of the objective function and involved identification of non-linear dependencies of the variables. Also each iteration included a corrective construction of the approximate function and compared that to the real simulation. Then Pierret (2005) applied analogous technique which combined the use of GA and the radial basis function interpolation. From one perspective, the method of 'divide and conquer' of this thesis benefits in a similar way to deal with the complications that exist in solving a high dimensional history matching problems.

Arwini and Stephen (2010) verified that the proxy model was of limited use to replace the prediction close to minima; the location of minima was different in the proxy model compared to what was obtained by conventional use of the NA routine. Zubarev (2009) also concluded that the proxy models are successful for estimating objective function values for test datasets; however they failed to predict that the global minimum could be found by a stochastic algorithm. Our aim in this study is that we should not use the proxy model explicitly because, in our case, such an approach would lead to bias close to the global minimum in the misfit. For this reason we cannot search the proxy space directly. Instead we use it as a guide in the identification of decoupled parameter groups and also in the calculation part of the misfit related to the divided groups. We barely avoid unnecessary sampling in the inversion process and thus would speed up history matching.

We will show that the 'divide and conquer' approach is very successful when applied to the several high dimensional seismic history matching studies of the Schiehallion field where transmissibility of barriers are the dominant parameters along with permeability and net:gross. The entire parameter space of these cases could be decoupled into sub-volumes of lower dimensions and faster convergence in history matching process was achieved and the required number of models was smaller relative to the full SHM method.

3.3 Closing Review

The process of Seismic History Matching (SHM) of this thesis is an effort to merging the benefits of both production and 4D information to improve estimates of the reservoir model parameters. The SHM method and several challenges of this process which have been investigated were discussed. A major challenge is that the computational cost of history matching is high if a large number of parameters are updated and especially when it is assumed that they are interacting. The method of 'divide and conquer' of the unknowns is a new approach for efficient sampling of parameter space based on identification of insignificant interactions between model parameters and subdivision of the decoupled parameter space thus to make the problem straightforward. The proposed 'divide and conquer' method is an innovation to the usual SHM practice.

Basic concepts supporting the development of the method was explained in this chapter. In this approach first a numerical or analytical representation of a high dimensional misfit function is expanded so that it can be split into sub-misfit functions of fewer independent parameters. Two search methods of the parameter sub-domains including Parallel-SHM and Serial-SHM were then established. Also, in order to reduce the number of required ensemble models, an approach of integrating experimental design techniques with the Parallel-SHM method was described.

CHAPTER 4 Application of 'Divide and Conquer' Method to Seismic History Matching of Schiehallion Field

Introduction

This chapter represents the application of the 'divide and conquer' method to the Schiehallion field. Seismic History Matching (SHM) using the Neighbourhood Algorithm (NA) has been applied to the Schiehallion field (Stephen et al. 2006, Stephen and MacBeth 2008, Edris et al. 2008) previously. These studies showed that in the Schiehallion field, the transmissibility of flow barriers affects the fluid movement across the reservoir in a non-local manner. In such circumstances a group of the parameters updated during history matching may have a non-coupled impact (relative to other parameters groups) on the misfit objective function. Therefore, in this thesis it is sought to determine whether one can ignore interactions between certain reservoir model parameters in order to divide the parameter space into several lower dimensional sub-volumes. History matching would then be much more efficient leading to convergence by saving simulation runs and computation time.

This chapter is therefore laid out to show first the parameter sub-volume identification, following by the application of the parallel version of the NA routine for searching the decoupled sub-volumes. This method is called "Parallel-SHM". Also the NA approach is used to search each sub-volume sequentially, which is called the "Serial-SHM" method. Both techniques are compared against the usual SHM procedure which is referred to as "Full-SHM" since decomposition is not used and full interaction is assumed (see Chapter 3 for methods). It is shown that the Parallel-SHM can be applied to a 10-dimensional case of the Schiehallion field. The chapter begins with a case using the Schiehallion model to match the observed data from the field and proceed also with a synthetic case of this field. A simpler synthetic model is used to show an example of limitations of the method.

It is revealed that convergence was achieved very quickly requiring 30 per cent of the total number of models required for a Full-SHM. Application of the Serial-SHM improved convergence by using 40 per cent of the number of models required for Full-SHM. However this approach required about one and half times more models compared to the parallel method. The 'divide and conquer' approach is certainly very useful for history matching problems of many unknowns.

4.1 Schiehallion Field

The Schiehallion field is situated on the UK Continental Shelf (UKCS), to the west of Shetland. The Schiehallion Paleocene turbidite reservoir sands lie at a depth of 1800–2064 m. The Schiehallion depositional environment is interpreted as a submarine slope channel system, with structural dip of 2–3° to the northwest, crossed by a series of east–west faults dividing the field into four structural segments, labeled 1 to 4 as shown on Figure 4.1a. About two hundred of such faults and barriers were mapped from seismic data across the whole Schiehallion field (Macdonald et al. 2004) (see Figure 4.1b). They are shown on the reservoir Full Field Model (provided by operator) as in Figure 4.1c. Most of the mapped oil in place is contained in Segment 1 and Segment 4 (see Figure 4.1c and d). The degree of connectivity across the faults between these two segments is uncertain on a production timescale. However, in 1996, wells drilled in Segment 1 encountered depletion whereas wells in Segment 4 were not depleted, suggesting that the connectivity between the two segments is limited. More details on the Schiehallion field can be found in the works by Leach et al. 1999, Macdonald et al. 2004, Fletcher et al. 2005, Soldo 2004, Miranda 2007, and Edris 2009.

To reduce the CPU time and the number of variables that may need to be varied for such a large model in this study, we needed to focus on a smaller independent reservoir sector of the FFM. Thus, the reservoir of sand layer of the area of Segment 4 was extracted and selected for Seismic History Matching and verifying the application of 'Divide and Conquer' method of this thesis.

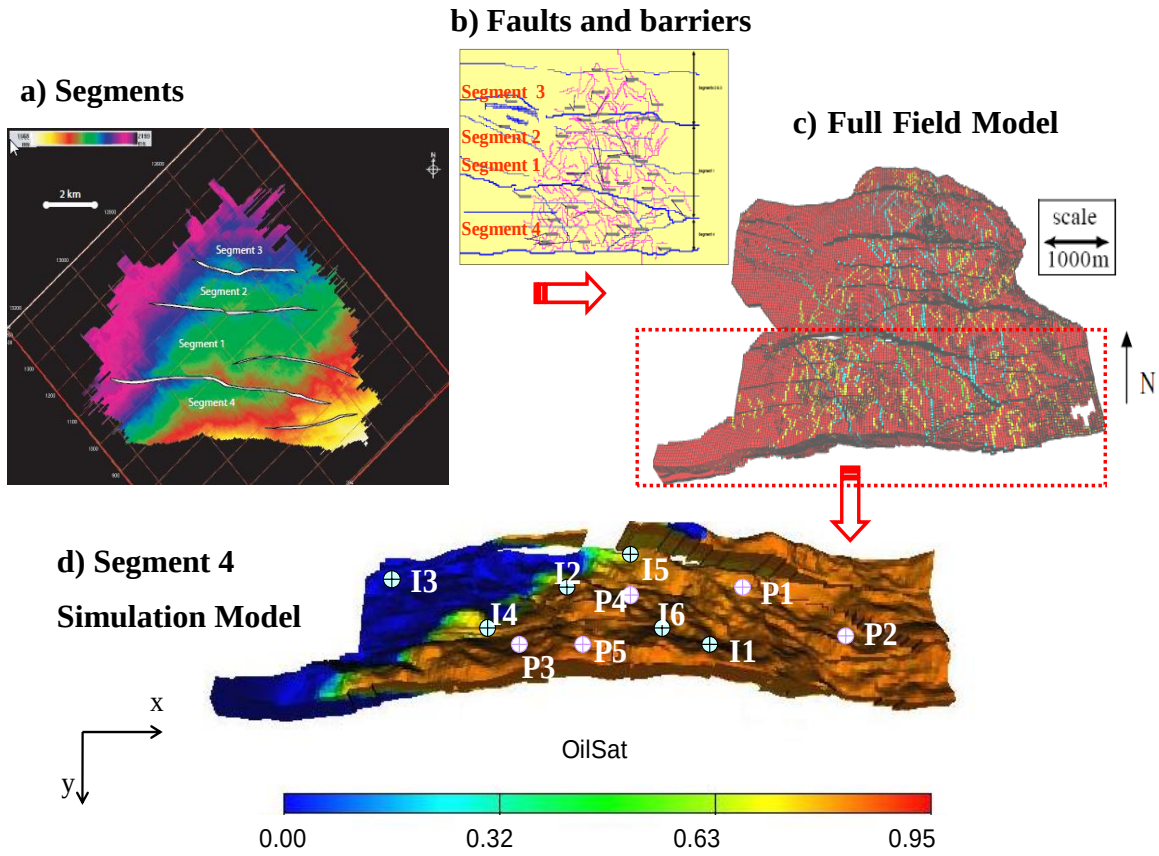

Figure 4.1: Schiehallion field top-view picture showing: a) the segments, b) the faults and barriers, c) the location of the extracted Segment 4 in the Full Field Model, and d) the reservoir simulation model of Segment.

4.1.1 Segment 4 Characteristics

Segment 4 is enclosed on three sides by faults and pinches out on the fourth side (see Figure 4.1c and d). At initial conditions the oil in the segment had the density in the range of 55.37-57.32 lb/cf and with the high viscosity ranging from 1.5-4.5 centipoise. The initial reservoir pressure was 2907 psia at a datum depth of 6365 ft TVDss, which is close to reservoir oil bubble point and the typical values for the gas-oil ratio (GOR) are 342 scf/bbl. Reservoir quality varies in character from thinly interbedded sands to substantial sands (Lancaster et al. 2000), which are of better quality. The porosity of Segment 4 sands lies between 27-29% while permeability varies from 10 to 2000 mD. It has been estimated that gas has come out of solution in some areas of the reservoir particularly early on in the field life. Sub-vertical water injectors were employed in the reservoir to prevent significant gas breakout via reservoir pressure maintenance, and to deliver reservoir sweep. However, the effective use of the water flood demands a high level of connectivity between injectors and producers in the reservoir. This is a

significant issue in a reservoir that is inherently heterogeneous. The segment has been producing since August 1998 and has continued up to the present. However in this thesis, the focus is on the history period up to 2004. In the reservoir a total of eleven wells, six injectors and five producers, were completed in the sandstone sequence in this period and several seismic surveys have been acquired on the field (preproduction baselines in 1993 and 1996, as well as monitor surveys in 1999, 2000, 2002, and 2004).

In this chapter the period of history matching considered ran from the start of production in August 1998 up to August 2000. For this period, the 4D seismic data was obtained from the baseline seismic acquired in 1993, while monitor surveys were acquired after one and two years of production, i.e. in early September 1999 and in late August 2000. The seismic dataset measured the P-waves of seismic volumes. The process of cross-equalization, calibration and transformation of migrated stack was performed by the operators and by a combination of phase rotation and filtering the coloured inversion stack was derived. By time-to-depth conversion, the location of the reservoir horizons were provided by the operator also and used to generate maps of Root Mean Square (RMS) attributes from the migrated stack by integrating the signal over a suitable time window. Then, the pre-production RMS attributes were mapped to net:gross (NTG), given the almost uniform porosity of the sand (Stephen et al. 2006). 4D seismic data were obtained using differences of the RMS attributes of the migrated stack. These attributes were used as a pseudo-impedance to detect pressure and saturation effects via the time-lapse seismic map of differences between the surveys as shown in Figure 4.2b. The attribute maps are normalised to the baseline by subtracting the mean and dividing by its standard deviation (refer to Equation 3.8 of Chapter 3), to gain a comparable change in magnitude and signs between surveys.

Based on seismic attribute analysis, the producers were drilled in the core of the reservoir channels where high pay properties were expected. The injectors were not placed in the same channels in order to avoid early water breakthrough and so maximize sweep. In the history period from 1998 to 2000, in total 6 wells including 3 horizontal producers and 3 near-vertical injectors, have been active in Segment 4. They are named in Table 4.1. The locations of the wells are shown in the 4D seismic map of 1993-1999 in Figure 4.2b. Initially the reservoir management strategy was mainly aimed at gas supervision and pressure maintenance to prevent gas releasing from oil. The oil production and water injection data of active wells are shown in Figures 4.2a and 4.2c.

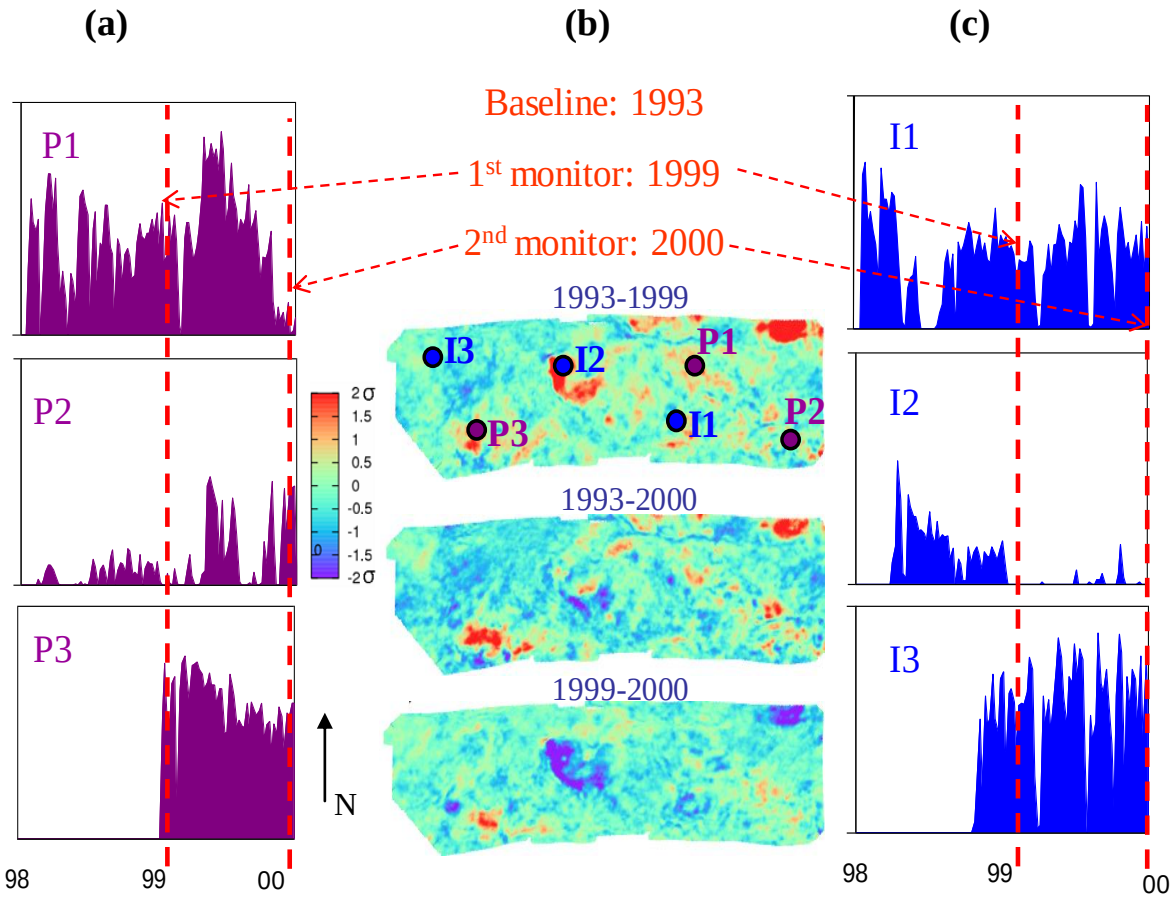

Figure 4.2: Observed data for the history period from 1998 to 2000 which include: a) production rates, b) maps of change in pseudo-impedance, and c) injection rates. The 4D signatures are normalised by subtracting the mean of the pre-production map (1993) and dividing by its standard deviation, and differences are presented in this scale. The colour bar is the same for all maps and is in units of the standard deviation. Changes in acoustic impedance indicate a pressure up signal around injector I2 in the first year, map 1993-1999. Injection stopped at that time and negligible net change is shown over two years, map of 1993-2000. The drop in pressure is seen between years 1 and 2, map of 1999-2000. Red indicates pressure up or gas exsolving which is a drop in impedance in map of 1993-1999, while blue indicates draw down or water injection which is an increase in impedance in map 1999-2000.

Table 4-1: List of active wells in Segment 4 for the history period starting from August 1998 up to August 2000 (see Figure 4.2 for location of wells).

Well		
Name	**Type**	**Active since**
P1	Producer	August 1998
P2	Producer	August 1998
P3	Producer	July 1999
I1	Injector	August 1998
I2	Injector	November 1998
I3	Injector	July 1999

In the sector the reservoir rocks are acoustically softer than the overlying shale. The contrast increases if something occurs to make the rocks softer, i.e. impedance decreases. When the reservoir pressure decreases the gas comes out from solution. On the other hand a compressible fluid into the pore space introduced by the gas free from solution causes an increase in the pore pressure (nearby) and consequently reduces the net effective stress on the rock frame. That makes the matrix softer and significantly reduces the overall fluid hardness. A reverse process leads to the opposite effect because of resolution of gas and an increase in pressure. A hardening effect occurs for reservoir rocks due to water injection because the compressibility of the hydrocarbon is higher than the water, but when water injection leads to significant increase in the pore pressure of reservoir sand, then the rocks become softer and the acoustic impedance will decrease (Marsh 2004). Therefore, an increase in the reservoir pressure results in the opposite effect compared to the increase in the water saturation by water injection. In Schiehallion, an increase in pressure of 500 psi could reduce the change of the acoustic impedance due to water replacement by half of the change from water alone. Also an increase in reservoir pressure of 1000 psi or more could completely mask the change in acoustic impedance due to water flood (Floricich 2006).

We can see from Figure 4.2b that there is a clear relationship between the well activities and the seismic response and reservoir behaviour. For example the main signal in the 4D seismic maps (difference in pseudo-impedance) is because of the injector I2 which is enclosed by flow barriers and baffles. In Figure 4.2b, in the first year, the softening

around injector I2 in the 4D signature map of 1993-1999, which is due to the activity of well pressuring up and injecting water. Then in the second year, the injector I2 is switched off and the reservoir pressure relaxes back to the equilibrium (Saxby 2001). Hardening occurs therefore around the injector, which is observable in the 4D signature seismic map of 1999-2000. The region around the injector I2 is important however as an infill well was added nearby in December 2001 and the injector turned out to be surrounded by barriers. The aim in this chapter is to match this strong seismic anomaly along with the injection rate for the well while we are adjusting the transmissibility of the barriers.

In the 4D signature maps of Figure 4.2b, there is also a less obvious signal for injector I1 and a quite small signal for injector I3. We see also some of the effects of two years of production near producers P1, P2 and P3. A slight increase in the velocities due to injector activities indicates that the reservoir sand sequence has more sensitivity to changes in pressure than changes in the fluid saturation. Moreover, there are two anomalies which cannot be explained in terms of production activities whose magnitude are comparable with the time-lapse seismic signal around injector I2. The anomaly close to producer P3 possibly may be caused by some shadowing production effect in the upper sandstones sequence (Soldo 2005). That is production from the upper sequence may be the origin of the 4D signature in the area, since depletion generates a release of gas that could create a shadow detectable in time-lapse seismic interpretation. Picking the horizons incorrectly may also cause the same effects (for more details see Castagna et al. 2003, Al-Maskeri et al. 2003, Soldo 2005). Also the anomaly observable to the northeast of the 4D signature map is related to well activity in Segment 1. This anomaly is located beyond the sealing fault that separates Segment 4 from the Segment 1 and no activity would be simulated to the north of this fault. As a consequence these effects can not be captured during this thesis.

By visual interpretation of maps of 4D seismic differences (Figure 4.2b), it has been recognized that there is clearly a high degree of compartmentalisation and heterogeneity, perhaps due to a combination of faulting and channelization in the reservoir (for more details, see Stephen et al. 2006). In particular the main 4D seismic anomaly around the injector I2 data have assisted in locally identifying the existence of a number of barriers and faults that affect the sweep efficiency of the area. Figure 4.3 illustrates the location of identified barriers and baffles (10 barriers labeled ‘a’ to ‘j’).

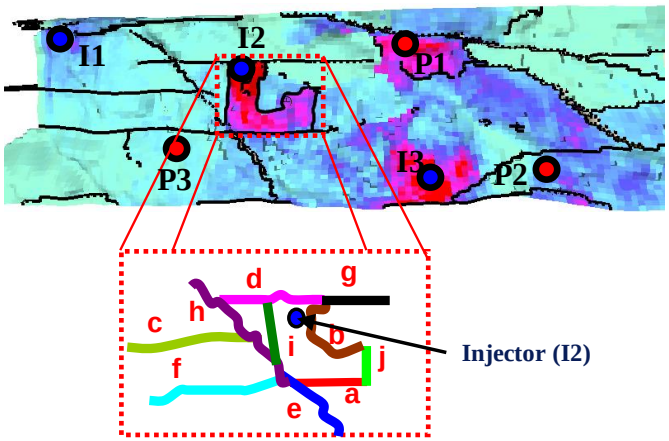

Figure 4.3: The transmissibility of 10 barriers around the injector I2 that were updated to improve the prediction of the seismic anomaly around that well in the seismic history matching in this study.

These barriers in the region close to injector I2 have resulted in poor well performance (Leach et al. 1999). Although, the barrier transmissibilities may be estimated from the geological model properties using the Shale Gouge Ratio (Manzocchi et al. 1999), they are inevitably highly uncertain or sometimes unknown because relationships between observed barrier permeabilities and shale content show order-of magnitude variations. Estimated transmissibilities are therefore useful starting points for history matching particularly when time-lapse seismic data are available.

4.1.2 Segment 4 Simulation Model

The Full Field Model (FFM) of the Schiehallion reservoir was constructed by the field operator using typical approaches where facies objects and static flow properties such as porosity and permeability were distributed stochastically. The Segment 4 reservoir model was extracted from the FFM and was then upscaled vertically by a factor of 4 giving 8 layers of sand and reducing the simulation run time. For history up to 2000, each Segment 4 simulation takes around 34 minutes while the upscaled simulation model takes around 8 minutes on 3.4 GHz processor. If we include six years of production up to 2004, then the simulation time will be about 140 minutes but only twenty minutes for the upscaled model. The upscaled Segment 4 model consisted of 146 × 44 × 8 grid cells. In total the model consisted of 51392 active cells typically measuring 100 × 100 × 6 m. The segment was four cells thick vertically in many parts, but to the East side of the model, it extended to eight cells in the aquifer.

In the model, the wells were completed in the sandstone sequence in the interval corresponding to the FFM model and the well controls were set to oil rate for producers and water rate for injectors. The barriers and baffles have been represented vertically, in a simulation k-direction, and by discretising areally, so that they stair-step through the simulation grid at the top of the reservoir. In the base case, the transmissibility multipliers of 10 barriers (Figure 4.3) that we updated were set to 0.001. Although, it is risky to justify a barrier addition without cross checking 3D seismic for any evidence, a new barrier was added to satisfy the 4D seismic signatures in the reservoir model (for more details refer to Edris 2009). This barrier (labeled 'i' in Figure 4.3) reduces the seismic misfit of the base case model and the existence of that barrier has been confirmed by the field operator.

In the following SHM application, the reservoir history period that we focused on ran from 1st August 1998 up to the 27th August 2000. The base case simulation of Segment 4 was run for this period (two years) and the oil production and water injection of wells was predicted. A petro-elastic transform (for more details see Chapter 2 and 3) was used to convert the outputs (saturation and pressure) of the simulation run to predicted seismic properties (for the parameters used in petro-elastic modelling, see Stephen et al. 2006c, Edris 2009). Maps of acoustic impedance were predicted pre-production, and at the time of the monitor seismic surveys in August 1999 and August 2000. Figure 4.4 shows the base reservoir simulation model predictions of the pressure, water saturation and gas saturation for the initial pre-production conditions and for 2000. The base model well and 4D seismic maps predictions are shown in Figures 4.5. and 4.6, respectively.

We can see that for most of the wells the history data (up to 2000) were well matched in the base case model but not for the injector I2 (see Figure 4.5). Besides, in the predicted seismic maps 1993-1999 and 1999-2000 (see Figure 4.6); we can see that the base simulation model allowed pressure leakage to extend in some distance from the injector I2. Thus the match to 4D seismic data was not attained.

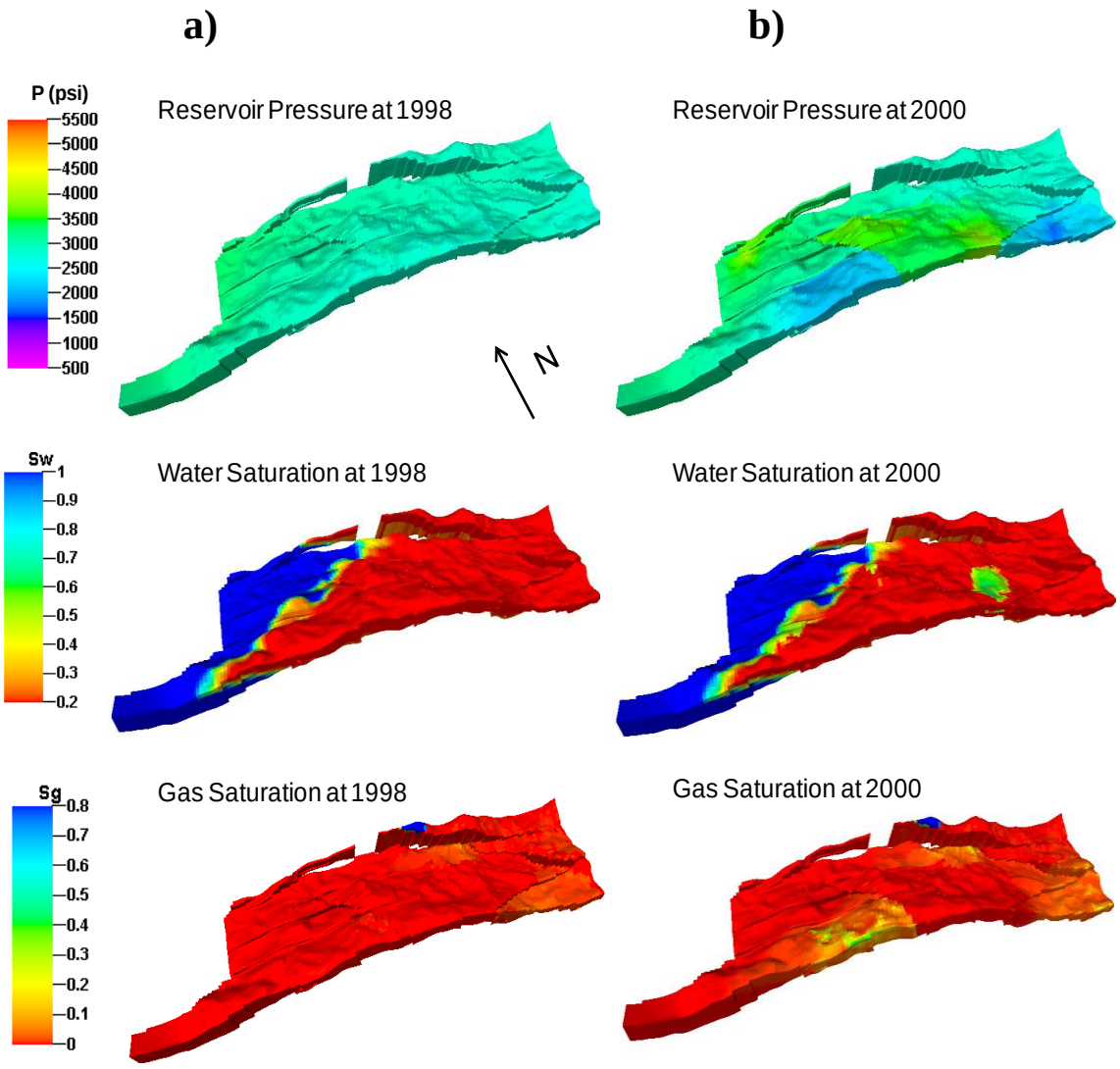

Figure 4.4: Pressure, water and gas saturation from the base case simulation model for: a) the initial pre-production conditions, and b) after two years production in 2000.

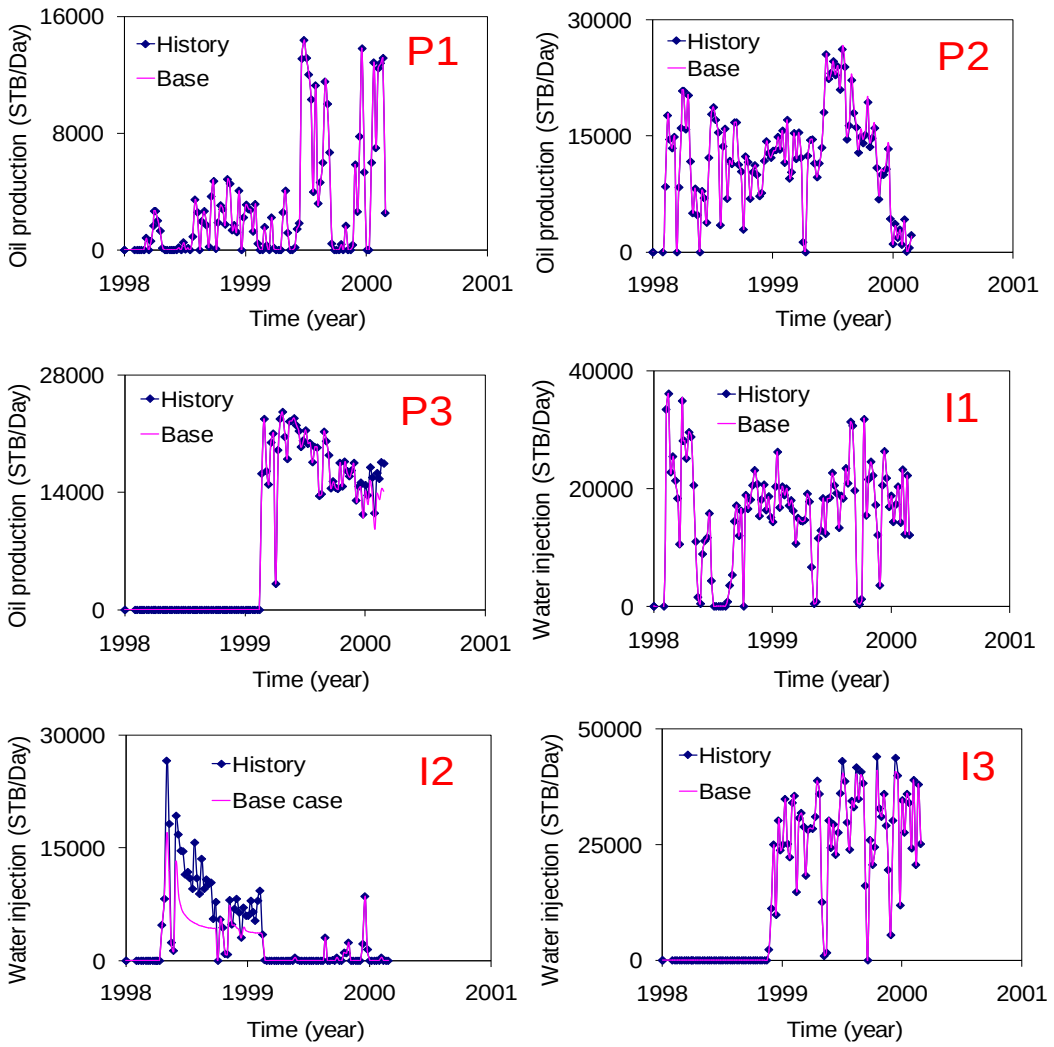

Figure 4.5: The base case simulation model predictions compared to well history data.

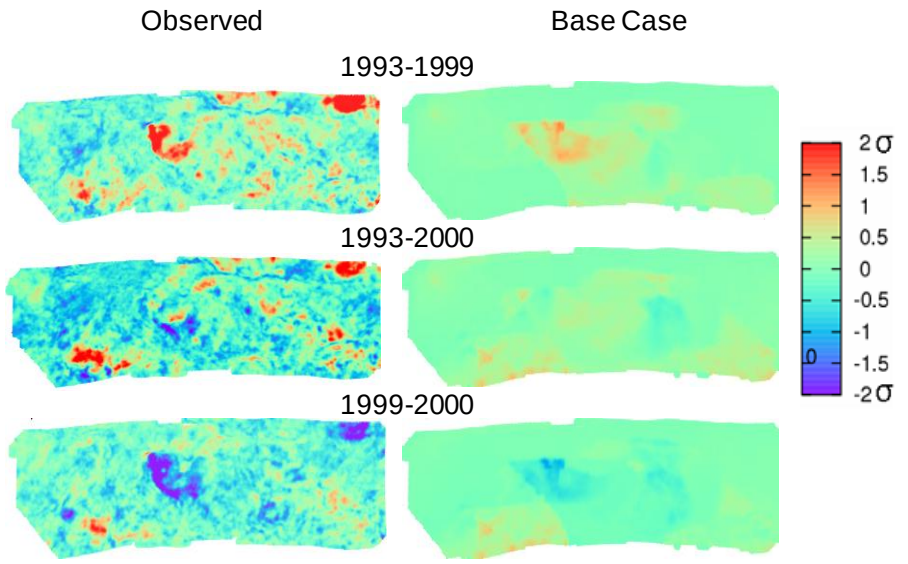

Figure 4.6: The base case simulation model predictions for 4D seismic maps of differences in impedance.

4.2 Application of the 'Divide and Conquer' Approach

Application of Seismic History Matching to the Segment 4 of the Schiehallion field has been presented previously (see Stephen et al. 2006, Stephen and MacBeth 2008, Edris et al. 2008). In this thesis the effectiveness of the 'divide and conquer' approach including Parallel-SHM and Serial-SHM methods, is investigated. Also the methods are compared against Full-SHM method of previous work.

To perform history matching, it was necessary to define a parameter space. In this case, we selected 10 barriers around the injector I2 (see Figure 4.3) as the most important parameters. The barriers consisted of a combination of faults and near vertical (on this scale) shale drapes. All were therefore modelled as transmissibility multipliers using the simulator's "Faults" keyword (Eclipse 100 Manual 2007) for pragmatism. The transmissibility multipliers of the barriers were modified by a second modifier parameter. The limits of these modifiers are listed in Table 4.2, and they were sampled on a $\log_{10}$ scale in history matching process, i.e. if the modifier parameter is 0.0 (on $\log_{10}$ scale), then there is no change from the base case model. We used this scale so that there is equal likelihood of sampling for reduced transmissibility than increasing it for a modifier range of 0.1 to 10.

Table 4-2: Ranges and mid value of parameters on a $\log_{10}$ scale. The base case is represented by a modifying factor of 1 on the linear scale (i.e. zero on the $\log_{10}$ scale).

modifier of barrier*	Min.	Mid.	Max.
a	-2	-0.5	1
b	-2	-0.5	1
c	-2	-0.5	1
d	-2	-0.5	1
e	1	0.5	2
f	0	1.5	3
g	-1	0.5	2
h	0	1.5	3
i	-2	-0.5	1
j	-1	0.5	2

**** The barriers are shown in Figure 4.3***

The limits of the multiplier values of barriers were assumed while the maximum values were chosen to be three orders of magnitude higher than their minimum values (on linear scale). Since the prior uncertainties of transmissibility multipliers of barriers are unknown, their parameter probability was assumed to be of a uniform distribution within the limits which means that in a Bayesian framework the prior parameter term (refer to Equation 2.4 of Chapter 2) can be ignored.

Initially, we investigated how the barriers control the mismatch between predicted and observed well data. For producers the misfit of 'oil rate' and for injectors the misfit of 'water rate' were calculated for a number of models (1024) while we perturbed the modifiers of the barriers using quasi-random sampling. We identified that since the active production and injection wells in the reservoir, and hence in the simulation model, are located remotely from the injector I2, their mean misfits and the variation of the misfits are not large (see Table 4.3). The mean misfit value and the variation of the misfit for producers P2 and injector I3 was zero. These values were also small for produces P1 and P3, and injector I3. Thus, the data of these wells were not included in the misfit evaluation of history matching in this chapter. The injector I2 switches to pressure control, however, when the compartment pressures up too much, and thus it would be a source of misfit for injector I2 which could be zero, otherwise. Hence, in addition to the 4D seismic data, the injection rate was also included in the misfit evaluation in a case.

Table 4-3: Sensitivity of oil production and water injection rate of misfit of wells to parameter perturbations.

Well	mean misfit and variation in the misfit of producers and injectors*	
	Mean	**Standard deviation**
P1	221	0.2
P2	0.2	1.4E-16
P3	117	3.6
I1	0.0	0.0
I2	23988	53.2
I3	558	2.7

1024 models were used in the calculation of mean and standard deviation of misfits.

Therefore, in this study two misfit scenarios were considered: a) the 'total 4D seismic data only' was used; i.e. the changes of impedance over the first, second and first two years of production against the equivalent time differences in the observed 4D seismic attribute were compared in history matching, and b) the '4D seismic plus injector data' where the injector misfit was also calculated. In the case of integrating of both seismic and injector data, the total misfit is calculated as:

$$J_T = W.J_S + (1-W).J_P \quad (4.1)$$

Where J_T, J_S and J_P are total, seismic and injector objective functions, respectively, and are calculated using Equation 2.3 (refer to Chapter 2), and W is the weighting factor between seismic and injector misfits. Choosing the proper weighting factor is not a straight forward task. This factor should be investigated in relation to the accuracy of the data. In this thesis, equal weights were considered for seismic and injector data. They were considered to be similar to the previous study (Edris 2009), so the total misfit was:

$$J_T = J_S + J_P \quad (4.2)$$

During history matching, once the flow simulation model results were obtained, using the saturation and pressure outputs at initial reservoir condition and at the time steps corresponding to the time of seismic monitors, the seismic impedances for each Colum of simulation cells were predicted. The simulated impedances were calculated through petro-elastic modelling (see Chapter 2) and using the elastic parameters of reservoir rock. Then vertical upscaling (Backus 1962) and areal downscaling (Equations 3.2 and 3.6, Chapter 3) were applied to map the simulated impedances into the observed grid cells (seismic bins), and to bridge the gap between the simulated and observed seismic scales. After this step we were able to compare simulated and observed impedances. The aim of 'divide and conquer' is to establish a speed up in the convergence rate of history matching and we principally focused on examining this new developed approach. In the case studies of this thesis, the modelling errors are ignored and thus are not included in the misfit objective function.

In the misfit calculation we need to include a covariance matrix due to correlated random error in the observed data. The covariance matrix provides weighting factors to scale observations of different type, according to data. The seismic data error for the Schiehallion has been studied previously (Soldo 2005, Edris 2009). In that study the pseudo-impedance attributes of each individual survey and their corresponding differences were analysed assuming that the covariance behavior can be represented as a function of a semi-variogram lag distance between traces in the two main seismic acquisition directions of inline and crossline (see Figure 4.7). The analyses concluded that at the simulation grid scale, the seismic covariance matrix could be represented as σI, where σ is the standard deviation of estimated noise of each map, and I is the identity matrix (for more details see Soldo 2005). A similar approach has been examined by Gosselin et al. (2003). Also, in this thesis, it was assume that there is the same level of data error in Phase II seismic data.

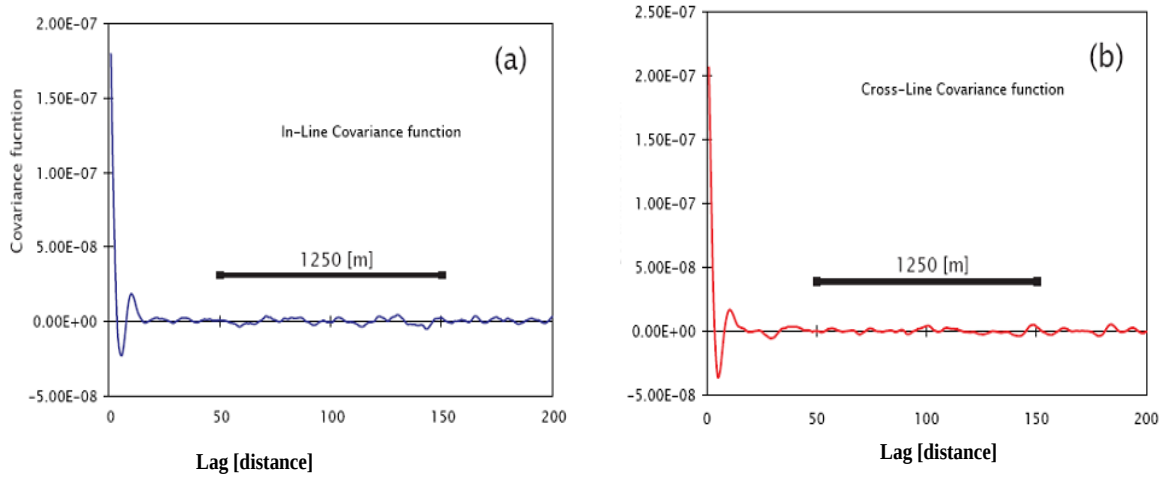

Figure 4.7: Covariance functions for seismic data error: a) in the inline direction, and b) in the crossline direction. The stationary state is reached at a distance corresponding to lag = 5 (62.5 m) which is smaller than simulation grid scale (100 m) (after Soldo 2005).

The covariance of the production data was also represented as a function of time lag in Figure 4.8. This Figure (as it is presented in the original reference, Edris 2009) do not show the zero lag information, although what is more important here is the structure of the changing of the covariance data error (i.e. vertical-axis on Figure 4.8) with time lag (horizontal-axis on Figure 4.8), which is showing production/injection rate

measurements contain uncorrelated errors. In fact, the covariance function demonstrated no evidence of correlation trend over time, and exhibited an irregular fluctuating and did not reach to a stationary. Yet if we interpreted a correlation for up to one lag, i.e. one week (see Figure 4.8), since the time steps in the reservoir production/injection data is one week, the data error was concluded to be uncorrelated (for more details see Edris 2009). Consequently, for both seismic and injector data, uncorrelated Gaussian errors were deployed.

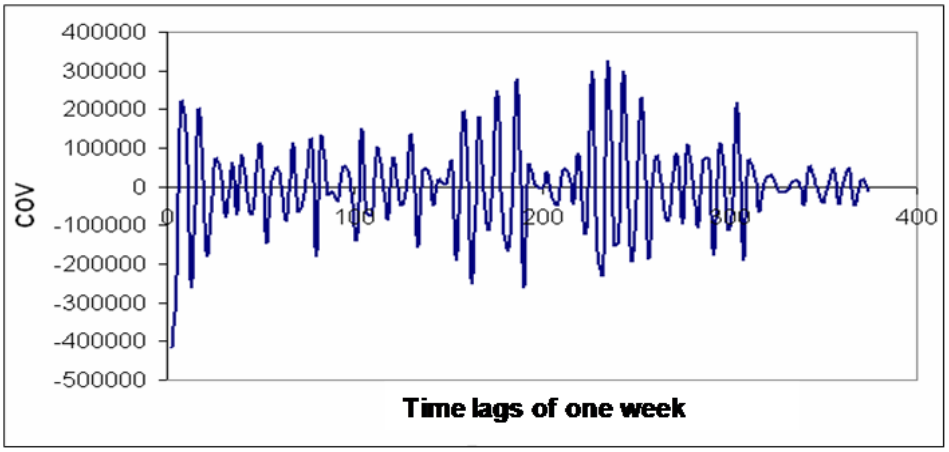

Figure 4.8: Covariance function for data error in the production and injection rates is shown for 400 lag where each time lag corresponding to one week.

The standard deviation of observed production/injection data was evaluated using the wavelet decomposition filter (for details see Edris 2009). The whole observed data set, which included the bottomhole pressure and GOR (Gas oil ratio), was used to define the right level of noise extraction and to characterise the truth signal. Subsequently the statistics of standard deviation of production data error was evaluated. Also, the power spectrum decomposition was used to filter the noise from raw seismic attributes (RMS amplitude). Then by inspecting the power spectrum of the raw and noise-free seismic data the standard deviation of each seismic map (observed pseudo-impedance) was estimated (for details see Soldo 2005). The standard deviations of relevant data are presented in Table 4.4. They were included as the weights specified as the inverse of the square of the standard deviation of the 'noise in the data' within their equivalent misfit calculation.

Table 4-4: The data error of water rate of injector I2 and 4D seismic data.

Data	Standard Deviation
Injector I2	63.2
4D Seismic 1999-1993	2.89
4D Seismic 2000-1993	3.36
4D Seismic 2000-1999	3.19

A prior sensitivity analysis was conducted in order to evaluate the influence of the transmissibility modifiers in the misfit function through a 'one parameter change at a time' investigation. The parameter values were varied in the interval of [-3,3] in $\log_{10}$ scale. Some parameters showed more influence on the misfit than others. For both scenarios mentioned earlier the sensitivity of the misfit to parameter changes are shown in Figure 4.9.

a) Sensitivity analysis for the total seismic misfit

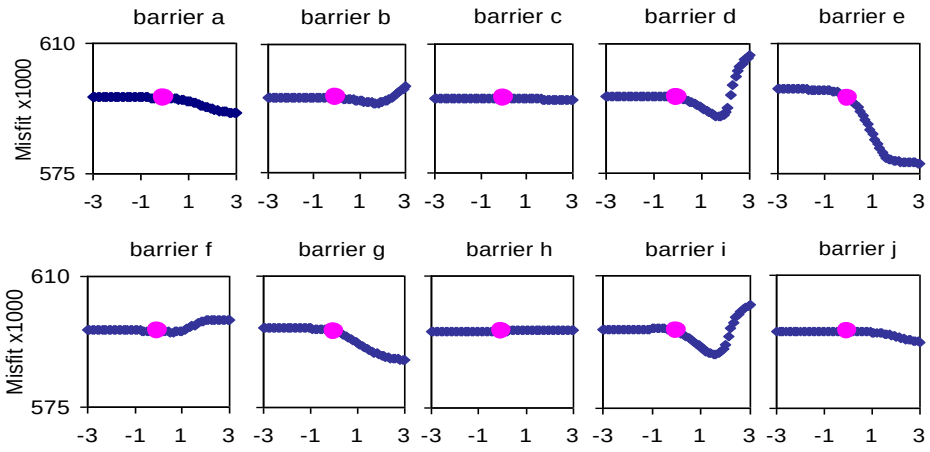

b) Sensitivity analysis for injector misfit

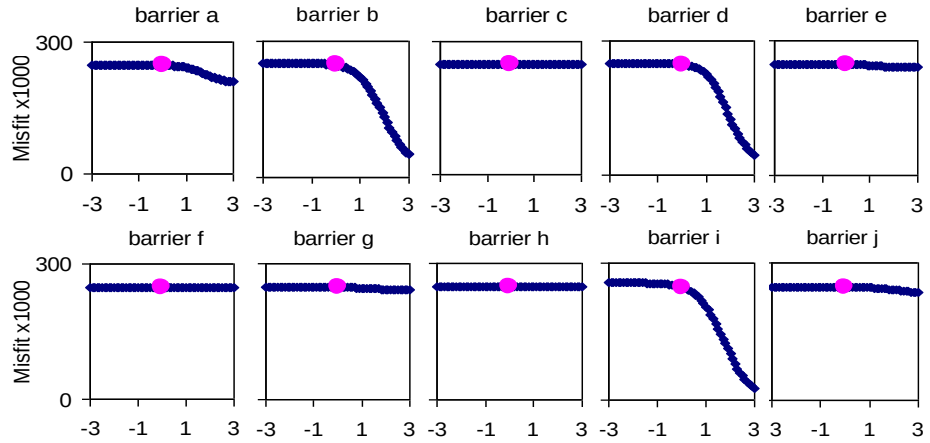

c) Sensitivity analysis for the total seismic plus injector I2 misfit

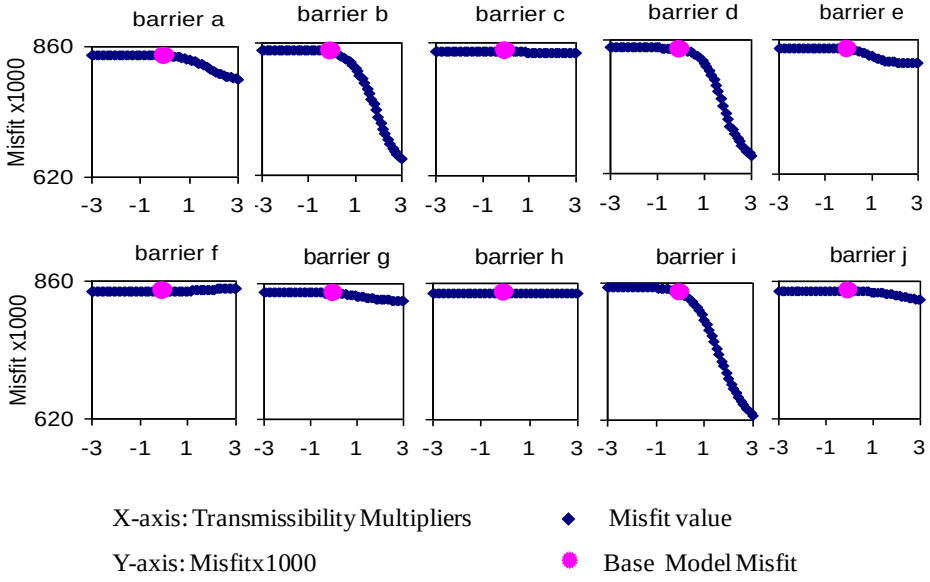

X-axis: Transmissibility Multipliers
Y-axis: Misfitx1000
Misfit value
Base Model Misfit

Figure 4.9: Sensitivity analysis of: a) total seismic misfit, b) injector misfit, and c) seismic plus well misfit. Transmissibility modifier of barriers on log_{10} scale (x-axis). The circle marks the base model misfit value.

The effect of the most dominant parameters on the misfit was non-linear. Also, the injector I2 misfit dominated the sensitivity of total misfit to parameter changes. This is because the range of the injector misfit was much higher than the misfit of the 4D seismic data. The seismic and injector misfits displayed negligible variation with respect to the change of parameters in the interval of [-3,0]. This is because in the base case simulation the transmissibilities of the barriers were already low such that a drop in transmissibility has no effect on flow in the reservoir model.

Moreover, for the transmissibility modifier of barriers 'c' and 'h', when they were the only perturbed parameters in the interval of [0,3], both 4D seismic and injector misfits exhibited little change, if any at all. At this stage in the analysis we regarded that there may be interaction of these parameters with other barriers that may show up later. Change to transmissibility of barriers 'a', 'f', 'and 'j' resulted in similar outcomes for both seismic and injector misfits, although the seismic misfit showed more sensitivity. Seismic and injector misfits consistently declined when the transmissibility modifier of barriers 'b', 'd' and 'i' were increased (from 0.0 to 1.5). However, these barriers result in opposing consequences for seismic and injector misfits when they allowed further pressure communication as the $\log_{10}$ of transmissibility multiplier increased (from 1.5 to 3). The seismic misfit increased but injector misfit decreased. This suggests the possibility of the existence of the multiple minima of the misfit function. The seismic misfit showed strongest sensitivity to barrier 'e' and medium sensitivity to the change to barrier 'g', while the sensitivity of injector misfit was small.

We then performed Full-SHM method. We used 1024 (n_i) models that we previously generated (in analysis of misfit of wells). These models were populated in the 10-dimensional parameter space of the problem (Figure 4.4), using Quasi-random (QR) sampling (for more details refer to Section 2.5 of Chapter 2). At each subsequent iteration, 96 (n_s) models were created in the vicinity of the best 48 models (n_r) of all models available from previous iterations. Thus two models (n_s/n_r = 2) were generated in each voronoi cell of the parameter space where the best models were located. The process was iterated 30 times. In current case studies a predefined number of iteration (models) was set based on making an allowance for the limited availability of computational resources and having an overall convergence towards the minimum misfit as termination criteria. The Neighbourhood Algorithm (NA) usually exhibits rapid evolution toward minimum at the beginning and then flattens out at the end

indicating that the convergence to a minimum misfit is reached. When we continually manually checked the results and if we reached a point where we reasoned that the quality of match would not improve if we continue for further iterations. More automatic termination criteria could be considered as a future work in the SHM workflow (for more details see Section 2.5.2 for stopping criteria).

The initial models (n_i) were used to calculate the coefficients of the regression proxy model of misfit functions (see Equation 3.10 of Chapter 3). Separate regression models of the misfits were generated for each of the two misfit scenarios i) where the ‘ total 4D seismic misfit only’ was used, and ii) ‘4D seismic plus the injector misfit’ were used. The coefficients of the polynomials were estimated using least square regression and singular value decomposition techniques. The regression models had a correlation coefficient, R^2, of 0.976 and 0.967 for the above two scenarios, respectively, when they were compared to true misfits as shown in Figurer 4.10. In both cases only about 10% of the coefficients of the misfit polynomial were significant as illustrated in Figure 4.11. The other 90% of coefficients were very small and they were not related to any valid effect in the misfit function.

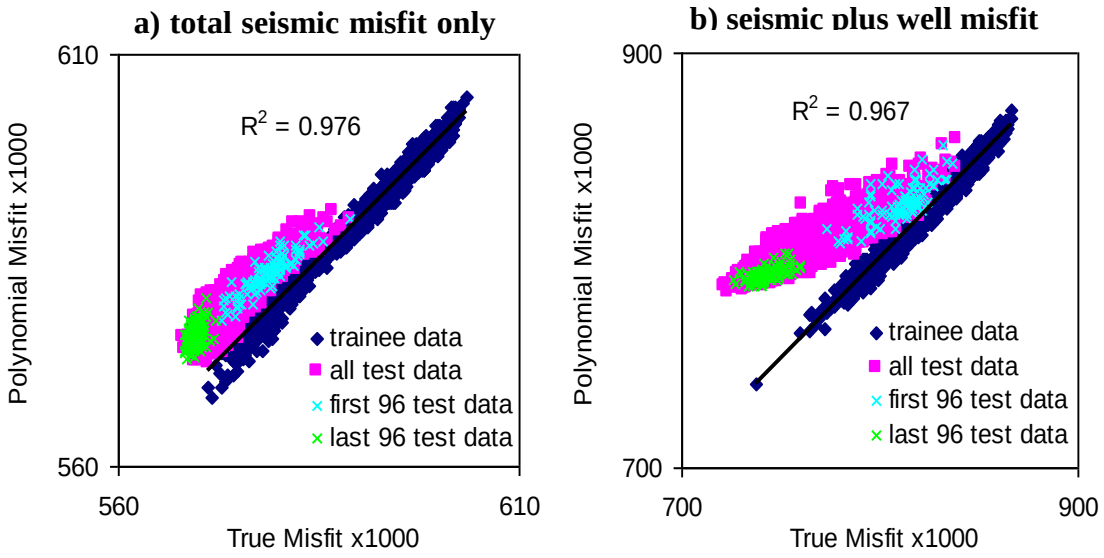

Figure 4.10: Comparison of misfits predicted by the polynomial response surface against the true misfit values where we used: a) the ‘total 4D seismic misfit only’, and b) the ‘seismic plus injector misfit’. On the plots dark blue symbols show the misfit of models used to generate the misfit polynomial and the pink symbols represent all test models generated in the subsequent Full-SHM for Segment 4. The blue and green crosses represent models generated in the first and last iteration of the Full-SHM process.

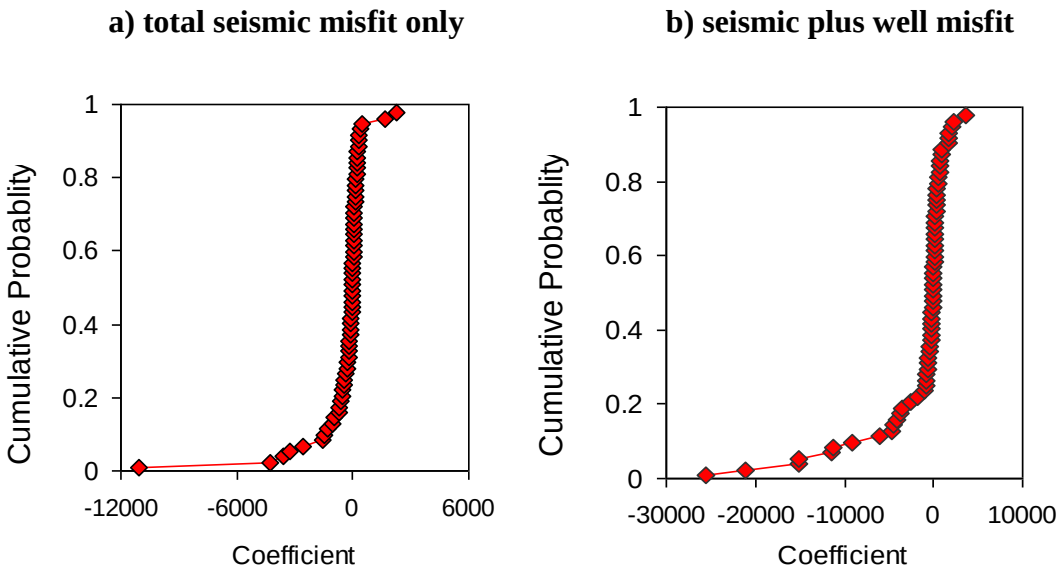

Figure 4.11: The probability distribution of coefficients in the polynomial misfit shows that only 10% of the coefficients of the misfit polynomial are significant.

The reliability of the regression proxy was verified through prediction of the test models and by calculating a mean absolute error, ***D***, which may be considered to be the deviation from reality. ***D*** is the average of differences between estimated misfits by polynomial and true misfits and is calculated using the L1 norm as follows:

$$D = \frac{1}{n}\sum_{i=1}^{n}\left|\frac{J(\underline{\theta}) - f(\underline{\theta})}{J(\underline{\theta})}\right|_i \times 100 \qquad i\text{=1 to number of models } (n) \qquad (4.1)$$

Where: $f(\underline{\theta})$ is the estimated misfit by multidimensional polynomial regression, $J(\underline{\theta})$ is the true misfit, $\underline{\theta}$ is the vector of parameters (here $\log_{10}$ of the transmissibility modifier of the 10 barriers), and n is the number of test points. During validation, the test models were obtained from an ensemble generated in the Full-SHM work flow. Three subsets of test points were considered as shown in Figure 4.8 and consisting of: i) all models of 30 iterations, ii) models in the first iteration, and iii) models in the last iteration (each iteration contains 96 models). These test models are therefore different from the training models used in building the misfit polynomial.

Table 4.5 outlines the mean absolute error calculated considering different combinations of test datasets and for: a) 'the total 4D seismic misfit only' scenario, and b) the 'seismic plus injector misfit' scenario. The error was larger when considering the

seismic with well misfit compared to the seismic misfit only scenario. This might be because of the noise in the injector data. The errors did not change significantly when iterating to the last 96 models in the 'seismic misfit only' case. However there was significant increase of error when iterating to the last iteration in the 'seismic plus injector misfit' case. This signifies that when injector data are combined with 4D seismic data the characteristic of the shape of the misfit surface alters especially when converging towards a minimum. The comparisons between predicted and true misfits for these test models are shown in Figure 4.8.

Table 4-5: The mean absolute error, D (Equation 4.1) calculated considering different combination test datasets and for: a) the seismic misfit only scenario, and b) the seismic and injector well misfit scenario.

Test Dataset	Standard Error (D)	
	Seismic misfit only scenario	Seismic and injector misfit scenario
All (2880) points	1.0%	5.2%
First iteration(96) points	0.83%	2.7%
Last iteration(96) points	1.1%	6.8%

The Pareto plots of the significant effects on the misfit polynomial for the 'total 4D seismic only misfit' and for the 'seismic and injector misfits' scenarios are shown in Figure 4.12 and Figure 4.13. In these figures the most significant coefficients of the polynomial misfits are shown for those effects that capture 95% of the total true misfit behaviour. These effects are presented for total seismic misfit, for injector misfit and for each individual 4D seismic maps of 1993-1999, 1993-2000, and 1999-2000. The misfits are separable in this way because they are additive.

'total 4D seismic misfit only' scenario

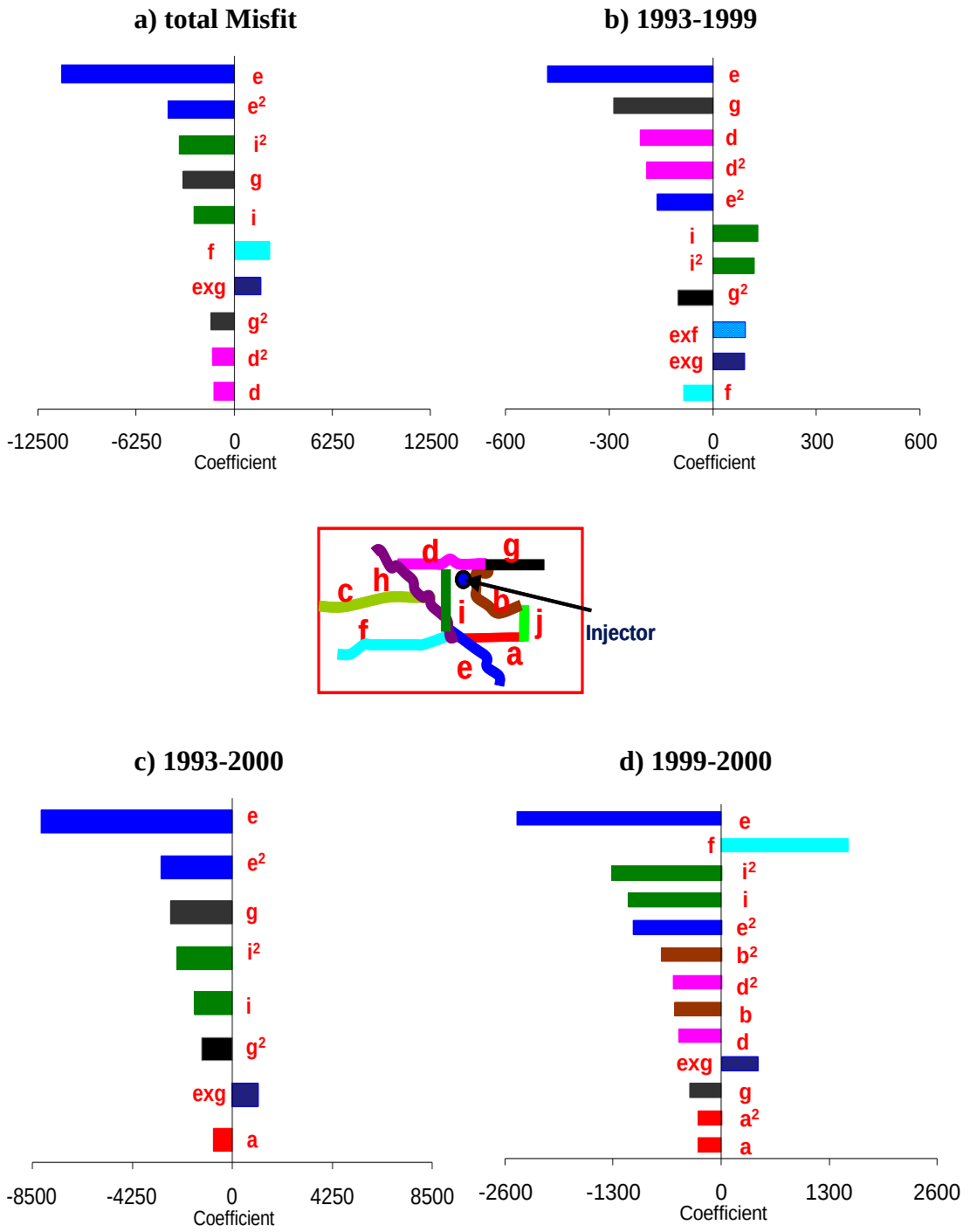

Figure 4.12: Pareto charts of significant effects from the regression polynomial of the total seismic misfits as well as for each time step between monitors for the scenario of the 'total seismic only misfit'. Each letter on the plots refers to the transmissibility modifier of a barrier as shown in the legend. The single character shows a linear effect, squared letter indicates quadratic effect, and cross product of two letters (e.g. e×g) represents interaction effects.

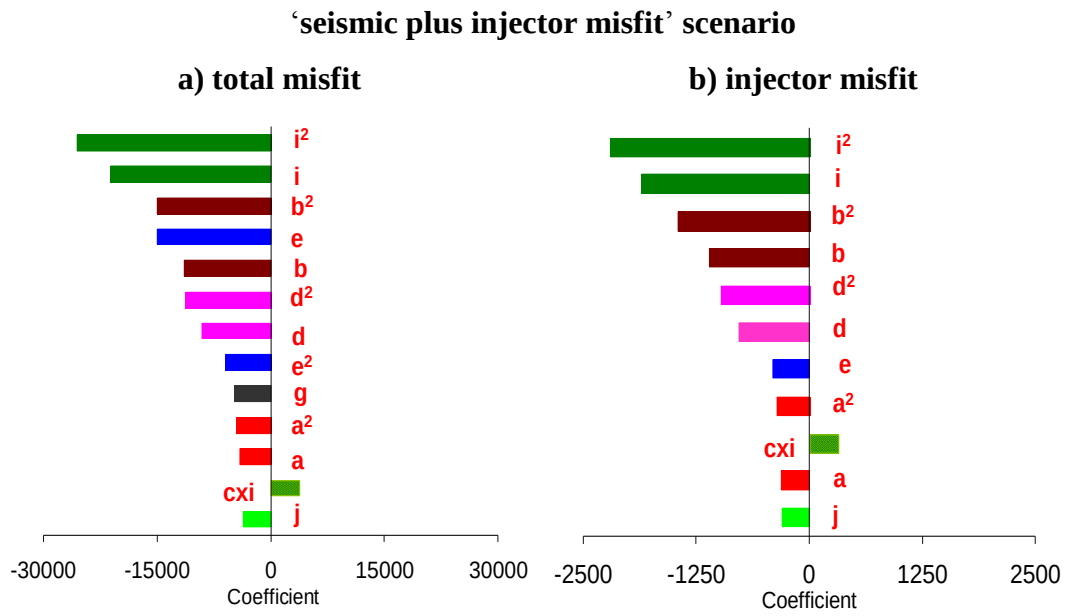

Figure 4.13: Similar plots (as of Figure 4.12) but for significant coefficients from the regression polynomials for a) the 'total 4D seismic plus injector misfit' and for b) injector only misfit.

Transmissibility of the barriers 'e', 'i', 'g', 'f' and 'd' (ranked by significance) were found to have major effects on controlling the total 4D seismic misfit surface in the 'seismic only misfit' scenario. Also there was a significant interaction between the two transmissibility modifiers of barriers 'e' and 'g'. These parameters had influential effects on each of the individual time differences of seismic surveys including: 1993-1999, 1993-2000, and 1999-2000. The transmissibility of other barriers including 'a' and 'b' also played an influential role in the later seismic survey as they were observable in the 1999-2000 plot. They may turn out to be more significant due to interference of: i) the producer P1 activity which is located to the east of the barrier 'b' and had an increase in production rate in year two (1999), and ii) the injector I3 which is placed to the south-east of barrier 'a' and was active from year two (1999). The parameters most influential in the injector misfit were transmissibility of barriers 'i', 'b', 'd', 'j', 'a' (in their order of significance) and interaction between 'c' and 'i'. When the seismic misfit is combined with the 4D seismic misfits, barriers 'e' and 'g' also came to the fore (see Figure 4.11). It seems that the positions of the previously mentioned barriers strongly control the extent of pressure propagation in the horizontal directions relatively close to the injector. Barriers 'e' and 'g' effects on the other hand are less-localized.

In both scenarios, the derived misfit proxy models were quadratic with simple polynomial structure, so we considered applying direct differentiation to find the zero gradient locations on these surfaces. However, we found that the misfit proxy models are concave downwards with a maximum in some parameters, i.e. for the parameters with negative quadratic coefficients in the polynomials (see Figure 4.12a and 4.13a). Therefore, the application of the direct gradient approaches was not practical.

Next, the terms with insignificant coefficients were discarded as the deterioration of the correlation between polynomial and true misfits was measured, (see Figure 4.14). We considered that 95% correlation between true misfits and misfits predicted by regression model to be adequate, but also a significant reduction in R^2 could be observed after we dropped below that number. Thus a threshold for decoupling parameters was acquired. Following this interacting parameter groups could be separated out by considering just those parameters with interactions above the derived threshold (see Chapter 3).

Based on the analysis of interactions, we obtained 9 decoupled sub-volumes in the parameter space for both scenarios under study as shown in Table 4.6. For the 4D seismic misfit, barriers 'e' and 'g' were coupled while the rest were separate. The combined 4D seismic and injection misfit was dependent on coupling between barriers 'c' and 'i', and the rest were uncoupled. The magnitude of the coefficient of the interacting term of 'e × g' for the 'seismic only misfit' case was '1650'; which was 15% of the largest coefficient in the polynomial. The magnitude of the coefficient for interacting term of 'c × i' in the misfit polynomial for the 'seismic and well misfit' case was '3710', it was also 15% of the largest coefficient in the polynomial, so both effects were of similar strength in the polynomials.

Table 4-6: Decoupled parameter sub-volumes.

Scenario	**number of sub-spaces**	**decoupled parameters in separated parentheses**
total 4D Seismic misfit only	9	(e g) (a) (b) (c) (d) (f) (h) (i) (j)
Seismic and injection misfit	9	(c i) (a) (b) (d) (e) (f) (g) (h) (j)

a) 'total seismic misfit only' scenario

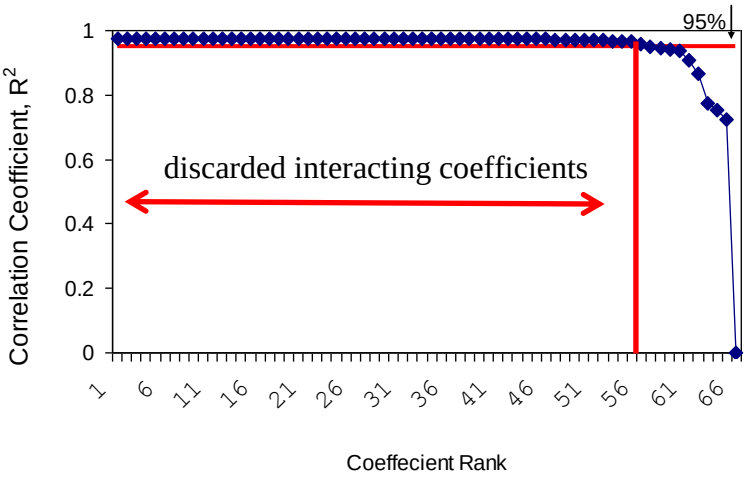

b) 'seismic plus injector misfit' scenario

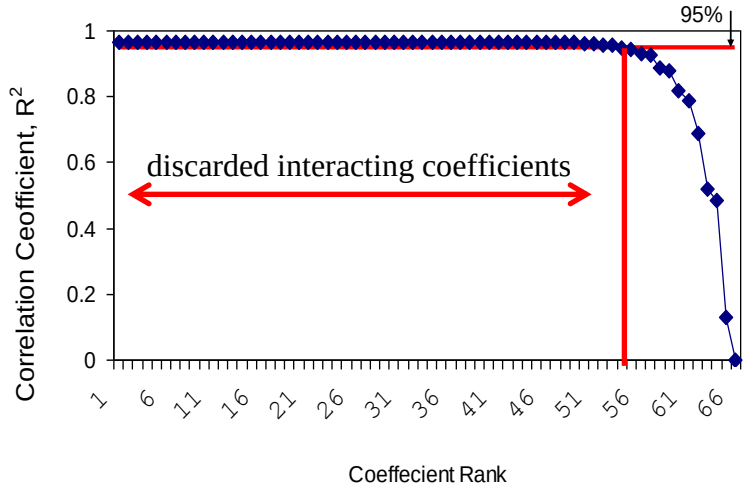

Figure 4.14: Correlation coefficient (R^2) comparing the true total misfit against the regression model predictions as the interacting coefficients are discarded the in order of increasing size (i.e. rank, the smallest first), for: a) the 'total seismic misfit only' scenario, and b) the 'seismic plus injector misfit' scenario.

In the base case model, the transmissibility of barriers was set to '0.001' such that the pressure around the injector I2 increases too much locally. Then in order to improve the match of the major seismic anomaly around the injector, the barriers needed to be opened. There were negative effects (coefficients with negative sign) in the polynomial misfits of both scenarios. These effects implied a need to increase transmissibility. For the scenario of 'total 4D seismic misfit only' the barriers 'e' and 'g' were the most critical, indicating that there was more opportunity for the pressure to propagate away

from injector I2. However the interaction between these barriers gave us an idea that there was an optimal role for each of these barriers.

For the 'seismic plus injector misfit' scenario, the mismatch of injector prediction also suggested that the barriers should be opened with strongest prominence for barrier 'i'. It appeared that the regions close to and beyond the barrier 'i' would provide a channel for injected water and therefore for pressure propagation from injector I2. If this barrier was opened the injector rate mismatch would be zero, however the seismic data match would deteriorate. It seems that barrier 'c' was coupled to barrier 'i' to encompass the optimal transmissibility of these barriers for simultaneous match of the injector and seismic data.

4.3 Applications of Parallel-SHM and Serial-SHM Methods

The convergence to the minimum of misfit value, using the Full-SHM method was achieved, see Figures 4.15 and 4.16. We used the same 1024 models which previously were used to derive the misfit regression equation, as the initial models (n_i) required for using NA. During the search for the minimum, 2880 models were evaluated including 96 (n_s) models at each subsequent iteration (for 30 iterations, and with n_r = 48). Again the same 1024 models were utilized, but this time to initialise the parallel search. When the parallel version of the neighbourhood algorithm was applied to search the parameter sub-volumes a similar result to the Full-SHM approach was achieved but using a much smaller number of model evaluations. This time we also used n_s = 96 and n_r = 48 (to be comparable with the Full-SHM method) but the number of required iterations was just 2. Then only 192 models were called for convergence compared to 2880 models used in the Full-SHM (see Figure 4.15a and b for the two misfit scenarios).

After dividing the parameter space we at most needed to deal with a 2D problem when searching parameters in parallel. Accordingly, the tuning parameters for the neighborhood algorithm can be set for such situation. Another run of the Parallel-SHM was carried out with n_s = 8 and n_r = 4 for 2 iterations. The same result was obtained but this time with much smaller number of model evaluations of 16 models. The convergence of this case is illustrated in Figure 4.15a.

Using the Serial-SHM, the parameters are searched in order of decreasing importance as determined from the coefficients and their effects on the correlation of the regression

equation predictions against the true misfits. The 2D sub-volume containing barriers 'e' and 'g' was searched first, and then the other eight 1D volumes were searched in turn. The NA tuning parameters were set for n_i = 32, n_s = 16 and n_r = 8 for 2D sub-volume, and n_i = 16, n_s = 8, and n_r = 4 for 1D sub-volumes, and the process was carried out with 10 and 5 iterations for the 2D and 1D sub-volumes, respectively. Convergence was achieved in 552 models which is one sixth of the number of models required for the Full-SHM approach. In Figure 4.16 the serial convergence is shown together with Full-SHM convergence results. Nevertheless, this result was not as attractive as the Parallel-SHM approaches which was accomplished with a 70% speedup of the convergence rate (if we count over initial models). In the Serial-SHM method when the nieghbourhood algorithm was applied to sub-volumes sequentially, each time the parameter was searched, there was a need to initialise with the appropriate sampling consistent with the dimension of the sub-volumes. This was not required for the Parallel-SHM method which starts searching with the same initial models used to obtain the misfit regression model.

In Figure 4.17 convergence of the 10 parameters towards the best solution using the Parallel-SHM approach is compared with that of the Full-SHM. The Parallel-SHM resulted in a much faster convergence. In Figure 4.18 the evolution of models in convergence of the Serial-SHM method are shown but only for each serial application of neighbourhood algorithm (i.e. where that parameter was changed).

Figure 4.17a shows that for the Full-SHM method to converge we required 2000 models at least (more than 20 search iterations using NA) to obtain the convergence of transmissibility multipliers of barriers 'f' and 'b' in the 'seismic only misfit' scenario, and for the barriers 'a', 'd', 'g' and 'j' in the 'seismic plus well misfit', see Figure 4.17a. The model parameter evolution showed a potential bi-modal solution for barrier 'b' until convergence to solution is reached, i.e. where the minimum misfit does not improve any more in the 'seismic only misfit' scenario (Figure 4.17a). Further, the barriers 'd' and 'j' in the 'seismic only misfit' scenario, and the barriers 'c', 'f' and 'h' in the 'seismic plus well misfit' scenario were very much non-convergent using Full-the SHM method. However, using Parallel-SHM and Serial-SHM there was apparent convergence after the first iteration of each search routine (Figure 4.17 and 4.18).

a) 'total 4D seismic misfit only' scenario

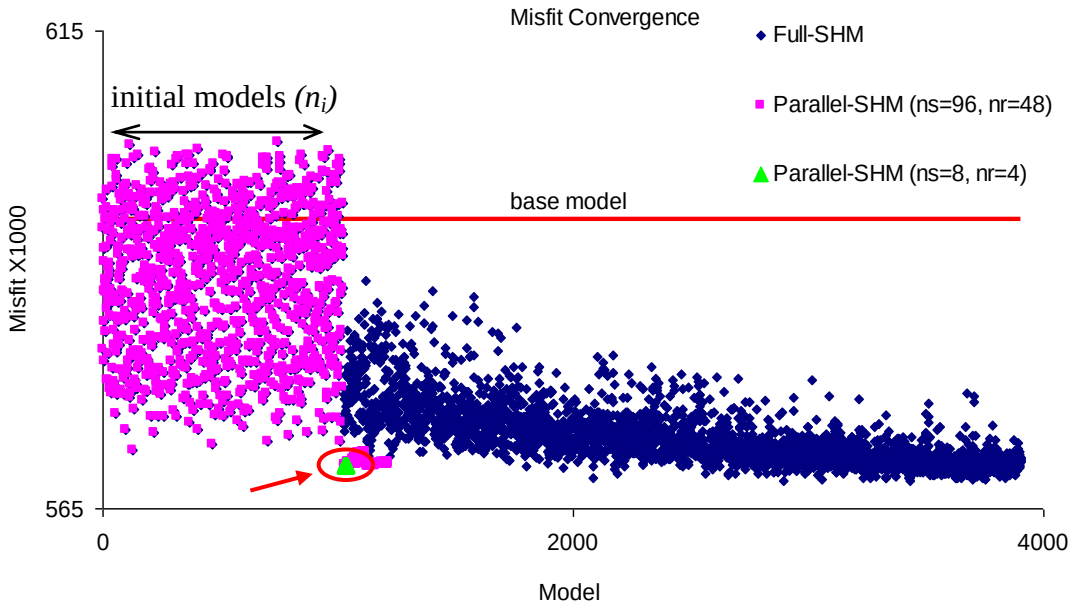

b) 'seismic plus injector misfit' scenario

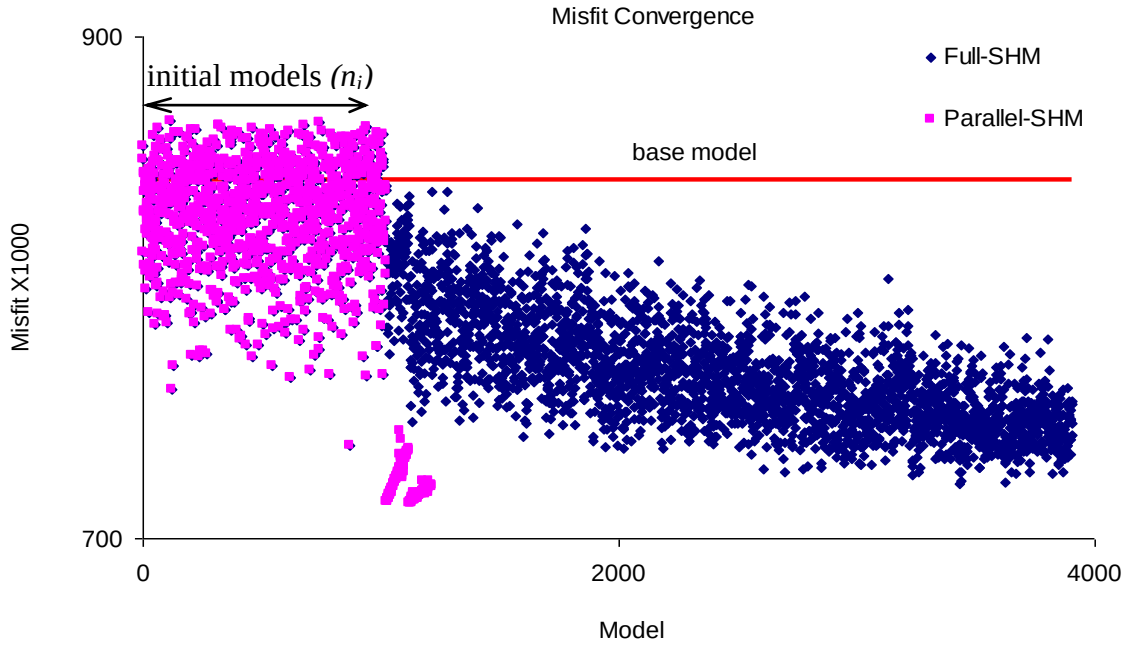

Figure 4.15: Comparison of misfit convergence of the Parallel-SHM approach to the Full–SHM: a) 'total 4D seismic misfit only' scenario, for two cases of using 'n_s = 96, n_r = 48' and 'n_s = 8, n_r = 4', and b) 'seismic plus injector misfit' scenario. The solid line indicates the base case simulation misfit. The dark blue symbols represent the evolution of the models during converge to minimum misfit using the Full-SHM method, and pink symbols show the models for Parallel-SHM method (plus the initial models- also used in Full-SHM). Green symbols (marked in red circle) show Parallel-SHM result for the case with 'n_s = 8, n_r = 4'.

a) 'total 4D seismic misfit only' scenario

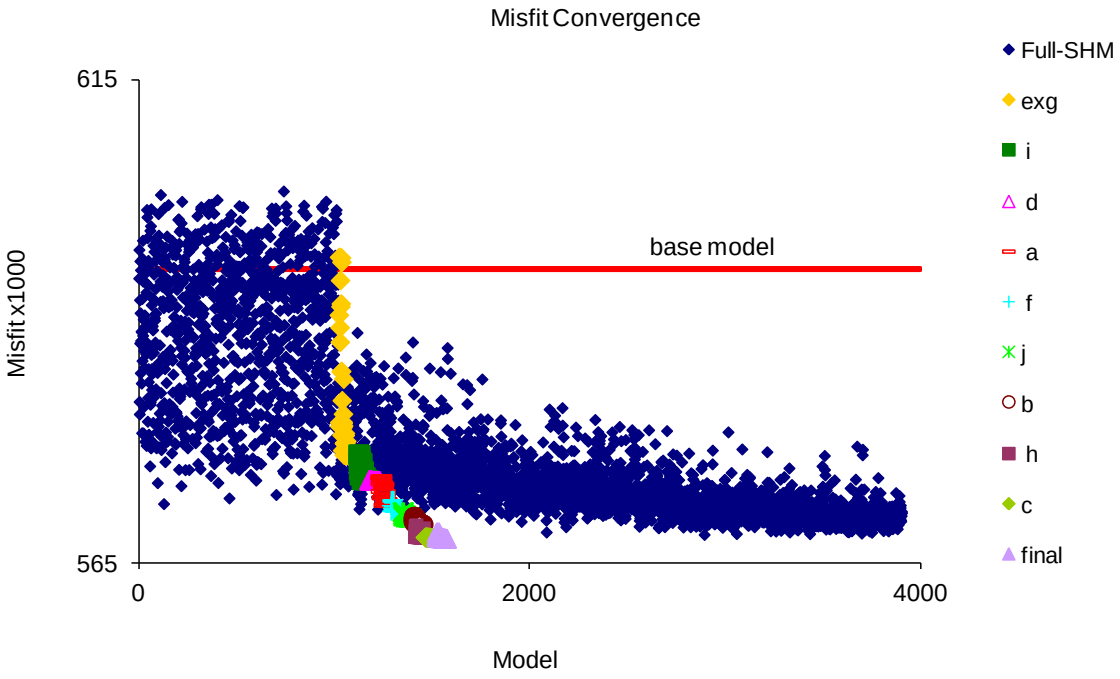

b) 'seismic plus injector misfit' scenario

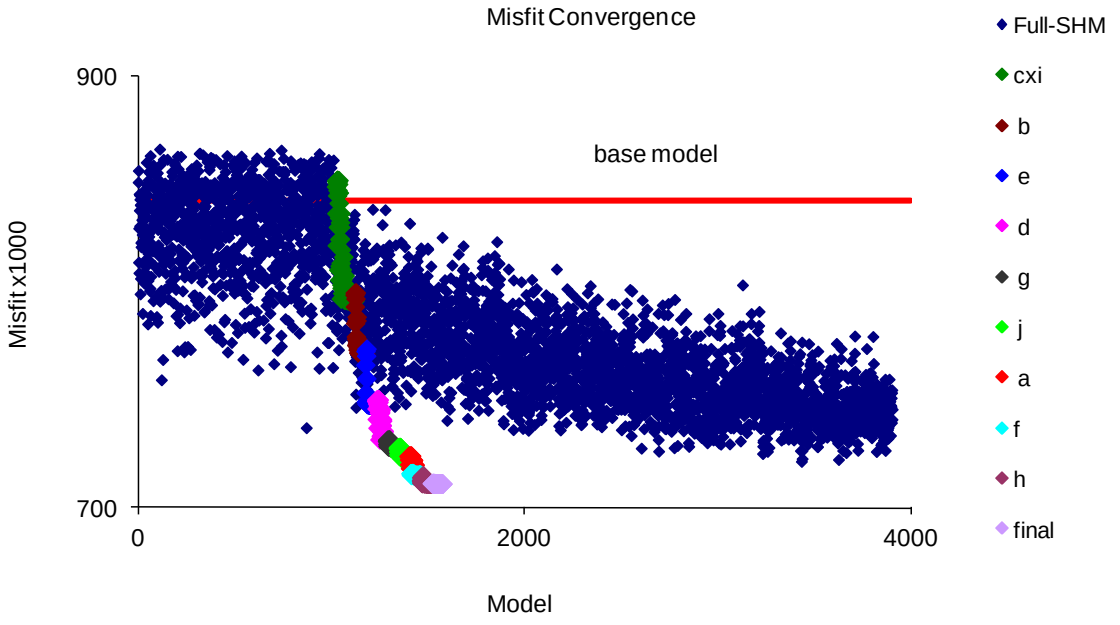

Figure 4.16: Convergence to the solution by applying serial 'one sub-volume at a time' or Serial-SHM for: a) the 'total 4D seismic misfit only' scenario, and b) the 'seismic plus injector misfit' scenario. The solid line indicates the base case simulation model misfit. Each coloured symbol is related to a sub-volume search as specified in the legend.

a) 'total 4D seismic misfit only' scenario

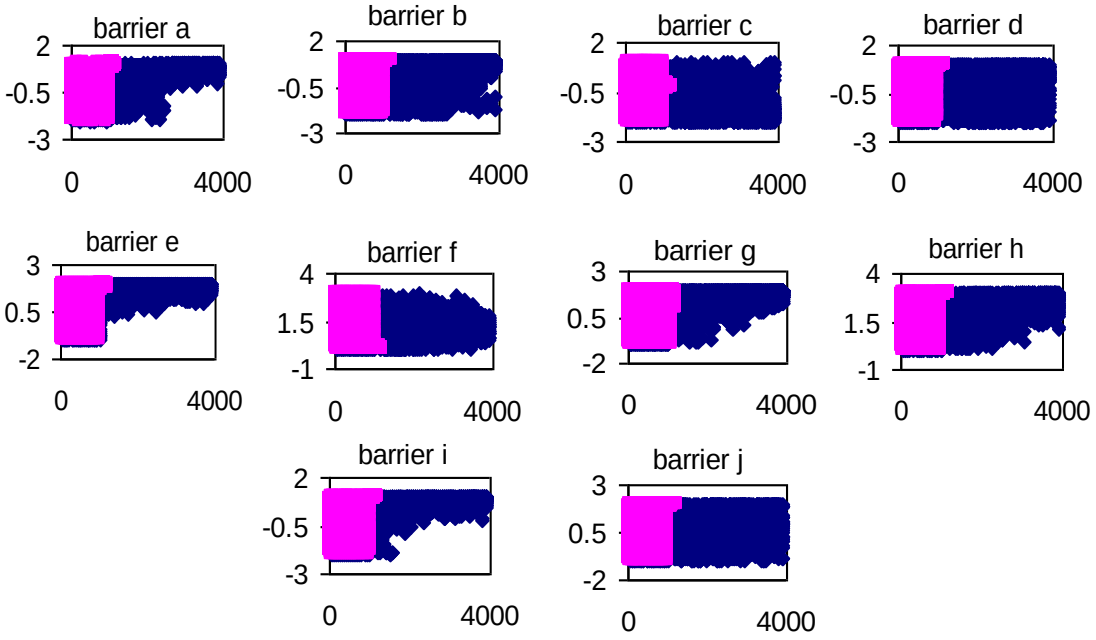

b) 'seismic plus injector misfit' scenario

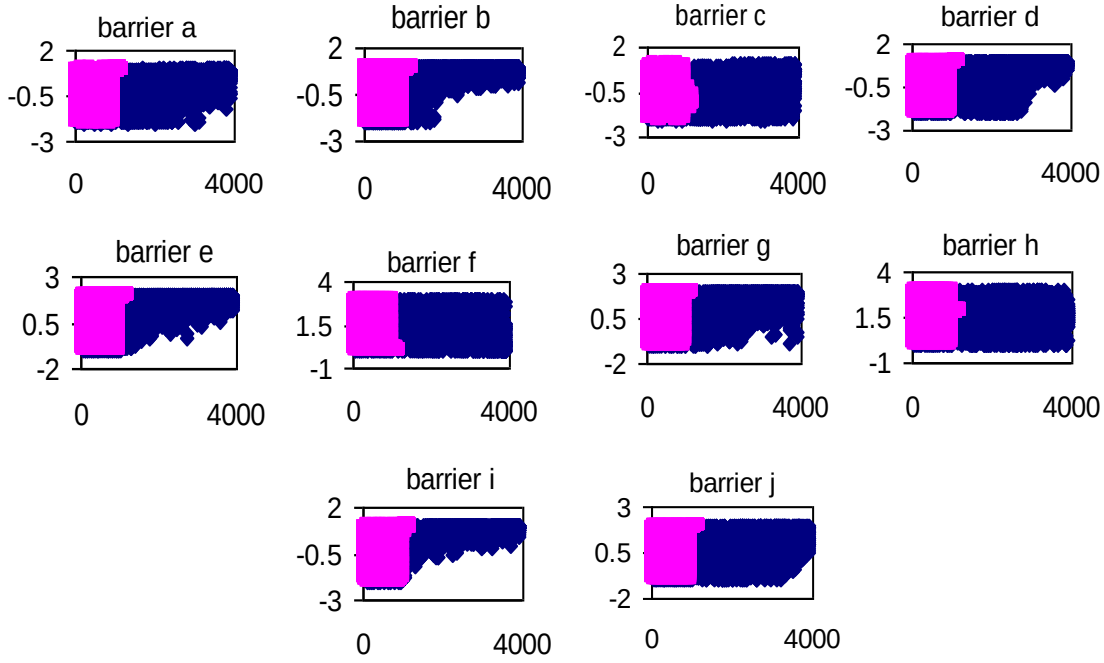

Figure 4.17: Convergence of the parameters by Parallel-SHM (pink symbols) and Full-SHM (dark blue symbols) for: a) the 'total 4D seismic only misfit', and b) the 'seismic plus injector misfits' scenarios. The x-axis is the model index and y-axis is log_{10} of the modifier applied to barrier transmissibility.

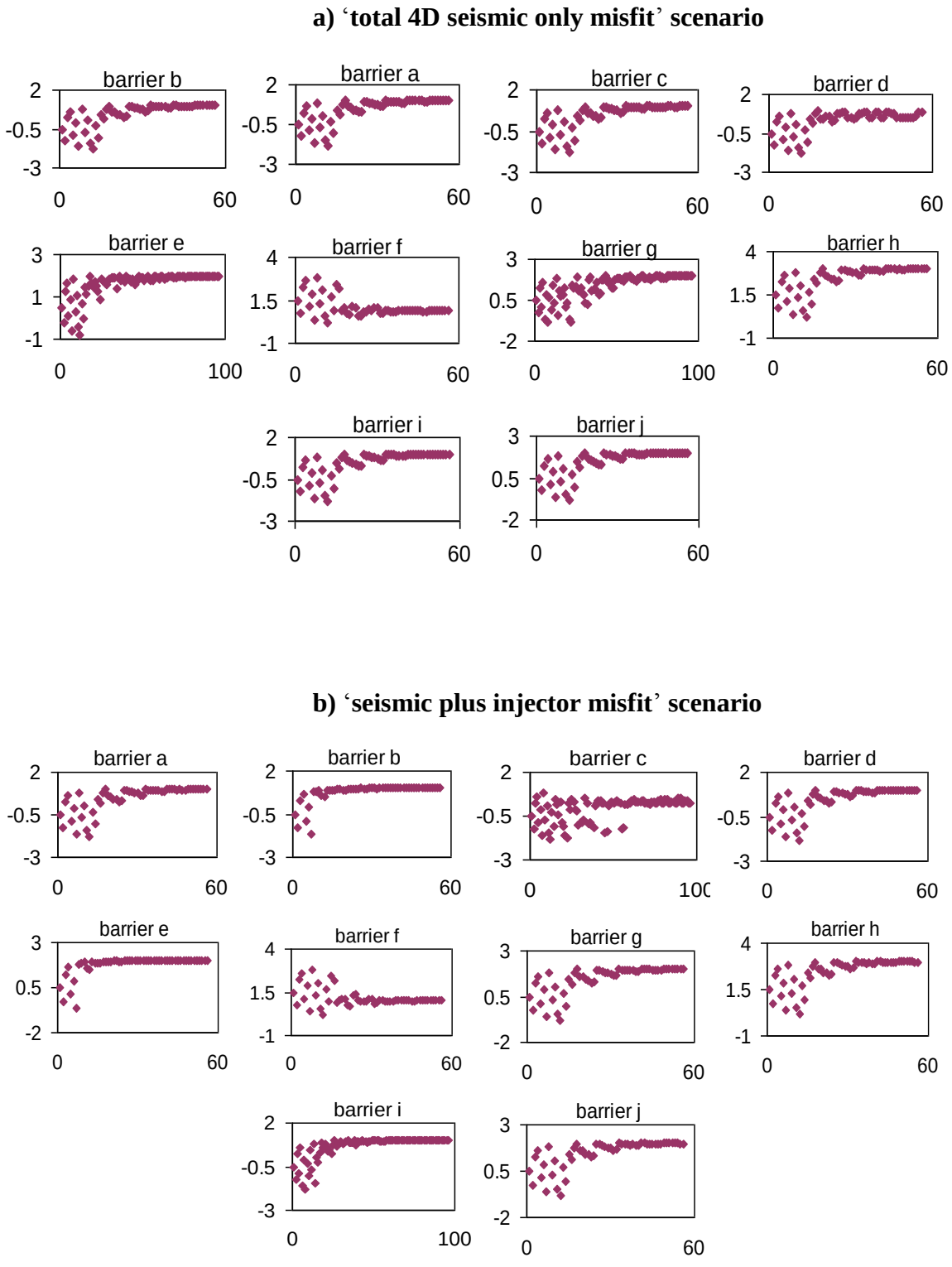

Figure 4.18: Convergence of the parameters when the Serial-SHM is applied to the two scenarios of: a) the 'total seismic misfit only', and b) the 'seismic plus well misfits'. We only show the models as the parameters are modified. The x-axis is the model index and y-axis is log_{10} of the modifier applied to barrier transmissibility.

4.4 Comparison of Final Model Results

Maps of predicted change in impedance for the best models obtained by the three different approaches (Full-SHM, Parallel-SHM and Serial-SHM) are compared to corresponding maps of observed data and those of the base model in Figure 4.19. These comparisons are for the two scenarios of: a) the 'total 4D seismic data only in misfit', and b) 'the seismic and injector in misfit'. The Parallel-SHM and Serial SHM results were very close to those obtained by Full-SHM method. In Figure 4.19, since the resulting match of seismic maps was the same for the two scenarios of 'total 4D seismic misfit only'; and 'seismic plus injector misfit' merely the results of former one are illustrated. The match of the signal around injector I2 is improved noticeably in all methods.

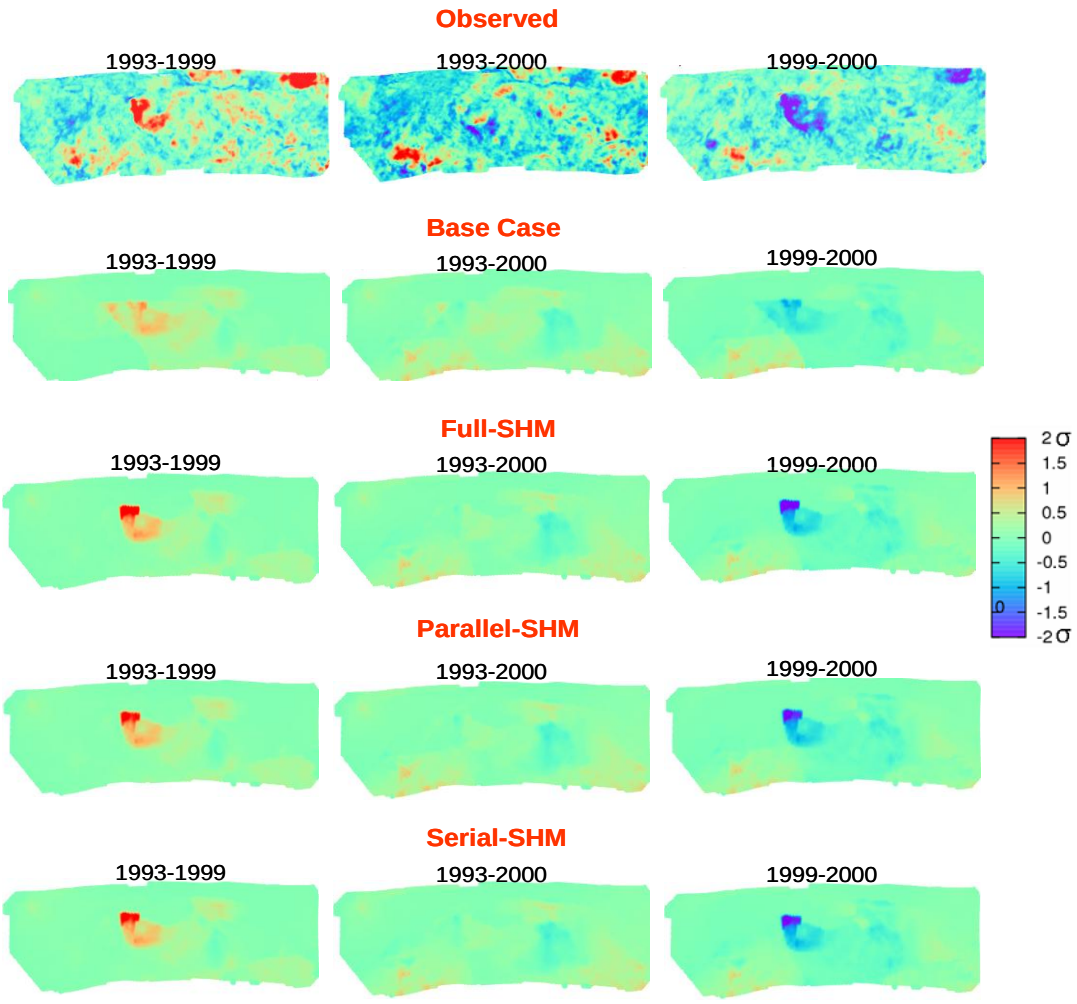

Figure 4.19: Comparison of predicted seismic maps by best model obtained by various methods to observed data and base model predictions. This figure shows the results for the 'total 4D seismic misfit only' scenario but the scenario that used the injection rate misfit as well gave the same results.

Comparison of the injector I2 history to the predictions by the base model and by the best models acquired by various methods is shown in Figure 4.20. The match of the injector I2 using full, parallel and serial approaches is improved relative to the base case model. For parallel and serial approaches there was even slightly more improvement compared to the Full-SHM approach. However a complete match to the injector was not achieved by any of the approaches. This result reveals that for reducing the mismatch of injector I2, it is necessary to acquire insight to both the ability of flow across barriers and the capacity of injection in the reservoir sand (i.e. petro-physical properties) of the area where the well is located. We have investigated this in the next chapter.

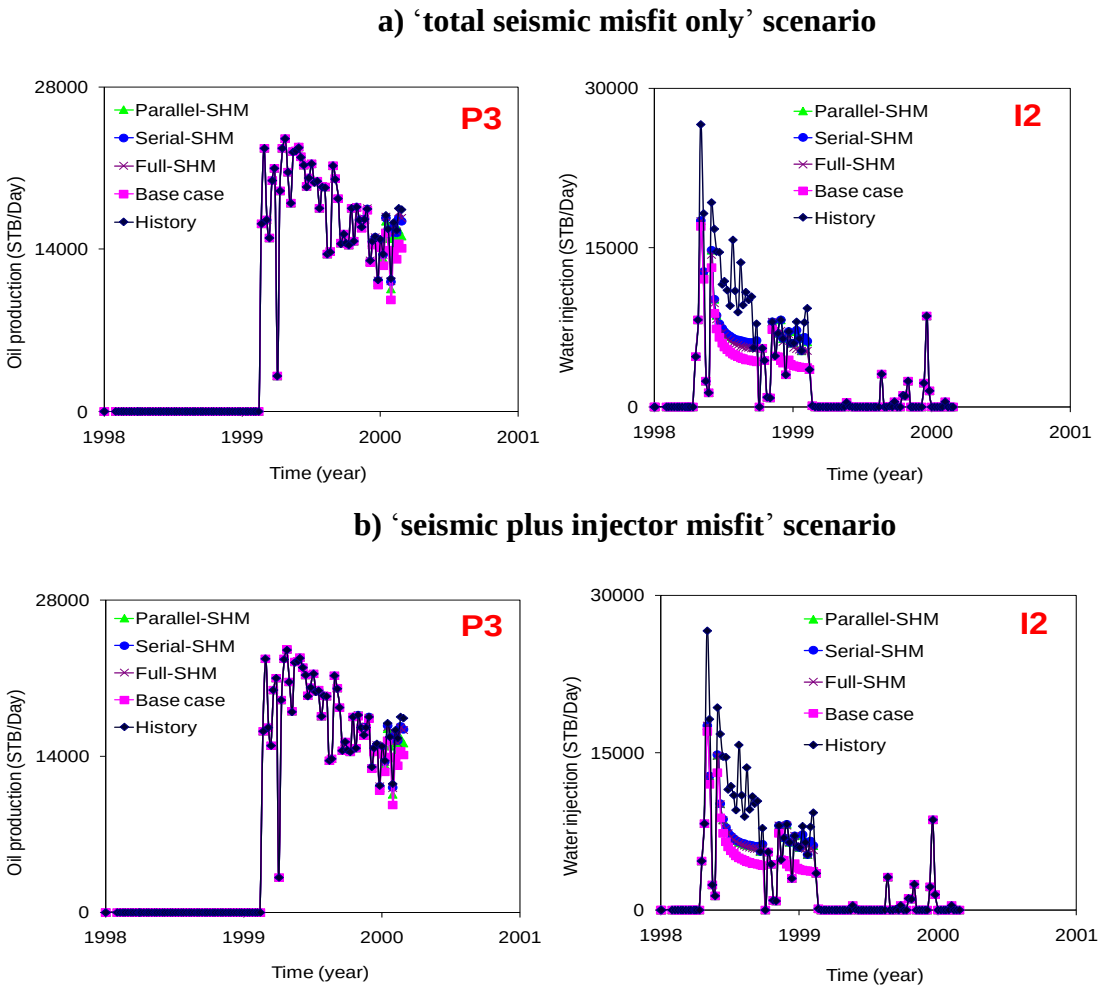

Figure 4.20: Comparison of predicted well data by the best model obtained by various methods of Parallel-SHM, Serial-SHM, and Full-SHM to observed well history and base model prediction for the two scenarios of: a) 'total 4D seismic misfit only', and b) 'Seismic plus well misfit'.

For the producer P3, we also obtained small improvements in the match by various SHM methods relative to the base model (see Figure 4.20). The match of the history data of other wells was attained in the base model and remained unchanged by the best models prediction, thus they are not shown. The results obtained by the new approaches show a similar quality to the Full-SHM method, but it has been achieved in a smaller number of flow simulations. Improvements to the water injection rates were also obtained. Comparison of the parameter values of the best models achieved by the three approaches is shown in Figure 4.21. The standard deviation of the best parameter values was estimated based on the variation of parameter values in the 10 best models obtained by each of the three various methods; they are displayed as error bars on Figure 4.21.

For most parameters of the transmissibility modifier, the results were consistent although there are some exceptions. Barriers 'a', 'b', 'e', 'g', 'i' and 'j' are consistent and close to the injector I2 and control the build up of the pressure and thus the shape of the seismic anomaly around the injector. The other parameters can be improved around the best parameter value of these barriers, and have mostly competing effects on the observed data variables (seismic and well data).

Barriers 'c' has negligible influence on the seismic misfit response, but has an interaction effect with barrier 'i' for injector I2 misfit. Barrier 'f' has negligible influence on the injector misfit but has opposing significant effects on seismic misfits of 1993-1999 and 1999-2000, also it has an interaction effect with barrier 'i' on seismic misfit of 1993-1999. Barrier 'h' does not have significant effects on either seismic or injector misfits. Barrier 'd' has linear and quadratic influences on both the injector misfit and the seismic misfit (see Figures 4.12 and 4.13). These barriers 'd' and 'h' have consistent effects on the seismic and injector misfits but they were changed to the most largest degree along with when different combinations of changes to the other parameters, particularly for barriers 'c' and 'f'.

Consequently, we concluded that for the current history matching exercise multiple solutions may exist or at least there are saddle points such that there is no unique minimum for the misfit function. The transmissibility multipliers were updated for barriers 'd', 'j', 'h', 'c', and 'f' also were estimated with higher uncertainty using the Full-SHM method (see the error bars in Figure 4.21). This also supports the conclusion

that there may be multiple combinations of the parameters which provide a good match to observed field behaviour.

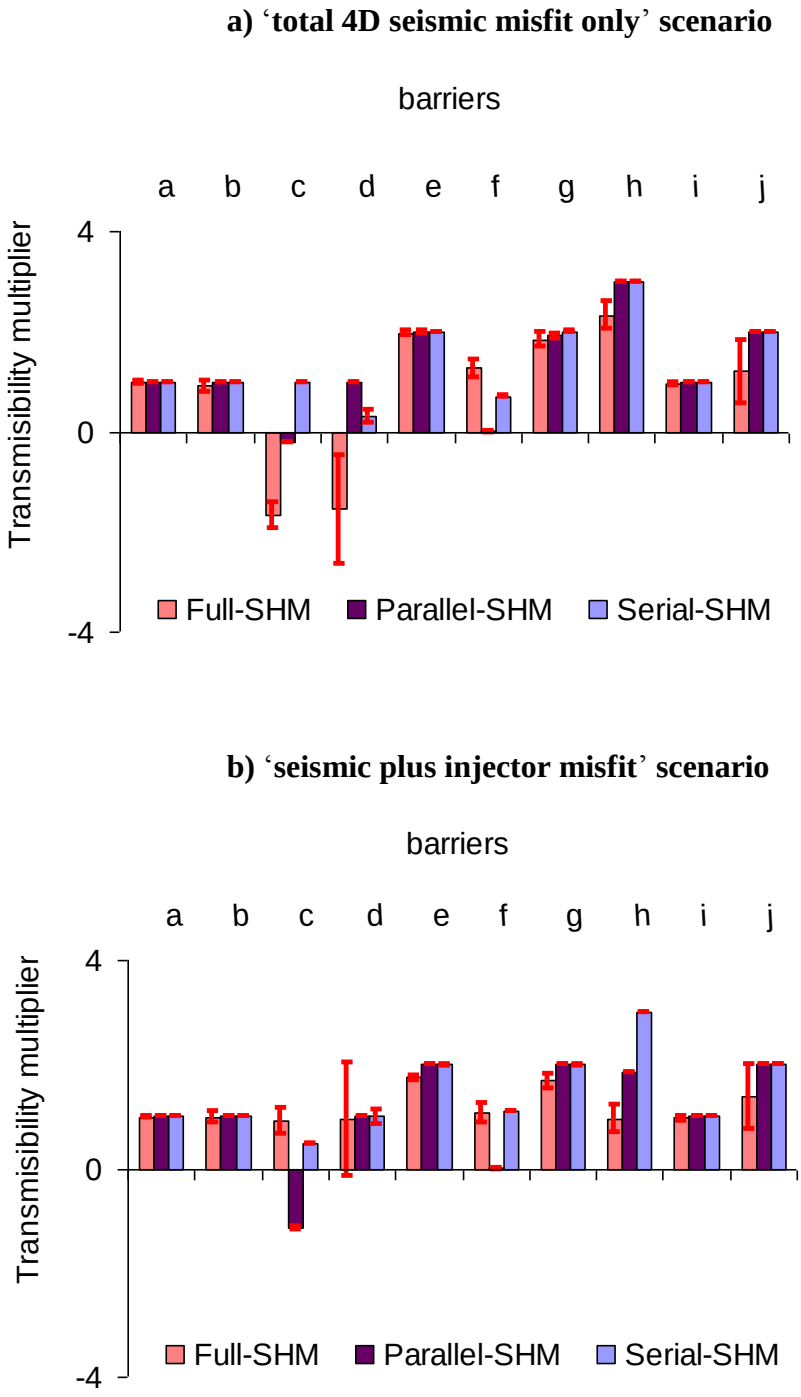

Figure 4.21: Comparison of the parameter values for the best models obtained by various methods for the two misfit scenarios: a) the 'total 4D seismic misfit only', and b) the 'seismic plus injector misfits'. The error bars of parameter values are calculated from of the 10 best models generated by various methods of SHM.

Further investigations on the quality of results obtained by the Full-SHM, Parallel-SHM, and Serial-SHM approaches were carried out through sensitivity analysis. The best models of each method were modified via 'one parameter change at a time'. In Figure 4.22, we can see that the sensitivity of the misfit surfaces is small for further perturbation around the best models for most transmissibility multipliers (notice the range of y-axis of plots). The seismic misfit increases sharply if the transmissibility of barrier 'e' is reduced and the injector misfit increases when barrier 'i' and 'b' are closed relative to best model. They are the most important parameters and have converged to identical results by the various methods and in both misfit scenarios.

The **s**ensitivity analysis of the updated parameters (see Figure 4.22) indicates that many optimal parameter values have been found at the boundaries of their defined search domain (i.e. the range of parameters allowed for sampling). This wider domain was chosen initially for history matching based on preliminary analysis and also where the **s**ensitivity of the seismic and injector misfits were examined through one at the time parameter changes (see Figure 4.9). In these studies, the $\log_{10}$ of the multipliers were varied in the range [-3,3]. The feasible domain for the neighbourhood algorithm was then chosen span three orders of magnitude. The ultimate **s**ensitivity analysis on the updated parameters (see Figure 4.22), however, indicated that many optimal parameter values lay at the boundaries of this domain. This may be because seismic and production misfits are pulling the parameters in opposite directions for several reasons:

- The weightings were calculated for seismic and injector misfits and these could be incorrect.
    - For seismic data, the errors were estimated by assuming that high spatial frequency components of the data are noise which was found to be uncorrelated. However there could be lower frequency or correlated, e.g. from multiples, band pass filtering, etc., that induced errors in the 4D seismic data.
    - For the injector misfit the appropriate relative weight is not known, and there is a possibility that the injection rate was less accurate than assumed.

- There may be parameters missing from the history matching process. If the seismic and production misfits draw in opposite directions then that could be a sign that some other parameters needs to be modified.

- There may be uncertainty in scaling of the 4D signals. Normalization to baseline should capture geological imprints but other 4D related parameters (e.g. stress sensitivity) may be incorrectly calibrated or otherwise normalized.

- The bounds of the parameter values were restricted based on the preliminarily analysis that was considered compelling for the purpose of obtaining good quality results for the history matching application. There are always the possibilities of having solution/solutions in some other places in the parameter space (e.g. wider parameter space or restricted to other bounds) which are not included in the history matching process.

- However it is most likely that some combinations of all the above explain the observed trend.

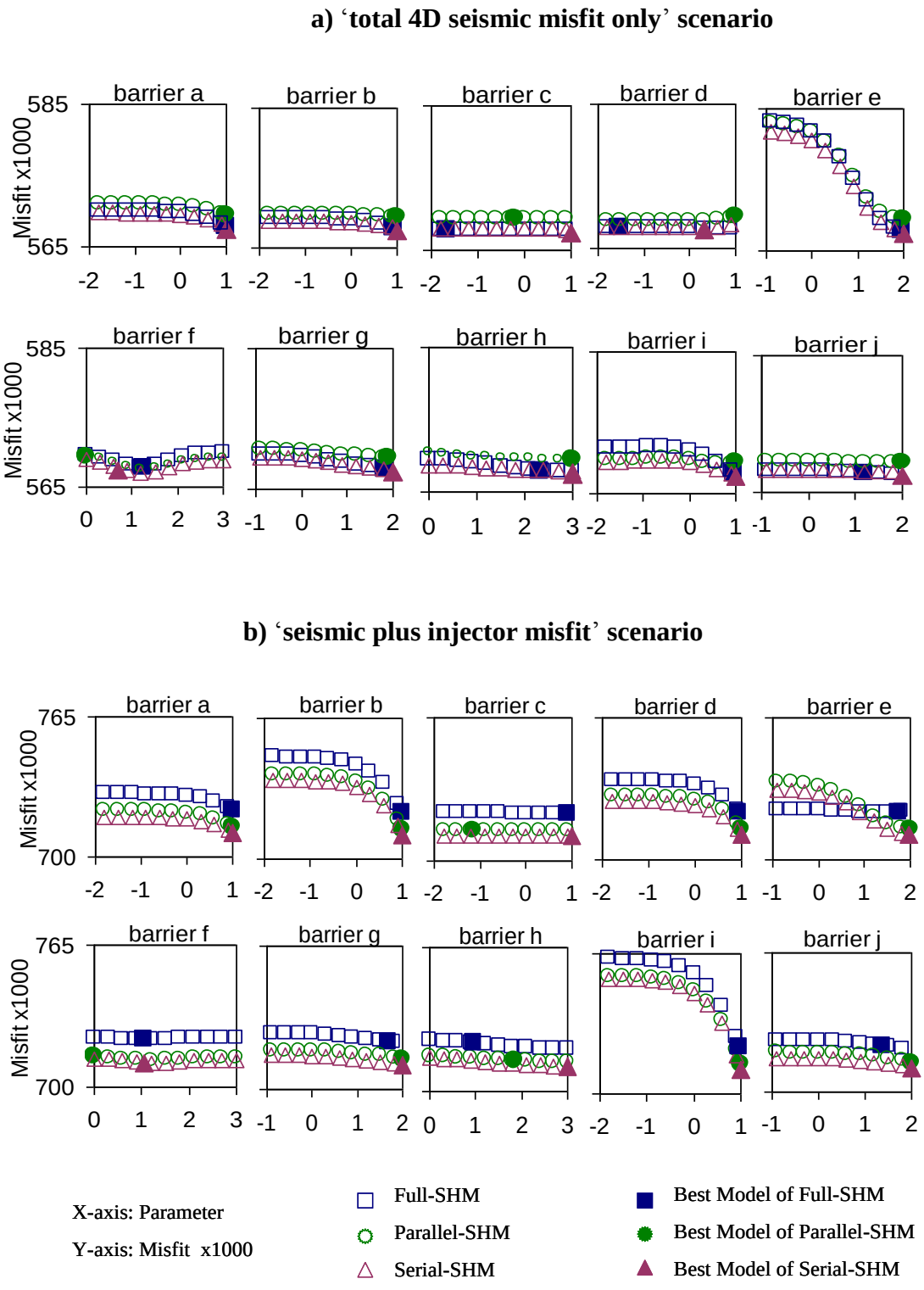

Figure 4.22: Sensitivity analysis for the best models obtained by various methods for: a) the 'total 4D seismic only misfit', and b) the 'seismic plus injector misfits' scenarios. Each parameter is varied one at a time. Filled symbols indicate the best value found from SHM methods.

Tables 4.7 compares the simulation models and CPU time required by each of the various methods for two misfit scenarios.

Table 4-7: Summary of simulation data for each of the methods in the two misfit case.

Misfit Scenario	Method of SHM	Number of models excluding initialisation*	CPU excluding initialisation (days)**
'total 4D seismic misfit only'	Full-	2880	16.0
	Parallel-	192	1.07
	Serial-	552	3.07
'seismic plus injector misfit'	Full-	2880	16.0
	Parallel-	192	1.07
	Serial-	552	3.07

1024 models were used to initialise the study during which both misfits were recorded taking 5.7 days of CPU to compute. These were then used for all remaining studies.

****Each model takes around 8 minutes on a 3.4 GHz processor.***

The initialization models were not counted at this stage of evaluating the performance of methods against each other; as they are common to all models. It is often found that such a large set of initial models is necessary for the NA approach. The degree of speedup is quite large and could be increased further, though we opted for similar preference to the full inversion initial ensemble (n_i = 1024 in NA) for the two new methods; and similar explorative and exploitative options (n_s = 96 and n_s = 48 in NA) for Parallel-SHM. We examined a second option (i.e. n_s = 8, and n_r = 4) for the Parallel-SHM which is not used in the comparison of the performance of methods, though this is more representative, however this case gave similar history match results as the first case.

Table 4-8: Comparison of the performance of the various search methods in the two misfit scenarios.

Misfit scenario	**Method of SHM**	**Drop in full seismic misfit (%)**	**Drop in seismic misfit for area around injector (%)***	**Drop in injector rate misfit (%)**	**Drop in total seismic and injector rate misfit (%)**	**Drop in seismic misfit of area around injector and injector rate misfit (%)***
'4D seismic misfit only'	Full-	4.6	19.6	31.5	12.5	28.6
	Parallel-	4.4	18.7	41.5	15.3	35.9
	Serial-	4.7	19.5	40	15.0	32.7
'Seismic plus injector misfit'	Full-	4.4	19.1	38.4	14.4	33.7
	Parallel-	4.3	18.7	41.7	15.3	36.1
	Serial-	4.6	18.9	42	15.6	36.3

****The seismic map contains noise plus several anomalies that we do not attempt to match, one outside of the area of simulation and one large one within (see "shadowing" discussion in Section 4.2.1). Therefore only the misfit in the area immediately around the injector indicated by the box in Figure 4.6 is considered.***

Table 4.8 compares the performance of the three methods in the two misfit scenarios. The minimum seismic misfit achieved and the reductions in the seismic misfit by various methods are very close. Nevertheless there is a further drop in the injector misfit by new methods compared to the Full-SHM, which has propagated into the evaluation of the total misfits in both of the 'total 4D seismic misfit only' and 'seismic plus injector misfit' scenarios, particularly for seismic 'plus injector misfit' scenario (see Table 4.8).

Two regions of misfit were considered for the seismic data in order to compare the different methods against each other. First, the seismic misfit was calculated for the entire area of the reservoir model during history matching, and this was used during the whole process. However, this region actually contains two further anomalies that we

did not try to match (refer to Section 4.1.1). The total reduction of misfit for the entire area of the reservoir therefore appears to be quite small. Thus a region around the injector I2 was considered (similar to the box in Figure 4.3), where the percentages of misfit drop was quite large. Although the injection rate misfit is significantly reduced by using all of the SHM methods, a perfect match was not obtained however. Even in the case of 'seismic plus injector misfit' scenario almost similar result to the 'total 4D seismic misfit only' scenario was obtained. It appears that some other geo-cellular properties such as net:gross and permeability may need to be updated for adjustment of injector rate (see Section 5.4 of Chapter 5).

Considering only the misfit of the region around the injector I2 lead to almost similar conclusions about the performance of the methods against each other, compared to the case when the entire reservoir is incorporated. This is because the perturbation of the transmissibility multiplier of barriers dominantly affects the misfit of the area around the injector. The NA approach is based on misfit ranking and the regions that are not perturbed would equate to a constant addition term to the misfit of all models in the inversion process.

It should also be remembered that there is some noise or "data error" due to the amount of contributed data in the misfit computation. Here the noise contributes to approximately sixty per cent of the misfit over the whole region while for the region around the injector it is only twenty per cent. The "data error" contribution was estimated with the assumptions that there is no model error due to insufficient parameterisation and the variance of the model error is zero. Also it was assumed that the noise in the data is uncorrelated random Gaussian with zero mean. For more detailed of calculation on "data error" contribution see Appendix B.

4.5 Application of the Parallel-SHM to a synthetic Schiehallion case

Application of the 'divide and conquer' approach was validated for the Parallel-SHM and Full-SHM methods using a synthetic Schiehallion case study similar to the first experiments detailed in Section 4.2. The aim was to determine that the method works under conditions where the answer is known, there is no data or model error and the solution exists in the search space. The first 10 dimensional case (including the transmissibility of barriers as uncertain parameters, see Figure 4.3) was rerun with the

total 4D seismic and injector misfit used. For this purpose synthetic 4D acoustic impedance maps were derived from the best model obtained in the equivalent real data case study and these were used as observed data. The base case model for seismic history matching was the same as before (see Section 4.2 for the details of the base case description).

The cross-plot of seismic versus injector misfits for 1024 models (n_i models used later on) for both real and synthetic cases is shown in Figure 4.23. The scales of the misfits were different. In the real case there were more observed seismic data, i.e. typically 64 measurements for each simulation cell and we used these in the misfit. However, in the synthetic case, seismic data were estimated on the simulation grid. In addition, the synthetic truth is much closer to the base case prediction, which also reduces the misfit (of both seismic and injector). Finally, in the real case not all regions of the 4D map were addressed so there was a constant misfit we did not attempt to reduce. We assumed that similar levels of data uncertainty should be applied. Accordingly, to adjust previous figures, a weight factor of value 0.828 was derived and applied to the injector misfit in this study to preserve the relative degree of variation of the seismic and injector misfits as occurred with the real data. This ensured that the ratio of the range of seismic misfit to the range of injector misfit in Figure 4.23a was the same as equivalent properties in Figure 4.23b. These weights were used in the following history matching runs.

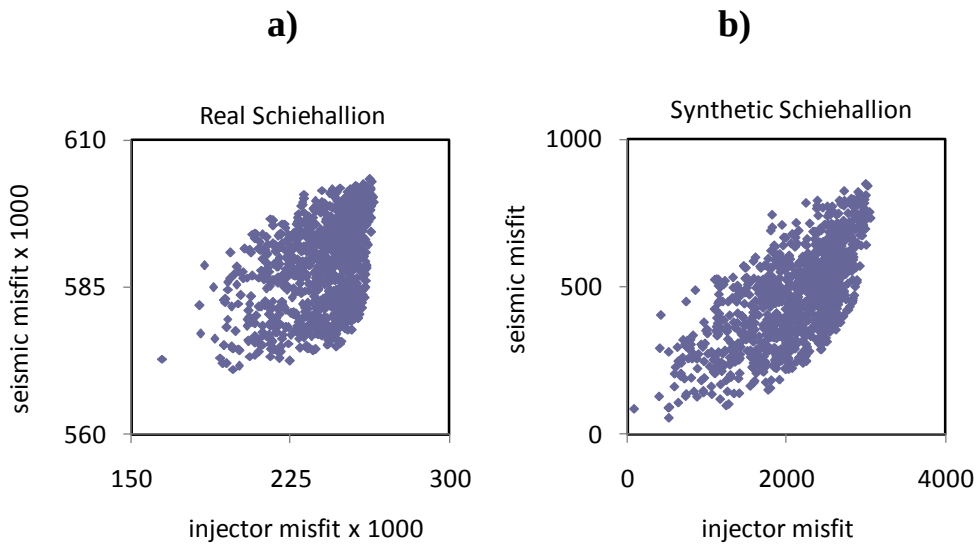

Figure 4.23: Cross-plot of seismic versus injector misfits for 1024 for: a) real and b) synthetic Schiehallion case studies prior to misfit weight adjustments.

The NA parameters were also set as before for both Full- and Parallel-SHM (i.e. n_i = 1024, n_s = 96 and n_r = 48). First Full-SHM method was performed. Then using the initial, n_i, 1024 models the proxy to the misfit function was constructed. The correlation between proxy misfits and the true misfits were very good, it was $R^2 = 0.97$. The Pareto plots of the significant effects on the misfit polynomials are shown in Figure 4.24. The most significant coefficients of the polynomial misfits were similar to the previous result of Figure 4.12. Then the parameter decoupling and misfit decomposition were carried out. Based on these analyses, 9 decoupled sub-volumes in the parameter space were identified; they are shown in Table 4.9. Again results were similar to the previous real case (refer to Table 4.6). Barriers 'e' and 'g' were interacting parameters while the rest were separate parameters.

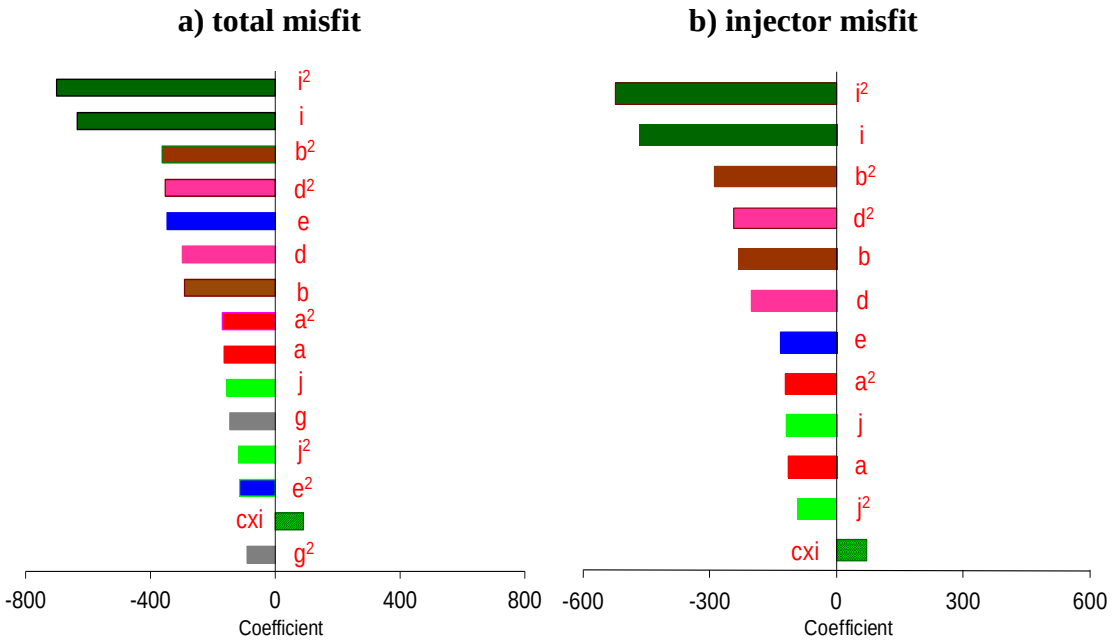

Figure 4.24: Pareto charts of significant effects from the regression polynomial of the misfit for the synthetic case (legends are similar to Figure 4.12 for: a) total misfit and b) injector misfit).

Table 4-9: Decoupled parameter sub-volumes.

number of sub-spaces	decoupled parameters in separated parentheses
9	(e g) (a) (b) (c) (d) (f) (h) (i) (j)

For Full-SHM, 5760 models were evaluated during the search (i.e. 60 iterations). Parallel-SHM only required 5 iterations generating 480 models in total. Figure 4.25 shows convergence towards zero misfits using these methods. Figure 4.26 also shows convergence of the 10 parameters towards the true solution by Parallel-SHM which is compared to Full-SHM. These figures reveal that Parallel-SHM obtained an improved convergence and confirms the efficiency of the method.

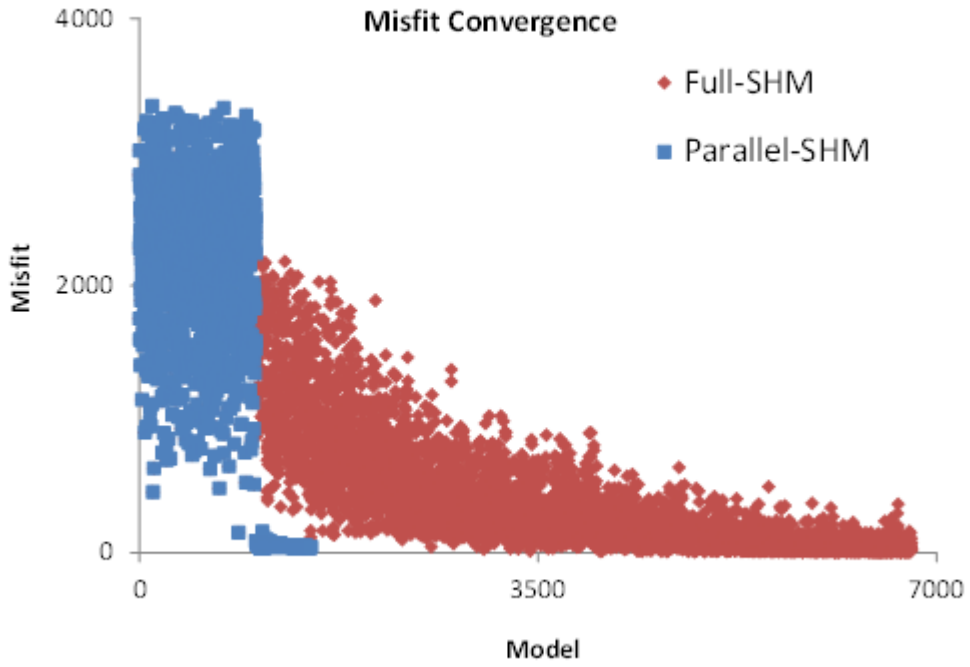

Figure 4.25: Misfit evolution as models are generated by Parallel-SHM compared to Full-SHM.

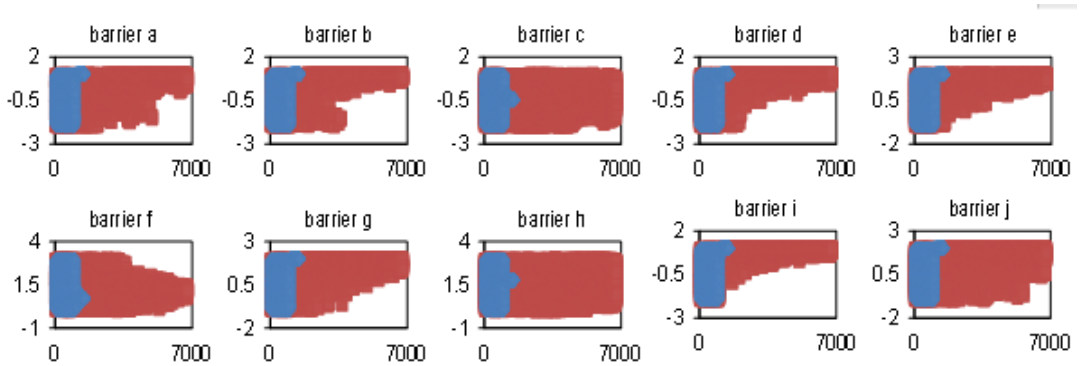

Figure 4.26: Convergence of the parameters by Parallel-SHM (blue symbols) and Full-SHM (dark red symbols). The x-axis is the model index and y-axis is log_{10} of the modifier applied to barrier transmissibility.

Maps of predicted change in 4D impedance maps and the injector rate for the best models obtained by Full-SHM and Parallel-SHM are compared to the corresponding truth (synthetic) and to the base model predictions in Figure 4.27 and 4.28. The results were very close to the true parameter values.

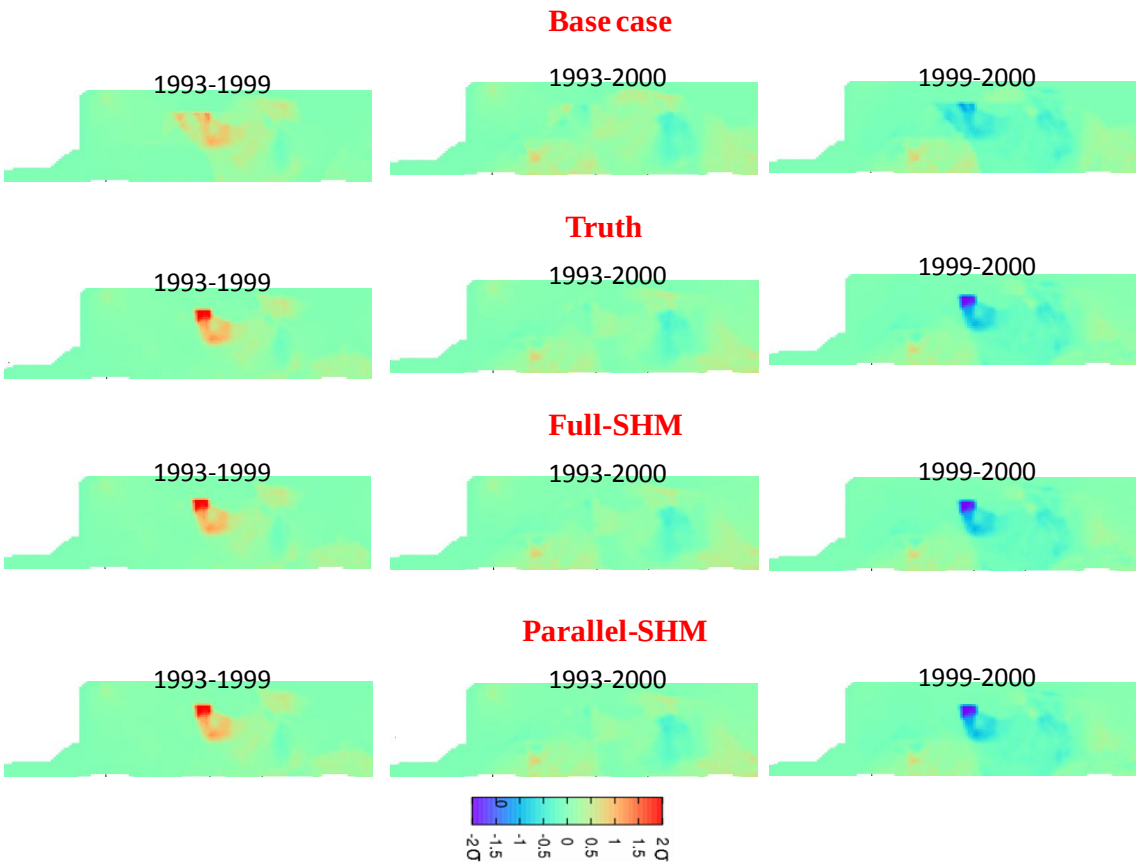

Figure 4.27: Comparison of predicted 4D impedance maps data for the base case, truth case and best models obtained by Parallel- and Full-SHM.

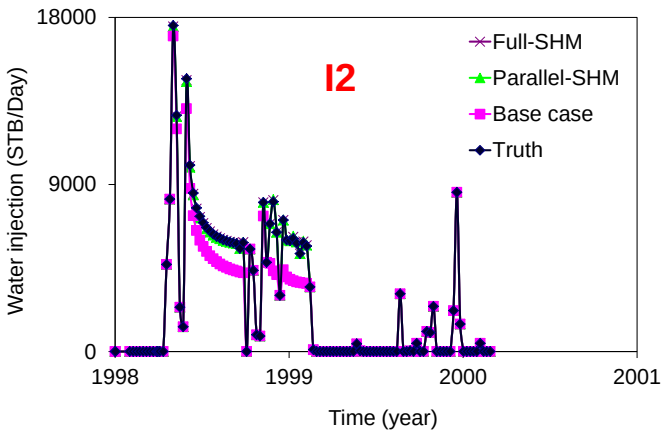

Figure 4.28: Comparison of prediction of injector I2 data for the base case, truth case and best models obtained by Parallel- and Full-SHM.

Comparison of the parameter values of the best models achieved by the methods is shown in Figure 4.29. The standard deviations of the parameter values were estimated based on the variation of their values in the 10 best models obtained by each method; they are represented as error bars on Figure 4.29. The standard deviations are an approximation of the true uncertainty based on a conjecture that if we use more models we over-predict the error estimates while fewer models will under sample the variation. The proper measure of uncertainty of parameter estimates would be the weighted by likelihood, i.e. $L = (exp(-M/2))$, where M is the misfit value and L is likelihood for each model. This analysis was not carried for this research work (refer to Equation 2.13). Although the error bars (Figure 4.29) are an approximation of the uncertainty of the estimated parameter values, we found that the resulting transmissibility multipliers appear to have higher uncertainty using the Full-SHM method, see the error bars. This is because greater convergence has been obtained by the Parallel-SHM method. The results of this synthetic case study show that for most parameters of the transmissibility modifier, the results were consistent with truth case parameter values. However, barrier 'c' did not converge to the truth value, but this parameter did not have a strong influence on the misfit response (see Figure 4.24) and is changing to some degree without affecting the quality of history matching results. Moreover, the path to convergence for parameter values for important barriers 'a', 'b' and 'j' were also slow and all of these were suggestive of a saddle point, a flat point or perhaps a local minimum, particularly for barrier 'j'.

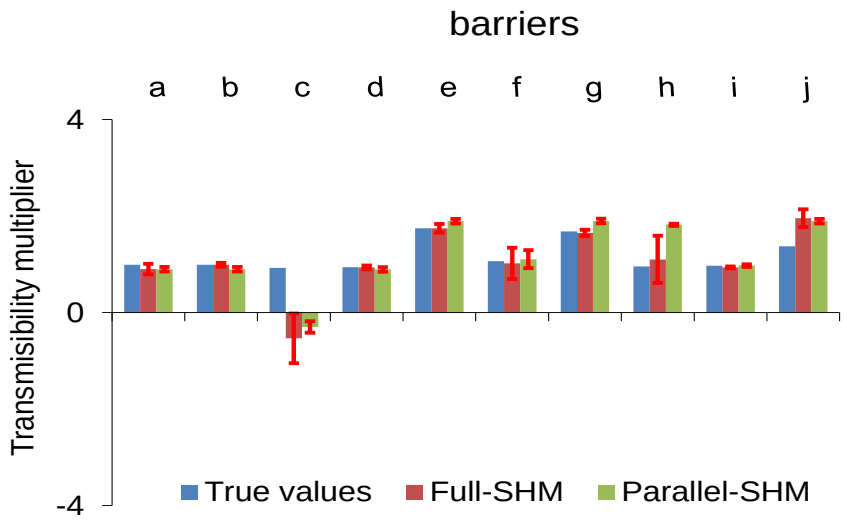

Figure 4.29: Comparison of the parameter values for the best models obtained by Full-SHM and Parallel-SHM to the truth case parameter values. The error bars of parameter values are calculated from of the standard deviation of the 10 best models obtained by each method.

4.6 Limitation of the 'Divide and Conquer' approach

The present approach is not without limitation. The second order nature of the misfit polynomial response surface can be expanded with additional, higher order terms or multiple interactions if the correlation to the true misfit is not high enough. The drawback here though is that more models are then required to determine the polynomial coefficients and parameter values.

In addition the general shape of the misfit may follow a more complex structure. In a seismic history matching synthetic study (the model used by Stephen 2007), permeabilities were modified using the pilot point approach by selection of six permeability multipliers at various locations in the reservoir model, see Figure 4.30. These parameters are labeled from 1 to 6 in this figure. In the base simulation model which was also considered to be the truth, the value of each multiplier was 1.0 (i.e. the parameters were 0.0 in $\log_{10}$ scale).

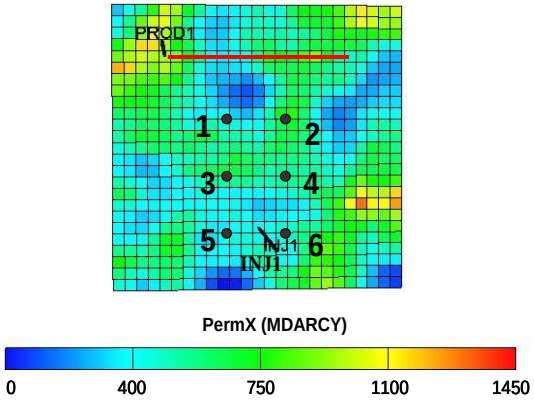

Figure 4.30: Seismic history matching of a synthetic reservoir where 6 Pilot Points of transmissibility multiplier of permeability are perturbed across the reservoir.

For this synthetic model, the 'divide and conquer' method was applied to the case when only seismic data was used in computing the misfit function. Although the method of 'divide and conquer' worked well when the parameters were changed in an interval [0, 1] and [-1, 0] (in $\log_{10}$ scale), it failed when the parameter space was increased and was sampled in [-1,1] space. The results of regression analysis showed that none of the second and third order forms of the polynomial could fit the misfit surface in the parameter interval [-1,1] and having enough correlation factor (i.e. 95% value). We

identified that the shape of the misfit function was quite different on either side of the base model in the interval [-1,1], see Figure 4.31.

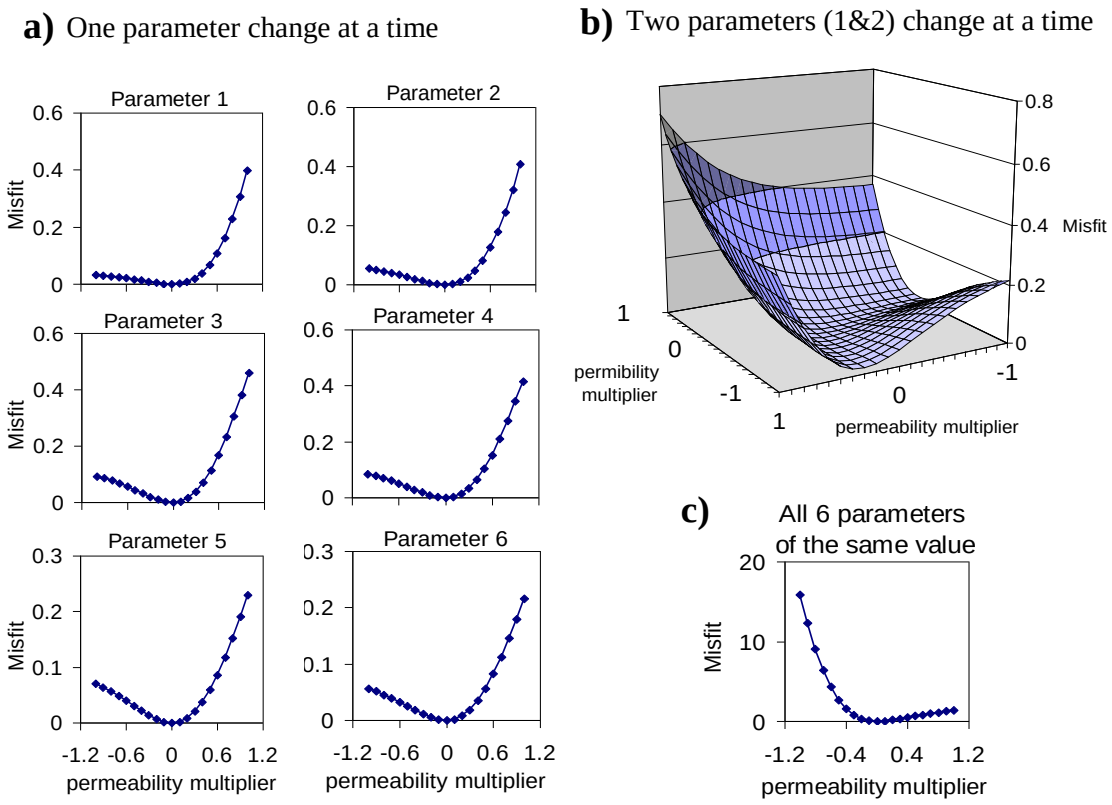

Figure 4.31: Sensitivity of misfit to parameters in the interval of [-1,1] (in log_{10} scale). The permeability multipliers of 6 pilot points were changed in the base case model in three ways: a) one parameter at a time, b) two parameters at a time, and c) all parameters are changed but of similar values.

We concluded that no unique function could adequately define the misfit surface and the parameters were strongly coupled in the interval [-1,1]. In other words, the misfit surface was very asymmetrical and could not be represented well enough by the symmetrical quadratic polynomial for the wider parameter spaces. In this case the correlation between the true misfit and the regression equation (quadratic polynomial) was only that 0.8% (see Figure 4.32a). Also a technique of transformation of parameters to new domains including natural log, powers of 0.5, 1.5, 2.5, and exponentials did not improve the fitted misfit proxy in this interval. Conversely, when the parameters were perturbed in the interval [0,1] the regressed quadratic polynomial misfit was achieved with high correlation factor, R^2 of 0.999 (see Figure 4.32b). Similar

results were obtained for the interval [-1,0], only the results of analysis for interval [0,1] are presented here and in following paragraphs.

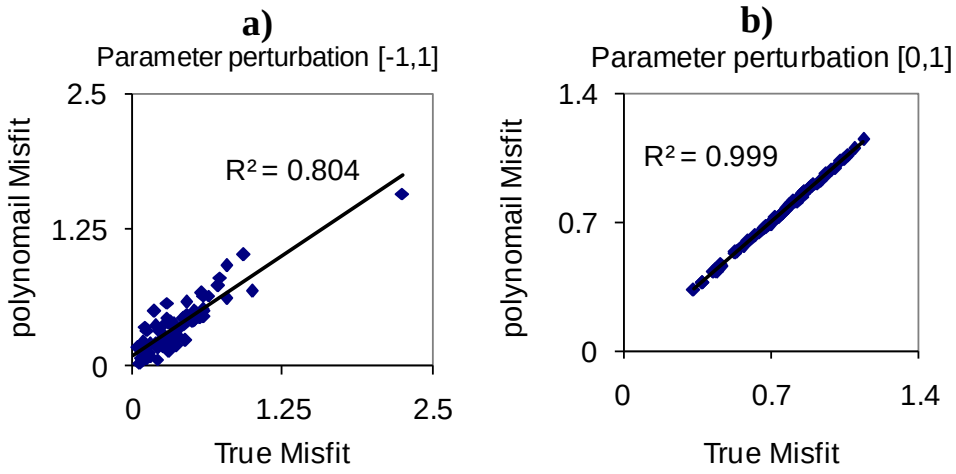

Figure 4.32: Comparison of misfits predicted by polynomial versus the true misfit values when the parameters perturbed: a) in the interval of [-1,1], and b) in the interval of [0,1]. Parameter intervals are in log_{10} scale.

For decoupling parameters in the case of parameter interval [-1,1], we then considered a 50% threshold for the correlation between the true misfits and the misfits predicted by the proxy. While for the case where the sample interval was [0,1], a 95% correlation was used as a threshold as before. Based on the analysis of the remaining interactions coefficients for both cases, the sub-volumes of the parameter space were identified as shown in Table 4.9. Based on these thresholds, there were decoupled sub-volumes for the case [-1,1], and we obtained 3 parameter sub-volumes for the case [0,1]. When the parallel NA routine was applied, for the case [-1,1],we found out that the Parallel-SHM approach did not work. It was as we anticipated because in this case the interactions between the parameters were very strong, and by using a 50% correlation to set the threshold we practically ignored the effect of interaction of parameter 1 with the other parameters during the search for solution of the problem. The method did not converge to the minimum misfit (see Figure 4.33a). Also, since the Parallel-SHM method actually uses the proxy misfit for guiding the search of the parameter sub-volumes, the wrong solution was found as evidenced by convergence to a misfit that was not a minimum. As such the parameters did not reach to the expected values i.e. '0.0', of the truth model (particularly for parameter 1 and 2) (see Figure 4.34a).

Table 4-10: Decoupled sub-volumes in the interval of [-1,1] and [0,1], in log_{10} scale.

Case: Parameters interval	Threshold	number of decoupled parameter sub-spaces	decoupled parameters in separated parentheses
[-1,1]	$R^2 \geq 0.50$	2	(1) (2 3 4 5 6)
[0,1]	$R^2 \geq 0.95$	3	(1 2) (3 4) (5 6)

a) parameter interval [-1,1]

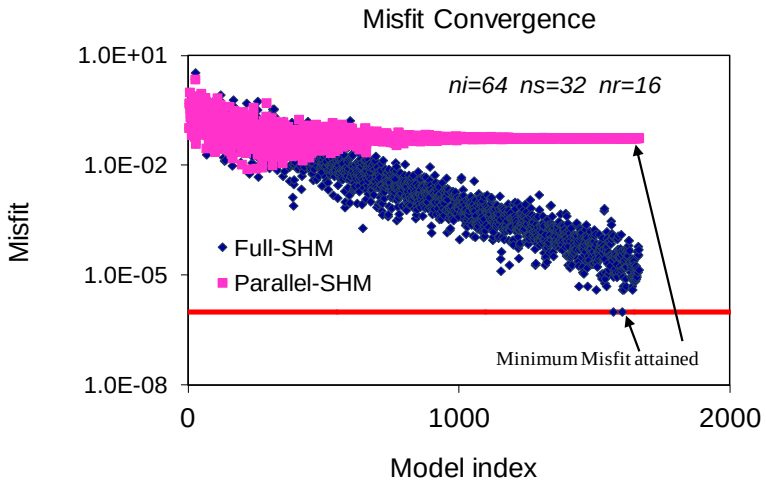

b) parameter interval [0,1]

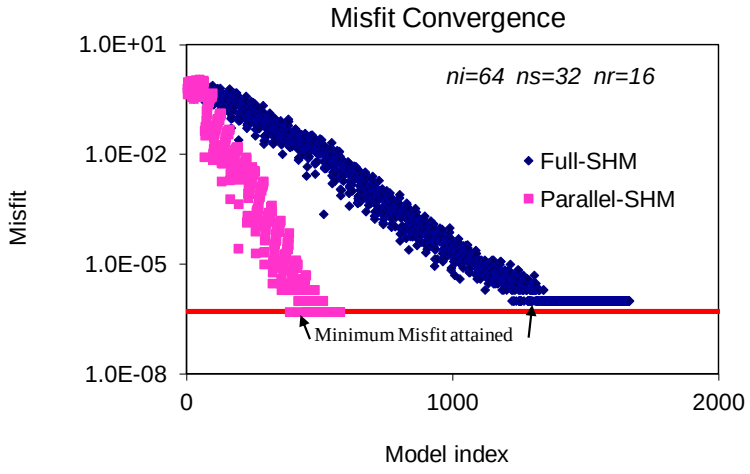

Figure 4.33: Comparison between the misfit convergence of Parallel-SHM and Full-SHM methods for the synthetic example of Figure 4.23. The parameters perturbed in the interval: a)[-1,1] and b))[0,1] in log_{10} scale.

a) parameter interval [-1,1]

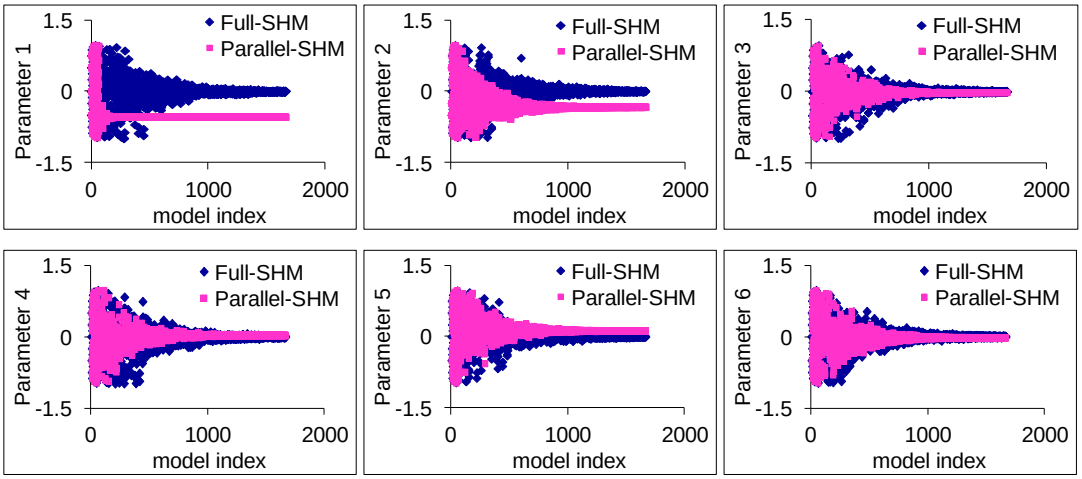

b) parameter interval [0,1]

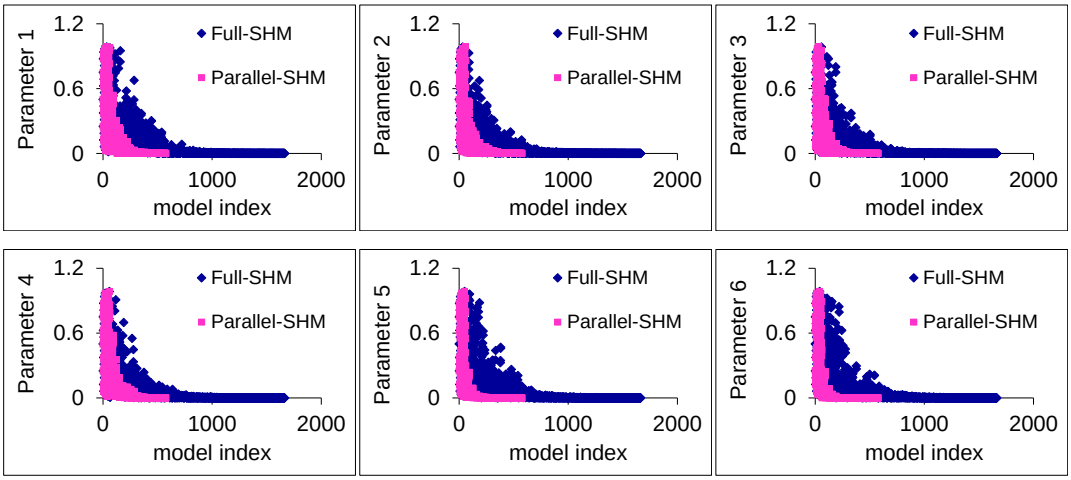

4.34: Comparison between the parameter convergence of Parallel-SHM and Full–SHM methods for the synthetic example of Figure 4.23. The parameters perturbed in the interval: a) [-1,1] and b) [0,1] in log_{10} scale.

The Serial-SHM method did not work in this case either. Initially, we searched the 1D sub-volume (of parameter 1) separately, while the values of the other five parameters (of 5D sub-volume) were '0.0' in the base case model. Since in the truth case the parameter values were also '0.0', the serial search converged to the true solution. However, setting the base case model parameters values of the 5D sub-volume to values other than '0.0', resulted in the serial search of the 1D sub-volume of parameter 1 to converge to the wrong value. This analysis could be used as a check for confirming the result of decoupling of the parameters. Also, the result of dividing of the parameter space could always be checked through construction of misfit proxy for the individual

sub-volumes and comparing the obtained coefficients with the coefficients of the misfit proxy constructed for whole parameters space. If we obtain the same values for coefficients (within the confidence interval) the decoupling of parameter space should be correct.

Nevertheless, for the case [0,1] the method succeeded through application of Parallel-SHM (see Figure 4.33b). The parameters converged to the value of true model. Also, there was 65% improvement in the convergence toward minimum misfit relative to Full-SHM method (see Figure 4.33b). Therefore, in the application of the 'divide and conquer' approach, the correlation between true misfits and polynomial misfits should be quite good, e.g. 95%. Multiple minima may also be ignored by the regression equation but again the correlation coefficient may show this effect, the regions of the parameter space that may show large divergence from the proxy model can be explored. Generally, there is every reason to believe that the 'divide and conquer' approach is very promising and may be extended to other inversion schemes including the Genetic Algorithm or even gradient based methods. The expectation is that any method may be improved if it is over-searching of the parameter space when parameter interactions are low.

In the application of the method in this thesis, the misfit quadratic proxy model itself points to a simple a misfit response with simple structure. We may opt for a direct solution to find the zero gradient locations on the surface. However, we find that the misfit proxy model can be concave downwards with a maximum in some parameters (e.g. for the parameters with negative quadratic coefficient in the polynomial misfit). We also search on a limited range of parameters which may not contain the zero gradient location. There may be multiple minina and they may lie at the extrema. This makes this application of the direct gradient based approaches somewhat more awkward.

4.7 Discussion

A high dimensional problem must be solved in inversion of seismic history matching. Most techniques including the SHM procedure which use stochastic routines such as NA have not always been practical for such high dimensional applications. They need too many flow simulations. In the 'divide and conquer' approach, decoupled sub-

volumes of the parameter space are identified and searched separately more efficiently. The method avoids sampling many unnecessary models that bring no information about misfit surface in the search of the parameter space. The studies presented reveal that including the training dataset (needed in dividing the parameter space), convergence can be achieved requiring 30 per cent of the number of the models required for a full history matching run. If the training models are discounted, only 7 per cent of models are required. Using the Serial-SHM, one sub-volume was searched at a time approach, still the convergence can be obtained using 40 percent of the full SHM set of models but require nearly three times as many models compared to the parallel approach if the training data set are excluded.

In the Full-SHM approach, the large set of initial models is essential when using the NA; it is common in most stochastic search routines. It would make the deconvolution method more attractive if one can find a more efficient means of sampling the parameter space initially in order to construct the misfit response surface for the purpose of misfit decomposition and parameter space decoupling to sub-domains. Experimental design methods are an obvious candidate for this aim and they have been explored and the results of the study are presented in the next chapter of this thesis.

The decoupling approach is particularly useful for amalgamating the local effects of particular parameters on the time-lapse seismic data and well responses. This is complimentary to the localization approaches used with the Ensemble Kalman, EnKF (e.g. Skjervheim et al. 2007, Chen et al. 2009) where more heuristic approximations are used. We could adopt a similar approach using the 'divide and conquer' approach. The misfit of various wells and seismic data could be grouped spatially and then associated sub-volumes of the parameter space could be searched separately. For this some knowledge of the localization is required and appropriate spatial relationships are needed. It may be more appropriate to use present method as shown here as it will find the spatial relationships implicitly. The possibility of localized effects of parameters has been investigated and an approach for spatial decomposition has been invented as part of research work of this thesis (for details see Chapter 6).

4.8 Conclusions

In this chapter the details of application of the 'divide and conquer' approach for efficient solution of the history matching problem was presented. It is given that one could identify the decoupled sub-volumes of the parameters and search them separately more efficiently. The 'divide and conquer' method circumvents the redundant sampling in the search of the parameter space for the minimum misfit. The results subsequently revealed that the convergence of the history matching can be improved significantly in particular using parallel search method and also by serial search of parameter sub-volumes. The conclusions may be summarized in the following points.

- A successful approach for decoupling the parameter sub-spaces and misfit decomposition in high dimensional seismic history matching problems was demonstrated.
- Separate sub-volumes of the parameters as well as dominant parameters were identified in an effective way.
- The 'divide and conquer' method was applied to history matching of observed data from the Schiehallion field with similar improvements in efficiency of the process.
- Further demonstration was carried out using a synthetic case based on the Schiehallion field with great success and leading to saving a great amount of computational cost.
- Convergence was improved by 70 per cent using parallel search of decoupled sub-domains, but by nearly 60 per cent using the serial search.

CHAPTER 5 Improved Convergence in Seismic History Matching Combining Experimental Design with a 'Divide and Conquer' Approach

Introduction

In previous chapter the successful application of the 'divide and conquer' method was presented. The method was based on identification of insignificant interactions between model parameters and subdivision of the parameter space. This was performed using the information obtained by analysis of the ensemble of initial models that the search routine begins with. However, initialization of stochastic inversion routines such as Neighbourhood Algorithm (NA) relies on a large number of models to effectively sample the parameter space, particularly if pseudo- or quasi-random sampling are used which is usually the case for these methods. In this chapter, in order to reduce the number of initial models an approach of integrating experimental design techniques with the 'divide and conquer' method are adopted. Conventional quadratic experimental designs that are commonly used in the modelling of the objective functions of multi-dimensional optimization problems are employed for this purpose and the method are examined on history matching of Schiehallion field.

In this chapter, through the application of method, first we have shown using experimental designs; the number of initial ensemble of simulations runs required in seismic history matching could be reduced by about 85% for a 10-dimensional SHM case of the Schiehallion field (the same real case study from Chapter 4). Moreover, when this new initialization step are combined with Parallel-SHM to search the decoupled parameter sub-spaces of the problem, there are 91% speed up in the convergence rate of the SHM process.

The new method is also applied to a case of 18-dimensional seismic history matching of the Schiehallion field. Normally the inversion of such case requires too many models to be completed using any stochastic minimization routine. For this case the results of

application of combining experimental design with 'divide and conquer' are also accomplished very promising and are attained with an affordable number of simulation runs, 741 model using a parallel search and 1557 models using a serial search, compared to full inversion using Neighbourhood Algorithm (NA) which practically needs many more models.

The major achievement in this chapter is thus additional improvement in convergence of history matching problems. We conclude experimental designs perform efficiently to train a proxy to misfit, which can then be used to decouple the parameter sub-volumes, giving an order of magnitude saving in simulation rums. The approach of 'experimental design combined with divide and conquer' is a practical way to be used in particular for high dimensional SHM cases.

5.1 Experimental Designs Combined with the Parallel-SHM

The basic idea behind using Experimental Designs (ED) method is to vary multiple parameters at the same time so that maximum inference can be attained with minimum cost. Once the appropriate design is established and the corresponding experiments (simulations) are performed, the results can be investigated by fitting them to the response surface. Central Composite Design (CCD), Box-Behnken Design (BBD), and D-optimal (D-opt) are quadratic designs that assume no lack of fit. They are variance-based designs which are generated in such a way that the random variation would be minimized. For more details on experimental design see Chapter 2 and Appendix A. A comparison of the designs used here is presented below.

5.1.1: Overview of Different Design Strategies Used

Central Composite design is an efficient way of providing sufficient amounts of information to test the fitness of a model in a minimum number of required runs. It is partitioned into two subsets of model samples; the first subset estimates linear and two-factor interaction effects while the second subset estimates curvature effects. In this study, to reduce number of experiments, resolution **R(V)** applied to experimental design (for details see the Matlab scripts "CCDESIGN.m"). In resolution **R(V)**, the main effects are aliased (also known as confounding) with 4-parameter interactions, and 2-parameter interactions are aliased with 3-parameter interactions (for more details about

aliasing the parameters and resolution of the sampling in CCD design refer to Mason 2003). The Box-Behnken design has three levels per factor with no points at the vertices of the cube defined by the ranges of the factors. Therefore in contrast to the CCD design, the feature of BBD design is that it is "corner free". Because it is an exact quadratic design, at least one of the factors is at its midpoint in all experiments. BBD design should be considered to be used when there is no interest in predicting behaviour in the corners of the design space of a quadratic surface. Such designs are especially useful when it is desirable to avoid extreme points due to engineering considerations or limitations.

For irregularly shaped domains, or when the number of experiments to be performed does not fit any of the standard designs (due to limitation of the sample size), it is common to numerically determine the best set of sampling points using the popular D-optimality search criterion. Typically, a candidate set of models (samples) is generated, on a grid of the parameter space. Then an optimal subset with a given number of samples is searched to maximize the determinant of the matrix used for solving the least squares formulation of the regression method (for least square regression see Numerical Recipes, Press 1992). This optimal criterion minimizes the volume of uncertainty around the vector of estimated coefficients of the regressed model. To be similar to other variance-based criteria, the optimization algorithms used to construct the D-optimal designs place most of the selected points on the boundary of the parameter region albeit irregularly. In contrast, this is always the case in the CCD design. In D-optimal design, one measure of the quality of the design is the size of the relative variance of the coefficients which is lower than other designs.

Quasi-Random (QR) sampling seeks to randomly place the data points on the parameter space. Nevertheless the relative ratio of the sampling points in the boundary of the parameter region relative to the total design samples is still less than that it is in the CCD design. For BBD, D-opt and QR sampling, the consequence of these characteristics is higher uncertainty of prediction near the vertices compared to the CCD design.

In the CCD design only a small numbers of centre runs are added to the first-order design to detect the existence of curvature and to better resolve the response surface around the quadratic effects. Further, the orthogonality property is preserved, but the

design is not variance optimal anymore. In other words, the variance of regression coefficients is no longer minimized on a per observation basis. However it has better outcome in the prediction of other design sampling points.

5.2 Application to the 10-dimensional SHM Case in the Schiehallion Field

The details of the application of the 'divide and conquer' approach to a 10-dimensional case study of seismic history matching of the Schiehallion field, for the 'total 4D seismic misfit only' scenario, were given in Chapter 4. There, 1024 of samples were generated to initialize the full inversion process and these were used to construct the misfit polynomial proxy. The models were primarily based on Quasi-Random (QR) sampling. Here, the three sampling designs of Central Composite (CCD), Box-Behnken (BBD), and D-optimal (D-opt) were used to sample the parameter space of the same problem. The CCD and BBD designs required 149 and 161 model evaluations to sample the 10-dimensional parameter space efficiently, respectively. For a user-defined D-opt design 150 models were drawn. In this application, to follow the above sampling strategies, the reservoir simulation models were run to calculate the misfit values where only the 4D seismic data were used in the objective function (see Equation 2.1 of Chapter 2). Based on these data the misfit regression polynomials were constructed for use of each of the three designs.

The misfit predictions by polynomials were compared to the true misfit values from the objective function. The correlation, R^2, between the misfits recalculated by regression models and the true misfits, was 0.998, 0.991 and 0.996 for CCD, BBD, and D-opt cases, respectively. Figure 5.1, shows the cross plots of the misfits re-calculated by polynomial versus true misfit values for the three cases. They were compared with corresponding cross plot when quasi-random sampling was used in the full inversion process of the problem. All results were consistent.

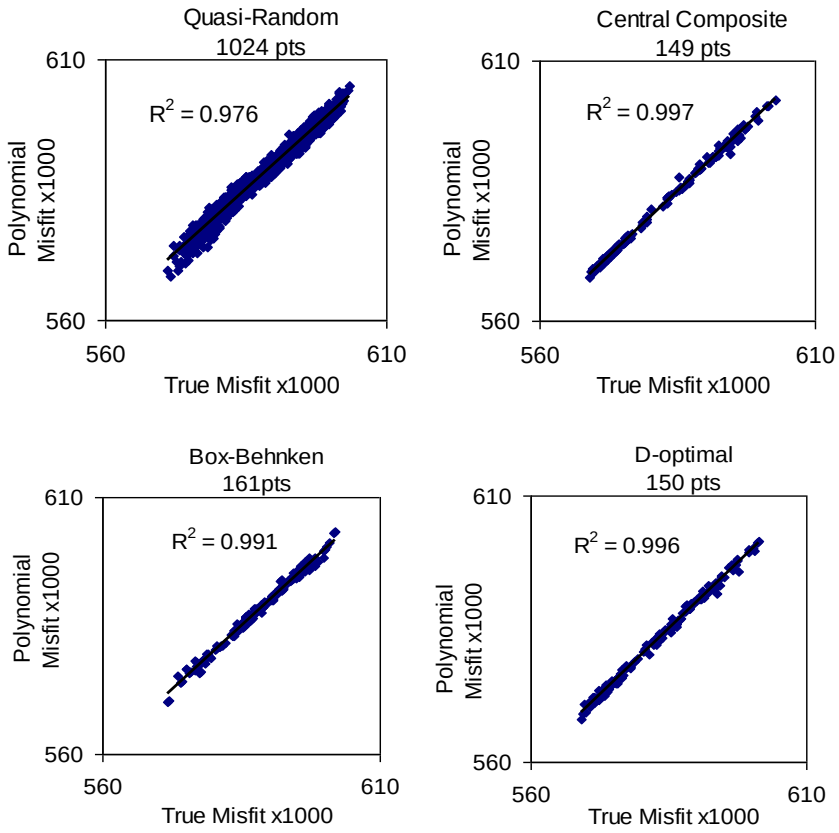

Figure 5.1: Cross plots of polynomial misfits against true misfit for different experimental designs. The number of sampling models (points) used to construct the proxy model by each design method is shown in the plots.

We then verified whether or not the proxy model equation actually has a statistical significance. In other words, we tested whether the relationship we derived when setting up each of the quadratic polynomial models has any meaning in the specified parameter space when compared to the true misfit data. As a result we applied a kind of bootstrap technique. This was performed using the misfit polynomials obtained by a particular experimental design to predict the misfits of all the other designs. The cross plots of the prediction of design polynomials against all other design datasets are shown in Figure 5.2, in most cases the correlation, R^2, between these data was around 90%. The exception was for the correlation of the predictions of the CCD data points using the misfit equations obtained by other sampling designs, for which the correlations, R^2, was about 80%. It was due to the dissimilarity of the sampling scheme of the CCD design compared to BBD and D-optimal designs and also QR sampling (refer to previous section).

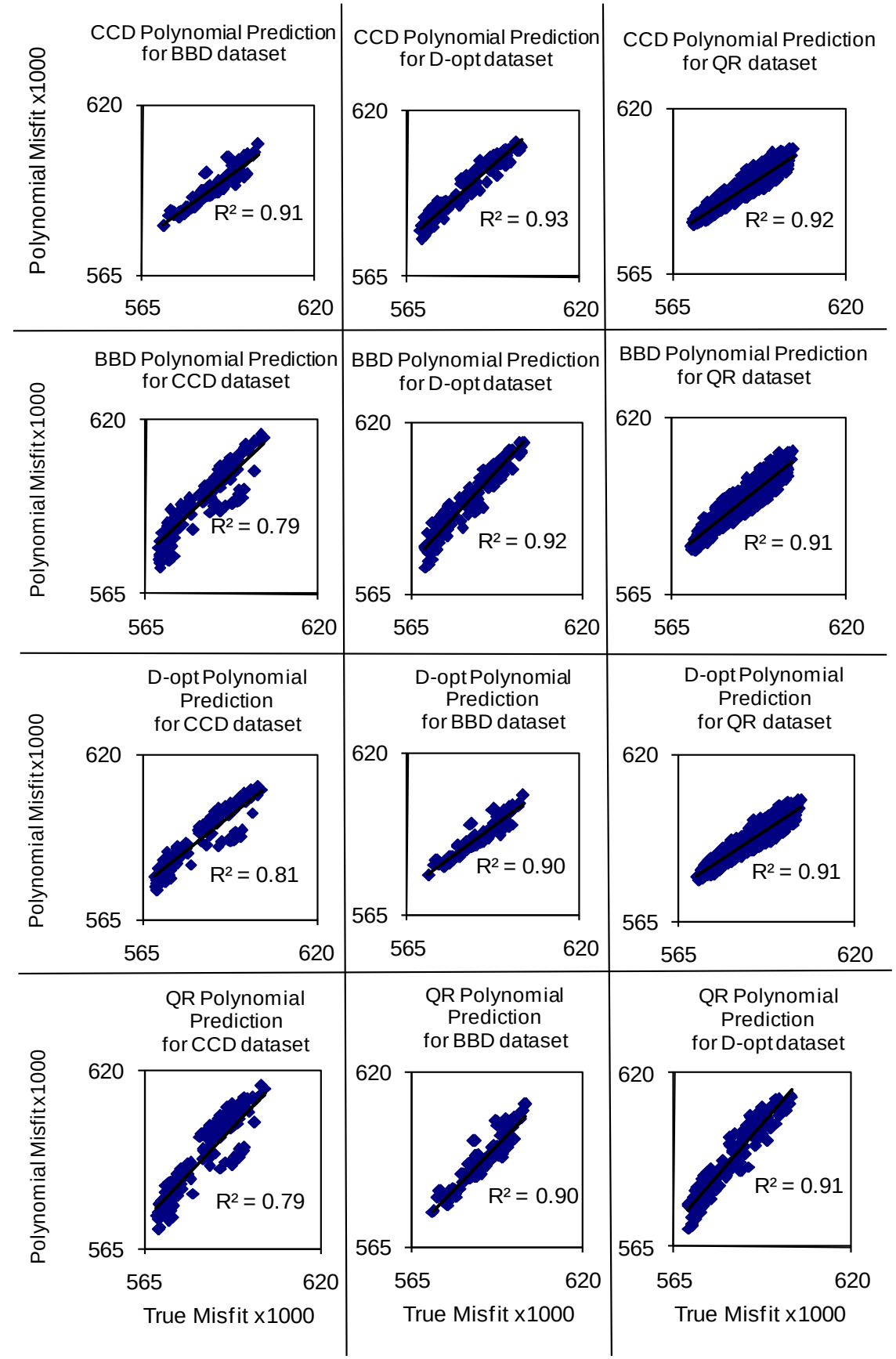

Figure 5.2: Correlation between the misfit predictions of each polynomial model (by row) and using the data points of the other designs (by column). The analysis is applied for each of the proxies obtained by CCD, BBD, D-opt and QR sampling strategies.

The prediction variance is a diagnostic tool for evaluating and comparing the response surface designs and validating the polynomial misfits using different experimental designs. The average relative prediction errors were calculated in each case. They were computed as the mean of the sum of the relative differences between the predicted misfits by the polynomials and the true misfits (see Equation 4.1 of Chapter 4). The results are presented in Table 5.1. They are of small values and are between 0.6% and 1.9%. Because of the random characteristic of Quasi-Random sampling, the average relative prediction errors of these data points by all misfit polynomials are smaller, while for designed samplings, especially for systemised D-optimal design they are of higher values.

Table 5-1: Average relative prediction errors by polynomial misfits for models from other experimental designs

Constructed Misfit Polynomial based on Experimental Design of:	Average Relative Prediction Error (%)			
	Prediction for models from:			
	CCD	BBD	D-opt	QR
CCD	-	0.92	1.89	0.92
BBD	1.83	-	1.92	0.98
D-opt	1.47	0.58	-	0.6
QR*	0.72	1.61	1.68	-

QR is Quasi-Random Sampling.

Similar to Chapter 4, the regression models were further validated by testing different sets of data points obtained in the Full-SHM inversion of the example (for details see Chapter 4). They consisted of: i) the first 96 models, ii) the total set of 2980 models, and ii) the final 96 models. These models were different from the trainee models used to build the misfit polynomials. For all cases the mean relative errors were calculated. They were of small values; i.e. around 1% for first 96 test points, less than 1.5 % for all 2980 test points, and at most 2 % for last 96 test points (see Figure 5.3).

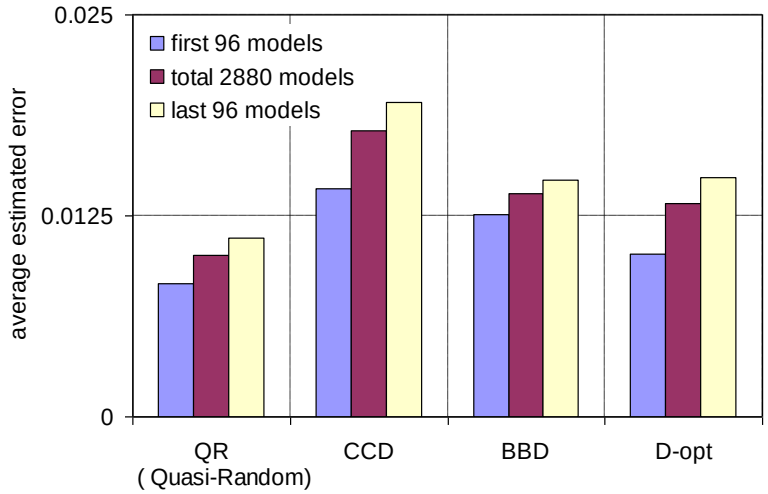

Figure 5.3: Mean relative error of predictions by polynomial misfits for test data points in different cases of using experimental designs compared to using Quasi-Random sampling.

Figure 5.4 compares the main effects (main significant coefficients) in the misfit polynomials obtained by the various design cases. Also, the error bar obtained based on 95% confidence interval for each coefficient is shown in Figure 5.4 (for more details on estimation of standard error and confidence interval of the coefficient see Montgomery 2000). They were quite similar apart from the relatively insignificant effects of barriers 'f' and 'd'. Barrier 'f' only shows a linear effect for the case of quasi-random sampling and it does not reveal any significant effect using other experimental designs. Barrier 'd' does not show any influential linear effect for the case of using BBD design nor any significant quadratic effect when using D-opt design.

Barrier 'f' is located to the southwest and barrier 'd' is situated to the northwest of the injector I2. The pressure propagation to the left of the injector I2 is mainly controlled by transmissibility of the barrier 'i' which is elongated to the west and close to the injector I2. Therefore, other barriers to the west of injector I2 beyond the barrier 'i', generally would have less influence in controlling the pressure propagation of the injector and thus the seismic misfit (compared to barrier 'i'). In particular, for barriers 'c' and 'h' there are negligible effects (not displayed in the plot of Figure 5.4), and there are effects for barriers 'f' and 'e', which are quite small. There are multiple interferences of effects as found by using various design methods. It seems that when both linear and quadratic effects of barrier 'e' are negative then barrier 'f' should be of

positive effect. There is an anti-correlated interaction, i.e. as one effects goes up the other goes down to have the same effect.

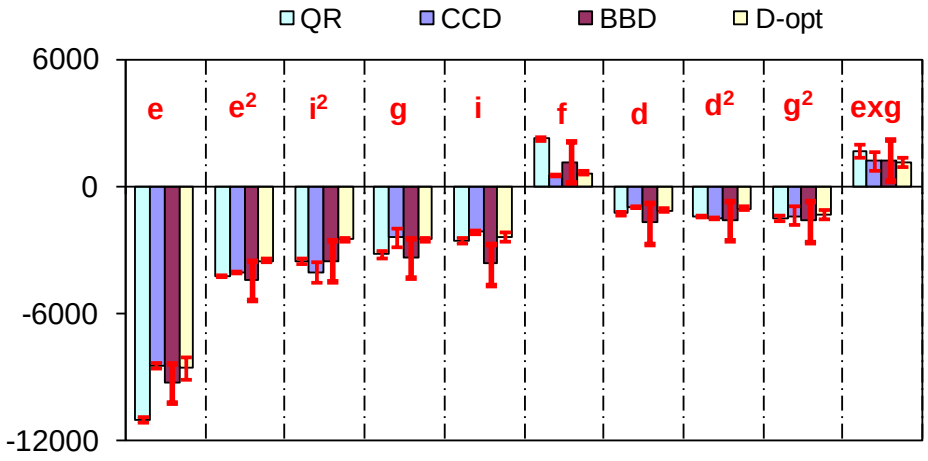

Figure 5.4: Comparison of the significant effects (coefficients) in the misfit polynomials obtained by various experimental designs. The error bars are based on 95% confidence interval obtained for each coefficient prediction (for more details see Montgomery 2000).

Obviously, the deduced effect of parameters by various sampling methods is to some extent different since each method is based on only a limited number of models for each particular strategy. In fact, the more exact calculation of parameter effects and their interactions for a 10-dimensional parameter space requires numerous models to be run using full factorial designs (of at least 3-levels). In the conventional approach (using QR sampling) the parameter space is sampled randomly for many models. However there remains lack of confidence that the effects identified are more accurate, despite the large computational cost. Alternatively, using the design sampling they could give us equivalent information but with much less cost.

Having obtained the misfit polynomials, the parameter sub-volumes were then decoupled. This was performed by gradually discarding the insignificant interaction coefficients in the polynomial misfits and measuring the deterioration of the correlation between polynomial misfits and the true misfits. The correlation minimum of 95% was used as a threshold for keeping significant interaction coefficients. Subsequently, based on the remaining significant interaction coefficients in the polynomials, the non-

interacting parameter groups were decoupled. We sought out links between the parameters and subdivide accordingly, e.g. if we found that Parameter 1 interacts with Parameter 2 and Parameter 2 with Parameter 3 but with no other parameters, this defined a 3D sub-volume. Table 5.2 shows the decoupled parameter sub-domains obtained using different designs. The results are identical and are the same as the previous result presented in Chapter 4 where the initial models were generated using QR sampling.

Table 5-2: Decoupled parameter sub-volumes.

Design method	Number of sub-volumes	Decoupled parameter sub-volumes in parentheses
QR*- 1024 models CCD- 149 models BBD- 161 models D-opt- 150 models	9	(e g) (a) (b) (c) (d) (f) (h) (i) (j)

**** Quasi-random sampling***

The parallel version of the NA routine was used once more. The NA tuning parameters were set as before (see Chapter 4). That is, we used n_s = 96 and n_r = 48. Thus two models (n_s/n_r = 2) were generated in the vicinity of the space of the best models (n_r) in each NA search, for which there were two iterations (it=2). In each case, the design models used to construct the polynomial misfits were also used. They were deployed as initial models (n_i) for applying the parallel NA routine. As a result of using experimental designs the number of initial simulation runs was reduced dramatically.

When the parameter sub-domains were searched using this 'Parallel-SHM combined with experimental design' method, 91% speed up in the full inversion process of SHM process was obtained. Figure 5.5 shows the misfit evolution using various experimental designs in comparison to the Parallel-SHM (of Chapter 4 with QR sampling) and the Full-SHM methods. Figure 5.6 illustrates the convergence of parameters toward the best model by these methods. In Table 5.3 comparison of the simulation and performance of various methods are summarized.

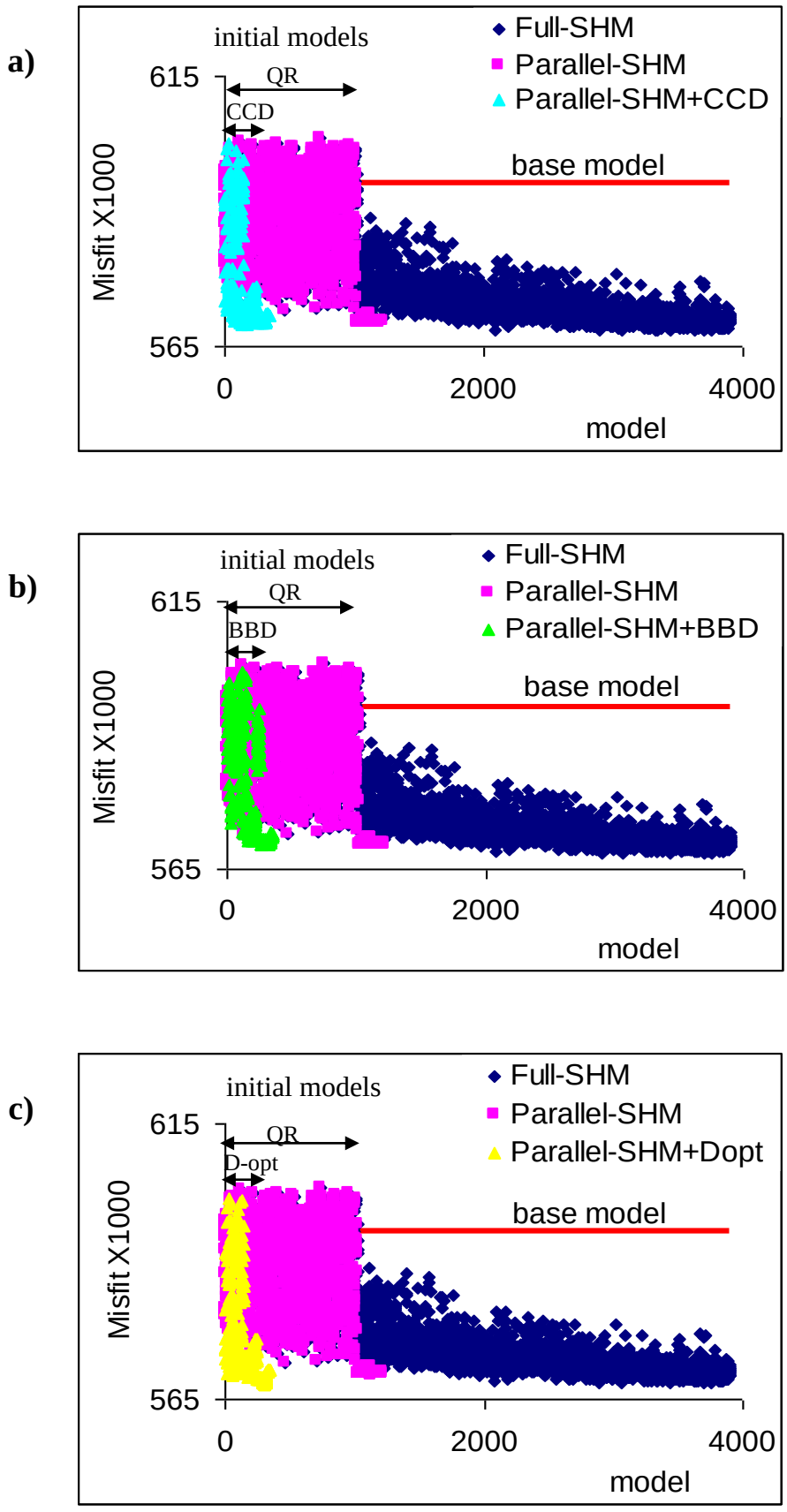

Figure 5.5: Misfit evolution by the 'Parallel-SHM combined with experimental design' method compared to Parallel-SHM and Full–SHM process for various designs: a) CCD, b) BBD, and c) D-opt designs.

a) Parallel-SHM combined with CCD

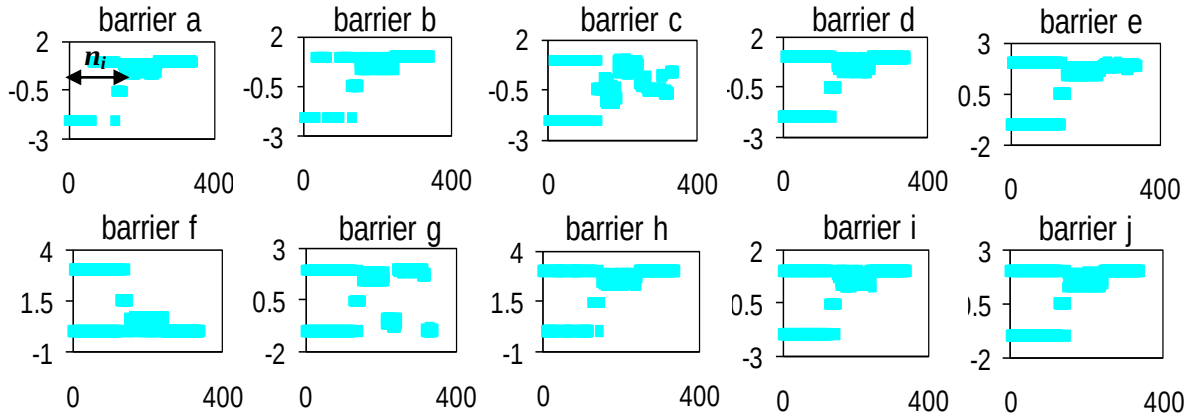

b) Parallel-SHM combined with BBD

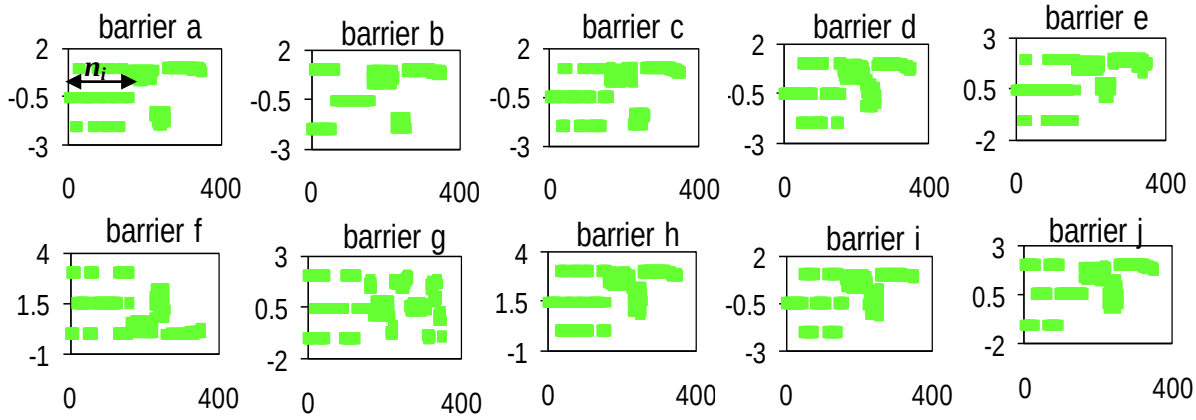

c) Parallel-SHM combined with D-opt

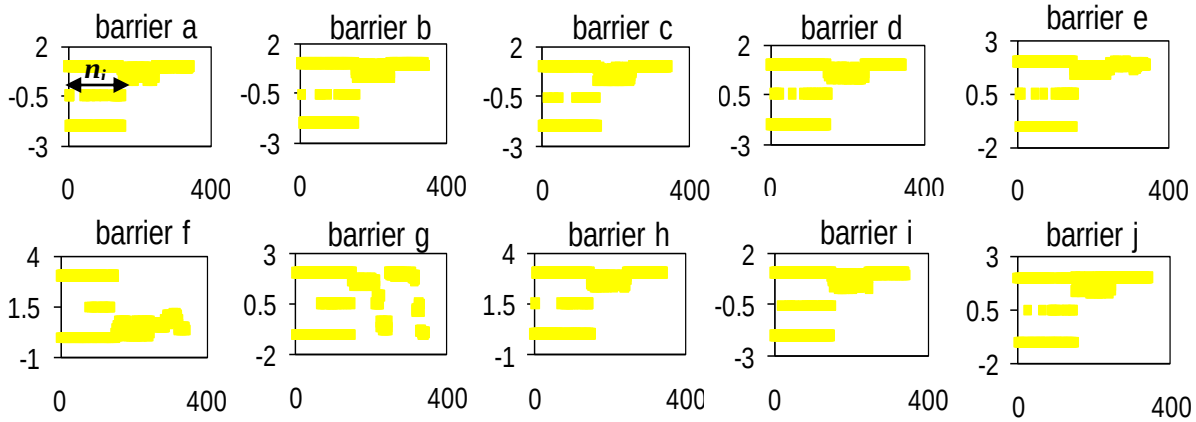

Figure 5.6: Convergence of the parameters toward best models using 'Parallel-SHM combined with experimental design' in various cases: a) CCD, b) BBD, and c) D-opt designs.

Table 5-3: Summary of simulation performance for various SHM approaches.

Method	Initial models sampling method	Number of initial models*	CPU for initial models (days)	Number of models after initial models	CPU after initial models (days)	Total CPU (days)
Full-SHM	QR	1024	5.69	2880	16.0	21.7
Parallel-SHM	QR	1024	5.69	192	1.07	6.76
	CCD	149	0.83	192	1.07	1.90
	BBD	161	0.89	192	1.07	1.96
	D-opt	150	0.83	192	1.07	1.90

Simulation run of each model takes around 8 minutes on a 3.4 GHz processor.

Updated parameters values for the best matched model obtained by various methods are compared in Figure 5.7. For the most significant parameters the results are consistent. The exceptions are mainly for barriers ‘c’ and ‘d’ in the case of Full-SHM method, and for barrier ‘f’ in various cases. We concluded that either a saddle point or multiple minima exist in the solution because of the variation in the best values we obtained for significant parameters such as barriers ‘h’ and ‘j’. The results signify the non-uniqueness of history matching problems. Multiple best models were obtained by various methods probably because of the existence of multiple minima in the misfit surface of the problem. It is common that the use of different inversion routines leads to various minima, thus inconsistent updated parameter may be obtained especially for less dominant parameters. In our case, the best model predictions for seismic maps by different approaches are very similar however. They are compared with the observed seismic maps in Figure 5.8.

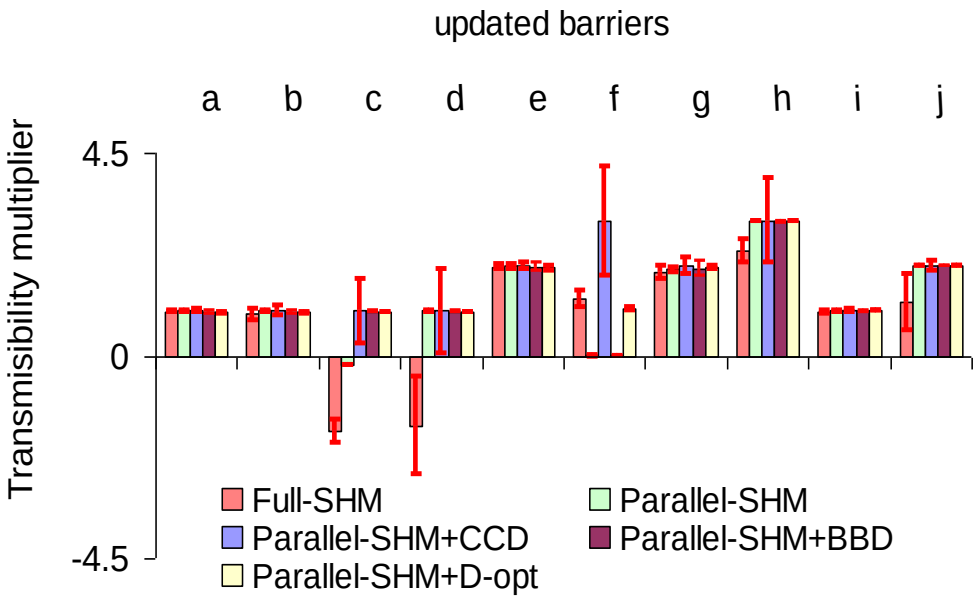

Figure 5.7: The best value obtained for parameter values, with error bars calculated based on 10 best models acquired in each method.

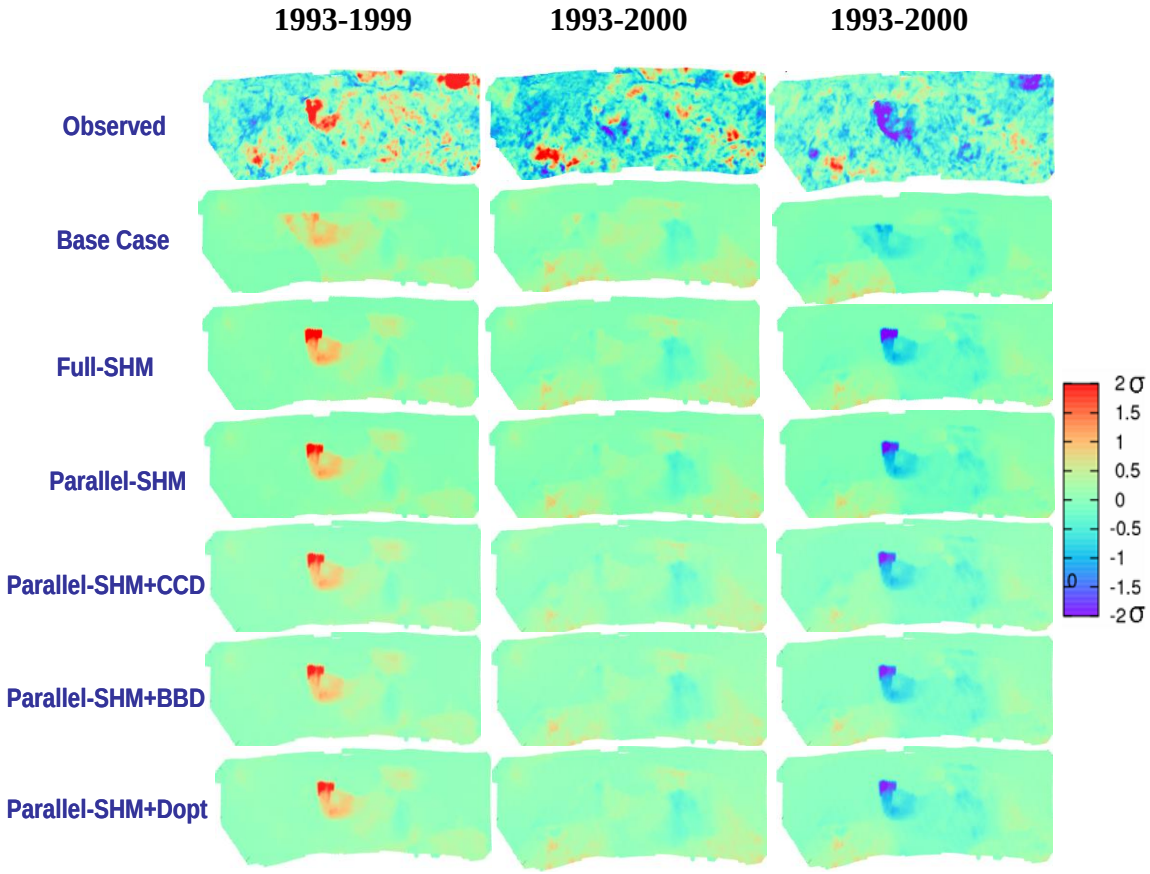

Figure 5.8: Match for seismic predictions of differences in acoustic impedance maps obtained by various approaches is compared to observed data.

5.3 Application to the 18-dimensional case

Simultaneous updating of several parameters that control changes to permeabilities, transmissibility of barriers and the petro-elastic transform parameters was carried out using the SHM method previously (Stephen et al. 2006). Here, we have applied the 'Parallel-SHM combined with CCD design' method on a large dimensional example that includes simultaneous updating of the transmissibility of barriers as well as permeability and net:gross. In this case, 18 parameters were considered for updating which is too large for the Full-SHM application. Also a longer history period for reservoir production and 4D seismic data was considered which increased simulation time (each model run took twenty minutes).

The case study included the previous 10 transmissibility multiplier of barriers 'a' to 'j' plus transmissibility multipliers of 2 new barriers ('k' and 'l') that have impact on the later history data (i.e. history added from 2000 up to 2004). In addition, 6 more new parameters that take account of two multipliers of net:gross (NTG), two multipliers of horizontal permeability (PermH) and two multipliers of vertical permeability (PermZ) were included. They were perturbed by two groups of pilot points (see Section 2.6 of Chapter 2 for more details on the pilot point method). In each group several individual pilot points were changed to control the petro-physical properties locally in the area with high seismic mismatch particularly where there are strong seismic anomalies around the injectors I2 and I5. Figure 5.9 illustrates the position of the new barriers ('k' and 'l'), and the two groups of pilot points on the Schiehallion Segment 4 reservoir model. The individual pilot points of the two grouped pilot points are also shown in Figure 5.9.

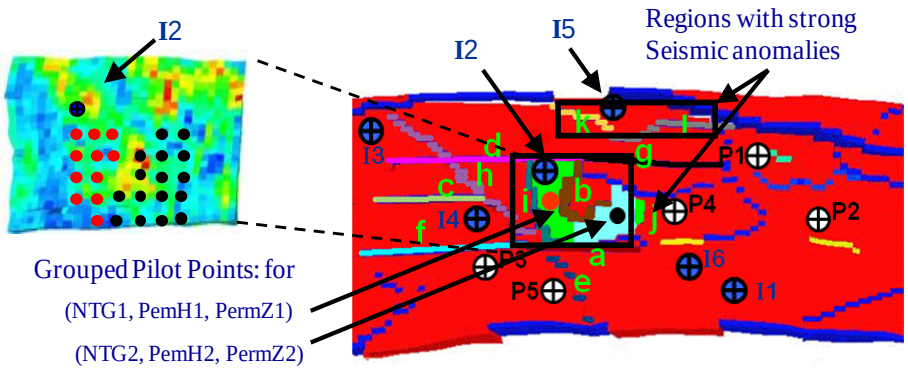

Figure 5.9: Parameters updated in the18-dimensional SHM case of Schiehallion field.

The pilot points were placed with equal spacing on a grid that is coarser than the reservoir grid cell, referred to as the pilot point grid (see Figure 5.10). Multipliers of the net:gross, horizontal permeability and vertical permeability were applied to the pilot points and changes to the properties of the neighbouring grids (area around the injector I2) were made through application of kriging. For this case the parameters describing the pilot point and kriging method are shown in Table 5.4 (for more description on these parameters, see KT3D code in the GSLIB manual).

Table 5-4: Parameters describing the applied techniques of pilot point and kriging.

Pilot point grid separation in x direction	2
Pilot point grid separation in y direction	3
Layers modified	1-8
Minimum horizontal range for the kriging variogram*	2
Maximum horizontal range for the kriging variogram	3
minimum data used for kriging	4
maximum data used for kriging	8
search radii in x, y and z directions	50
angles capturing geometric anisotropy x, y and z directions	0.0

****The ranges are measured in the grid cell. It is best to set the range of the variogram equal to the size of the pilot point separation.***

As in the previous 10-dimensional example, the transmissibility multiplier of each barrier was modified by a second controlling modifier. For barriers 'a' to 'j', they were changed in the same intervals as for the previous 10-dimensional SHM example (see Table 4.2). The lower and upper bound as well as mid values (in $\log_{10}$ scale) for the new parameters/multipliers that were added to current SHM example are listed in Table 5.5. Similar to the previous example, in the base model, the value of multipliers are 0.0 in $\log_{10}$ scale (or 1.0 in linear scale).

Table 5-5: Ranges and mid values of the modifiers to transmissibility expressed on a log_{10} scale. The base case is represented by a modifying factor of 1 (or zero on the log_{10} scale).

Parameter*			**Range**
Multipliers	Min.	Mid.	Max.
k	-1	1	3
l	-3	-1	1
NTG 1	-0.3	0.0	0.3
NTG 2	-0.3	0.0	0.3
PermH 1	-0.15	0.0	-0.15
PermH 2	-0.15	0.0	-0.15
PermZ 1	-0.15	0.0	-0.15
PermZ 2	-0.15	0.0	-0.15

**** The barriers and groups of pilot points are shown in Figure 5.9***

In this example, the history matching began in 1998 and continued up to the end of 2004. During this period a total of eleven wells (including 6 producers and 5 injectors) were active in the reservoir. The producer's oil and injector's water rate history data are shown in Figure 5.10. In addition to the preceding observed seismic dataset (refer to Section 4.2 of Chapter 4), additional 4D seismic data have been used. Therefore, there are 6 seismic surveys consisting two acquired pre-production surveys of 1993 and 1996 as well as four monitor surveys which captured in 1999, 2000, 2002 and 2004. We refer to these two datasets as 'Phases I' and 'Phase II', by the difference in their acquisition and processing used. The Phase I dataset was collected for three seismic surveys of 1993 as baseline and 1999 and 2000 as monitors and the remainder are Phase II. For these data the process of cross-equalisation, calibration and transformation of Migrated Stack was performed by a combination of phase rotation and filtering, to produce the Coloured Inversion Stack. Time-to-depth conversion and the location of the reservoir horizon was provided by the operators and used to generate a map of Root Mean Square (RMS) amplitudes from the Migrated Stack by integrating the signal over a suitable time window (Leach et al. 1999). Then for Phase I data, a second attribute, the Sum of Negative Values, was obtained by summing the negative amplitude in the Coloured Inversion stack from the picked horizon to 20 ms below. This was used as pseudo-impedance. However, Phase II 4D seismic data which consisted of 1996 as of the

baseline, and 2002 and 2004 as monitors. 4D attributes was obtained using the RMS amplitudes of the coloured inversion stack. This was obtained by integrating the signal from 5 ms above the picked horizon to 25 ms below, and was also considered as pseudo-impedance. Both Phase I and Phase II dataset 4D attributes were used as a difference in pseudo-impedance to detect pressure and saturation effects via the time-lapse maps, these data are shown in Figure 5.11.

The noise in the seismic data was analysed previously (Soldo 2005). It was identified that for the Phase I dataset the errors were not correlated in space (on the simulation grid scale) and could be represented by the standard deviation of data for each 4D monitor map. For Phase II seismic data, it was assumed that the same level of data error was present (Edris 2009). The normalization of Phase I data was made by Stephen et al. (2006), the same procedure was used again (refer to Equation 3.8 of Chapter 3). That is, for both datasets the 4D attribute maps were normalised to the baseline by subtracting the mean and dividing by its standard deviation, to gain a comparable change in magnitude and signs between surveys. As it is observable from Figures 5.10 and 5.11, there is a relationship between the well activities and the seismic response. The main signal in Phase I seismic data is due to the injector I2, whereas for injector I1 and I3 there are less obvious signals. For the Phase I dataset, the major seismic anomaly is as a feature of softening in the first year of production (map 93-99 in Figure 5.12) that occurs around injector I2, followed by hardening for the next year when the well is switched off (map 93-00 in Figure 5.11).

For Phase II data the main signal in the maps were observed around the injector I5 (maps 96-04 and 02-04 in Figure 5.11), and there is a pronounced effect of softening due to recognizable pressure increase around the well. As the production continues, the responses of producers P1 and P5 become stronger; however for injectors I1 and I3, which are constantly injecting water into the reservoir, still there is no clear response. Around producer P2 a signal is observable probably due to the effect of the gas coming out of the solution. By simple visual interpretation, it is understandable that there is clearly a high degree of compartmentalisation and heterogeneity, perhaps due to a combination of faulting and channelised structures in the reservoir, which is recognizable by 4D differencing (for more details, see Stephen et al. 2005 and Edris et al. 2008).

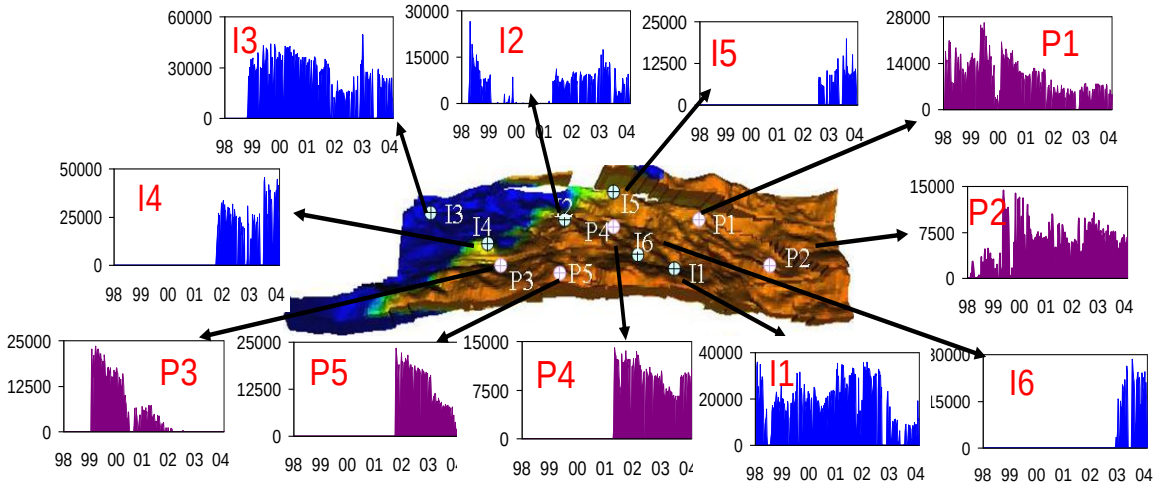

Figure 5.10: Producers oil rates and injectors water rates history data for the active wells in the period of 1998 to 2004.

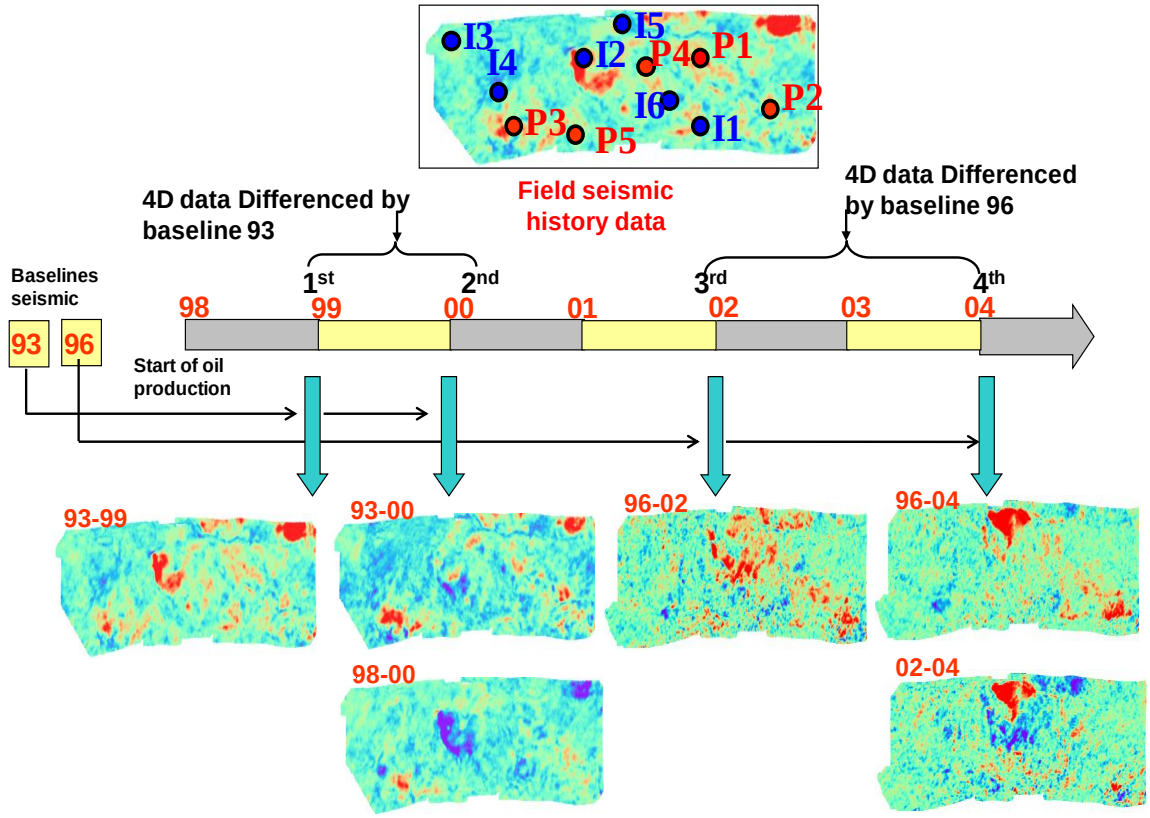

Figure 5.11: Available 4D seismic history data (baselines and monitor surveys), for the period starting from 1998 up to 2004. Maps in the figure show the differences in pseudo-impedance for two datasets of: i) Phase I comprised 1993 as a baseline for 1999 and 2000 monitors, and ii) Phase II comprised 1996 as a baseline for 2002 and 2004 monitors. Prior to differencing the attributes, each survey was normalized by subtracting the mean for corresponding baseline and dividing by its standard deviation (Stephen et al. 2005).

Figure 5.12 shows the base reservoir simulation predictions of the pressure, water saturation, and gas saturation for 2002 and 2004 conditions. For the initial pre-production and conditions at 2000, see Figure 4.4 of Chapter 4. The base model well data predictions are shown in Figure 5.13 for the producers and in Figure 5.14 for the injectors. For the majority of producers (except producer P4 and P5) and most the injectors (except injector I2), their historical rates are predicted quite well by the reservoir base case model.

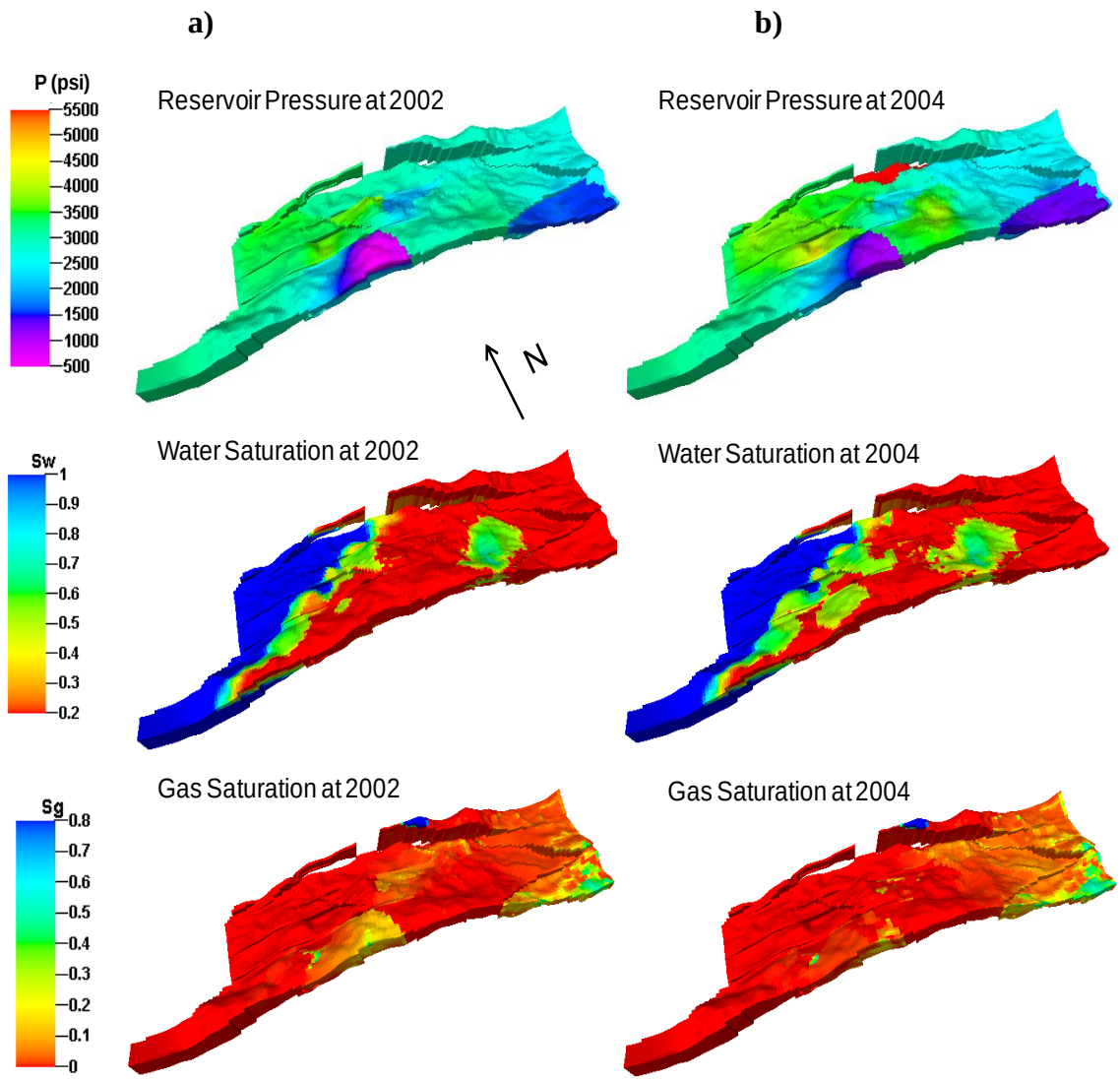

Figure 5.12: Pressure, water and gas saturation from the base case simulation model for: a) 2002, and b) 2004. For the initial pre-production and conditions at 2000, see Figure 4.4 of Chapter 4.

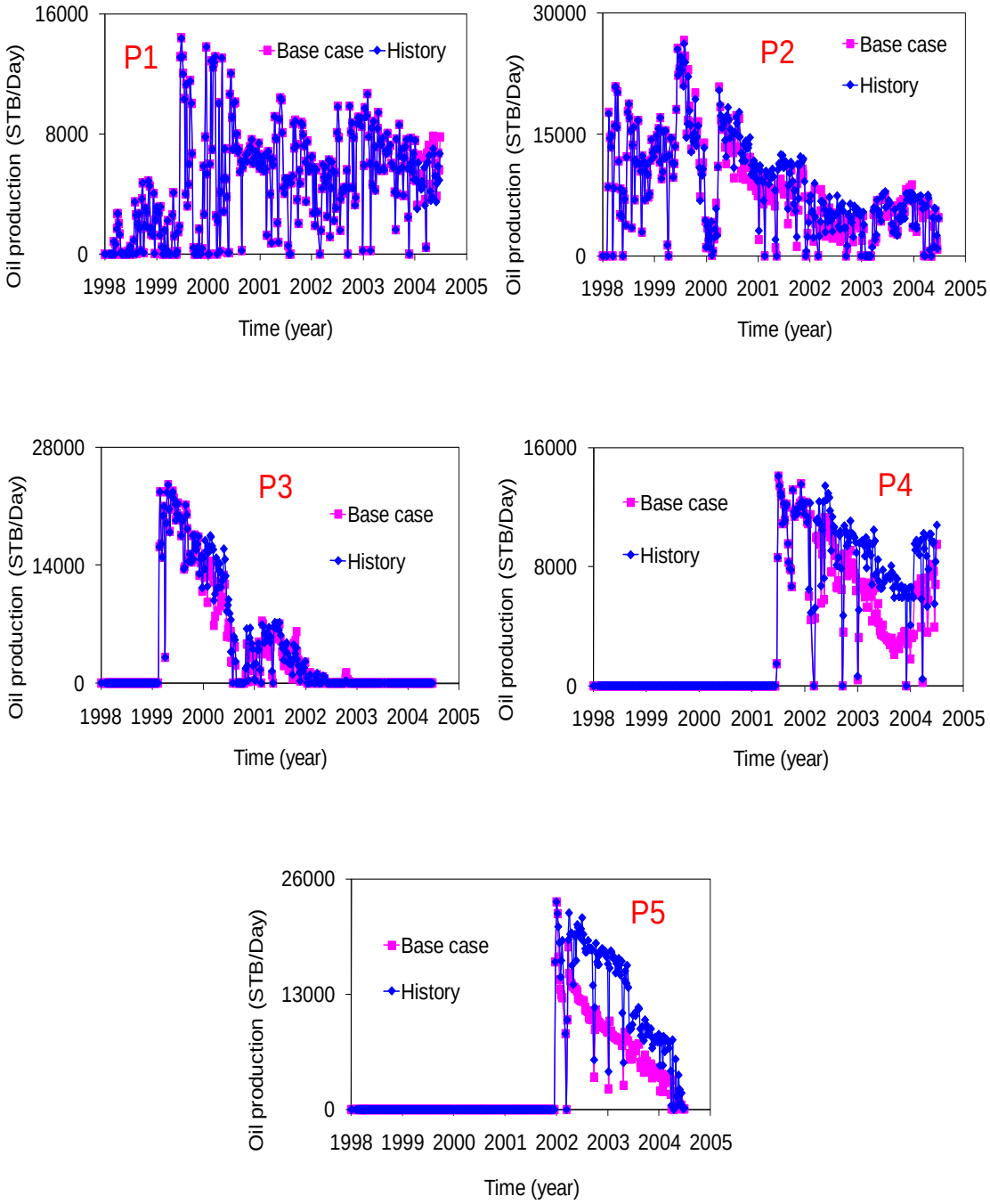

Figure 5.13: Comparison of historical data oil production rates of producers to the predictions for wells by the base case model.

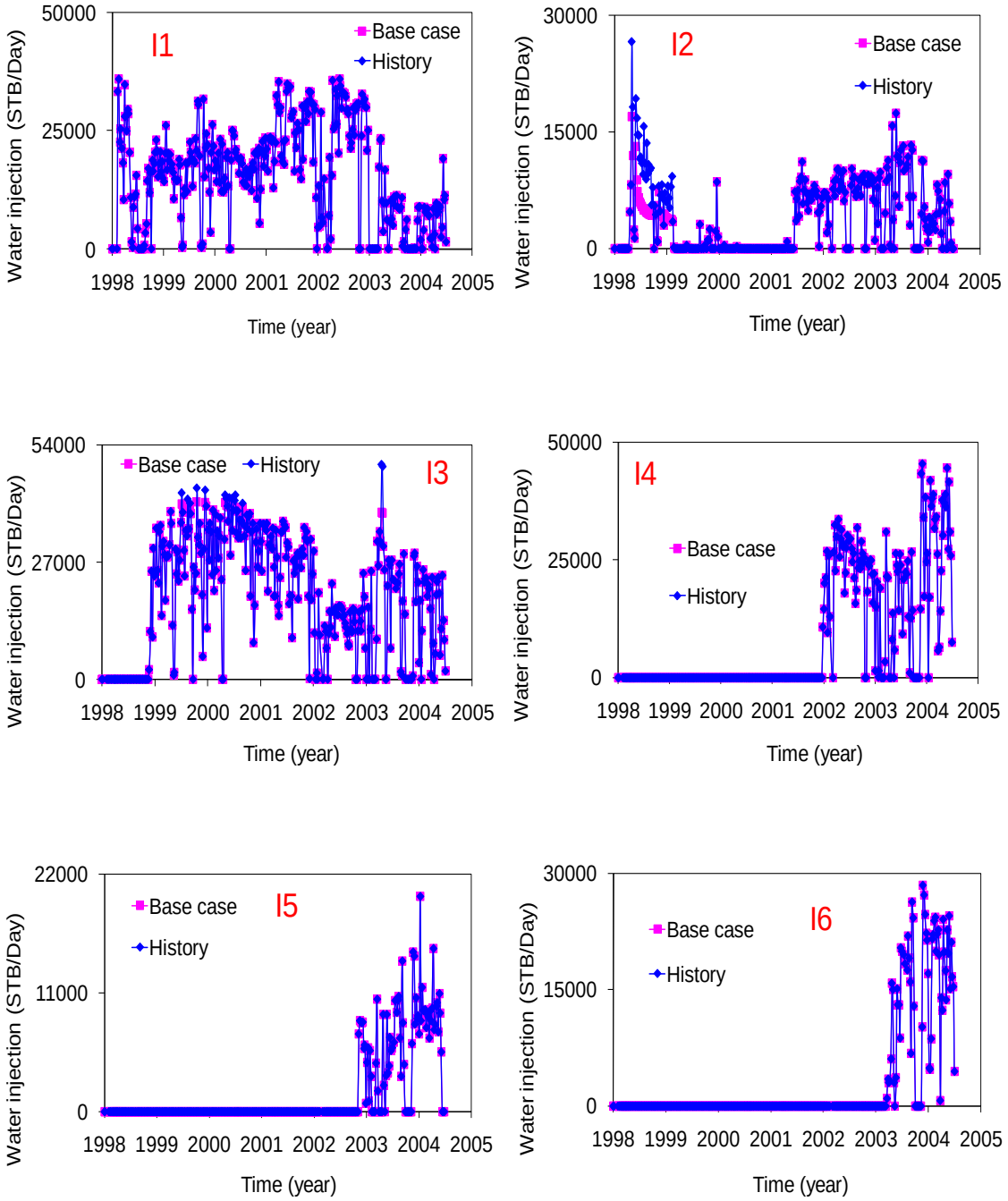

Figure 5.14: Comparison of historical water injection rates of injectors to the predictions for wells by the base case model.

The reservoir model was perturbed by varying the 18 multipliers in 549 models using CCD sampling in the parameter space of the example and the mean and standard deviation of the individual well misfits were calculated (see Table 5.6). The mean misfit and the variation of the misfit for wells P2, I1, I4 and I6 are negligible, and for wells P1, P3 and I3 are quite small. These values are moderate for wells P4 and I5, however,

producer P5 and injector I2 had high values of mean misfit. For well P5 the variation of the misfits is not high (relative to its mean), because the well is positioned in a location far from the multipliers.

Table 5-6: Sensitivity of misfit of oil production rates and injection rates of wells to parameter perturbation (549 models were used in calculating mean and standard deviation of well misfits).

Well	**Mean misfit and variation of the misfits of producers and injectors**	
	Mean	**Standard deviation**
P1	8902	50
P2	21	0.0
P3	4275	62
P4	12433	322
P5	50971	1221
I1	0.0	0.0
I2	21009	552
I3	6699	29
I4	0.0	0.0
I5	18090	921
I6	0.0	0.0

On the other hand, the base case predictions of 4D seismic data did not sufficiently resemble the observed seismic data. Comparison between observed and base case 4D seismic data is demonstrated for Phase I and Phase II datasets in Figure 5.15.

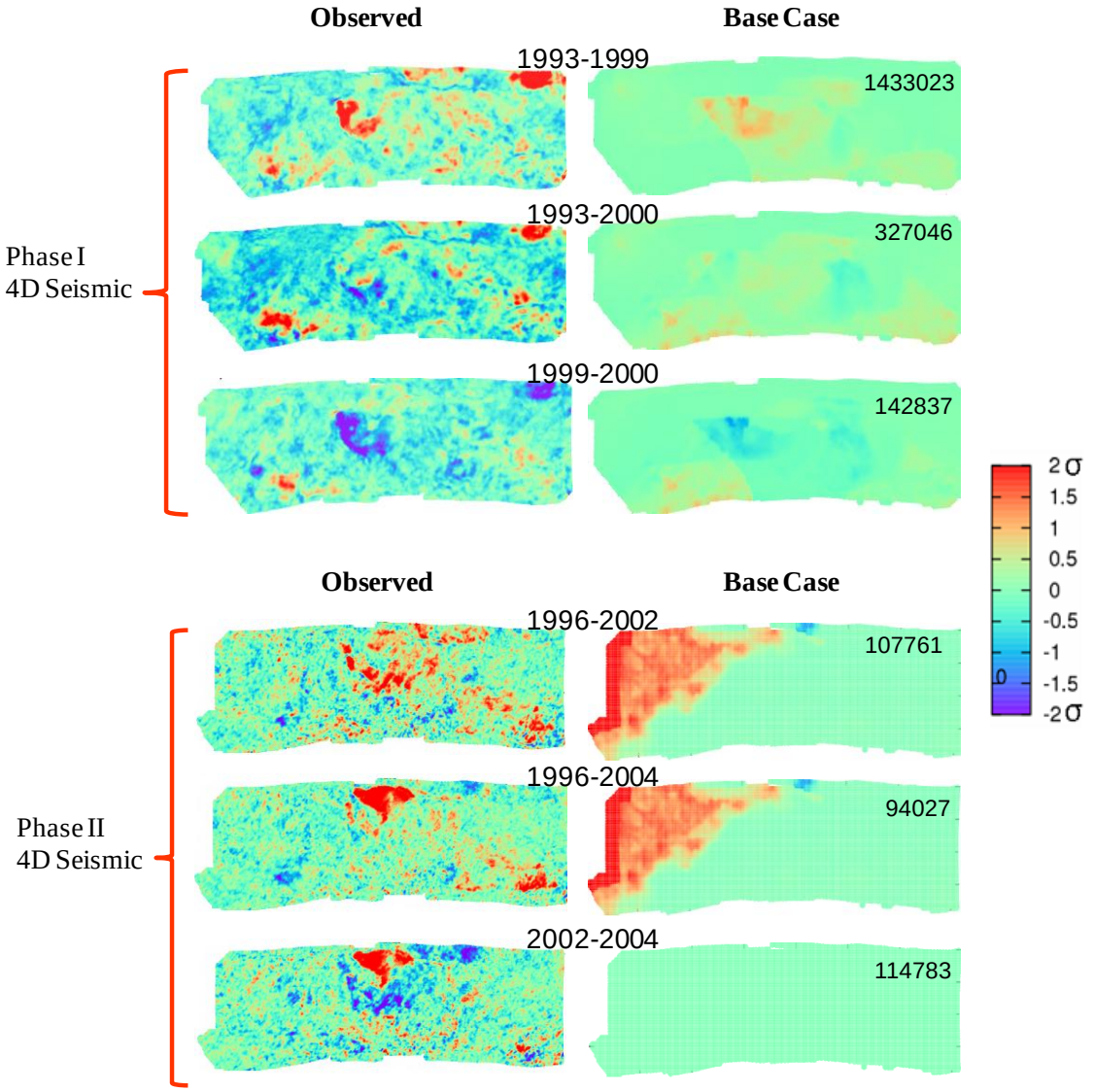

Figure 5.15: Comparison of observed and the base model predictions for Phase I and Phase II 4D seismic data (attribute maps of difference in impedance). The colour bar is the same for all the images and is in units of the 1993 standard deviation for Phase I and 1996 for Phase II. The 4D maps are in old-new which gives positive values (red colour) corresponding to the increase in pore pressure and thus decrease in the effective pressure. A positive value may also represent decrease in the water saturation or increase in the gas saturation. Negative values (blue colour) may be due to opposite effects, i.e. decrease in the pore pressure or increase in the water saturation. The misfit value of each time interval is shown in the predicted 4D seismic map.

The aim of this history matching was to capture the two strong seismic anomalies that are mostly affected by the performance of the injector I2 (detectable in the observed seismic difference map 93-99 and 99-00) and the injector I5 (recognizable in the observed seismic difference map 96-04 and 02-04) in Figure 5.15. Other anomalies in

the Phase I data were not addressed. In Phase II, there was a smaller number. An initial investigation revealed that the misfit of injector I2 was sensitive to both the petro-physical properties around this well and the flow barriers close to the well. Nevertheless, the misfit of injector I5 is only sensitive to fluid flow properties of the barriers in the regions close to the well. Therefore, as part of the history matching process we attempted to adjust the transmissibility of the flow barriers around the two injectors and the net:gross and permeability around the injector I2. Since the injector I5 history data have already been reasonably matched in the base case model, they were not included as variables in the misfit function. Consequently, the 'misfit of the injector I2 together with the sum of the all 4D seismic misfit data' was regarded in this history matching study.

In the application of SHM using the 'divide and conquer' approach the parameter space was sampled (in $\log_{10}$ scale) utilizing a Central Composite Design (CCD) for an 18-factor case (the same models used in analyzing the well mean misfits and variation of misfits, previously). Generally, for a quadratic response the CCD involves slightly fewer simulations relative to the BBD for some number of design factors including an 18-factor one. When D-optimal designs are constructed for problems consisting more than 15 factors would require a lot of CPU time and are not used here. Moreover, the three CCD, BBD and D-optimal schemes achieved quite similar results in predicting the quadratic polynomial misfit coefficients previously. Therefore, only CCD was used for the current 18-dimensional case.

Based on the ensemble of models generated by CCD (549 models) and their corresponding misfits, the proxy regression model to the misfit was created. The misfits were recalculated by polynomial. There was a correlation coefficient, R^2, of 0.999 when they compared to true misfit values, see Figurer 5.16a. Figure 5.16b shows the cumulative probability distribution of derived coefficients in the proxy polynomial misfit. In the polynomial misfit 90% of coefficient values (including many of two parameter interaction terms) were close to zero and therefore had negligible effect on the misfit response surface.

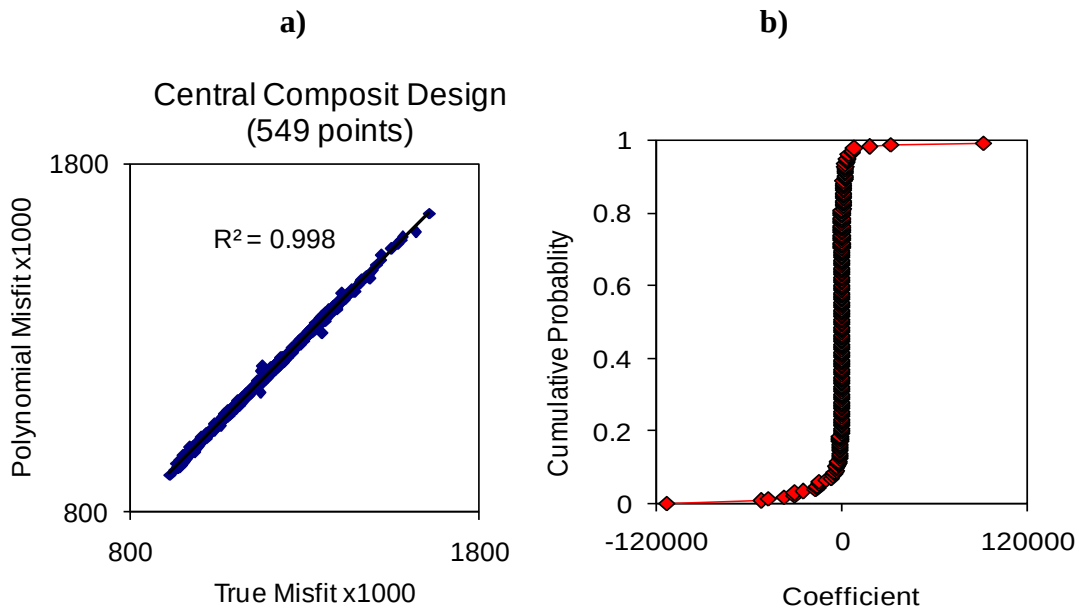

Figure 5.16: a) Misfits predicted by polynomial response surface against the true misfit and, b) Probability distribution of coefficients in the polynomial misfit.

The Pareto plots of the significant effects, which define up to 95% correlation between true and proxy misfits, are shown in Figure 5.17 (for the total the injector and 4D seismic misfit). It is apparent that the net:gross, horizontal permeability and the transmissibility of the two recently added barriers ('k' and 'l') have major effects on controlling the injector I2 and 4D seismic misfits. Furthermore, there was an interaction effect between the transmissibility multipliers of two barriers ('l' and 'k') and the (net:gross and horizontal permeability) multipliers of the grouped pilot points that are closer to injector I2.

Figures 5.18 illustrates the Pareto charts of the significant effects of the injector I2 misfit and Figure 5.19 shows the misfit of each individual 4D seismic data misfit. The displayed effects in these plots capture 90% of the correlation between the true misfits and their corresponding polynomial misfits. For the injector I2 misfit (Figure 5.18), it was recognized that net:gross and horizontal permeability of the sand around this well affects the volume injected and the resulting pressure propagation in the region. They therefore contributed as the most significant effects. These properties are major parameters that need to be updated to get a match of the dynamic well data as well as the 4D seismic data through history matching. Otherwise the injector I2 match would not be achieved. Besides, the transmissibility of barrier 'i' had a significant effect on

the injector I2 misfit. This result is consistent with what was obtained in the previous 10-dimensional example (refer to Figures 4.12 and 4.13 of Chapter 4), for the 'total 4D seismic misfit only' and 'seismic plus injector misfit' scenarios. This result indicates that the transmissibility of barrier 'i' is locally the most important parameter in controlling the pressure propagation to the left of the injector I2 and thus has major role in order to attain the match of the shape of the seismic anomaly and the well simultaneously.

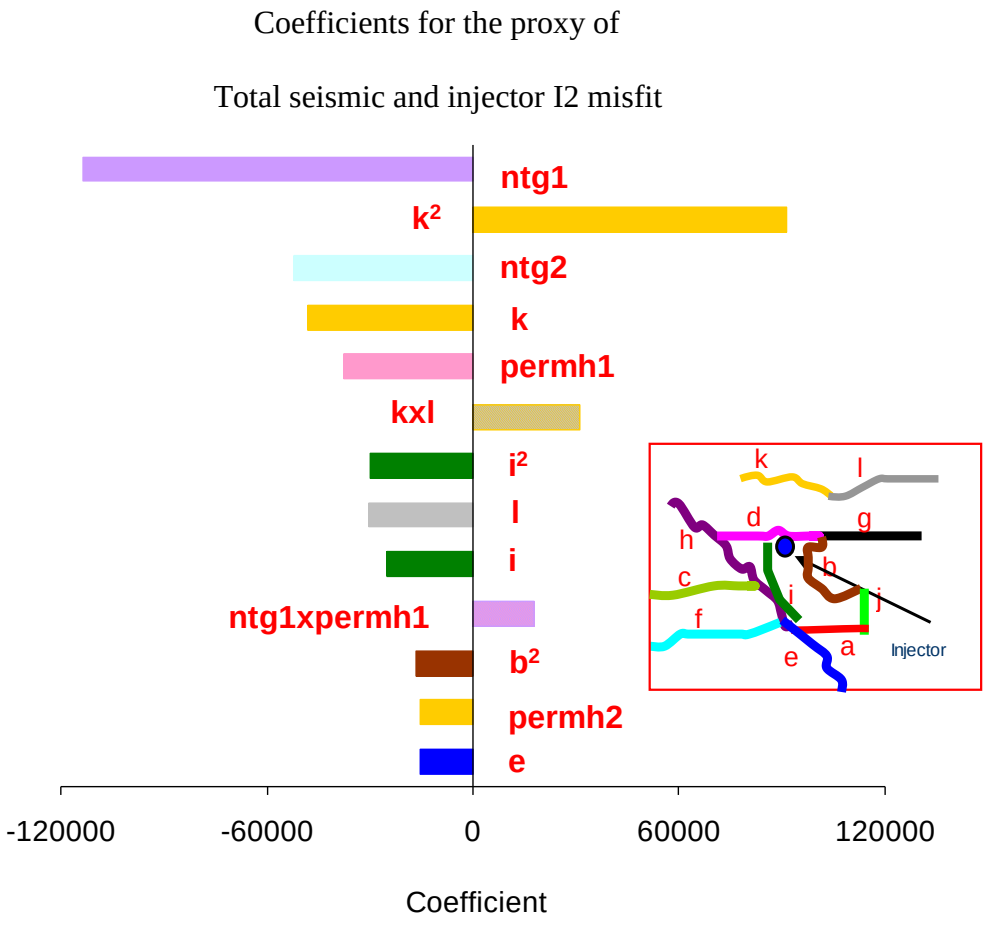

Figure 5.17: Significant effects in the total misfit response surface. Single symbols show linear effects, symbols to the power of two represent quadratic effects, and cross products represent interacting effects.

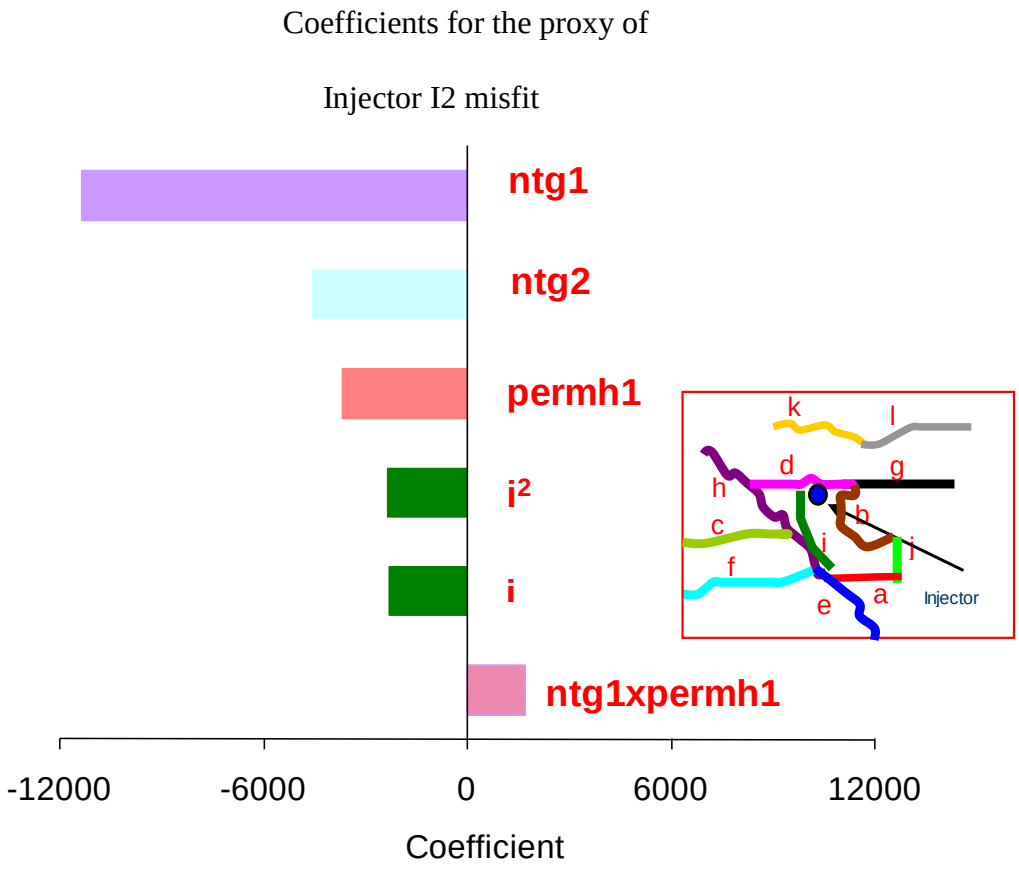

Figure 5.18: Significant effects on the injector I2 misfit response surface. Symbols as described in Figure 5.17.

We now compare the effect of adding extra parameters relative to the 10-dimensional case study. The plots of the significant effects of the 4D seismic misfits of each individual time difference are shown in Figure 5.18. From comparison of these Pareto plots in Figure 5.19, we see that the coefficients of the proxy misfit of the 1993-1999 (see Figure 5.19a) and 1996-2002 (Figure 5.18d) 4D misfits are of smaller values compared to the other time intervals. This indicates that the misfits of these time frames are less affected by the updated parameters.

The coefficients of the proxy for the 2002-2004 4D seismic misfit (Figure 5.19f) are the largest which signifies that the updated parameters have more effect on this time period. For the1993-1999 4D seismic misfit (Figure 5.19a), the net-to gross, permeability, and transmissibility of barriers ‘i’ and ‘e’, have stronger effects. When net:gross and permeability properties of the region around the injector I2 were included as the updated parameters in the SHM process, they reduced the influence of the transmissibility of barriers in comparison to 10-dimensional case, Figure 4.13b of Chapter 4.

From Figure 5.19b one could recognize that for the 1993-2000 4D seismic data the net-to gross is as important as the barriers ‘e’, ‘i’ and ‘g’, but the effect of transmissibility of barrier ‘e’ was reduced (compared to the 10-dimensional case, Figure 4.13c). Also the effect of barrier ‘i’ appears dominant over the effect of barrier ‘g’ now. In Figure 5.19c, for the 1999-2000) 4D seismic misfit, the net:gross, permeability and transmissibility of barrier ‘k’ were added to the influential effects. Meanwhile, the effect of transmissibility of barriers ‘g’ and ‘a’ was reduced compared to the 10-dimensional case (Figure 4.13d) as a result, the effects of the barriers were similar but the order of the influence of them was changed.

In the plots relating to the 1996-2002 4D seismic data (Figure 5.19d), the net:gross around the injector I2 and two new barriers were not influential. This was because at this time the seismic anomaly around the injector I2 had disappeared. This meant that there was a need for pressure propagation which was controlled by the ability of flow within the areas close to the injector I2. Therefore the effect of transmissibility of barriers and horizontal permeability, including parameters: ‘h’, ‘PermH1’, ‘PermH2’ ‘g’, ‘b’, ‘f’, and ‘d’, became dominant. As a result the effect of net:gross was suppressed. Moreover, the transmissibility of barriers ‘k’ and ‘l’ had no influence at this time, since injector I5 is active from 2003.

Figures 5.19e and 5.19f demonstrate the significant effects for the late time seismic misfits 1996-2004 and 2002-2004 which include the linear, quadratic and interaction effects of transmissibility of barriers ‘k’ and ‘l’. They were quite close to the injector I5 which had been active since 2003. The variation of these parameters would enable the match of the history of the injector I5 and would help the match to the shape of the seismic anomaly around this well.

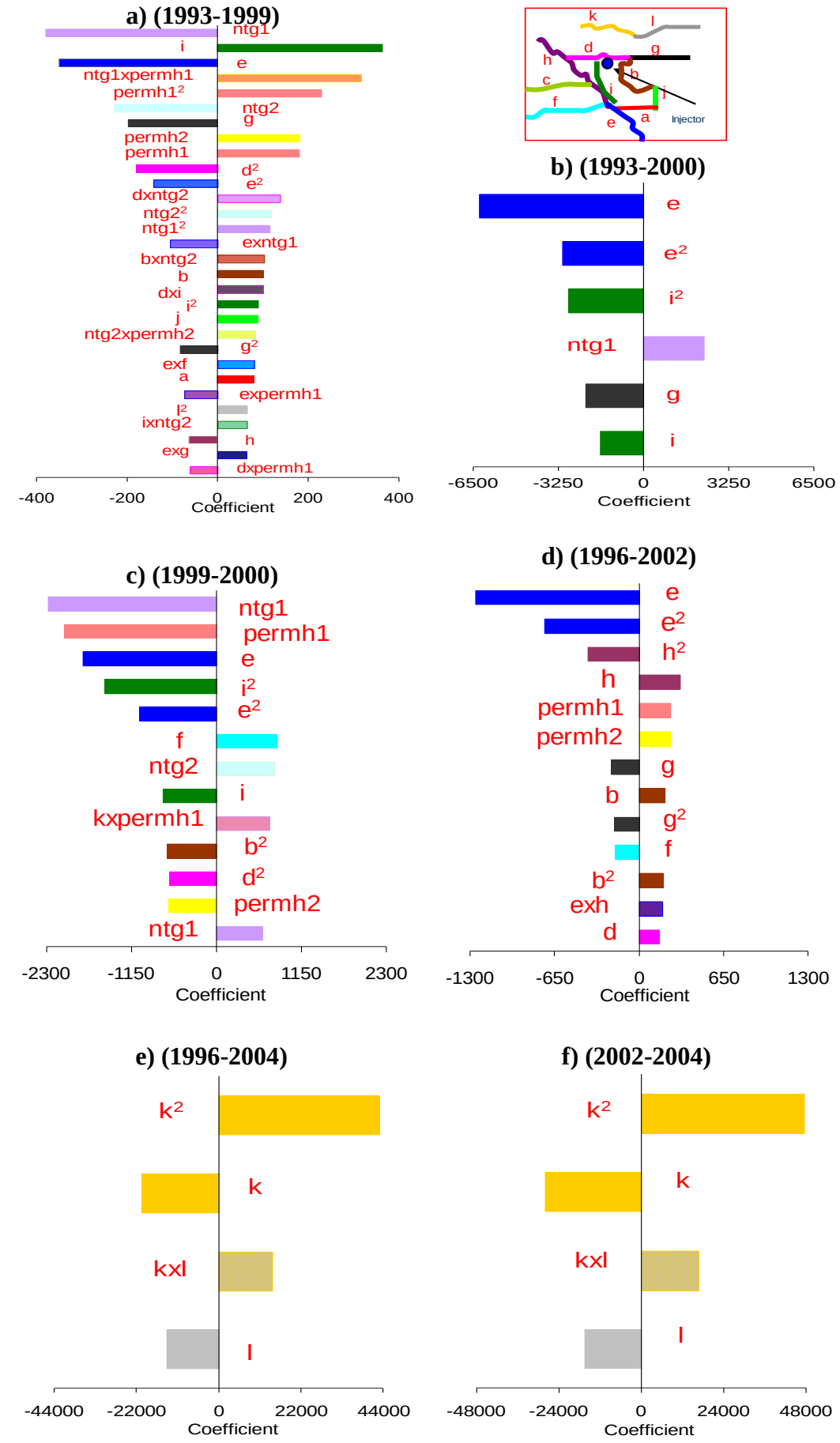

Figure 5.19: Significant effects in the seismic misfit response surface for various times. Symbols as described in Figures 5.17.

The interaction terms with insignificant coefficients were abandoned in the polynomial misfit proxy and only the coefficients giving 95% correlation between polynomial and true misfits were kept (see Figure 5.20). It was performed by measuring the correlation coefficient, (R^2) between the true misfits against the regression model predictions as the interacting coefficients were discarded in their order of increasing size (i.e. rank, the smallest first).

Then by analyzing the retained interaction coefficients in the polynomial misfit, the groups of non-interacting parameters were determined. As a result, the independent parameter sub-spaces were decoupled. Accordingly, the misfit function was decomposed into the sub-misfits. There were 16 decoupled sub-volumes as shown in Table 5.5.

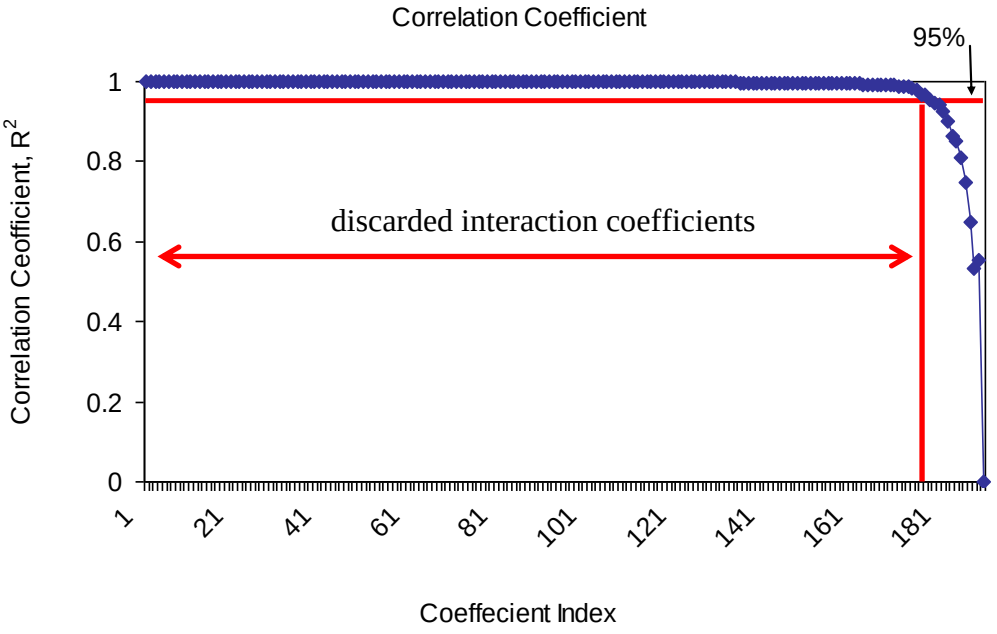

Figure 5.20: Deterioration of correlation factor (R^2) as we discarded interacting coefficients in order of increasing size (i.e. rank of their importance, smallest first).

Table 5-7: Decoupled parameter sub-volumes.

number of sub-volumes	decoupled parameters in separated parentheses*
16	(k, l) (NTG1, PermH1) (NTG2) (i) (b) (d) (PermH2) (e) (a) (j) (g) (f) (h) (c) (PermZ1) (PermZ2)

****They are ordered based on the size of coefficients in the polynomial proxy of the misfit, smallest first.***

The Parallel-SHM and Serial-SHM approaches were applied to search the parameter sub-volumes. As mentioned before, 549 models were used to derive the proxy model. These models were also used to initialize NA, i.e. provide the ensemble of initial models for the parallel search. In the parallel search we considered two cases. In the first instance the NA routine tuning parameters were set as n_s = 96, n_r = 48, and the routine was ran for 2 iterations (in total 192 models). Therefore, 741 models in total were ran to find the minimum misfit using the Parallel-SHM method (see Figure 5.21a). In the second instance we set the NA routine parameters for n_s = 16, n_r = 8, and the number of iterations was equal to 2 again (in total 32 models). We used these settings since following division of the parameter space eventually the largest sub-volume was a 2D one when searching in parallel. Then we effectively obtained the same result but in a fewer model calls of 581 in total (see Figure 5.21a).

Using the Serial-SHM, the parameter sub-spaces were searched in turn. In each serial search we needed to sample the ensemble of initial models consistent with the dimension size of that particular sub-volume. These models were different from the models that were used to construct the misfit proxy and also used in the parallel search of NA for initializing the sub-volume searches. First the higher dimensional sub-volumes were searched. Subsequently, for those sub-volumes with identical dimension, the search was followed in order of their importance which was determined based on their coefficients in the polynomial misfit model. The 2D sub-volume of transmissibility of barriers ('k' and 'l') and pilot point parameters (ntg1 and permh1) were searched using the NA routine with: n_i = 32, n_s = 16, n_r = 8, and was run for 5 iterations. For the

rest of the 14 sub-spaces, each of 1D, the NA parameters were set to: n_i = 16, n_s = 8, n_r = 4, and run for 5 iterations.

These NA parameters were set based on the fact that in practice for low-dimensional problems the potential exists to be trapped in a local minimum of the objective function, because the constructed voronoi cells are isolated (see Section 2.5 of Chapter 2 for more description on voronoi cells and NA routine). So the algorithm should be tuned for larger n_s, and also should be starting with extra initial ensemble of models, n_i (refer to Sambridge 2001). Searching the sub-volumes of the parameter spaces in the serial mode meant that convergence could be obtained in only 1008 model calls. When they were added to the 549 models required for decoupling the parameter sub-spaces, a total of 1557 models was required (see Figure 5.21b).

Seismic maps of difference in impedance predicted by the best models using the parallel and serial search approaches are compared to maps of observed data in Figure 5.22. The misfit value of each individual seismic map is also shown in maps. These misfit values, for corresponding time difference maps were close and at most there was a 1.6% difference for the map of time difference 1999-2000, which is still very small. From comparison of these maps it was also noticeable that there were great improvements in the match of the shape of the two main anomalies around the injector I2 and injector I5 by parallel and serial methods relative to the base case (for the 4D seismic map predictions by the base case model, see Figure 5.15).

5.4 Results

Significant improvement in the match of history data of injector I2 rates by using either parallel or serial methods was obtained. Although the misfit of the producers P4 and P5 were not included in the inversion process, the match of the history data of these wells were also been improved. The history match of other wells was attained in the base model and remained unchanged by the best model predictions. For the wells with improved match, the comparison of the well history data to the predictions of the base and the best models using the Parallel-SHM and Serial-SHM approaches are displayed in Figure 5.23.

a) Parallel-SHM

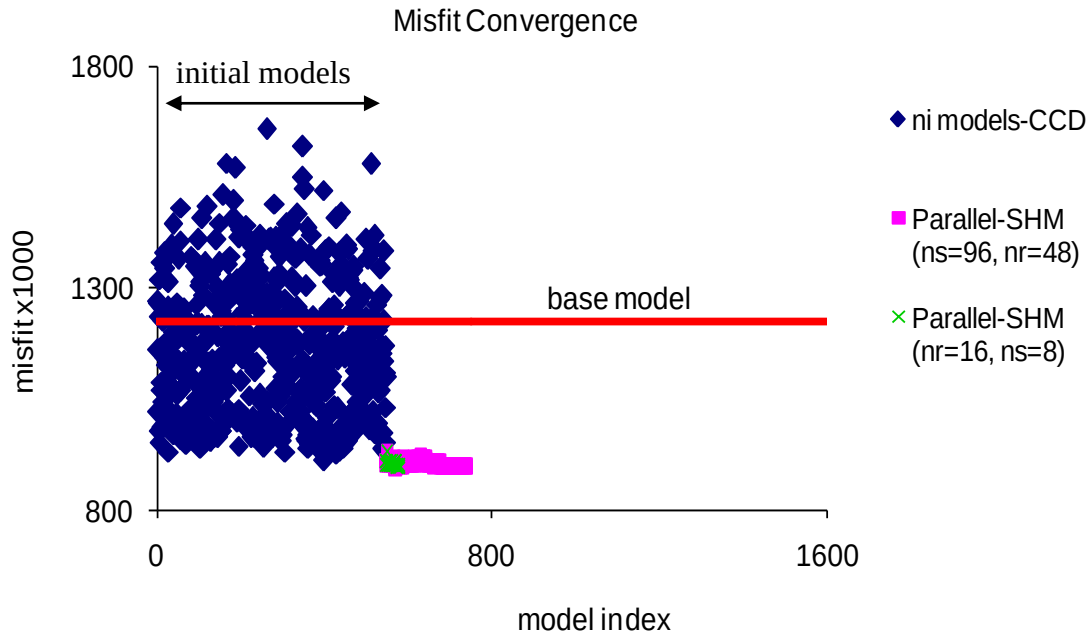

b) Serial-SHM

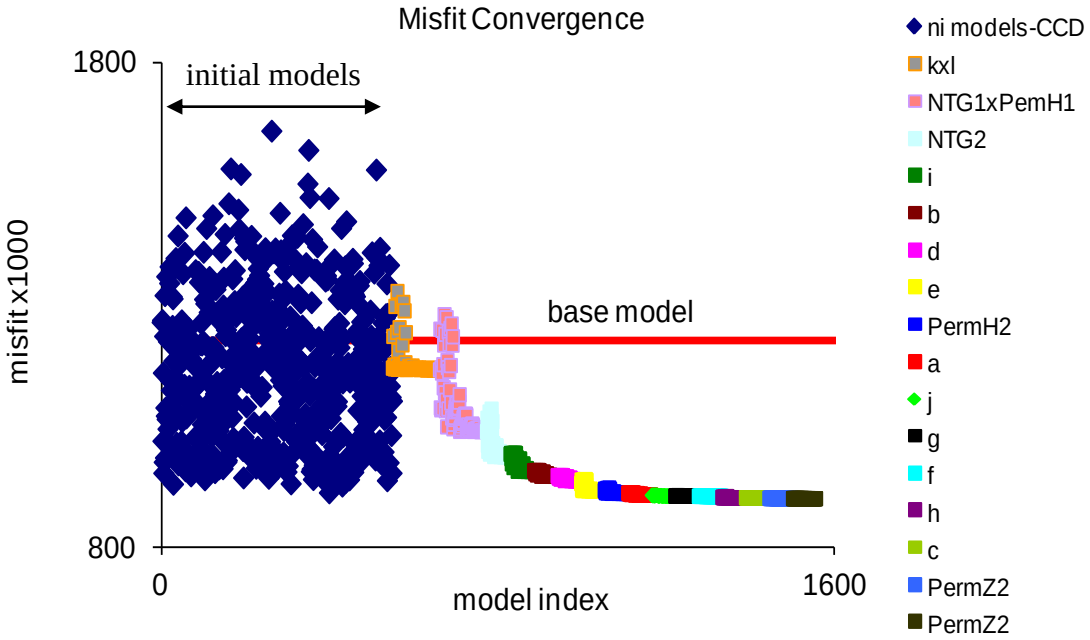

Figure 5.21: Misfit convergence using technique of 'Central Composite Design combined with: a) Parallel-SHM for two cases n_s = 96, n_r = 48 and n_s = 16, n_r = 8, and b) Serial-SHM. The dark blue markers are the 549 samples used in decoupling parameter sub-spaces and also in initialization (initial ensemble of models) of parallel search. The solid line indicates the base case model misfit.

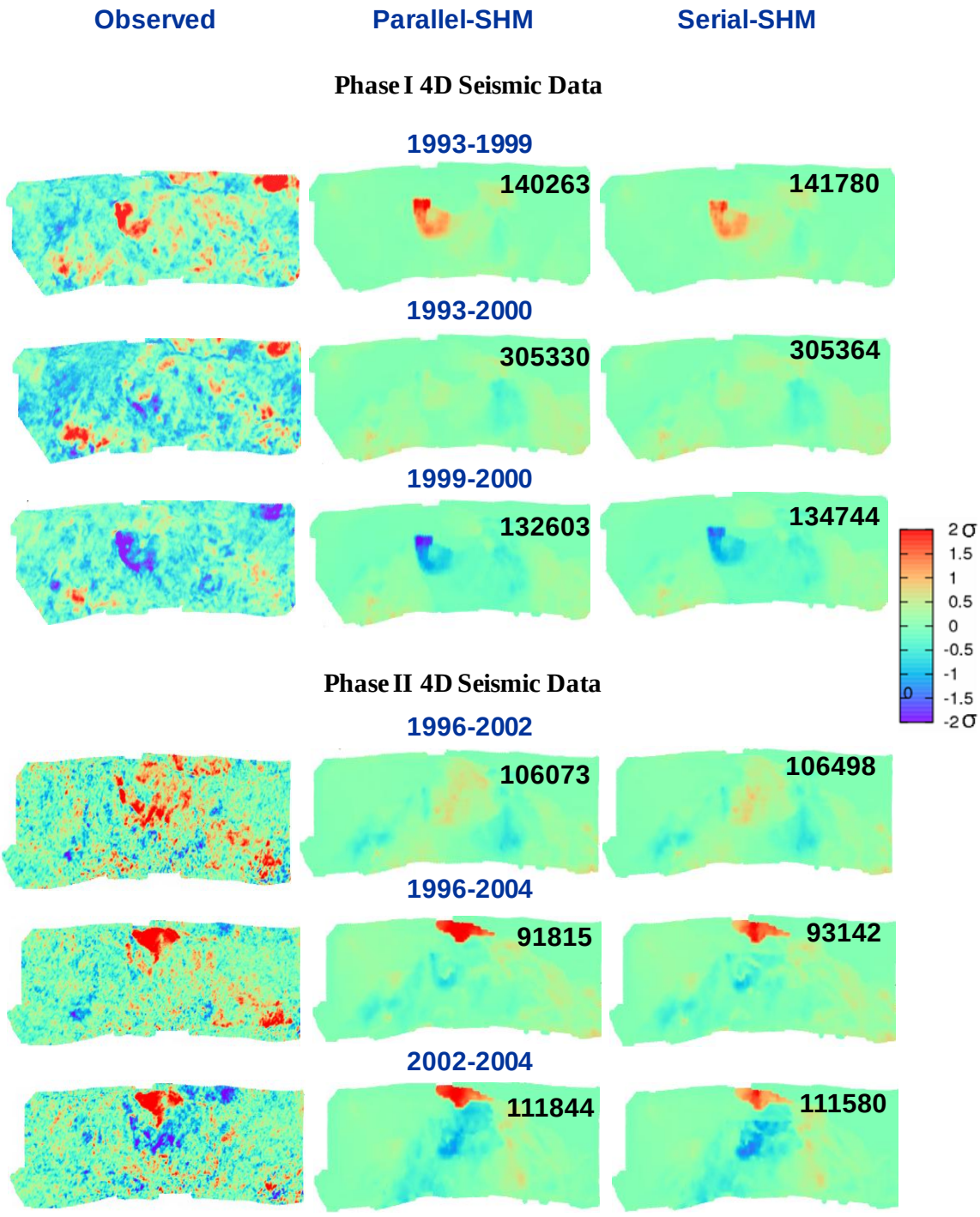

Figure 5.22: Maps of change in impedance predicted by the best models obtained by the parallel and serial search approaches compared to the equivalent observed data. The misfit value of each individual seismic map is shown in each map.

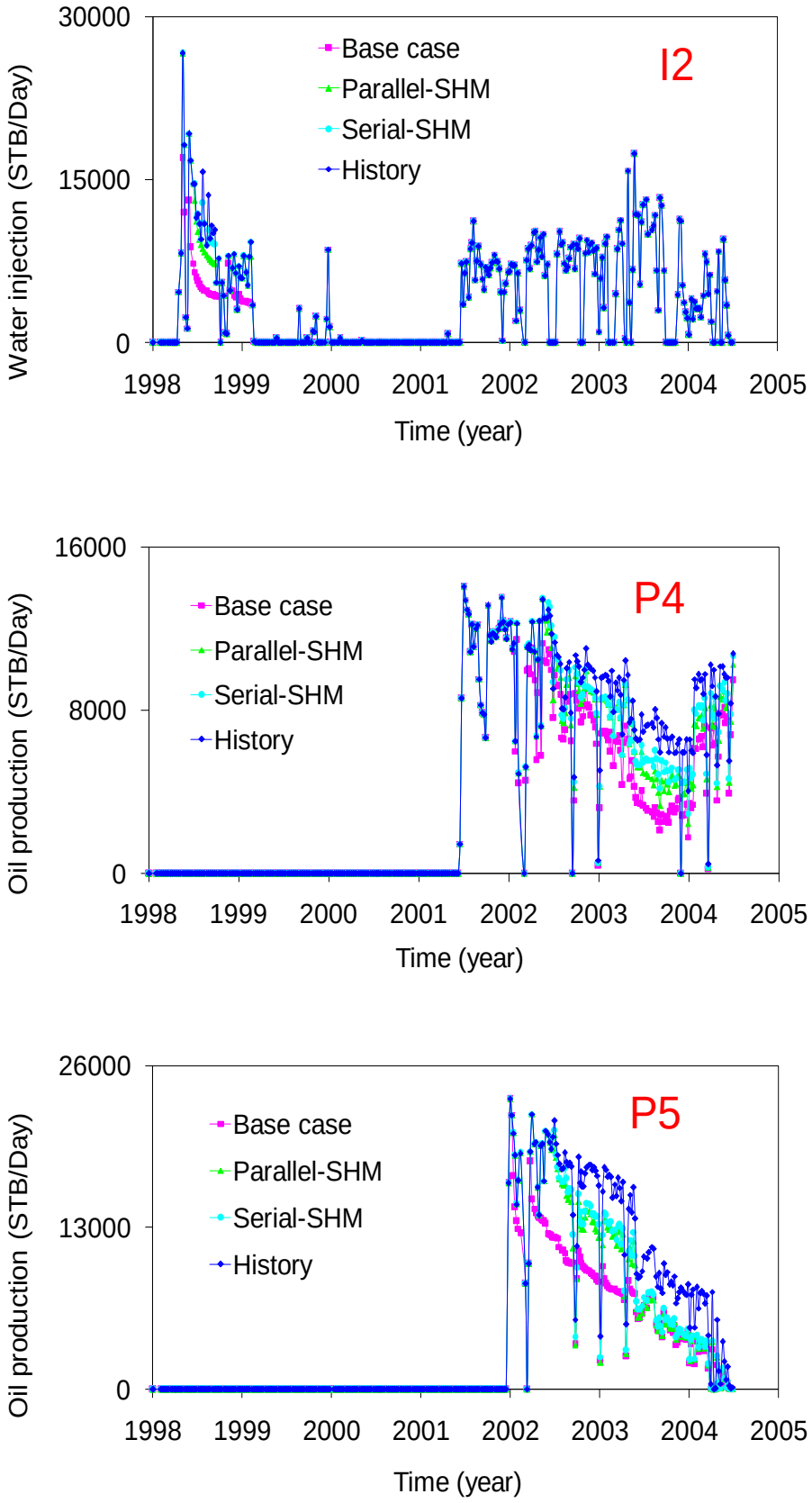

Figure 5.23: Comparison of history data to the predictions from the base model and the best models obtained by the parallel and serial methods.

Tables 5.8 and 5.9 summarises the simulation data and the comparison of the performance of the two parallel and serial approaches. The simulation information (Tables 5.8) confirm that whereas the Full-SHM approach is difficult to apply in practice, the number of model calls and the CPU time required for the 18-dimensional case are affordable reasonably if we use 'divide and conquer' approaches.

A large drop in injector I2 and the 4D seismic misfits was attained by Parallel- and Serial SHM applications (Tables 5.9). The seismic maps contain noise plus several anomalies that we did not intend to match (e.g. they are outside the simulation region etc.). However in the present study we sought to match the 4D seismic anomalies in the area immediately around the updated parameters. Although the decrease in the entire reservoir seismic misfits was computed, to determine the effect of SHM, the regions adjacent to the injectors I2 and I5 were considered also.

Table 5-8: The simulation and computer time requirements for an 18-dimentional case of Schiehallion using the Parallel-SHM and Serial-SHM approaches.

Search choice	Initialization of decoupled sub-spaces		After initialisation		Total	
	number of models	required CPU (days)*	number of models	required CPU (days)*	number of models	required CPU (days)*
Parallel- $n_s = 96$, $n_r = 48$	549	7.63	192	2.76	741	10.29
Parallel- $n_s = 16$, $n_r = 8$	549	7.63	32	0.46	581	8.07
Serial-	549	7.63	1008	14.0	1557	21.63

Each model takes around 20 minutes on a 3.4 GHz processor.

Table 5-9: Performance of the two search methods.

Method of SHM	Drop in total 4D seismic misfit (%)	Drop in injector rate misfit (%)	Drop in sum of total seismic and injector rate misfit (%)	Drop in total seismic misfit of area around strong anomalies (%)*	Drop in sum of seismic misfit of area around strong anomalies and injector rate misfit (%)*
Parallel-**	4.5	84.5	21.0	19.8	55.0
Serial-	4.0	91.8	22.3	19.3	59.5

**** The misfit in the area immediately around the updated parameters and strong seismic anomalies were considered. They are marked in Figure 5.9 and are observable in the 4D seismic maps of Figure 5.22. They are around the injector I2 in Phase I and around injector I5 in Phase II 4D seismic data.***

***** Similar results obtained by both the Parallel-SHM cases: i) n_s = 96, n_r = 48 and ii) n_s = 16, n_r = 8.***

The updated parameter values of the best models achieved by the parallel and serial searches are shown in Figure 5.24. For most parameters the results are consistent and quite close. The exceptions are mainly for barriers 'g', and 'l' which provide the pressure communication between the two regions of strong seismic anomalies. It seems that when the barrier 'g' is of high transmissibility (several orders of magnitude larger in size) then the barrier 'l' should be less transmissible to adjust the pressure communication between these regions and their immediate surroundings. Because of the stochastic nature of search algorithm, they may approach various solution minima of objective function in the parameter space of the problem. In fact the various updated parameter values for the best models were obtained by the different methods indicate the non-uniqueness of the current history matching problem.

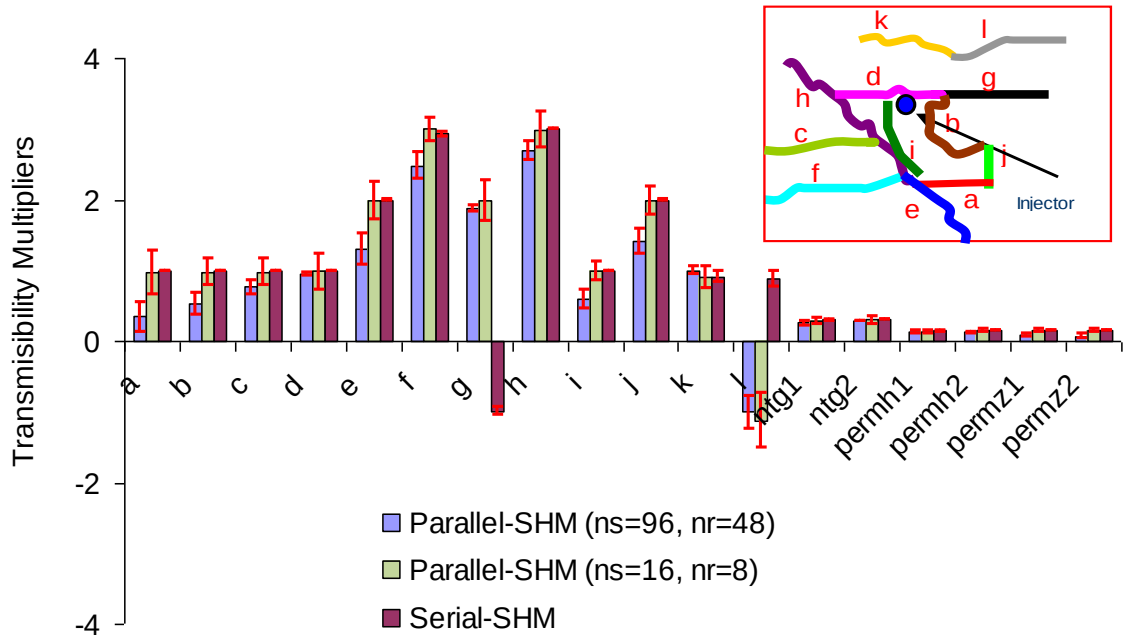

Figure 5.24: The updated parameter values achieved in the best models obtained using the parallel and serial search. The error bars are calculated based on 10 best models acquired in each method.

5.5 Conclusions

Stochastic inversion routines such as Neighbourhood Algorithm (NA) require a large ensemble of initial models to effectively sample the parameter space. In this chapter we adopted an approach of integrating experimental design techniques with 'divide and conquer' and gained more improvement in the convergence of history matching procedure. Through application of this approach we were able to reduce the number of required initial simulations to about 15% of what was required for a conventional full inversion using NA. When this initialization step was combined with Parallel-SHM to find the minimum misfit we obtained more gain, and 91 per cent speed up in the convergence for the history matching of a 10-dimensional case of the Schiehallion field was achieved. The method of 'combining experimental design with divide and conquer' was also applied to a problem of 18-dimensional SHM of the Schiehallion filed. Such case usually requires too many simulations and in practice may not be completed using any stochastic search routine. The convergence of this example also was reached very fast and efficiently with an affordable number of simulation runs. While we attained the objective of handling even higher dimensional history matching problems, the other important conclusions were summarized in the following paragraphs.

- Experimental design is a useful way to train proxy models to misfit function giving an order of magnitude saving over random sampling.
- Using ‘experimental design combined with a divide and conquer‘ method; convergence can be obtained very quickly in the history matching.
- Results of the approach are independent of experimental design methods used, and better understanding of the reservoir parameter effects on misfit response can be obtained.
- ‘Experimental design combined with divide and conquer’ approach is especially very attractive to the SHM cases of large number of reservoir unknown parameters that are involving many simulation runs.

CHAPTER 6 'Divide and Conquer' Approach to Spatial Decomposition of the Seismic Misfit

Introduction

In this chapter the approach of the 'divide and conquer' method to spatial decomposition of the misfit function to identify seismic territories is extended. Reservoir simulations contain sets of 'grid blocks' in the reservoir rock volume. The sets may be grouped parametrically but also by the effect that their properties have on local response variables and history matching misfits. This fact motivates us to find a way to identify such structure in the models and could lead to spatial decomposition of the misfit function to simplify the problem and then reduce computational cost. The approach presented in the following sections is based on the above initiative. This method also uses a polynomial response surface to help identifying the separable sub-domains and uses the neighbourhood algorithm in finding the minimum of sub-domains misfits.

For a number of SHM cases such as the Nelson reservoir (see Kazemi and Stephen 2008) and the Schiehallion field (Stephen et al. 2006, Stephen and MacBeth 2008, Edris et al. 2008) it was revealed that parameter modifications could be made in a very local manner. In Nelson, changes in the properties of net:gross, horizontal permeability, and vertical permeability of a region influence the 4D seismic map in a limited area. In the Schiehallion field the major seismic anomaly around the injectors are affected particularly by transmissibility of nearby surrounding faults and barriers (refer to Chapter 4 and 5 case studies). The spatial decomposition approach finds components of the objective function which depend only on a smaller number of the elements of the vector of updated parameters in reservoir sub-domains. Then each spatial sub-misfit function is treated individually, along with updating the parameters on which it depends.

This method is called 'divide and conquer to identify seismic territories' and it relies on the experimental design and response surface modelling techniques (discussed in earlier chapters) to analyse dominant parameters and, to decompose the misfit spatially, and to define the separable sub-domains. The method also deploys the neighbourhood algorithm in find the minimum of the spatial sub-domain misfits. The major advantage of this method is that the true misfits are used instead of misfits from the proxy models in the inversion of local misfits. The seismic maps are divided into several separate regions consistent with a set of flow barriers, and the modifiers to the barrier transmissibilities are linked to variations in the seismic misfit. In the following sections the details of spatial decomposition method are described. It has been revealed that many simulation runs would be saved in the SHM process through illustration of the application of this new approach.

6.1 'Divide and Conquer' of Spatial Domains

The criteria for sub-region decomposition should simultaneously take into consideration the spatial characteristics of the reservoir features and their separability. Often reservoirs are composed of several different sedimentary classifications and facies, of different petrophysical properties (i.e. net:gross, porosity, permeability) which affect their flow behavior and divided the reservoir to various sub-regions. Sometimes reservoirs are heavily faulted and there are many flow barriers dividing the reservoir to sub-regions. One way of decomposing the sub-regions would be to capture distinct differences induced by these features. In this thesis, the spatial subdivisions were based on the geology and structure of the reservoir and picking out the pressure discontinuities in the heavily faulted Schiehallion reservoir.

Reservoir region decomposition has been implemented before through the delineation of least correlated, most sensitive sub-regions by Zhang et al. (2001). They stated that on extreme occasions while one is dealing with a multi-scale complicated reservoir simulation of millions of grid blocks, the history matching may be described simply for domains distinguished by the parameters correlated in space. Correlation of parameters does not occur over large distance even when the reservoirs are geologically very complex with many faults and flow barriers.

Srinivasan et al. (2004) introduced domain delineation which utilizes streamline density (in streamline simulators). That is the regions whose streamlines were dense, were recognized by sensitivity analysis from the parameter perturbations and by adjustment of the reservoir model to attain a good history match. Bryant et al. (2005) offered a basis for decomposing the flow simulation for increasing the effectiveness of a parameter perturbation scheme. First they considered a set of permeability perturbation parameters for a given reservoir. Each parameter was applied to a particular sub-region in the reservoir which was non-overlapping with other domains. They used a sensitivity analysis to determine the influence of the value of permeability at any given location upon the production data using Principal Component Analysis (PCA), and identified domain sensitivity and least correlation. They increased the effectiveness of the history matching in terms of computational time.

The optimal choice of identifying the sub-regions must satisfy two conditions. First, the parameters, in the sub-regions that we wish to modify (such as barrier transmissibilities or permeability multipliers) should have the greatest influence on the performance of any associated injection and production wells. Second, the sub-regions should exhibit the least possible correlation with one another. There are several methods for obtaining sensitivity matrices. For example, the Hessian matrix calculated internally by a flow simulator and a covariance matrix calculated using a suite of realizations (Yadav et al. 2007).

As an alternative, Principal Component Analysis (PCA) of sensitivity matrices could readily identify the regions meeting both the above conditions (Kim et al. 2008). However, calculation of sensitivities is computationally costly and it restricts the approach of domain delineation to some specific simulators. To tackle this problem, a technique of evaluating sensitivities from a set of equi-probable initial realizations was deployed by Bryant et al. (2006). Sensitivities were calculated only at a few locations and were interpolated to remaining locations in the reservoir.

In this chapter we have derived a new and less costly approach based on the domain of seismic territories using response surface modelling. Proxy models are used to identify the sensitivity of sub-regions to parameters and correlation between sub-regions. Consequently, partial separability of domains is determined, and also the parameters that affect the seismic misfit locally are identified. This means that the 'divide and

conquer' approach can be implemented spatially as well as in the parameter domain. We found that our method is successful in terms of representing fluid flow connectivity, and even more effective in terms of computational time and simplicity to implement.

6.1.1 Spatial Decomposition of the Misfit Function

Initially several sub-regions of the reservoir model are identified based on the reservoir structural and geological features. We mainly use flow barriers that mostly affect the simulation performance and its predictions of seismic anomalies. The parameter space of the history matching problem is sampled to create an ensemble of initial models; and simulation models are run. The misfit of each region is labeled and calculated separately instead of merely computing one lump sum for the misfit.

A misfit regression model in the form of a quadratic polynomial is created for the misfit of each region. The sensitivity of the misfit of each sub-region to each parameter is determined and the significant effects on the misfit response surface of individual regions are identified. Then the criteria of spatial decomposition are applied. Below we outline the steps involved in the decoupling of the regions:

- First we identify the sub-region with highest sensitivity to parameter perturbations (which as a rule is the sub-region with highest misfit value). This is implemented through comparison of the size of the coefficients of the misfit polynomials of the sub-regions.

- For this sub-region we only keep the significant effects (the coefficients) in the polynomial misfit (which delineate 95% correlation between the true misfit and the misfit recalculated by polynomial misfit) and reject the other insignificant coefficients for this sub-region.

- We identify the smallest effect (coefficient) among the significant effects of the polynomial misfit of this sub-region and exploit that as a threshold to find the first group of coupled sub-region (i.e. spatial domain).

- Regions that have effects larger than the threshold for at least one of the similar significant effects of the most sensitive sub-region are coupled. Thus we classify

the first of grouped sub-regions which we call the first 'domain'. However there are still other sub-regions which are not linked to this domain.

- Then among the remaining sub-regions we detect the one with the most sensitivity to the parameter changes. The same process (as described for the first the domain) is used to resolve the sub-regions that are coupled to this one. Thus we identify the second domain.

- The procedure is repeated several times until all Domains are decoupled.

6.2 Application to Segment 4 of the Schiehallion Field

In Chapters 4 and 5, the details of a 10-dimensional case of seismic history matching of the Schiehallion field were explained. For that case we showed that for the active production and injection wells, their mean misfits and the variation of their misfits are small (see Table 4.3). This is because they are located remotely from the injector I2. In Chapter 4, we showed that for the injector I2 a perfect match was not obtained even when the 'seismic plus injector misfit' scenario was considered in the inversion process, and a similar result to the scenario of 'total 4D seismic misfit only' was obtained for injector I2. Here, we intend to show the feasibility of the approach of 'spatial decomposition of the seismic misfit' through the application of the method to the same 10-dimensional example. The method was applied to the scenario when 'total 4D seismic misfit only' is used.

First the separate sub-regions were postulated (Figure 6.1), then the correctness of the decoupled sub-regions was evaluated, and finally those sub-regions that should not be separated at all were grouped to have the grouped sub-domains. In the Schiehallion reservoir the area around the injector I2 with the strongest 4D seismic anomaly was divided into twelve (12) sub-regions. In Figure 6.1 these sub-regions are labelled (from A1 to A12). Each of these sub-regions are surrounded by several flow barriers (12 barriers named 'a' to 'l') as they are illustrated in Figure 6.1.

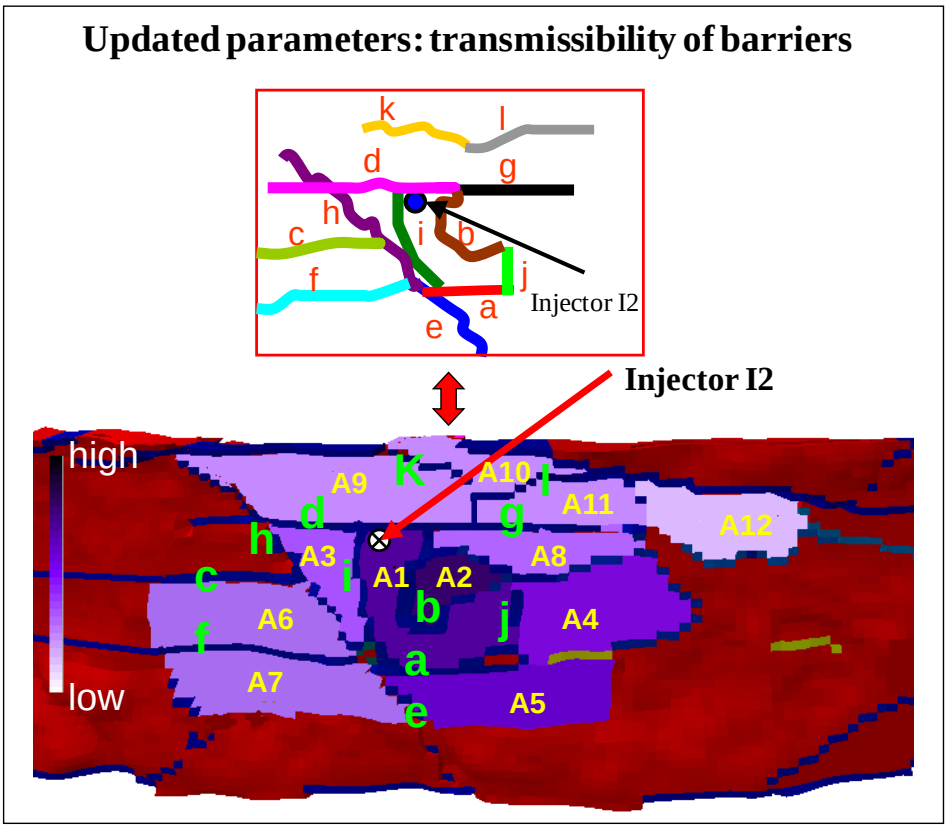

Figure 6.1: Sub-regions around the injector I2 and the change in the normalized misfit across the area in the vicinity of the injector. Dark purple colour indicates high misfit and light purple colour indicates low misfit value.

The component misfit of each sub-region in the base case simulation model of the reservoir was calculated and compared in Figure 6.2. Besides, the normalized misfit of each sub-region was computed by dividing the component misfit of each sub-region by the number of its constituting grid blocks. They are compared on Figure 6.2

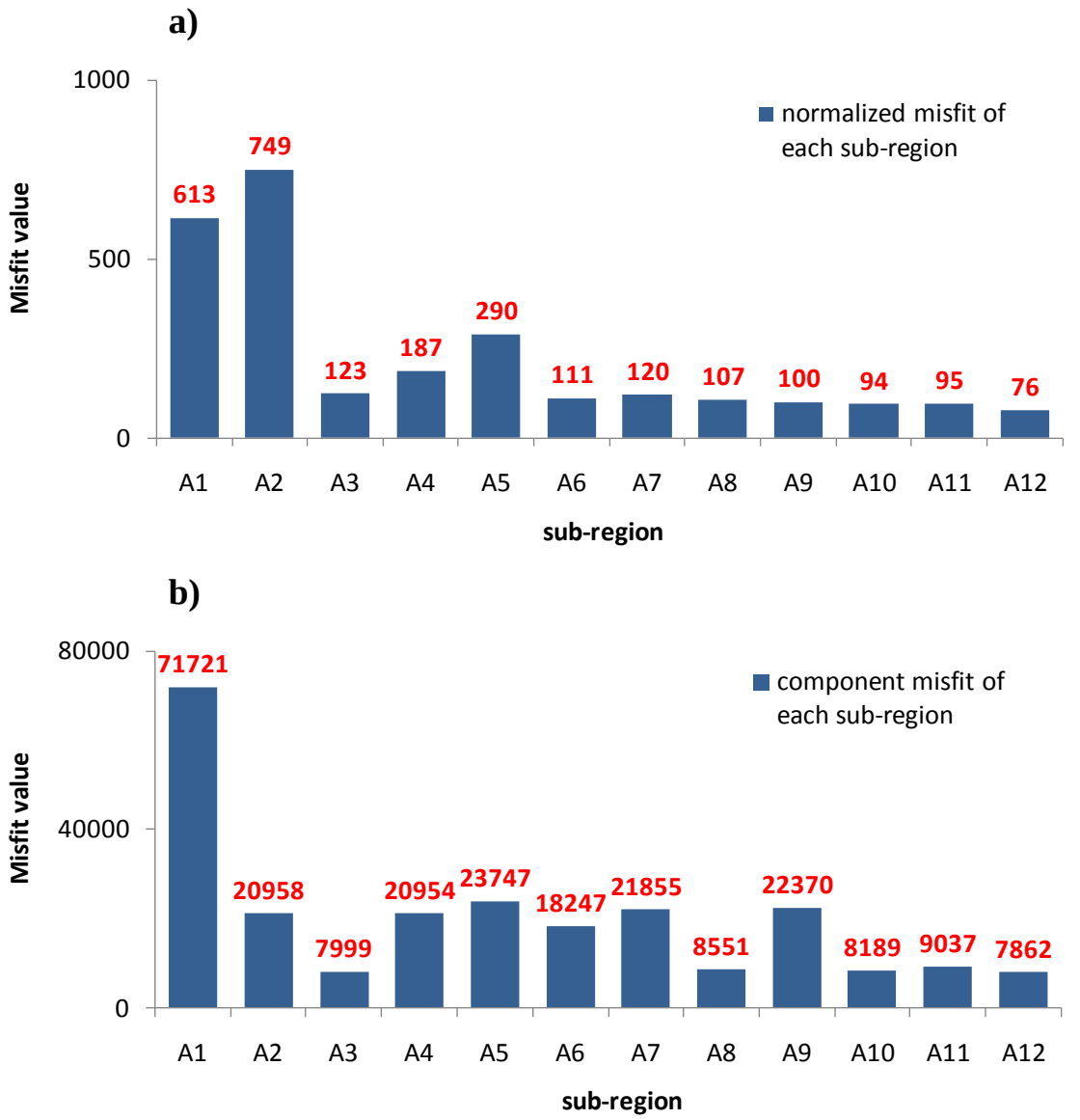

Figure 6.2: a) the component misfit of each sub-region in the base case reservoir model, and b) the normalized misfit of each sub-region calculated by dividing the component misfit by the number of its constituting grid blocks of each sub-region.

Using the Central Composite Design, to sample the 10-dimensional parameter space of the problem 149 models were required. Thus, the Schiehallion simulation model was run for that number of cases to calculate the misfit of the sub-regions. Using the Central Composite Design, to sample the 10-dimensional parameter space of the problem 149 models were required. Then for each of the 12 sub-regions a quadratic polynomial misfit (Equation 3.1) was constructed. Maps of the influence of the effects on the misfit for the area around the injector were determined based on the relative contrast of the coefficients in the polynomial misfits acquired for the separated sub-regions. Figure 6.3

shows several examples of such maps for linear effects of transmissibility of barriers 'd', 'e' and 'f', and Figure 6.4 shows examples of such maps for quadratic effect of transmissibility of barriers 'e', 'g' and 'i'.

Linear effect of parameters

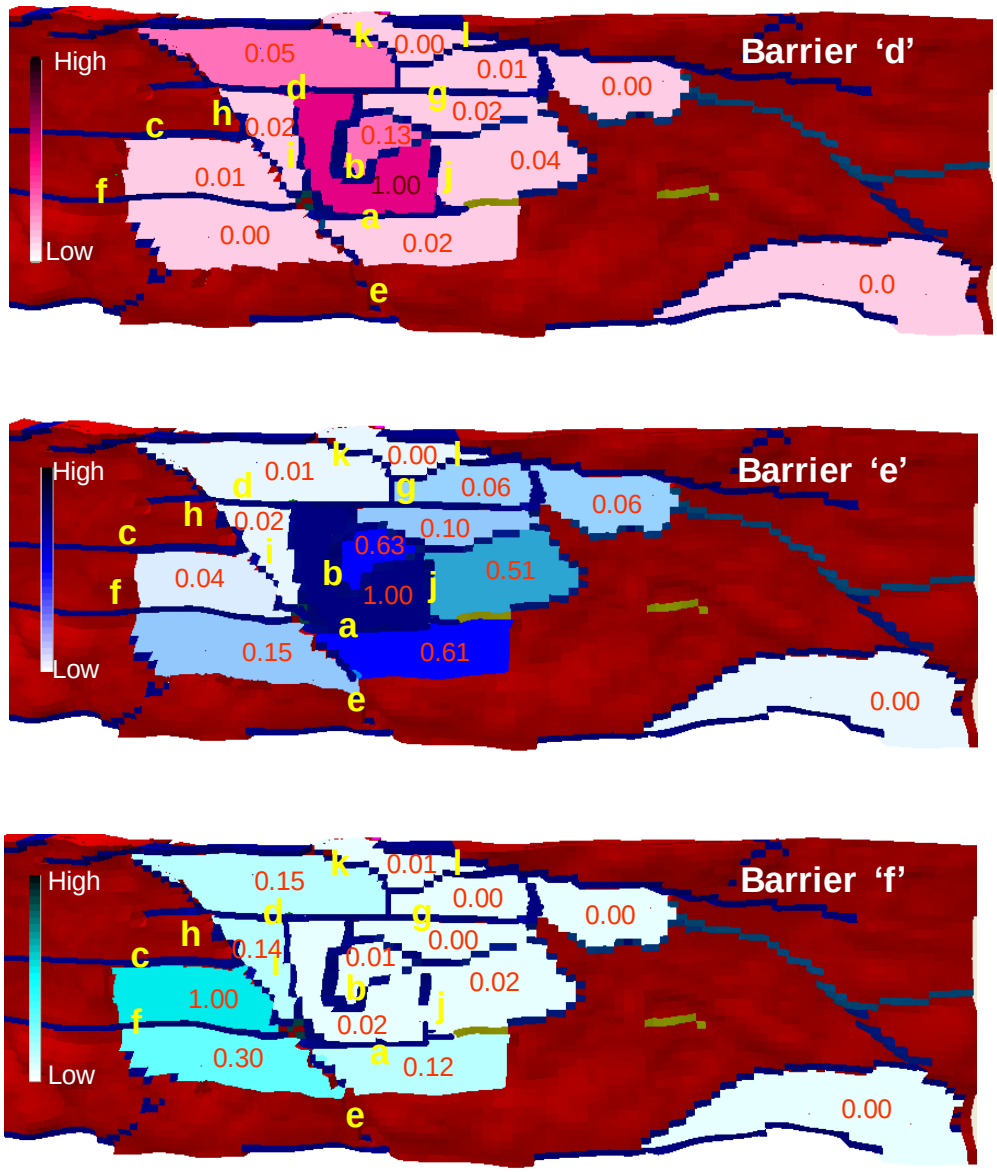

Figure 6.3: Example maps of the linear effect of three parameters on the misfits of areas around the injector I2. They were normalized, i.e. the value of 1.0 was assigned to maximum effect (shown in darkest colours) while the minimum effect acquires the value of 0.0 (shown in lightest colours). The area picked at the bottom right of the maps confirms that the misfit of regions far from the injector I2 and barriers showed no sensitivity to the parameter variations.

Quadratic effects of parameters

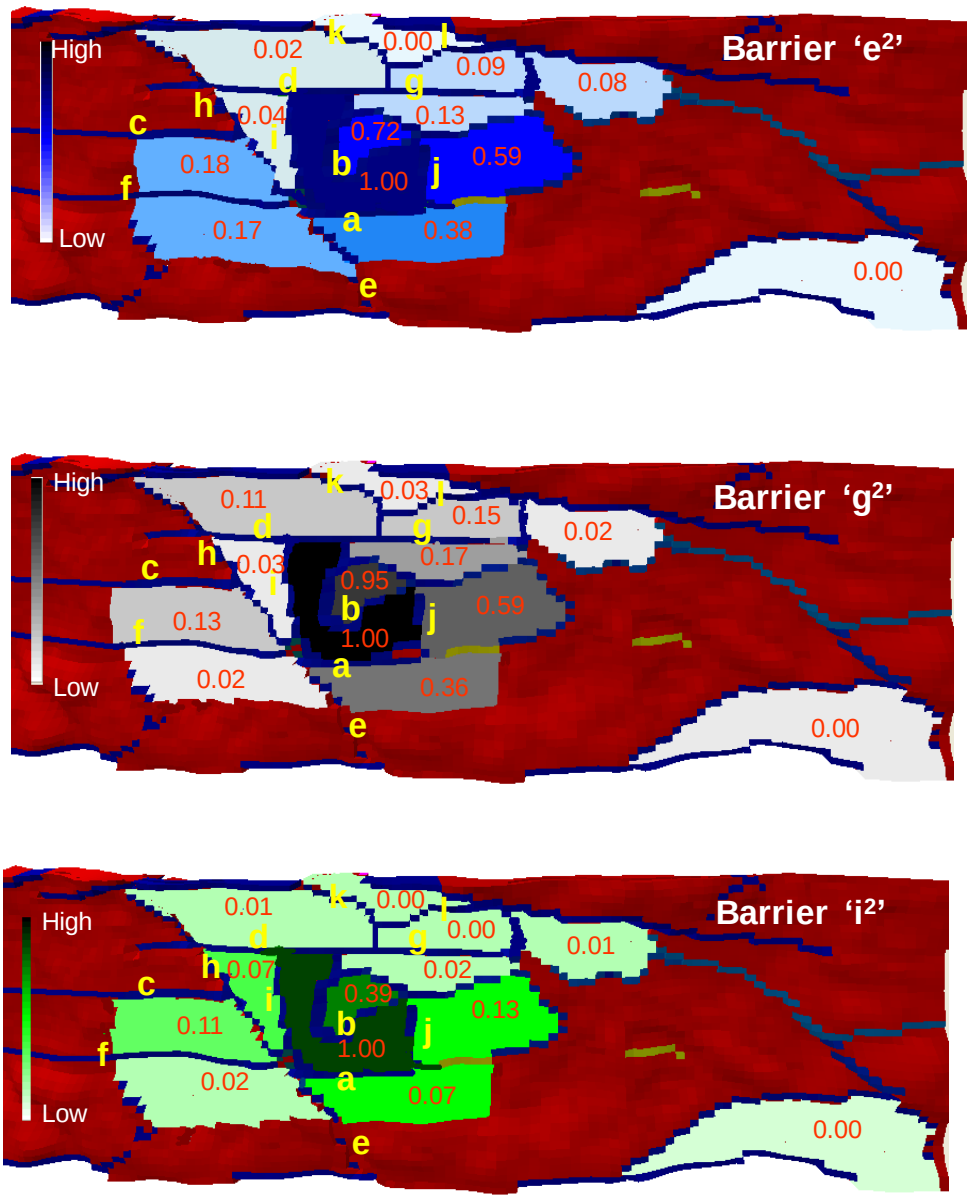

Figure 6.4: As Figure 6.3 but for the quadratic effect of three parameters on the misfits of areas around the injector I2.

The sensitivity of the misfit of a sub-region to the parameter variation, Ψ_s, may be determined through the absolute sum of the derivatives of the misfit polynomial of a sub-region, f_s, with respect to all the parameters, as below:

$$\psi_s = \sum_{i=1}^{n_d} \left| \frac{\partial f_s(\theta)}{\partial \theta_i} \right| \qquad i = 1,\ldots, n_d \tag{6.1}$$

That is, for each sub-region we have (see Equation 3.10 for polynomial model):

$$\psi_s = \sum_{i=1}^{n_d} |a_i| + \sum_{i=1}^{n_d} |2b_i . \theta_i| + \sum_{i=1}^{n_d} \sum_{j \neq i}^{n_d} |b_{ij} . \theta_j| \tag{6.2}$$

where n_d is the number of updated parameters. We utilize the normalized sampled parameters to construct the misfit polynomials (to avoid distortion), i.e. all parameter values are mapped onto the domain of [-1,1] (on a $\log_{10}$.scale). When the parameters give the same value in the polynomial misfits of the sub-regions, then the absolute sum of these coefficients can be used as an intuitive approach to compare the sensitivity of sub-regions against each other. Then for each sub-region we compute:

$$\psi_s = \sum_{i=1}^{n_d} |a_i| + \sum_{i=1}^{n_d} |2b_i| + \sum_{i=1}^{n_d - 1} \sum_{j=i+1}^{n_d} |b_{ij}| \tag{6.3}$$

The region with the highest value of 'absolute sum of the linear and quadratic coefficients' was considered as the region with most sensitivity. The region with the smallest value of the 'absolute sum of the coefficients' was considered as the least sensitive region. Figure 6.5 demonstrates the change in the sensitivity of misfits to the parameter perturbations for the areas around the injector I2. Consequently, the sub-region with highest sensitivity was identified, i.e. sub-region A1. It is an important sub-region since we started the process of spatial decomposition by identifying the sub-regions that were coupled to this one. This sub-region is displayed in darkest colour in Figure 6.5.

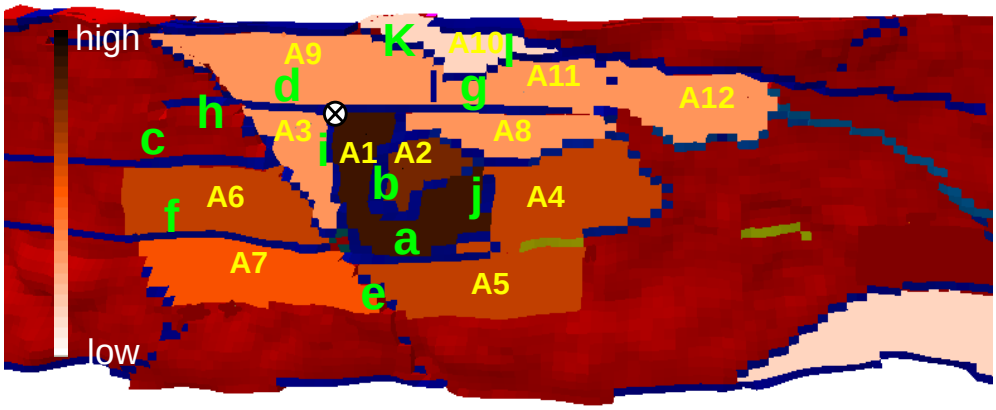

Figure 6.5: Change in the sensitivity of the misfit of sub-regions to the parameters perturbation. Dark brown colour indicates high sensitivity and light brown indicates low sensitivity sub-regions.

From the coefficients of the polynomials, the significant effects on the component misfit of each sub-region were determined. Figure 6.6 illustrates the Pareto charts of influential effects for the misfits of the sub-regions. For each sub-region these effects define 95% of correlation between true misfits and the corresponding misfits re-calculated by the regression polynomial. The correlations between the true misfits and the full polynomial misfits were higher, for example for the sub-region A1, there was 99.7% correlation between the true misfits and the misfits recalculated by the polynomial.

The dominant coefficients of the polynomial were only used in the decoupling process of the seismic territories. For sub-region A1, the misfit was mostly influenced by the linear and quadratic effects of the transmissibility of the barriers 'a', 'b', 'd', 'g', and 'i' (see, Figure 6.6a). The coefficient of the smallest absolute effect of the misfit polynomial of this sub-region was marked out. It had the absolute value of '956' and was found for the linear effect of the transmissibility of barrier 'a'. It was used as a threshold (see Figure 6.6a), such that for any other sub-region, they are concluded to be coupled to this sub-region, if: i) they had any effects equal to or larger than this threshold, and ii) at least one of them were identical to the significant effect of the polynomial misfit of sub-region. In this way the first group of coupled sub-regions was identified to consist of four sub-regions: A1, A2, A4, and A5 (called first domain). They were as shown in Figure 6.7b, c and d.

The same procedure was repeated for the remaining, as yet uncoupled sub-regions, to determine the remaining domains. It means that among the remaining sub-regions the one most sensitive to the parameters perturbation was identified, i.e. sub-region A6. The significant effects of this sub-region only consisted of the linear and quadratic effects of the transmissibility of barrier 'f'. The coefficient of the smallest absolute effect was for the quadratic effect of barrier 'f' and had the absolute value of '1458'. It was used as a second iteration threshold. However, the remaining sub-regions did not have any similar significant effect of 'f', equal to or higher than this threshold. Therefore no sub-region was considered coupled with it. It was considered as the second spatial domain, see Figure 6.6e.

Of the rest of the sub-regions the next most sensitive was sub-region A7. The coefficient of the smallest effect was found for the linear effect of transmissibility of barrier 'h' and had the absolute value of '144'. It was employed as a third threshold. The polynomial misfit of sub-regions A3, A8, A9, A11, and A12 had at least one similar effect to one of the effects of sub-region A7 larger than this threshold. Therefore, these sub-regions were considered to be coupled. They comprised the third domain, see Figure 6.6f-k. We completed the process of dividing the seismic territories. The misfit of sub-region A10 had negligible sensitivities to parameter changes (see the range of x-axis for coefficients in Figure 6.6l). This gave reason to ignore this sub-region in the SHM procedure. Moreover, the transmissibility of barrier 'c' displayed negligible effect on the misfit of all sub-regions. Hence, it was not used in the parameters updated for any of the domains.

In Figure 6.7 the decoupled spatial domains along with the parameters that affect their misfit are illustrated. As a result of the spatial decomposition of the misfit, the 10-dimensional SHM problem was divided into three simpler ones of lower dimensions. They consisted of: i) one 6-dimensional (6D), ii) one 1-dimensional (1D), and iii) one 2-dimensional (2D).

a)

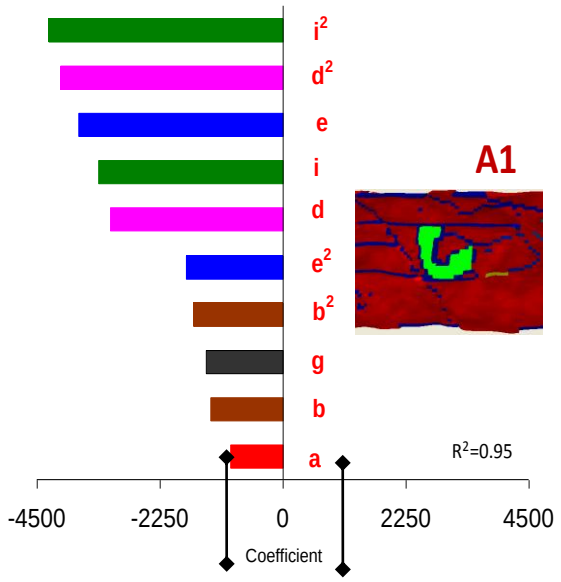

-956 956

b)

common effects (b d e g i) larger

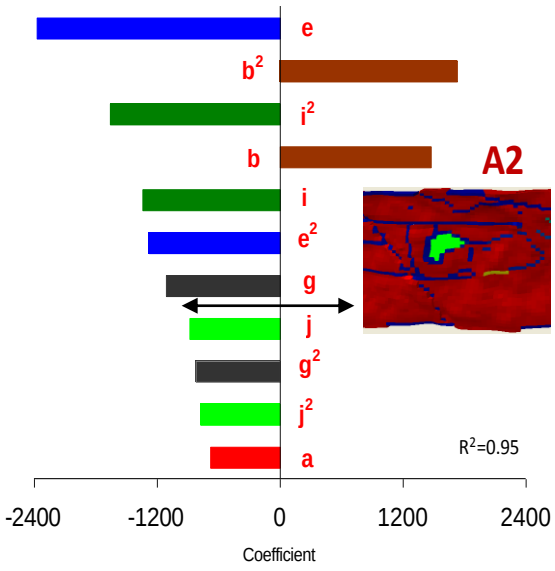

c)

common effects larger than smallest effect of A1

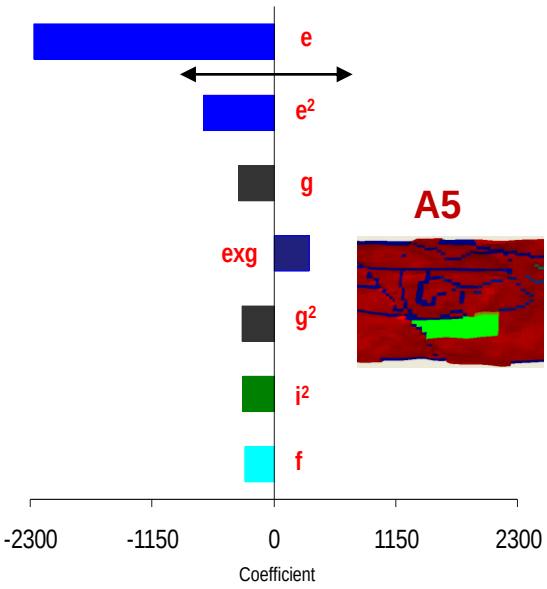

d)

common effects larger than smallest effect of A1

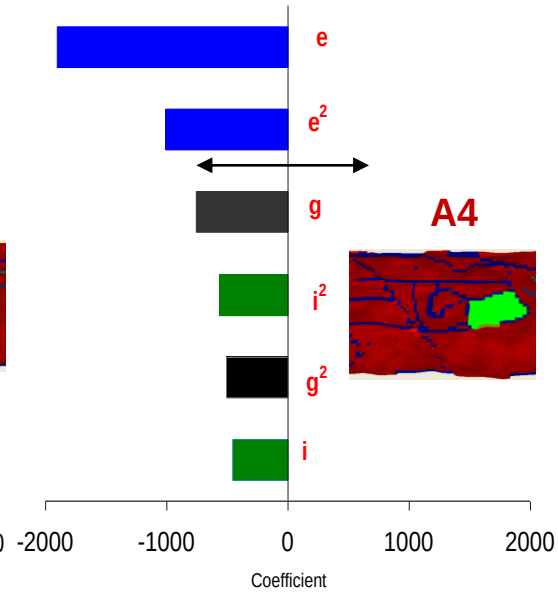

e)

no significant common effects

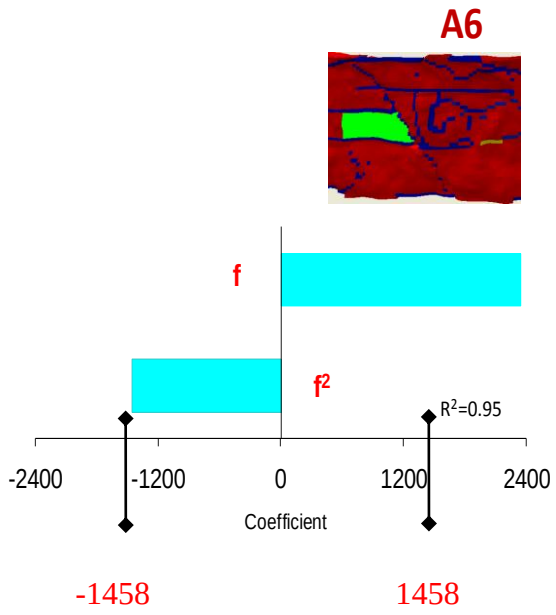

-1458 1458

f)

common effect (f) is less than

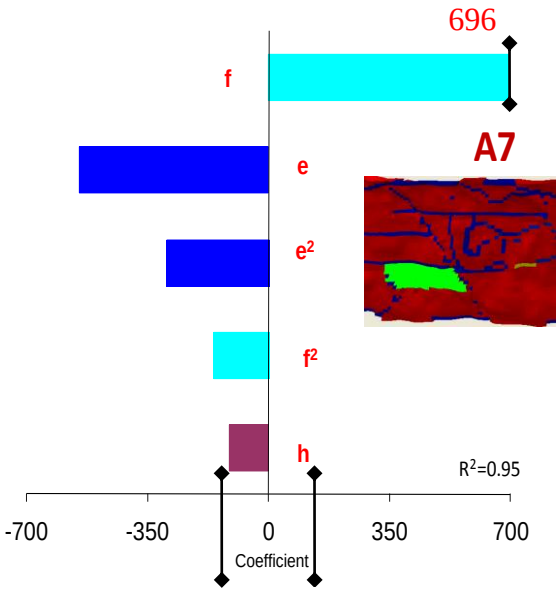

-114 114

g)

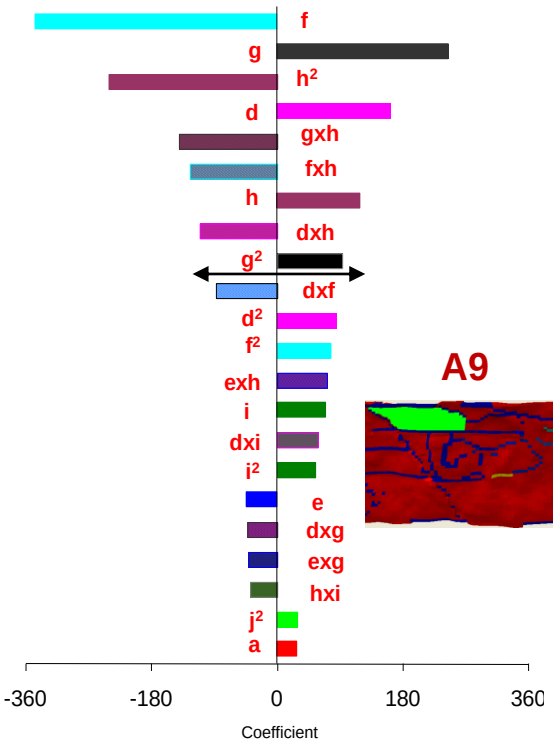

h)

common effects to A9 larger than smallest effect of A9

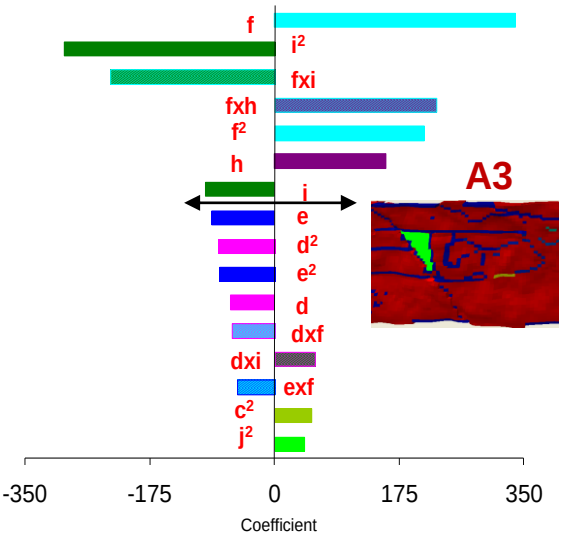

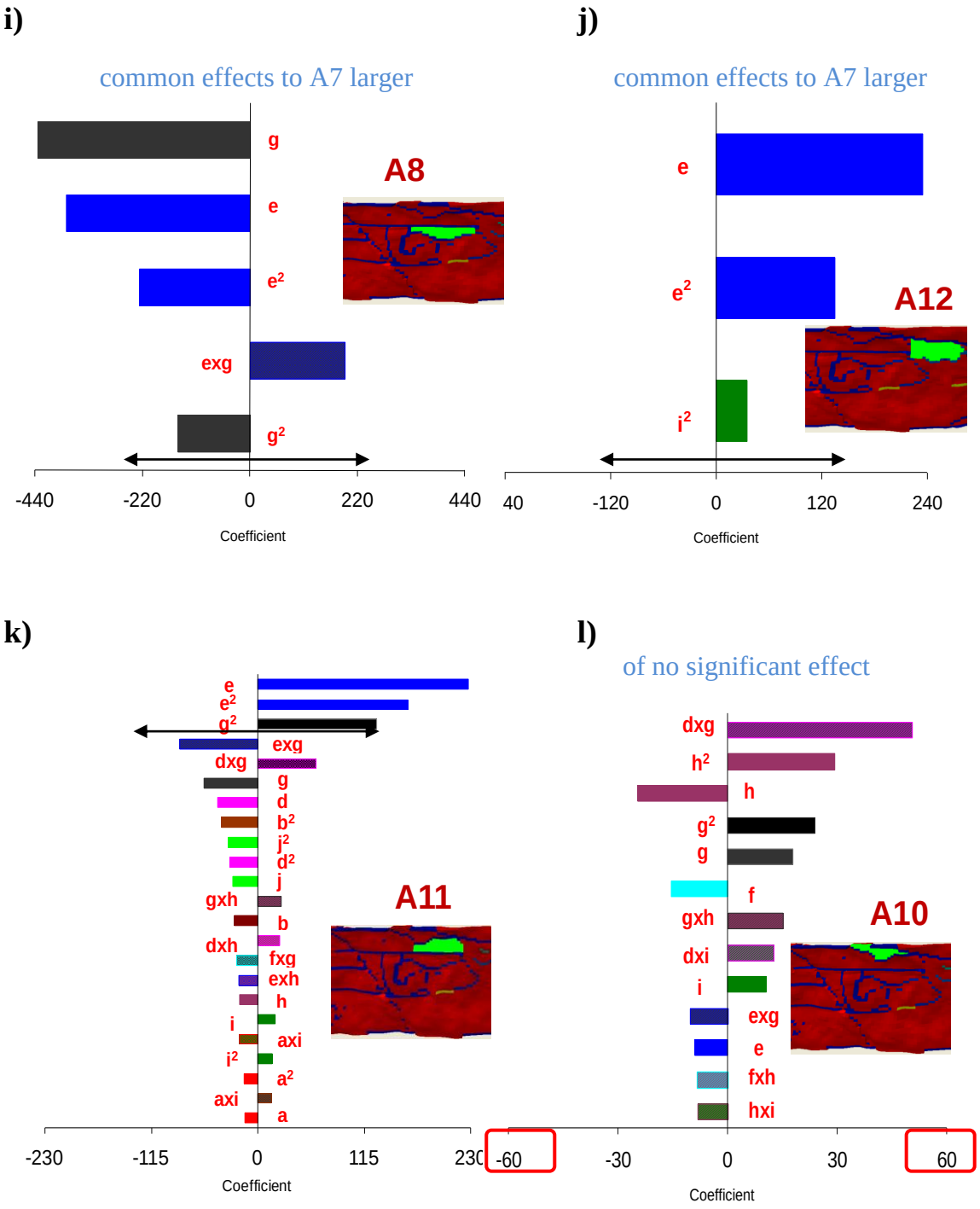

Figure 6.6: Pareto charts of the influential effects of the misfit of the sub-regions. They represent the coefficients in the polynomial misfit obtained for each sub-region. Single letters on plots show linear effects, letters to the power of two show quadratic effects, and product of letters are interacting effects. In this figure the threshold coefficients that were used in investigation of the coupled sub-regions in the three iterations (explained in text) are marked in their relevant plots. Also the coefficients larger than the threshold are highlighted by segregating arrows in the plots. Moreover, the red rectangle on the x-axis of plot (l) highlights the negligible sensitivity of this sub-region to parameter changes.

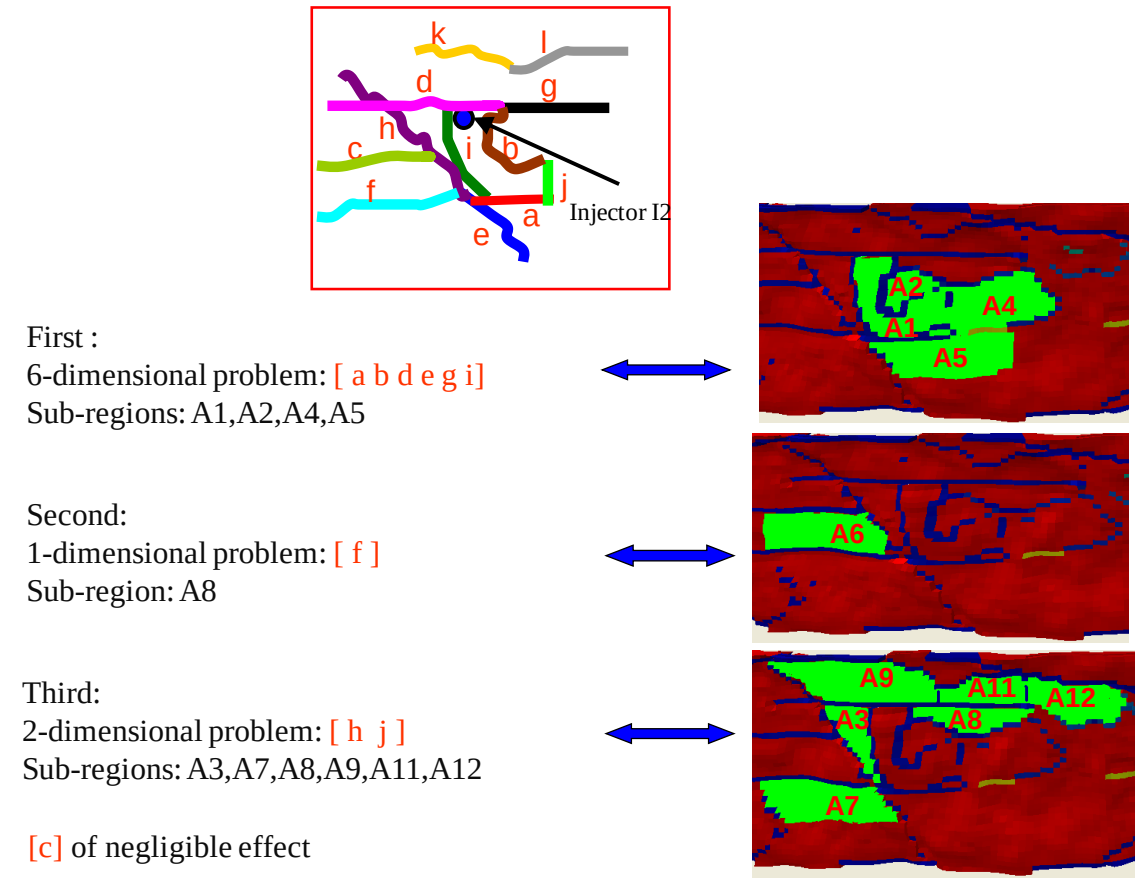

Figure 6.7: The decoupled domains and the parameters that affect their misfit.

The Neighbourhood Algorithm (NA) was then applied and the parameter space of each of decoupled region was searched separately, it meant that Full-SHM was applied on three lower dimensional problems of (6D), (1D) and (2D), instead of one (10D) case, thus fewer models ware required to obtain convergence to the minimum misfit. For the first (6D) spatially decoupled domain the NA tuning parameter was set to be as n_i = 128, n_s = 64, n_r = 32 and it = 5, and in total 448 model was performed. For the second (1D) decoupled domain the NA parameters was set as n_i = 8, n_s = 4, n_r = 2 and it = 5 which resulted in 28 model calls. Finally for the third (2D) decoupled domain the NA parameters were put as n_i = 16, n_s = 8, n_r = 4, and it = 5, and there were 56 runs of the simulation model. Therefore, in total only 685 models were deployed with application of the 'divide and conquer' method, while application of Full-SHM method required 3096 models in finding the minimum misfit.

Moreover, the parameter space of (6D) problems by itself can be decoupled to: one (2D) and four (1D) sub-volumes (the knowledge gained by the results of Chapter 4 and 5).

Consequently, in another approach instead of using the Full-SHM application to the (6D) spatially decoupled domain, the Parallel-SHM was applied, and further saving in model runs were made. That meant that the first full inversion of (6D) was implemented, and next Parallel-SHM used to search the one (2D) and four (1D) parameter spaces separately but simultaneously. These approaches are compared in Figure 6.8a. Figure 6.8 shows the misfit convergence of three spatially decoupled regions. For (1D) and (2D) spatial decomposed domains only Full-SHM was deployed, see Figure 6.8b and c.

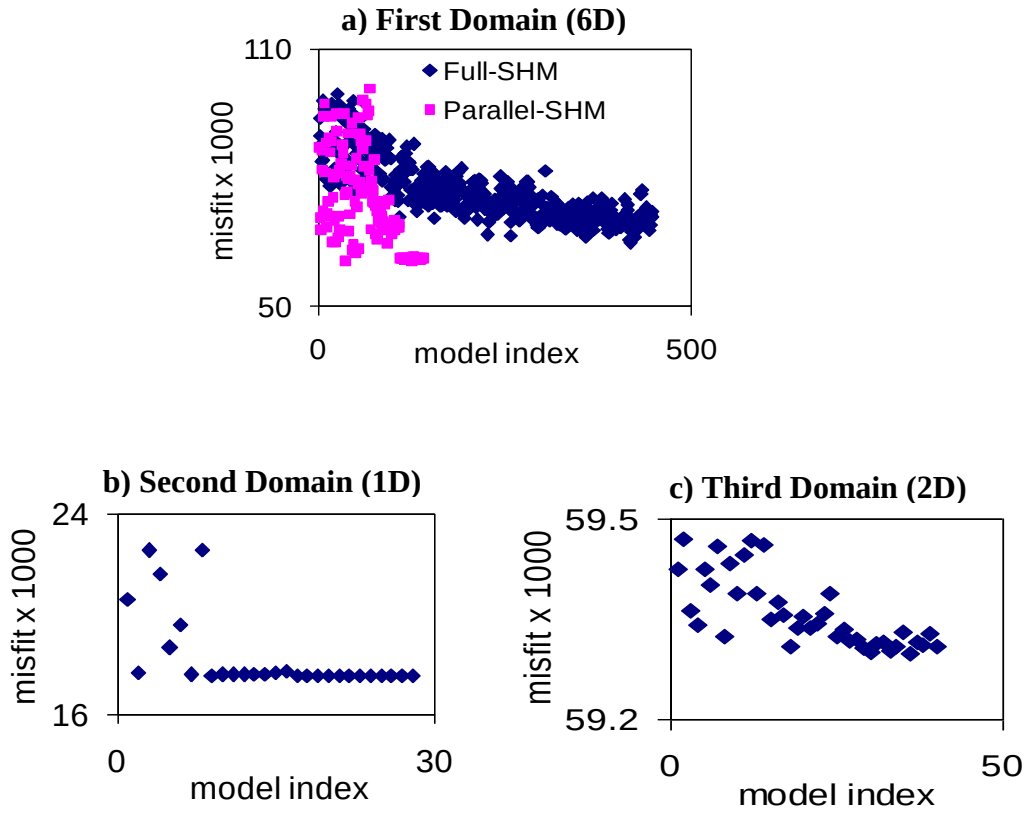

Figure 6.8: Convergence of misfit to minimum for: 6D, 1D and 2D spatially decoupled domains.

6.3 Results

Table 6.1 summarizes the number of models required for searching the spatially decomposed parameter space with Parallel-SHM'. The latter approach only required 374 model evaluations. The 78% and 88% speed-up in seismic history matching of this problem were achieved using these methods, respectively.

Table 6-1: Summary of number of models required in searching the parameter space by using spatial decomposition approaches.

Number of required models					
initialization CCD	searching parameter spaces of decomposed regions				
	1st decomposed domain (6D)		2nd decomposed domain of (1D)	3rd decomposed domain of (2D)	
	Full-SHM	Parallel-SHM			total
149	448	_	28	56	685
149	_	141	28	56	378
Number of required models used by Full-SHM (no decomposition)					3904

Predictions of 4D seismic maps by the best model obtained by the 'divide and conquer' approach are compared to the prediction by the Full-SHM method in Figure 6.9. They are consistent. Updated parameter values for the best model (with minimum misfit) acquired by the various approaches are compared in Figure 6.10. Also the standard deviations of the updated parameters were calculated based on the best 10 models (Figure 6.9). The results for the best updated parameter values are consistent; the exceptions are mainly for the parameters with negligible influence on the misfit response which is the transmissibility of barrier 'c'. In addition, for barriers 'b', 'd' and 'f', there are a few discrepancies by various methods. These results may signify the non-uniqueness of this history matching problem and the existence of the multiple solutions that have been obtained using NA as a stochastic search method. It also may indicate that the reservoir flow behaviour of this example is a complex and non-linear system such that the topography of the misfit objective function away from the minimum may exhibit many multiple local minima. Also there may be stationary points in the surface of misfit function, where the gradient of the function with respect to the parameters is zero, in particular for barriers 'b', 'c', 'd', and 'f'.

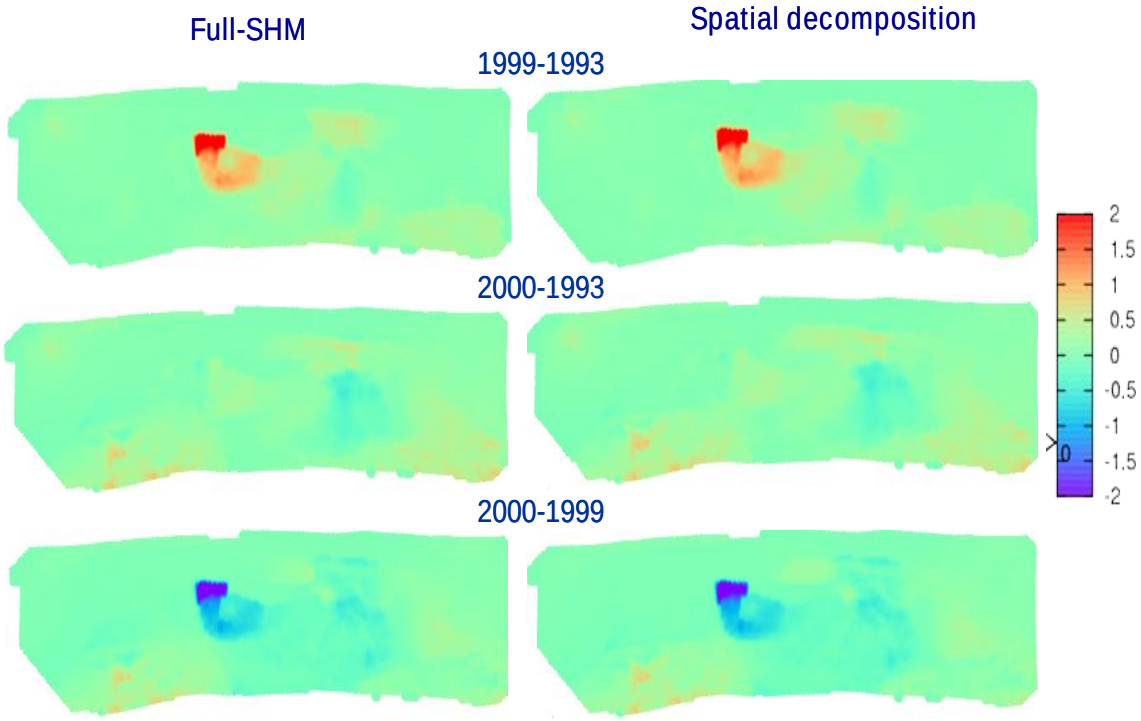

Figure 6.9: Comparison between the maps of seismic predictions for difference in acoustic impedance obtained by spatial decomposition and those obtained by Full-SHM method.

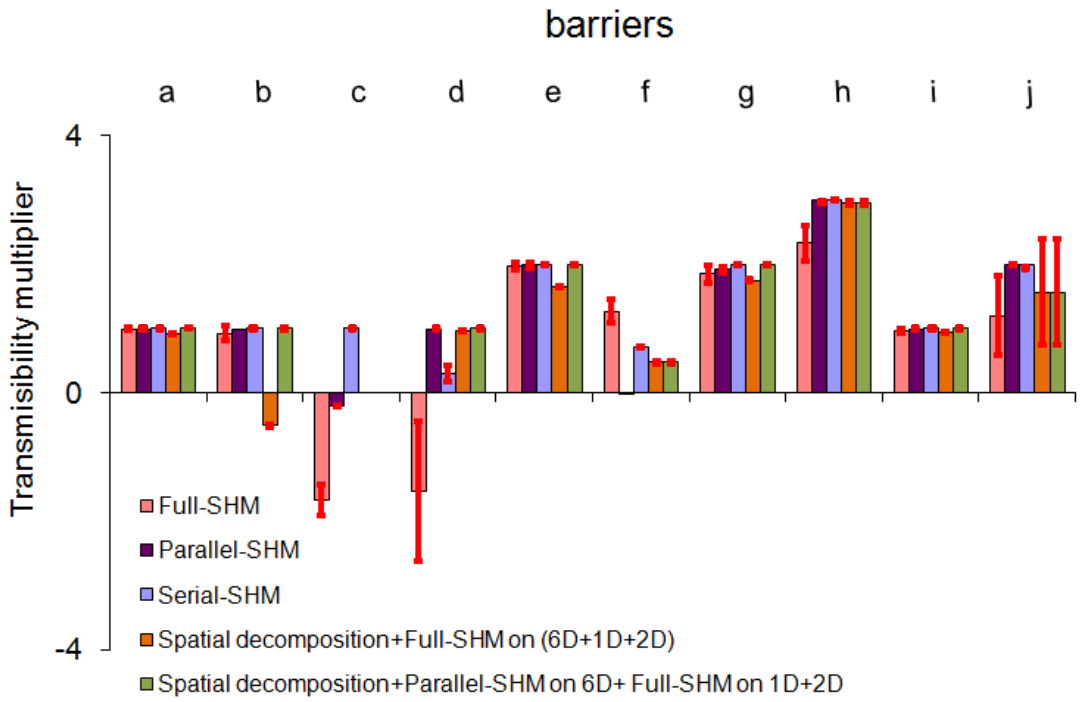

Figure 6.10: Comparison of the best parameter values obtained by various approaches. The error bars are calculated based on 10 best models acquired in each method.

6.4 Discussion

The proposed technique in this chapter uses data partitioning, or sensitivity analysis, to reduce the number of simulations. The misfit objective function can be separated as the sum of local components related to wells or seismic territories. The parameter sensitivities are different for each component. A local component might depend only on a few influential parameters. Therefore, fewer simulations are used to calculate the minimum misfit for a local component. In this approach, full independence of sub-regions or components with respect to the parameters is not required, but for significant parameters. The proposed technique was tested on the case study example of this thesis, i.e. Schiehallion field including 10 updated parameters, and showed the efficiency of the approach.

Generally, the information offered by 4D seismic data is considered to prompt such a local decomposition approach. 4D seismic data bring flexibility in the choice of local components for spatial division of the problem, and provide information about the parameters to be perturbed. In this application, the sub-regions were initially defined manually based on the position of flow barriers. However, they were still implicitly mapped via seismic data.

The method demonstrated here is not restricted to the spatial division based on only the seismic zones. It can be applied in history matching to separate the problem into other local components such as wells and. Then as a rule a local component would depend on a smaller number of parameters. The approach may alleviate the problem of multiple solutions when using a stochastic search routine which is as result of presuming full interactions between parameters and local components of the objective function

For very large fields, it is difficult and even unfeasible to use conventional optimization methods in history matching. The method shown here enables history matching of large fields. It is particularly attractive where a large number of local parameters exist. One point in this approach is that it splits the objective function based on the sensitivity of its local components to parameters. To apply this approach to a wider range of history matching problems, an automatic procedure is required in determining the sensitivity of the local objective functions. This could be considered as future work for further improvement of the method.

The supposition of this method is that the regions of related geological attributes and relatively similar properties which are inter-connected hydraulically are also amalgamated to show similar sensitivity to changes in the variables and the resulting production and 4D seismic responses. In this context this method seems more sensible geologically in comparison to the parameter de-convolution and numerical decomposition of the objective function of the methods proposed in Chapter 4. However, this method involves more analysis to derive the sensitivity of the regions. Also, the method involves more simulation runs than the misfit decomposition method particularly when the degree of parameters convolution is low as it was in the case study of this thesis.

Production and seismic attributes are affected in a complex way by reservoir properties such as lithology, porosity, fluid saturation, layer thickness, permeability, etc; it is possible that different combinations of these variables generate the same production and seismic responses. The excellent feature with this method is that this non-uniqueness does cause less difficulty since the different geologic regions are spatially separated.

6.5 Conclusions

The spatial decomposition method appears more sensible geologically. The history match results obtained by this method were similar to those acquired by parallel and serial methods and also Full-SHM. Although the method requires more simulation runs than the Parallel-SHM and Serial-SHM, on the other hand we were able to use properly calculated misfits, not the proxy misfit. It is very appropriate method to be applied to large reservoir history matching of many unknowns where flow performance of various regions in the reservoir do not effect by all the updated parameters but a few of them. In such cases there would be a great amount of computer cost by applying spatial decomposition method. The major conclusions of this chapter are as following.

- A local misfit function component might depend only on a few influential parameters.

- The spatial decomposition of misfit could be achieved; while full independence of sub-regions or misfit components with respect to the parameters is not required, but for significant parameters.

- Spatial misfit decomposition is a promising approach to tackle high dimensional SHM problems and segregate them to simpler ones. Successful application of this method to a 10-dimensional SHM case of Schiehallion field was shown.

- Integration of misfit decomposition and spatial decomposition approaches leads to even faster convergence in SHM workflow.

CHAPTER 7

Summary, Recommendations and Conclusions

7.1 Summary

In automatic SHM, stochastic optimization routines such as the Neighbourhood Algorithm (NA) are used to guide modifications of the model parameters by minimization of an objective function which quantifies the misfit between observed and predicted data. The computational and financial cost for convergence to a minimum is high. This cost increases exponentially with the dimensionality of the problem particularly if it is assumed that there is interaction between updated reservoir parameters. However, when there are non-interacting groups of parameters and we solve the problem as being fully coupled, a great number of models would be sampled in the inversion process that brings no information about the misfit surface. This leads to waste of simulations. History matching often shows that the interactions between the updated parameters in misfit function do not always occur however. In fact, in such instances the parameter hyper-volume of the problem can be divided into independent sub-volumes; then a more efficient search can be performed by applying any optimization routine to each of the sub-volumes separately in parallel or in serial. The aim of this study was to develop an approach to make the optimization part of history matching more efficient thus to reduce the number of simulations.

We offer a 'divide and conquer' approach that has been developed based on identifying the parameter space sub-volumes. The proposed approach is a development of the existing SHM procedure (Stephen et al. 2006). The development of parameter space decomposition converts the search for the solution of a multidimensional problem into the search for a solution of couple of problems of reduced dimensionality. This dramatically reduces the hyper-volume of the search space and thus the required number of function evaluation and simulation runs.

This 'divide and conquer' approach uses response surface modelling. We employ simulations from initialization of the full inversion using the NA algorithm. We begin by using singular value decomposition techniques with least squares regression and obtain the multi-dimensional polynomial proxy representation of the misfit function. Next, we eliminate the insignificant interaction terms, successively from the polynomial from the smallest up to a coefficient threshold. Parameters are then grouped or separated depending on whether interaction coefficients are above or below the threshold, respectively. The sub-domains of the misfit are identified and the misfit then is decomposed, accordingly.

Several methods were proposed based on the 'divide and conquer' approach in this study. They resulted in significant speed up of the convergence rate in the history matching process. When we searched the independent sub-volumes in parallel, the method was called Parallel-SHM. This method contrasts against a method where the sub-volumes are searched in serial, called Serial-SHM, and also against the application of conventional full inversion, called Full-SHM method. In Full-SHM the problem was solved assuming all the updated parameters are coupled. We successfully applied the Parallel-SHM method to a 10-dimensional SHM case of the Schiehallion field. The results revealed that the convergence can be achieved requiring 30 per cent of the total number of models required for a Full-SHM run. Using the Serial-SHM, still the convergence can be obtained using 40 per cent of the full SHM set of models but required nearly one and half times more models compared to the parallel approach.

Stochastic inversion routines such as NA require a large ensemble of models to effectively sample the parameter space for initialization and to decompose the misfit, particularly if quasi-random sampling is used. In order to reduce the number of initial models, we also adopted an approach of integrating experimental design techniques with the method of Parallel-SHM. We considered conventional quadratic experimental designs that are commonly used in modelling of objective functions of multi-dimensional optimization problems including Central Composite, Box-Behnken, and D-optimal Designs. We were able to reduce the number of initial simulations to about 15% of initial models required for a full inversion. When this initialization step was combined with Parallel-SHM to search the sub-parameter space and find the minimum misfit, then we obtained a 91 per cent speed up in the convergence for the 10-dimensional case study of the Schiehallion field (Sedighi and Stephen 2010).

The method of 'combining experimental design with divide and conquer' was also applied to an 18-dimensional seismic history matching problem of the Schiehallion filed. Such a high dimensional case usually requires too many simulations and in practice, may not be completed using any stochastic search routine. The results in this example also were achieved efficiently with an affordable number of simulation runs.

Another method was presented based on spatial decomposition of the misfit function. The global objective function was decomposed into the sum of a number of local objective functions. Each local objective function measured the misfit on a separated domain and was related to a lower number of parameters, selected from among the parameters that had a significant impact on the seismic misfit of the region. The local coupled sub-regions were determined based on common significant parameter effects. The minimum of the local objective functions were estimated by means of a parameter perturbation technique using NA. Finally, the parameters calibrated based on spatial decomposition of the objective function, were integrated to build up the best history matched reservoir models. The method of 'spatial decomposition' of the misfit was also applied to the 10-dimensional case study of the Schiehallion field. We found that there were three independent domains in the area of the reservoir which we sought to match seismically. The method required fewer model evaluations relative to full inversion. A 78 per cent speed-up in the seismic history matching of this problem was achieved.

The 'divide and conquer' method makes use of a regression equation to derive a proxy response surface for the misfit function. This approach has been assessed several times in history matching studies previously. For example, Castellini et al. (2005) used a response surface model based on kriging interpolation as a proxy to the misfit function to rank and screen the number of parameters, and accelerating convergence to the minimum misfit while a Genetic Algorithm was applied directly on the kriged misfit proxy instead of on true misfit function. Zabalza et al. (2000) used response surface methods to model the objective function as a second order polynomial. Then instead of applying the inversion routines on the true misfit function, identification of the best parameter domain was performed by the minimization of the response surface of the objective function using the simplex method. In this study however, we could not use the proxy model explicitly because it would lead to bias close to the global minimum in the misfit surface due to inaccuracies of the proxy model. Instead it was used as a guide

in the identification of non-interacting or nearly non-orthogonal parameter groups and also in the calculation of misfits for those groups.

Multivariate analyses have been used in history matching studies in the past. They were used mainly to identify parameters which were not significant and reduce the dimension of the history matching problem. In this study, similar methods are used with the aim of identifying groups of non-interacting parameters. In one sense the sights are set lower but on the other hand, it retains more of the variability of the system while still significantly simplifying the inversion problem. In this way the method is more flexible. Besides, the set of problems where parameters can be removed from the system is probably a subset of those where a separation of parameter groups can be found.

Reduction of the number of simulation runs in the automatic history matching process based on independent objective functions has been examined before by Maschio and Schiozer (2008). They first defined several low dimensional independent objective functions each related to a well in the reservoir instead of a combined objective function. Then horizontal and vertical permeability parameters associated to each well were updated in a serial fashion. Sensitivity analyses showed that the parameters associated to each well influenced the misfit of other wells by less than ten per cent influence. The problem was then treated as a set of independent problems, one for each well. However, these criteria seemed to be unsuccessful in total field production history matching. In our approach we are able to determine more effectively how the parameter sub-spaces can be identified, retaining parameter interactions where necessary.

The limitation for dividing the parameter space was revealed through the application of the method to a synthetic field. In this model the parameters controlling permeability multipliers of pilot points was found to be strongly interacting. The response surface assigned to the objective function was strongly asymmetrical about the truth case (as the base model), and we considered a wide sample volume of parameters. Provided we just perturbed properties to one side of the truth case, we obtained a very good result and we could divide the parameter space to a few numbers of sub-volumes. This was a very artificial scenario however as we would expect to have to sample below and above the base case. On the other hand the method may be applicable when the parameters are perturbed in smaller intervals.

In the application of the method (to the Schiehallion field), the misfit quadratic proxy itself recounts a simple structure. We may choose to use a direct method to solve for the points on the surface misfit that have zero gradients with respect to parameters. However, we learned that the misfit proxy can be concave with a maximum in several parameters. We may also search on a limited range of parameters which may not contain the zero gradient points on the misfit surface. There may be multiple minina and they may lie at the extrema. These conditions make the application of the direct gradient based approaches to some extent more difficult to use.

The spatial decomposition method appears more sensible geologically in comparison to the dividing the parameter space by numerical decomposition of the misfit objective function. Although, the history match results obtained by this method were similar to the method of decoupling parametrically, it involved more analysis to derive the sensitivity of the subsequent decoupled domains. Also, the method requires more simulation runs than the misfit decomposition approach particularly when the degree of inter-dependency of the updated parameter effects is low. On the other hand, we were able to use properly calculated misfits, not the proxy misfit.

The application of spatial decomposition method to update properties such as relative permeability in a channelized turbidite reservoir with many flow barriers may not be straightforward. In such cases it is difficult to decouple the effect of a global property (relative permeability) and more local parameter effects (barriers) that may exist. Finding a consistent global parameter (being a coarse scale property) that could be conditioned to history data and could capture the entire channel flow characteristic should be carried out using a more global approach. Regional relative permeability could be used more effectively using spatial decomposition method, however.

7.2 Recommendations

In this study, the parameter space has been separated into several sub-volumes so that they can then be sampled separately but simultaneously using the Neighbourhood Algorithm. The approach is not limited to the choice of inversion method. The strength of the approach is that it reduces the number of models that are similar in terms of misfit response and efficiencies can be gained if other inversion methods are used. An equivalent increase in efficiency using stochastic approaches such as Genetic

Algorithms or Simulated Annealing could all be made more efficient by splitting the parameter space. The initiative of combining those algorithms with the parallel and serial search approaches should be considered in the future work.

The benefit of 'divide and conquer' to deterministic methods is similar. Gradient based methods require calculations of sensitivity coefficients. Usually one per parameter is needed and the computational requirement grows non-linearly with the dimension of the problem. Solution of an adjoint equation or numerical calculation of gradients would be faster if sub-volumes of the parameter space could be treated separately. The proposed method may provide some reduction in workload, therefore. When decoupling the parameter space some efficiency may also be gained by ensuring that new models obtained by estimation are generated in appropriate locations of the parameter space and unnecessary models are ignored. Investigating the gains of the integration of gradient based routines and present 'divide and conquer' approach could be deemed as one of the future studies as well.

The decoupling approach is particularly useful for amalgamating the local effects of particular parameters on the time-lapse seismic data and well responses. This is complimentary to the localization approaches used with the Ensemble Kalman (EnKF) (e.g. Skjervheim et al. 2007, Chen and Oliver 2009) where more heuristic approximations are used. The misfit of various wells and seismic data could be grouped spatially and then associated sub-volumes of the parameter space could be searched separately. However, some knowledge of the localization is required and appropriate spatial relationships are needed. This should be investigated in future studies.

Typically, it is attractive to use direct search methods such as steepest descent or gradient based methods to minimize the misfit proxy models. However, even if we detect a good fit between the true and quadratic regression equation misfits initially, we cannot tell if the form of the misfit surface is quadratic close to the minimum. We also have no information regarding the existence of the minima. From this point of view, it would be dangerous to assume from the initial analysis that the true misfit surface is fully quadratic. We deem therefore that there is benefit in just using the proxy of misfit to decouple the independent parameter space and combine that with the global search schemes. In fact in the Schiehallion case, the location of the minma is different in the regression equation. It is therefore possible that we lose the benefit of the direct use of

misfit proxy model and they could even work against us by directing the search in the wrong direction. One option may be updating the regression equation. We may consider to fit the regression model when the correlation deteriorates as we progress in the search process. Then in particularly we can interrogate as we converge toward a global minima, and see if in the true misfit the coupling effects of parameters diverges from the initial state. This progress could be considered also as one of the future studies.

The limitation of the spatial decomposition method is that we initially split the local components of the misfit function intuitively, and we then establish the emerge by investigating the inter-connections of the sub-regions. In order to apply the method to a wider range of history matching cases, it is required that the sensitivity of the local objective functions be determined in a more automatic way, e.g. using the Principal Component Analysis (PCA) approach. This could be considered as a future work for further improvement of the method.

7.3 Conclusions

- A 'divide and conquer' approach was used for decoupling the parameter space in high dimensional seismic history matching problems. The separate sub-volumes of the parameter space as well as dominant parameters were then identified.

- The sub-volumes of smaller dimension were searched very efficiently especially in parallel and also in serial search attempts. These search methods successfully improved the convergence rate of history matching process and reduced the number of simulation runs.

- When we could decompose the parameter space using any of the 'divide and conquer' methods, the quality of history matching results was equivalent to the case when the entire parameter space was searched during the inversion of the process but with reduced CPU cost.

- Combining experimental design with a 'divide and conquer' method result in convergence being acquired with significantly fewer number of model calls in the history matching procedure. Such an approach is then especially attractive of higher dimensional cases involving many simulation runs.

- A local misfit function component might depend only on a smaller number of updated parameters in history matching. Then spatial decomposition of the misfit is a promising approach particularly to tackle high dimensional problems and separate them into simpler ones each linked to a local domain.

REFERENCES

Aanonsen, S., Cominelli, A., Gosselin, O., Aavatsmark, I., and Barkve, T., 2002. Integration of 4D Data in the History Match Loop by Investigating Scale Dependent Correlations in the Acoustic Impedance Cube. European Conference on the Mathematics of Oil Recovery, Freiberg, Germany.

Aanonsen, S. I., and Eydinov, D., 2006. A multiscale method for distributed parameter estimation with application to reservoir history matching Computational Geosciences, Volume 10, 97 117 (2006), DOI: 10.1007/s10596-005-9012-4.

Aanonsen, S. I., 2005. Efficient history matching using a multiscale technique, SPE 92758, in 2005 SPE Reservoir Simulation Symposium.

Aanonsen S., Nævdal G., Oliver D., Reynolds A., and Vall`es B., 2009. The ensemble Kalman filter in reservoir engineering - a review, SPE Journal, SPE 117274.

Aarre, V., 2006. Estimating 4D velocity changes and contact movement on the Norne field: 76th Annual International Meeting, SEG, Expanded Abstracts,3115-3119.

Abacioglu, Y., Oliver, D. S., and Reynolds, A. C., 2001. Efficient reservoir history matchingusing subspace vectors, Computational Geosciences, 5(2), 151-172.

Abdollahzadeh, A., Reynolds, A., Christie, M., Corne, D., Davies, B., and Williams, G., 2011. Bayesian optimization algorithm applied to uncertainty quantification. EUROPEC/EAGE Annual Conf. and Exhibition, Vienna, Austria, 2011, SPE 143290.

Agarwal, B. and Blunt, M. J., 2004. A Streamline-Based Method for Assisted History Matching Applied to an Arabian Gulf Field. SPE Journal 9(4), pp. 437-449.

Aggio, A. and Burns, C. S., 2001. Seismic visualization for dynamic and static reservoir characterization. EAGE 63rd Conference & Technical Exhibition, Amsterdam, The Netherlands, 11-15 June 2001.

Aggrey G. H., 2007. A Study of Intelligent Oil and Gas Fields' Real Time Optimization and its Value Quantification, PhD thesis. Heriot Watt University.

Al-Maskeri, Y., Fulton, J., and MacBeth, C., 2003. Model-Controlled Quantitative Interpretation of 4D Signatures in Turbidite Reservoirs. In International Congress of The Brazilian Geophysical Society, Rio de Janeiro, Brazil.

Anderson, M.J., Whitcomb, P.J., 2005. RSM simplified: optimizing processes using response surface methods for design of experiments. Productivity Press, New York.

Anterion, F., Eymard, R., and Karcher, B., 1989. Use of Parameter Gradients for Reservoir History Matching. Paper SPE 18433 presented at the Reservoir Simulation Symposium, Houston, Texas, 6-8 February.

Arenas, E., Van Kruijsdijk, C., and Oldenziel, T., 2001. Semi-Automatic History Matching Using the Pilot Point Method Including Time-Lapse

Seismic(SPE71634). Annual Technical Conference and Exhibition, New Orleans, Louisiana.

Arts, R., 2005. 4D seismic quantification of a growing CO2 plume at Sleipner, North Sea Petroleum Geology Conference series 2005, 6:1385-1399; doi:10.1144/0061385.

Arwini, S. and Stephen, K.D., 2010. A New Method to Improve Convergence Rates with Seismic History Matching. SPE 131545, 72nd EAGE Conference & Exhibition incorporating SPE EUROPEC 2010 held in Barcelona, 14-17 June.

Arwini, S., and Stephen, K.D., 2011. Combining experimental design with proxy derived sensitivities to improve convergence rates in Seismic History Matching. SPE 143528, EUROPEC/EAGE Annual Conference and Exhibition Vienna, Austria, 23-26 May.

ASPO International, 2011. The Association for the Study of Peak Oil and Gas. Headline News, www.peakoil.net/news-type/headline-news.

Audet, C., and Dennis J.E., 2003. Analysis of generalized pattern searches. Siam J. Optimize., 13: 889-903. DOI: 10.1137/S1052623400378742.

Avansi, G. D., and Schiozer, D. J., 2011. Quantitative Analysis Involving Scaling Procedures for Integration between History Matching and 4D Seismic. (SPE 143599), 73rd EAGE Conference and Exhibition, Viena, Austria, 2011.

Avseth, P., 2000. Combining Rock Physics and Sedimentology for Seismic Reservoir Characterization of North Sea Turbidite Systems, PhD dissertation, Stanford University.

Aziz, K., and Settari, A., 1979. Petroleum Reservoir Simulation. Applied Science Publishers. New York and London, 476 p.

Backus, G. E., 1962. Long-wave elastic anisotropy produced by horizontal layering. J. Geophysical Research, 67 (11), p4427- 4440.

Badru, O., and Kabir, C. S., 2003. Well Placement Optimization in Field Development. Paper SPE 84191 Annual Technical Conference and Exhibition, Denver, Colorado, 5-8 October.

Ballester, P.J., and Carter. J.N., 2004. Tackling an Inverse Problem from the Petroleum Industry with a Genetic Algorithm for Sampling. Genetic and Evolutionary Computation Conference, June-04, Seattle, USA. Computer Science 3103, Springer, pp. 1299-130.

Ballester, P.J. and Carter, J.N., 2007. A parallel real-coded genetic algorithm for history matching and its application to a real petroleum reservoir. J. PETROL. SCI. ENG., 2007, Vol:59, Pages:157-168, ISSN: 0920-4105(doi).

Barker, J.W. and Dupouy, P., 1999. An analysis of dynamic pseudo-relative permeability methods for oil-water flows, Petroleum Geoscience 5, 385-394.

Barnes, R. L., 1964. A technique for maximizing details in numerical weather map analysis. J. Appl. Meteorology. 3, p396-409.

Barrera, A., and Srinivasan, S., 2009. History Matching by Simultaneous Calibration of Reservoir Geological Models at Pore Level and Field Scales. SPE: 124939-

MS. Annual Technical Conference and Exhibition, 4-7 October 2009, New Orleans, Louisiana DOI: 10.2118/124939-MS.

Batzle, M., and Wang, Z., 1992. Seismic properties of pore fluids. Geophysics, 57(11):1396-1408.

Benson, S. M., and Surles, T., 2006. Carbon Dioxide Capture and Storage: An Overview with Emphasis on Capture and Storage in Deep Geological Formations. The Proceedings Special Issue, Institute of Electrical and Electronics Engineers (IEEE), Vol. 94, No 10, October 2006, DOI: 10.1109/PROC.2006.883716.

Bertrand, A., McQuaid, S., Bobolecki, R., Leiknes, S., and Ro, H., 2005. A high-resolution workflow for 4D-friendly analysis: Application to gas-oil contact monitoring at Troll West: 75th Annual International Meeting, SEG, Expanded Abstracts, 2422-2426.

Bettomvil, B., and Kleijnen, J. P. C., 1992. Identifying the Important Factors in Simulation with Many factors. Tilburg University, Tilburg, The Nederland.

Bissell, R. C., Dubrule, O., Lamy, P., Swaby, P. and Lepine, O., 1997. Combining Geostatistical Modelling With Gradient Information for History Matching: The Pilot Point Method. SPE 38730, Annual Technical Conference and Exhibition. San Antonio, Texas, 5-8 October 1997.

Bissell, R.C., Sharma, Y., and Killough, J.E., 1994. History Matching Using the Method of Gradients: Two Case Studies. SPE 28590 Annual Technical Conference and Exhibition, New Orleans, LA, 25-28 September,.

Bittencourt, A. C., and Horne, R. N., 1997. Reservoir Development and Design Optimization. SPE 38895 Annual Technical Conference and Exhibition, San Antonio, Texas, 5-8 October.

Bogan, C., Johnson, D., Litvak, M., and Stauber, D., 2003. Building reservoir models based on 4D seismic & well data in Gulf of Mexico oil fields, SPE 84370, Annual Technical Conference and Exhibition.

Box, G. E. P., and Draper, N. R., 1987. Empirical Model Building and Response Surfaces, John Wiley and Sons, New York, United States.

Bryant, S., Srinivasan, S., Barrera, A., and Yadav, S., 2005; 2006. History Matching In Parallel Computational Environments. Annual Report Submitting organization: Center for Petroleum and Geo-systems Engineering. The University of Texas, Austin.

Burgers, G., van Leeuwen P. J., Evensen, and G., 1998. Analysis Scheme in the Ensemble Kalman Filter. Monthly Weather Review, Vol. 126, No. 6, 1998, pp. 1719-1724. doi:10.1175/1520-0493.

Burkhart, T., Hoover, A.R., and Flemings, P.B., 2000. Time-lapse (4-D) seismic monitoring of primary production of turbidite reservoirs at South Timbalier Block 295, offshore Louisiana, Gulf of Mexico: Geophysics, 65, 351.367.

Caers, J., 2003. History Matching Under Training-Image-Based Geological Model Constraints. SPE J., 8, 218-226 (Sept. 2003).

References

Caers, J., 2004. The Probability Perturbation Method: An Alternative to Traditional Bayesian Approaches for Solving Inverse Problems, presented at 9th European Conference on the Mathematics of Oil Recovery, Cannes, France.

Carrera, J., and Neuman, S. P., 1986. Estimation of aquifer parameters under transient and steadystate conditions:. Application to synthetic and field data. Water Resour. Res., 22(2),228-242, 1986c.

Calvert, R., 2005. Insights and methods for 4D reservoir monitoring and characterization, EAGE/SEG Distinguished instructor short course, No. 8, 2005.

Cao, D., Bevdoun, W. B., Singn, S.C., and Tarantola, A., 1989. A simultaneous inversion for background velocity and impedance maps: Geophysics, 55, 458-469.

Carter, J.N., 2004. Using Bayesian Statistics To Capture the Effects of Modelling Errors in Inverse Problems. Mathematical Geology, 2004, 36, No. 2, 187.

Carter, J.N., Ballester, P.J., Tavassoli, Z., and King, P.R., 2004. Our Calibrated Model has No Predictive Value: An Example from the Petroleum Industry. Los Alamos National Laboratory, 2005.

Castellini, A., Landa, J.L., and Kikani, J., 2004. Practical Methods for Uncertainty Assessment of Flow Predictions for Reservoirs with Significant History- A Field Case Study, 9th European Conference on the Mathematics of Oil Recovery, Cannes, France.

Castellini, A., Gullapalli, I., Hoang, V., and Condon, P., 2005. Quantifying Uncertainty in Production Forecast for Field with Significant History: A West African Case Study. International Petroleum Technology Conference, Doha, Qatar, 21-23 November.

Castro S, 2007. A probabilistic approach to jointly integrate 3D/4D seismic, production data and geological information for building reservoir models. PhD Thesis, Stanford University, USA.

Castro, S., Caers, J., and Durlofsky, L., 2006. Improve modelling of 4D seismic response using flow-based downscaling of coarse grid saturations. A024 the 10th European conference on the mathematics of Oil Recovery, Amsterdam, Netherlands, 4-7 September.

Chavent, G., 1991. On the theory and practice of non-linear least-squares, Adv. Water Resources,14(2), 55-63, 1991.

Chen Y., and Durlofsky L. J., 2006. Adaptive Local-Global Upscaling for General Flow Scenarios in Het-erogeneous Formations. Transport in Porous Media 62:157-185.

Chen, W.H., Gavalas, G.R., Seinfeld, J. H., and Wasserman, M. L., 1974. A New Algorithm for Automatic History Matching, Soc. Petrol. Eng. J., 14(12), 593-608.

Chen, Y., Oliver, D, S., Zhang, D., 2009. Data assimilation for nonlinear problems by ensemble Kalman filter with reparameterization. Journal of Petroleum Science and Engineering 66, 1-14.

References

Cheng, W. B., Wang, T. K., Lee, C. S., Liu, C. S., 2009. Seismic reflectivity and AVO studies of BSRs on the convergent margin in south-western Taiwan: OBS data analysis, Geophys. Res. Abstracts, 11, 3344, European Geosciences Union.

Christie, M. A., Glimm, J., Grove, J. W., Higdon, D. M., Sharp, D. H., and Wood-Schultz, M. M., 2005. Error analysis and simulations of complex phenomena. Los Alamos Science, 29, p 6-25.

Christie, M A., and Blunt, M. J., 2001. Tenth SPE Comparative Solution Project: A comparison of Upscaling Techniques, SPE 66599, presented at the SPE Reservoir Simulation Symposium, Houston, Texas, 11-14 February.

Christie, M., MacBeth, C., and Subbey, S., 2002. Multiple History Matched Models for Teal South. The Leading Edge, 21(3):286-289.

Christie, M., Demyanov, V., and Erbas D., 2006. Uncertainty Quantification for Porous Media Flows. Journal of Computational Physics, 217, 143-158, 2006.

Chu, C., 1990. Prediction of steam flood performance in heavy oil reservoirs using correlation development by factorial design method. SPE 20020 Proceedings of the 60th SPE California Regional Meeting, Ventura, California, U.S.A., April 4-6.

CSEG 2011. Geophysical Applications – Using Geophysics for Reserves and Resources Classification and Assessment. Chief Geophysicists Forum, DRAFT 09 June 2011

Cullick, A.S., Johnson, D., and Shi, G., 2006. Improved and More-Rapid History Matching With a Nonlinear Proxy and Global Optimization. SPE 101993, Annual Technical Conference and an Exhibition, San Antonio, Texas, 24-27 September.

Dadashpour, M., Martin Landrø, M., Kleppe, J., 2008. Nonlinear inversion for estimating reservoir parameters from time-lapse seismic data. J. Geophys. Eng. (5), pp. 54-66.

Dadashpour, M., Rwechungura, R., and J. Kleppe, J., 2011. Fast reservoir parameter estimation by using effect of principal components sensitivities and discrete cosine transform. 141913-MS SPE Reservoir Simulation Symposium, 21-23 February 2011. The Woodlands, Texas, USA. DOI:10.2118/141913-MS.

Daubechies, I., 1988. Orthonormal Bases of Compactly Supported Wavelets, Communications on Pure Applied Mathematics, XLI, 901-996.

Damsleth, E., Hage, A., Volden, R., 1992. Maximum information at minimum cost: A North Sea field development study with an experimental design. Journal of Petroleum Technology, 1350-1356.

Darcy, H., 1856. Les Fontaines Publiques de la Ville de Dijon, Dalmont, Paris.

Datta-Gupta, A, Lake, L. W., and Pope, G. A., 1995. Characterizing Heterogeneous Permeable Media With Spatial Statistics and Tracer Data Using Sequential Simulated Annealing. Mathematical Geology, 27 (6), 763-787.

Deutsch, C. V., and Journel, A. G., 1992, 1997. GSLIB: geostatistical software library and user's guide. Oxford University Press.

References

Deutsch, C. V., and Wang, L., 1996. Hierarchical object-based stochastic modelling of fluvial reservoirs. Math. Geol. 28, 857-880.

Ding, D.Y., 2011. Development of a Data-Partition Technique for Gradient-Based Optimization Methods in History Matching. SPE J. SPE-130473-PA. Doi: 10.2118/140811-MS.

Ding, D.Y., McKee, F., 2011. Using Partial Separability of the Objective Function for Gradient based Optimizations in History Matching, SPE 140811.

Ditzhuijzen, R., van, Oldenziel, T., and Kruijsdijk, van., 2001. Geological parameterization of areservoir model for history matching incorporating time-lapse seismic based on a case study of the statfjord field. SPE 71318, 2001.

Domenico, S.N, 1976. Effect of Brine-Gas Mixture on Velocity in an Unconsolidated Sand Reservoir. Geophysics, 41(5):882-894.

Dong, Y., and Oliver, D. S., 2005. Quantitative Use of 4D Seismic for Reservoir Description. SPE Journal, SPE 84571, March 2005, 91-99.

Dong, Y., Gu, Y., and Oliver, D. S., 2006. Sequential Assimilation of 4D Seismic Data for Reservoir Description Using the Ensemble Kalman Filter. Journal of Petroleum Science and Engineering, 53(1-2), 83-99, August 2006.

Doyen P.M., 2007. Seismic Reservoir characterisation an earth modelling perspective, EAGE 2007.

Dvorkin, J., and Nur, A., 1996. Elasticity of High-Porosity Sandstones: Theory for Two North Sea Datasets. Geophysics, 61, 1363-1370.

Eclipse 100 Manual, 2007. Schlumberger Geoquest

Edris, N., Stephen, K. D., Shams, A., and MacBeth, C., 2008. Updating Barrier Transmissibilies in Simulations by Successively Adding Data to an Automated Seismic History Matching Processes: A Case study. SPE113557. SPE Europec/EAGE Annual Conference and Exhibition, Rome, Italy, 9-12 June.

Edris, N., and Stephen, K. D., 2008. History matching with time-lapse seismic: will any starting model do? SPE Europec/EAGE Annual Conference and exhibition held in Rome, Italy, 9-12 June 2008.

Edris, N., 2009. Identification of an appropriate data assimilation approach in seismic history matching and effect on prediction uncertainty. PhD thesis. Institute of Petroleum Engineering, Heriot-Watt University.

Egeland, T., Hatlebakk, E., Holden, L., and Larsen, E. A., 1992. Designing better decisions. Proceedings of the SPE European Petroleum Computer Conference, Stavanger, Norway, May 25-27. SPE 24275.

Egorov, N., Kretinin, G. V., Leshchenko, I. A., 2002. Stochastic Optimization of Parameters and Control Laws of the Aircraft Gas-Turbine Engines-a Step to a Robust Design, Elsevier Science Ltd, Inverse Problem in Engineering Mechanics III, pp.345-353.

Eide, A. L., Holden, L., Reiso, E., and Aanonsen, S. I., 1994. Automatic history matching by use of response surfaces and experimental design. Proceedings of

the 4th European Conference on the Mathematics of Oil Recovery, ECMOR-IV '94, Roros, Norway, June 1994.

Enchery, A.C., Ravalec-Dupin, M., and Roggero, F., 2007. An improved pressure and saturation downscaling process for better integration of 4D seismic data together with production history, paper D003/SPE 107088 presented at the 69th EAGE conference and Exhibition, London, UK, 11-14 June.

Engelmark, F., 2002. Error propagation in Gassmann modelling for 4D feasibility studies. The Leading Edge; October 2002; v. 21; no. 10; p. 984-987; DOI: 10.1190/1.1518434.

Erbas, D., 2006. Sampling Strategies in Uncertainty Qualification in Oil Recovery Predictions. PhD thesis, HWU.

Erbas, D., and Christie, M., 2007. Effect of Sampling Strategies on Prediction Uncertainty Estimation. Paper SPE 106229, SPE Reservoir Simulation Symposium, Houston, TX, and 26-28 February 2007.

Evensen, G., 1994. Sequential Data Assimilation with a Non-Linear Quasi-Geostrophic Model Using Monte-Carlo Methods to Forecast Error Statistics. J. Geophys Res., 99 (C5), pp. 10143-10162.

Evensen, G., Hove, J., Meisingset, H. C., Reiso, E., Seim, K. S., and Espelid, Ø., 2007. Using the EnKF for Assisted History Matching of a North Sea Reservoir Model. SPE 106184, Reservoir Simulation Symposium, Houston, TX, 26–28 February.

Falcone, G., Gosselin, O., Maire, F., Marrauld, J., and Zhakupov, M., 2004. Petroelastic modeling as key element of 4D history matching: A field example. SPE 90466, Annual Technical Conference and Exhibition, Houston, Texas, September, 26-29.

Fanchi, J. R., 1999. Predicting 4D seismic performance using an integrated flow model: SPE 56517, Ann. Tech. Conf.

Finsterle, S., 2007. iTOUGH2 User's Guide, Report LBNL-40040, Lawrence Berkeley National Laboratory, Berkeley, Calif. USA.

Fishman, G.S., 1996. Monte Carlo: Concepts, Algorithms and Applications. New York, Springer-Verlag.

Fletcher, R., 1987. Practical methods of optimisation. Wiley.

Fletcher, J., Seymour, G., Flynn, T., and Burchell, M., 2005. Formation pressure testing while drilling for deepwater field development, SPE 96321. In SPE Offshore Europe Conference, Aberdeen, UK.

Floricich, M., 2006. An engineering-consistent approach for pressure and saturation estimation from time-lapse seismic data, PhD thesis. Institute of Petroleum Engineering. Heriot Watt University.

Floris, F., Bush, M., Cuypers, M., Roggero, F., and Syversveen, A. R., 2001. Methods for quantifying the uncertainty of production forecasts: a comparative study, Petroleum Geoscience 7(SUPP), 87-96.

References

Friedmann, F., Chawathė, A., and Larue, D. K., 2003. Assessing Uncertainty in Channelized Reservoir Using Experimental Designs. SPE Reservoir Evaluation & Engineering, August, pp264-274.

Fogel, L. J., Owens A. J., and Walsh, M. J., 1966. Artificial Intelligence Through Simulated Evolution, John Wiley, New York.

Fornel, A. M., Mezghani, M., and Langlais, V., 2007. Using production data and time domain seismic attributes for history matching. Geological Society, London, Special Publications 2007, v. 284, p. 147-159 . doi: 10.1144/SP284.10.

Foster, G., Dave, G., 2008. Lessons Learnt from over 20 Years of 4D Deployment. Presented in Indian oil and gas technical conference and exhibition held in Mumbai, India, 4-6 March 2008.

Fujita, K., and Kounoe, Y., 2005. High-Order Polynomial Response Surface with Optimal Selection of Interaction Terms Department of Mechanical Engineering, Osaka University, Suita, Osaka 565-0871, Japan.

Furre, A., K., Andersen, M., Smalø Moen, A., Tønnessen, R. K., 2009. Deriving effects of pressure depletion on elastic framework moduli from sonic logs. Geophysical Prospecting Volume 57, Issue 3, pages 427-437, May 2009, DOI:10.1111/j.1365-2478.2008.00744.x.

Gao, G., and Reynolds, A. C., 2004. An improved implementation of the LBFGS algorithm for automatic history matching, SPE 90058, SPE Annual Technical Conference and Exhibition.

Gassmann, F., 1951. Uber die elastizitat poroser medien. Vier. Der Natur. Gesellschaft, (96), pp. 1-23.

Gavalas, G.R., Shah, P.C., and Seinfeld, J. H., 1976. Reservoir History Matching by Bayesian Estimation. Soc. Petrol. Eng. J., 16(6), 337-350.

Glimm, J., Grove, J. W., Kang, Y., Lee, T., Li, X., Sharp, D. H., Yu, Y., Ye, K., and Zhao, M., 2004. Errors in Numerical Solutions of Spherically Symmetric Shock Physics Problems. Contemporary Mathematics. (submitted) University at Stony Brook Preprint Number SB AMS-04-03, Los Alamos National Laboratory number LA-UR-04-0713.

Goldberg, D., 1989. Genetic Algorithms in Search, Optimization, and Machine Learning. Addison-Wesley.

Gosselin, O., Aanonsen, S., Asvatsmark, A., Cominelli, A., Gonard, R., Kolasinski, M., Ferdinandi, F., Kovaic, L., and Neylon, K., 2003. History Matching Using Time-Lapse Seismic (HUTS) (SPE84464). Annual Technical Conference and Exhibition, Denver, Colorado.

Gosselin, O., Van den Berg, S., Comineli, A., 2001. Integrated history matching of production and seismic data. SPE 71599, SPE Annual Technical Conference and Exhibition held in New Orleans, Louisiana, 30 September-3 October 2001.

Gouveia, W. P., David, H., Solberg, J. A., and Lauritzen, M., 2004. Jotun 4D Characterization of fluid contact movement from time-lapse seismic and production logging tool data The Leading Edge, November 2004, v. 23, no. 11, p. 1187-1194, Doi: 10.1190/1.1825941.

Gu, Y., and Oliver, D.S., 2005a. The ensemble Kalman filter for continuous updating of reservoir simulation models. J. Energy Resour. Technol. 128 (1).

Gu, Y., Oliver, D.S., 2005b. History matching of the PUNQ-S3 reservoir model: using the ensemble Kalman filter. SPE J. 10 (2).

Guerin, G., He, W., Anderson, R. N., and Xu, L., 2000. Optimisation of reservoir simulation and Petrophysical Characterization in 4D seismic. OTC 12102, Offshore Technology Conference, Houston, Texas, 1-4 May 2000.

Guyaguler, B., Horne, R. N., Rogers, L., and Rosenzweig, J. J., 2000. Optimization of Well Placement in a Gulf of Mexico Water flooding Project. SPE 63221, Annual Technical Conference and Exhibition, Dallas, Texas, 1-4October.

Guyaguler, B., Horne, R. N., Rogers, L., and Rosenzweig, J. J., 2002. Optimization of Well Placement in a Gulf of Mexico Water flooding Project. SPE Reservoir Evaluation & Engineering, June, pp 229-236.

Hadamard, J., 1902. Sur les problems aux derivees partielles et leur signification physique. Princeton University Bulletin, 49-52, 1902.

Haldorsen, H., Damsleth, E., 1988. Review of the nature of reservoirs. In: Edwards, S., King, P. (Eds.), Mathematics in Oil Production. Clarendon Press, Oxford, pp. 109-209.

Han, D., 1986. Effects of porosity and clay content on acoustic properties of sandstones and unconsolidated sediments, PhD dissertation, Stanford University, pp 210.

Hashin, Z., and Shtrikman, S., 1963. A variational approach to the elastic behaviour of multiphase materials. J. Mech. Phys. Solids, 11, 127-140.

Haugen, V., Naevdal, G., Natvik, L. J., Evensen, G., Berg, A. M., and Flornes, K. M., 2008. History matching using the ensemble Kalman filter on a North Sea field case, SPE Journal, 13(4), 382-391.

Hawkins, K., Howe, S., Hollingworth, S., Conroy, G., Ben-Brahim, L., Tindle, C., Taylor, N., Joffroy, G., and Onaisi, A., 2007. Production-induced stresses from time-lapse time shifts: A geomechanics case study from Franklin and Elgin fields. The Leading Edge, 26:655.

Helgerud, M., B., and Miller, A., C., 2011. 4D in the deepwater Gulf of Mexico Hoover, Madison and Marshall fields. The Leading Edge; September 2011, v. 30, no. 9, p. 1008-1018, DOI:10.1190/1.3640524.

Herrera, F., Lozano, M., and Verdegay J.L., 1995. Fuzzy connective based crossover operators to model genetic algorithms population diversity. Tech. Rep. No. DECSAI-95110, University of Granada, 18071 Granada, Spain.

Higdon D., Lee, H., and Bi, X., 2002. A Bayesian Approach to Characterizing Uncertainty in Inverse Problems Using Coarse and Fine Scale Information. IEEE Transactions in Signal Processing. 50, 389-399.

Hoffman, B. T., and Caers, J., 2003. Geostatistical history matching using a regional probability perturbation method, SPE 84409 Annual Technical Conference and Exhibition, Denver, USA, 5-8 October.

References

Holland, J. H., 1975. Adaptation in Natural and Artificial Systems, Univ. of Mich. Press, Ann Arbor, Mich.

Hooke, R, and Jeeves, T. A., 1961. Direct search solution of numerical and statistical problems. J. Assoc. Comput. Mach., 8: 212-219. DOI: 10.1023/A:1013760716801.

Hu, L.Y., 2000a. Gradual deformation and iterative calibration of Gaussian-related stochastic models. Math. Geol., 32, 87-108.

Hu, L.Y., 2000b. Gradual deformation of non-Gaussian stochastic simulations. In Geostatistics 2000 Cape Town, W.J. Kleingeld and O.G. Krige (eds.).

Huang, X. R., 2001. Integrating time-lapse seismic with production data: A tool for reservoir engineering. The Leading Edge, (20), pp. 1148–1153.

Huang, X., Meister, L. and Workman, R., 1997. Reservoir Characterisation by Integration of Time-Lapse Seismic and Production Data (SPE38695). Annual Technical conference and Exhibition, San Antonio, Texas.

Jackson, D. D., 1972. Interpretation of inaccurate, insufficient, and inconsistent data, Geophys. J. Roy. Astr. oc., 28, 97-109.

Jacquard, P., and Jain, C., 1965. Permeability Distribution from Field Pressure Data. Soc. Petrol. Eng. J., 5(4), 281-294, 1965.

Jahns, H.O., 1966. A Rapid Method for Obtaining a Two-Dimensional Reservoir Description from Well Pressure Response Data, Soc. Petrol. Eng. J., 6(12), 315-327, 1966.

Jin, L., Alpak, F. O., and Hoek, P., Carlos Pirmez, C., Fehintola, T., Tendo, F., and Olaniyan, E., 2011. A Comparison of Stochastic Data-Integration Algorithms for the Joint History Matching of Production and Time-Lapse Seismic Data. SPE 146418. Annual Technical Conference and Exhibition, Denver, Colorado, USA, 30 October-2 November.

Jin, L., Stoffa, P. L., and Sen, M. K., 2009. Stochastic Inversion for Reservoir Properties Using Parallel Learning-Based VFSA and Pilot Point Parameterization. SPE 118818, SPE Reservoir Simulation Symposium, The Woodlands, Texas, USA, 2-4 February.

Jones D., Schonlau M., and Welch W., 1998. Efficient Global Optimization of Expensive Black Box Functions. Journal of Global Optimization, Vol. 13, pp. 455-492.

Jourdan, A., and Zabalza-Mezghani, I., 2004. Response Surface design for scenario management and uncertainty qualification in reservoir production. Math. Geol. 36(8), 965-985.

Kabir, C. S., Young, N. J., 2004. Handling Production-Data Uncertainty in History Matching: The Meren Reservoir Case Study. SPE Reservoir Evaluation & Engineering, 87823-PA, Volume 7, Number 2, Pages123-131.

Kalman, R. A, 1960. New Approach to Linear Filtering and Prediction Problems. Trans. ASME, J. Basic Eng., 82D, 35-45.

References

Kazemi, A., and Stephen, K. D., 2008. Improved Reservoir Description of the Nelson Field Via Seismic History Matching. SPE Europec/EAGE Annual Conference and Exhibition, Rome, Italy, 9-12 June.

Kazemi, A., and Stephen, K. D., 2009. Automatic Seismic and Production History Matching in Nelson Using Different Updating Schemes. presented at the 71st EAGE Conference and Exhibition, Amsterdam, The Netherlands, 8-11 June.

Kim, Y., Srinivasan, S., and Bryant, S. L., 2008. Efficient Region Decomposition for Parallel Simulation Accounting for Uncertainty in the Reservoir Model. SPE Annual Technical Conference and Exhibition, 21-24 September 2008, Denver, Colorado, USA.

Kirkpatrick, S., Gelatt, C. D. Jr., and Vecchi, M. P., 1983. Optimization by simulated annealing. Science 220, 671–680.

King P. R., Muggeridge A. H., and Price W. G., 1993. Renormalization calculations of immiscible flow, Transport in porous media, Vol. 12, p237-260.

Kleijnen, J.P. C., and Van Groenendaal, W.J. H., 1995. Two-stage versus sequential sample-size determination in regression analysis of simulation experiments. American Journal of Mathematical and Management Sciences, 15, pp. 83-115.

Kleijnen, J. P. C., 2005. Statistical testing of optimality conditions in multi-response simulation-based optimization. Seminar at the Statistics Department of Stanford University,26 July 2005.

Knight, R., Dvorkin, J., and Nur, A., 1996. Acoustic Signatures of Partial Saturation. Geophysics, 63, 1, 132-138.

Kostuchenko, S.V., and Bordzilovsky, A.S., 2008. Principle of Iteration Composition of Sector Models for Full Field Reservoir Simulation (Russian), SPE Russian Oil and Gas Technical Conference and Exhibition, 28-30 October 2008, Moscow, Russia

Krief, M., Garat, J., Stellingwerf, J., and Venter, J., 1990. A petrophysical interpretation using the velocities of P and S waves (full waveform sonic): The Log Analyst, 31, 355-369.

Kruijsdijk, C.P.J.W. van, 2001. Integrating reservoir engineering into Geosciences, Joule II– Reservoir Engineering Project, JOU2-0182, Delft University of Technology and TNO Institute of Applied Geoscience.

Kuster, G. T, and Toksoz, M. N., 1974. Velocity and attenuation of seismic waves in two-phase media: Pt. 1. Theoretical formulation. Geophysics, 39:587-606.

Kyte J.R., and Berry D.W., 1975. New pseudo functions to control numerical dispersion. SPEJ, August 1975, 269-275.

Lacombe C., Campbell, S., White, S., 2011. Improvements in 4D Seismic Processing - Foinaven 4 Years On. 73rd EAGE Conference & Exhibition incorporating SPE EUROPEC, Vienna, Austria, 23-26 May.

Lancaster, S., and Whitcombe, D., 2000. Fast-Track Coloured Inversion. In SEG International Exposition and Annual Meeting, Calgary, Canada

References

Landa, J. L., and Güyagüler, B. A., 2003. Methodology for History Matching and the Assessment of Uncertainty Associated with Flow Prediction. SPE 84465. Annual Technical Conference and Exhibition, Denver Colorado, USA, 5-8 October.

Landa, J. L. and Horne, R. N., 1997. A procedure to integrate well test data, reservoir performance history and 4-D seismic information into a reservoir description, SPE 38653, Annual Technical Conference and Exhibition.

Landrø, M., 2001. Discrimination between pressure and fluid saturation changes from time-lapseseismic data: Geophysics, 66, 836.844.

Landrø, M., Solheim, O. A., Hilde, E., Ekren, B.O., and Strønen, L. K., 1999. The Gullfaks 4D Seismic Study. Petroleum Geoscience, v. 5, pp. 213-226.

Lantuéjoul, C., 1997. Iterative algorithms for conditional simulation. In: Baffi, E.Y., Schofield, N.A. (Eds.), Geostatistics Wollongong96. Kluver Academic Publishers, pp. 27-40.

Le Ravalec-Dupin, M., Nœtinger, B., Hu L. Y., and Blanc,G., 2001. Conditioning to dynamic data: an improved zonation approach. Petroleum Geoscience; March 2001; v. 7; no. S; p. S9-S16; DOI: 10.1144/petgeo.7.S.S9.

Le Ravalec-Dupin, M., 2005. Inverse stochastic modelling of flow in porous media Application to reservoir characterization. Editions Technip.

Le Ravalec, M., Hu, L.-Y., 2007. Combining the Pilot Point and Gradual Deformation Methods for Calibrating Permeability Models to Dynamic Data. Oil & Gas Science and Technology, Rev. IFP, Vol. 62 (2007), No. 2, pp. 169-180.

Leach, H., Herbert, N., Los, A., and Smith, R., 1999. The Schiehallion Development. In Conference Petroleum Geology of Northwest Europe, London, United Kingdom. The Geological Society.

Leeuwenburgh, O., Brouwer, J., Trani, M., Peters, E., 2008. The Value of Seismic Data in Production History Matching.70th EAGE Conference & Exhibition, EAGE/EUROPEC, Rome, Italy.

Leeuwenburgh, O., Brouwer, J., Trani, M., 2010. Ensemble-based conditioning of reservoir models to seismic data. Computational Geosciences (16 September 2010), pp. 1-20-20. doi:10.1007/s10596-010-9209-z.

Leitão, H. C., and Schiozer, D. J., 1999. A New Automated History Matching Algorithm improved by Parallel Computing. SPE 53977, Latin American and Caribbean Petroleum Engineering Conference, Caracas, Venezuela, 21-23 April.

Levenberg, K., 1944. A method for the solution of certain nonlinear problems in least squares, Quart. Appl. Math., 2, 164-168.

Levy, G., 2002. An introduction to quasi-random numbers. Numerical Algorithms Group, published in Financial Engineering News, February.

Li, G., and Reynolds, A. C., 2009. Iterative ensemble Kalman Filters for data assimilation, SPE Journal, 14(3), 496-505.

References

Li, H., Ph.D., 2008. Hierarchic modelling and history matching of multi-scale flow barriers in channelized reservoirs. Stanford University, PhD thesis. 156 pages, AAT 3332867.

Li, B. and Friedman, F., 2005. Novel multiple resolution design of experiment/response surface methodology for uncertainty analysis of reservoir simulation forecasts. SPE Reservoir Simulation Symposium, Woodlands, Texas, U.S.A., 31 Jan. -2 Feb. 2005.

Li, R., Reynolds, A. C., and Oliver, D. S., 2003. History matching of three-phase flow production data, SPE Journal, 8(4), 328-340.

Li, S., and Petzold, L., 2004. Adjoint sensitivity analysis for time-dependent partial differential equations with adaptive mesh refinement. Journal of Computational Physics.

Lia, O., More, H., Tjelmeland, H., Holden, L., and Egeland, T., 1997. Uncertainties in reservoir production forecasts. American Association of Petroleum Geologists Bulletin, 81, 775-801.

Lines, L. R., and Treitel, S., 1984. A review of least-squares inversion and its application to geophysical problems: Geophysical Prospecting, 32,159-186.

Litvak M., Christie M., Johnson, D., Colbert, J., Sambride, M, 2005. Uncertainty Estimation in Production Predictions Constrained by Production History and Time-Lapse Seismic in a GOM Oil Field. SPE Reservoir Simulation Symposiums, Texas, 31 Jan-2 Feb 2005.

Liu, N., Oliver, D. S., 2005. Critical evaluation of the ensemble Kalman filter on history matching of geologic facies, SPE 92867.Reservoir Simulation Symposium.

Lorenc, A, 2009. The potential of ensemble Kalman filter for NWP- a comparison with 4D-var, Quarterly Journal of the Royal Meteorological Society, 14(3), 393(412).

Lumley, D. E., 2001. Time-lapse seismic reservoir monitoring. Geophysics, 66 50-53.

Lumley, D., Behrens, R., and Wang, Z., 1997. Assessing the technical risk of a 4D seismic project: The Leading Edge, 16, no. 9, 1287-1292.

Lumley, D., 2004. Business and Technology Challenges for 4D Seismic Reservoir Monitoring. The Leading Edge, 23(11):1166-1168.

Lumley, D. E., Nur, A., Strandenes, S., Dvorkin, J., and Packwood, J., 1994. Seismic monitoring of oil production: A feasibility study. SEG Expanded Abstracts.

Lumley, D., 2009. 4D Seismic Monitoring of Subsurface Fluid Flow. Telus Convention Centre, Calgary, November 2.

Lumley, D.E., Meadows, M.A., Cole, S.P. and Adams, D. C., 2003. Estimation of Reservoir Pressure and Saturations by Crossplot Inversion of 4D Seismic Attributes, 65th Mtg.: Eur. Assn. Geosci. Eng., A06.

Lygren, M., Dahl, G. V., Fagervik, K., Nickel, M., Borgos, H. G., Skov, T., Hetlid, A., Berge G. and Sønneland, L., 2002. Use of reservoir flow models in quantitative 4D analysis. EAGE 64th Conference & Exhibition, Florence, Italy, 27-30 May 2002.

References

MacBeth, C., 1995. How can anisotropy be used for reservoir characterisiation? First Break, 13(1), pp.31-37.

MacBeth, C., and Stephen, K., 2008. Seismic scale saturation relations in turbiditer reservoirs undergoing waterflood. European Association of Geoscientists & Engineers, Geophysical Prospecting, 56, 693-714.

MacBeth, C., 2004. A Classification for the Pressure-Sensitivity Properties of a Sandstone Rock Frame. Geophysics, 69(2):497-510.

MacBeth, C., Reid, F., McInally, A., Garnham, J., and Redondo-Lopez, T., 2002. 4D seismic signatures of OWC movement of the Nelson field- modelling and interpretation. 72nd Internat. Mtg., Soc. Explor. Geophys., Salt Lake City, USA.

Macdonald, C. J., Tosdevin, M., Tothill M. D., 2004. Report on the Schiehallion Full Field VIP Model FFM2003.

Marion, D., Mukerji, T., and Mavko, G., 1994. Scale effects on velocity dispersion: From ray to effective medium theories in stratified media: Geophysics, 59, no. 10, 1613-1619.

Makhlouf, E.M., Chen, W.H, Wasserman, M.L., and Seinfeld, J.H., 1993. A General History Matching Algorithm for Three-Phase, Three-Dimensional Petroleum Reservoirs. SPE Advanced Technology Series, 1(2), 83-92.

Manzocchi, T., Walsh, J. J., Nell, P., and Yielding, G., 1999. Fault transmissibility multipliers for flow simulation models. Petroleum Geoscience, 5, 53-63.

Marquardt, D.W., 1963. An algorithm for least squares estimation of nonlinear parameters, SIAM J. Appl. Math., 11, 431–441.

Marsh, M., 2004. The use of 4D seismic in reservoir management. EAGE/DLP course notes. February 2004.

de Marsily, G., Lavedan, G., Boucher, M., and Fasanino, G., 1984. Interpretation of Interference Tests in a Well Field Using Geostatistical Techniques to Fit the Permeability Distribution in a Reservoir Model. In Geostatistics for Natural Resources Characterization, Part 2, 831-849, Kluwer Academic Publishers.

Martínez del Rio, C., Silva, A., Medel, R., and Hourdequin, M., 1996. Seed dispersers as disease vectors: bird transmission of mistletoe seeds to host plants. Ecology 77: 912-921.

Maschio, C., and Schiozer, D. J., 2005. Assisted History Matching Using Streamline Simulation. Petroleum Science and Technology 23(7), pp. 761-774.

Maschio, C., and Schiozer, D. J., 2008. A new Methodology for Assisted History Matching Using Independent Objective Functions. Petroleum Science and Technology, 26(9), 1047-1062. Doi: 10.1080/10916460701208389.

Mavko, G., and Nolen-Hoeksema, R., 1994. Estimating seismic velocities in partially saturated rocks. Geophysics, 59, 252-258.

Mavko, G., Mukerji, T., and Dvorkin, J., 1998. The Rock Physics Handbook: Tools for Seismic Analysis in Porous Media, Cambridge University Press, Cambridge, pp 329.

McInally, A.T., Redondo-López, T., Garnham, J., Kunka, J., Brooks, A. D., Stenstrup Hansen, L., Barclay, F., and Davies, D., 2003. Optimising 4D fluid imaging. Petroleum Geoscience, 9(1), pp. 91-101.

McKinnon, K.I.M, 1999. Convergence of the nelder-mead simplex method to a non-stationary point. SIAM J Optimization, 9:148-158.

Meadows, M., 2001. Enhancement to Landrø's Method for Separating Time-Lapse Pressure and Saturation Changes. In SEG International Exposition and Annual Meeting, San Antonio, Texas.

Menezes, C., and Gosselin, O., 2006. From logs scale to reservoir scale: Upscaling of the petro-elastic model. SPE 100233,SPE/Europec Annual Conference and Exhibition, Vienna, Austria, 12-15 June 2006.

Mezghani, M., Langlais, V., Lucet, N., and Fornel, A., 2004. Quantitative Use of 4D Seismic Data for Geological Modelling and Reservoir Characterization Through History Matching. In EAGE Conference and Technical Exhibition, Paris, France.

Mindlin, R. D., 1949. Compliance of elastic bodies in contact. J. Appl. Mech., 16, 259-268.

Miranda, M., 2007. Fault-induced bends on Schiehallion's North Channel. Presented in DEVEX 15, 16 May 2007.

Mavko, G., and Mukerji, T., 1998. Bounds on Low Frequency Seismic Velocities in Partially Saturated Rocks. Geophysics, 63, 3, 918-924.

Mohamed, L., Christie, M. A., and Demyanov, V., 2010. Comparison of stochastic sampling algorithms for uncertainty quantification. SPE Journal, vol. 15, no. 1, pp. 31–38, 2010.

Montgomery, D. C., 2000. Design and Analysis of Experiments, 5th Edition, John and Wiley Sons, Inc., New York City.

Morrow, N. R., and Melrose, J. C., 1991. Application of Capillary Pressure Measurements to the Determination of Connate Water Saturation, Interfacial Phenomena in Petroleum Recovery, N.R. Morrow (ed.), Marcel Dekker, New York City (1991) 257-287.

Mosegaard, K., Vestergaard, P.D., 1991. A simulated annealing approach to seismic model optimization with sparse prior information. Geophys. Prospect. 39, 599-611.

Mosegaard, K., and Sambridge, M., 2002. Monte Carlo analysis of inverse problems, Inverse Probl., 18, R29-R54.

Mosegaard, K., and Tarantola, A., 2002. International Handbook of Earthquake & Engineering Seismology, chapter Probabilistic Approach to Inverse Problems, pages 237-265. Academic Press, 2002.

Murphy, W., Reischer, A., and Hsu, K., 1993. Modulus Decomposition of Compressional and Shear Velocities in Sand Bodie. Geophysics, 58, 227-239.

Mukerji, T., Mavko, G., Mujica, D., and Lucet, N., 1995. Rock physics Laboratory, Dept. of Geophysics, Stanford University, Stanford, CA 94305 Scale-

dependent seismic velocity in heterogeneous media. Geophysics 60, 1222(1995), doi:10.1190/1.1443851.

Myers, R. H., 1999. Response Surface Methodology -Current Status and Future Directions, Journal of Quality Technology 31, 30-44.

Myers, R. H., and Montgomery, D.C., 2002. Response Surface Methodology. Wiley, NewYork.

Nævdal, G., Mannseth, T., and Vefring, E. H., 2002. Near-well reservoir monitoring through ensemble Kalman filter. SPE 75235. SPE/DOE Improved Oil Recovery Symposium.

Narayanan, K., 1999. Applications for Response Surfaces in Reservoir Engineering. Thesis, University of Texas at Austin, May 1999.

Nelder, J. A., and Mead, R., 1965. A simplex method for function minimization. Computer Journal, 7(4), 308-313.

Nicotra G., Godi A., Cominelli A., Christie, M,. 2005. Production Data and Uncertainty Quantification: A Real Case Study. SPE 93280, Proceedings of the SPE Reservoir Simulation Symposium, Houston, Texas, USA, 31 Jan.-2 Feb. 2005.

Nicotra, G., Rotondi, M., Godi, A., and Christie, M., 2006. Uncertainty Quantification in Producing Fields using the Neighbourhood Algorithm. 10th European Conference on the Mathematics of Oi Recovery, Amsterdam, The Netherlands, 4-7 September 2006.

Neumaier, A., 1998. Solving ill-conditioned and singular linear systems: A tutorial on regularization, SIAM Rev., 40(3), 636-666, 1998.

von Neumann, J., 1951. The General and Logical Theory of Automata. in: L.A. Jeffress (ed.), Cerebral Mechanisms in Behaviour: The Hixon Symposium, New York: John Wiley, pp. 1-31.

Nes, O. M., Holt, R. M., and Fjær, E., 2000. The reliability of core data as input to seismic reservoir monitoring studies, SPE 65180, SPE European Petroleum Conference, Paris, France, October 24-25.

Niederreiter, H., 1988. Low-Discrepancy and Low-Dispersion Sequences. Journal of Number Theory, 30, 51-70.

O'Sullivan, A., Christie, M., 2006. Simulation Error Models for Improved Reservoir Prediction. Reliability Engineering and System Safety, Vol. 91, Issues 10-11, pp 1382-1389, Nov.

Oldenburg, D.W., Scheuer, T., Levy, S., 1983, Recovery of the acoustic impedance from reflection seismograms: Geophysics, 48, 1318-1337.

Oliver, D. S., 1996. Multiple Realizations of the Permeability Field from Well Test Data. SPEJ 1 (2): 145-154. SPE-27970-PA.

Omre, H., and Lødøen, O., 2004. Improved production forecasts and history matching using approximate fluid-flow simulators, SPE Journal, September 2004, 339-351.

References

Omre, H., and Tjelmeland, H., 1996. Petroleum geostatistics. Technical Re-ports, s-8. Department of Mathematical Sciences, Norwegian University of Science and Technology, Trondheim, Norway.

Ong, Y. S, Keane, A. J., Nair, P. B., 2002. Surrogate-Assisted Co-evolutionary Search. 9th International Conference on Neural Information Processing, Special Session on Trends in Global Optimization, pp. 2195-2199.

Osterloh, W. T., 2008. Use of Multiple-Response Optimization to Assist Reservoir Simulation Probabilistic Forecasting and History Matching. SPE 116196, Annual Technical Conference and Exhibition, Denver, Colorado, 21-24 September.

Ouair, Y., Strønen, L. K., 2006. Value Creation from 4D Seismic at the Gullfaks Field: Achievements and New Challenges. 76th Meeting, Society of Exploration Engineers.

Paige, C.C., 1985. The general model and the generalized singular value decomposition. Lin. Algeb. Applicat. 70, 269 -284.

Parr, R., Cowper, D., and Michener, B., 1999. The Search for Mountains of Oil: Exploration Activity in the Atlantic Margin, West of Shetland (SPE56897). In SPE Offshore Europe Conference, Aberdeen, Scotland.

Peake, W. T., Abadah, M., Skander, L., 2005. Title Uncertainty Assessment using Experimental Design: Minagish Oolite Reservoir. SPE 91820-MS , Reservoir Simulation Symposium, 31 January-2 February 2005, The Woodlands, Texas., DOI10.2118/91820-MS.

Peng, C.Y., and Gupta, R., 2004. Experimental Design and Analysis Methods in Multiple Deterministic Modelling for Quantifying Hydrocarbon In-Place Probability Distribution Curve. Paper SPE 87002, Asia Pacific Conference on Integrated Modelling and for Asset Management, Kuala Lumpur, Malaysia, 29-30 March.

Phan, V., and Horne, R. N., 2002. Fluvial channel parameter estimation constrained to static, production, and 4D sismic data. In: SPE Annual Technical Conference and Exhibition. San Antonio, Texas, USA.

Pickup, G. E., Ringrose, P. S., and Sharif, A., 2000, Steady-state upscaling: From lamina-scale to full field model, Soc. Petrol. Engr. Jour. 5(2), 208–217.

Pierret, S., 2005. Multi-objective and Multi-Disciplinary Optimization of Three dimensional Turbo-machinery Blades. 6th World Congresses of Structural and Multidisciplinary Optimization Rio de Janeiro, 30 May-03 June 2005, Brazil.

Portellaand, R. C. M. and Prais, F., 1999. Use of Automatic History Matching and Geostatistical Simulation to Improve Production Forecast. SPE 53976, Latin American and Caribbean Petroleum Engineering Conference. Caracas, Venezuela, 21-23 April.

Press, W. H., Teukolsky, S. A., Vetterling, W. T., and Flannery, B. P., 1992, 1998, 2002, 2007. Numerical Recipes in FORTRAN, the Art of Scientific Computing, Cambridge University Press, Cambridge.

References

Potter, M., 1997. The Design and Analysis of a Computational Model of Co-operative Co-evolution. Ph.D. thesis, George Mason University, Fairfax, VA.

Potter, M., Jong K. D., 1995. Evolving neural networks with collaborative species. In Proc. of Summer Computer Simulation Conference, pp. 340-345.

Potts, J. C., Giddens, T. D., and Yadav, S.B., 1994. The development and evaluation of an improved genetic algorithm based on migration and artificial selection. IEEE Trans. Syst. Man Cybern., Vol. 24, No. 1, pp. 73-86.

Queipo, N.V, Pintos S., Rincon, N., Contreras, N., and Colmenares, J., 2000. Surrogate Modelling Based Optimization for the Integration of Static and Dynamic Data Into a Reservoir Description. SPE 63065, Annual Technical Conference and an Exhibition, Dallas, Texas, 1-4 October.

Ramammorthy, R., Murphy, W.F., and Coll. C., 1995. Total porosity estimation in shaly sands from shear modulus. SPWLA 36th Annual Logging Symposium Transactions.

Rao, C. R., 1973. Linear Statistical Inference and its Applications. Wiley, New York.

Redondo-Lopez, T., and McInally, A., 2002. Quantitative Integration of 4D Seismic for Field Development. AAPG Annual Meeting, March 10-13, Houston, Texas.

Reuss, A., 1929. Berechnung der fliessgrense von mishkristallen Z. Angew. Math. Mech. (9), pp. 49-58.

Reynolds, A, C., He, N., Chu, L., and Oliver, D. S., 1996. Reparameterization techniques for generating reservoir descriptions conditioned to variograms and well-test pressure data. Soc. Petrol. Eng. J., 1(4):413-426.

Reynolds A. P., Abdollahzadehy, A., Corne D. W., Christiey, M., Daviesz, B., and Williamsz, G., 2011. A Parallel BOA-PSO Hybrid Algorithm for History Matching, IEEE 2011.

Rickett, J., and Lumley, D., E., 2001. Cross-equalization data processing for time-lapse seismic reservoir monitoring: A case study from Gulf of Mexico. Geophysics, 66(4), 1015- 1025, 2001.

Roggero, F., 1997. Direct Selection of Stochastic Model Realizations Constrained to Historical Data. SPE38731. Presented at the SPE ATCE, San Antonio, Texas, 5-8 October, 1997.

Roggero, F., and Hu, L. Y., 1998. Gradual Deformation of Continuous Geostatistical Models for History Matching. SPE 49004, Annual Technical Conference and Exhibition. New Orleans, Louisiana, 27-30 September 1998.

Roggero, F., Ding, D. Y., Berthet, P., Lerat, O., Cap, J. and Schreiber, P.E., 2007. Matching of Production History and 4D Seismic Data-Application to the Girassol Field, Offshore Angola. SPE 109929, Annual Technical Conference and Exhibition held in Anaheim, California, U.S.A., 11-14 November.

Romero, C. E., Carter, J. N., Gringarten, A. C., and Zimmerman, R. W., 2000. A modified genetic algorithm for reservoir characterisation, SPE 64765, International Oil and Gas Conference and Exhibition in China.

References

Ross, C., Cunningham, G., and Weber, D., 1996. Inside the Cross Equalization Black Box. The Leading Edge, 15(11):1233-1240.

Russell, B. H., 1988, Introduction to seismic inversion methods: Soc. Explor. Geophys., Course note series, v. 2.

Sablok, R., and Aziz, K., 2005. Upscaling and Discretization Errors in Reservoir Simulation. Paper SPE 93372 presented at the Reservoir Simulation Symposium, Houston, Texas, 31 January- 2 February. DOI: 10.2118/93372-MS.

Sacks, J., Welch, W. J., Mitchell, T. J., and Wynn H. P., 1989. Design and analysis of computer experiments. Statistical Science, 4(4):409-435.

Sacks, J., Schiller, S. B., and Welch, J., 1989a. Designs for computer experiments. Techno- metrics, 31(1), 41-47.

Sacks, J., Welch, W. J., Mitchell, T. J., and Wynn, H. P., 1989b. Design and analysis of computer experiments. Statistical Science, 4(4), 409-435.

Sambridge, M., and Drijkoningen, G. G., 1992. Genetic algorithms in seismic waveform inversion, Geophys. J. Int., 109, 323-342.

Sambridge, M, 1999a. Geophysical Inversion with a Neighbourhood Algorithm-I. Searching a Parameter Space. Geophysical Journal International, 138(2):479–494.

Sambridge, M., 1999b. Geophysical Inversion with a Neighbourhood Algorithm-II. Appraisal the Ensemble. Geophysical Journal International, 138(2):727-746.

Sambridge, M., 2001. Finding Acceptable Models in Nonlinear Inverse Problems Using a Neighbourhood Algorithm. Inverse Problems, 17, 387-403.

Sambridge M., Mosegaard K., 2002. Monte Carlo Methods in Geophysical Inverse Problems. Reviews of Geophysics, 40, 3.

Sarma, P., Durlofsky L. J., Aziz, K., 2006. Computational Techniques for Closed-Loop Reservoir Modelling with Application to a Realistic Reservoir, 10th European Conference on the Mathematics of Oil Recovery, Amsterdam, Netherlands.

Saxby, I., 2001. Impact of 4-D seismic reservoir monitoring in Schiehallion field, UKCS. AAPG Annual Meeting, Denver, Colorado.

Sedighi, F., and Stephen, K. D., 2009. Faster Convergence in Seismic History Matching by Efficient Parameter Searching. SPE-121210-MS, SPE Europec/EAGE Annual Conference and Exhibition, Amsterdam, 9-11 June.

Sedighi, F. and Stephen, K.D., 2010. "Improved Convergence in Seismic History Matching Combining Experimental Design with a Divide and Conquer Approach". 72nd EAGE Conference & Exhibition incorporating SPE EUROPEC 2010 held in Barcelona, 14-17 June, 2010.

Scheidt, C., and Caers., J., 2009. Representing spatial uncertainty using distances and kernels. Mathematical Geosciences, 41:397-419.

Schiozer, D. J., 1999. Use of Reservoir Simulation, Parallel Computing and Optimization Techniques to Accelerate History Matching and Reservoir

Management Decisions, SPE 53979, SPE Latin American and Caribbean Petroleum Engineering Conference, Caracas, Venezuela, 21-23 April.

Sen, M.K., Stoffa, P.L., 1991. Nonlinear one-dimensional seismic waveform inversion using simulated annealing. Geophysics, 56, 1624–1638.

Sen, M. K., Datta-Gupta, A., Stoffa, P. L., Lake, L. W., and Pope, G. A., 1992. Stochastic Reservoir Modelling Using Simulated Annealing and Genetic Algorithm. SPE 24754 Annual Tech.Conf., Washington, DC, October, 4-7.

Sen, M. K., and Stoffa, P. L., 1995. Global Optimization Methods in Geophysical Inversion, Adv. Explor. Geophys., vol. 4, Elsevier Sci., New York.

Sengupta, M., and Bachrach, R., 2007. Uncertainty in seismic-based pay volume estimation: Analysis using rock physics and Bayesian statistics. The Leading Edge, 26, 184-189, doi: 10.1190/1.2542449.

Sengupta, M., and Mavko, G., 1998. Reducing uncertainties in saturation scales using fluid flow models. SEG Technical Program Expanded Abstracts, 1998, 1012-1015.

Shapiro, S. A., and Troyan, V. N., 2002. Stress dependences of seismic velocities in porous and fractured rocks. EAGE 64th Conference, Florence, Paper B-35.

Shyeh, J.J., Johnston, D.H., Eastwood, J.E., Khan, M., and Stanley, L.R., 1999. Interpretation and modelling of time-lapse seismic data: Lena Field, Gulf of Mexico: SPE Paper 56731, 1999 SPE Ann. Tech. Conf., 12 p.

Simpson, T. W., Peplinski, J., Koch, P. N., and Allen J. K., 2001. Metamodels for computer based engineering design: Survey and recommendations. Engineering with Computers, 17(2):129-150.

Sirnivasan, S., and Bryant, S., 2004. Integrating Dynamic Data in Reservoir Models using a Parallel Computational Approach. SPE 89444.

Skinner, R.C., Jerauld, G.R., Bush, M.D., 2004. Simulation-Based EOR Evaluation of a North Sea Field. SPE Annual Technical Conference and Exhibition, 26-29 September 2004, Houston, Texas. DOI: 10.2118/90307-MS.

Skjervheim, J. A., Evensen, G., Aanonsen, S. I., Ruud, B. O., and Johansen, T. A., 2005. Incorporating 4D seismic data in reservoir simulation models using ensemble Kalman filter. SPE 95789.

Skjervheim, J. A., Evensen, G., Aanonsen, S. I. and Johansen, T. A., 2007. Incorporating 4D Seismic Data in Reservoir Simulation Model Using Ensemble Kalman Filter. SPEJ 12 (3), pp. 282-292.

Skopec, R. A., and Ross, C. P., 1994. Amplitude-versus-offset interpretation, scaling factors, and other challenges associated with acoustic data integration, paper SCA-9417, in SCA international symposium proceedings: Society of Professional Well Log Analysts, Society of Core Analysts, Chapter-at-Large, p. 183-196.

Slotte, P. A., and Smorgrav, E., 2008. Response Surface Methodology Approach for History Matching and uncertainty Assessment of Reservoir Simulation Models. SPE 113390 SPE Europec/EAGE Annual Conference and Exhibition, Rome, Italy, 9-12 June. Doi:10.2118/113390-MS.

Smith, T., Sondergled, C., and Rai, C., 2003. Gassmann Fluid Substitution: A Tutorial. Geophysics, 68(2):430-440.

Sobol, I. M., 1967. On the distribution of points in a cube and the approximate evaluation of integrals, USSR Comput. Math. Math. Phys., 7(4), 86-112.

Soldo, J.S., 2005. Quantitative Integration of Time-Lapse Seismic Information Using Multiple Model History Matching and Engineering Data, PhD thesis. Institute of Petroleum Engineering, Heriot Watt University.

Steinberg, D.M., and Hunter, W.G., 1984. Experimental design: Review and comment. Technometrics, 26, 71-130.

Stephen, K.D., 2006. Measuring the value of time-lapse (4D) seismic as part of history matching in the Schiehallion UKCS field. Presented at the 9th European on the Mathematics of Oil Recovery, Amsterdam, Netherlands, 4-7 September.

Stephen, K.D., 2007. Scale and process dependent model errors in seismic history matching. Oil and Gas Science and Technology-Revue de l'IFP 62 (2), pp. 123–136.

Stephen, K. D., Soldo, S., MacBeth, C., and Christie, M., 2006c. Multiple Model Seismic and Production History Matching: A Case Study. SPE94173-PA. SPE Journal, 11(4), 418-430

Stephen, K. D., and MacBeth, C., 2006. Inverting for the petro-elastic model via seismic history matching. Heriot-Watt University.

Stephen, K. D. and MacBeth, C., 2006. Reducing Reservoir Prediction Uncertainty Using Seismic History Matching (SPE 100295), SPE Europec/EAGE Annual Conference and Exhibition held in Vienna, Austria, 12-15 June 2006.

Stephen, K. D., and MacBeth, C., 2006b. Reducing Reservoir Prediction Uncertainty Using Seismic History Matching. SPE100295. SPE Europec/EAGE Annual Conference and Exhibition, Vienna, Austria, 12-15 June.

Stephen, K.D. and MacBeth, C., 2008. Reducing Reservoir Prediction Uncertainty by Updating a Stochastic Model Using Seismic History Matching. SPE 100295, SPE Reservoir Evaluation & Engineering 11(6), pp. 991-999.

Strebelle, S., 2000. Sequential Simulation Drawing Structure from Training Images, PhD thesis, Stanford University, CA (2000).

Subbey, S., Christie, M., and Sambridge, M., 2002. Uncertainty Reduction in Reservoir Modelling. In Chen, Z. and Ewing, R. (editors), Fluid Flow and Transport in Porous Media: Mathematical and Numerical Treatment, Volume 295 of Contemporary Mathematics, pp. 1-10. American Mathematical Society, Providence, Rhode Island.

Suzuki, S., and Caers, J., 2006. History Matching With an Uncertain Geological Scenario. SPE 102154, Annual Technical Conference and Exhibition, San Antonio, Texas, 24-27 September.

Tarantola, A., and Valette, B., 1982. Inverse Problems Quest for Information. Journal of Geophysics, 50(2):159-170.

Tarantola, A., 1984, Inversion of seismic reflection data in the acoustic approximation: GEOPHYSICS, 49, 1259-1256.

Tarantola, A., 1987. Inverse Problem Theory- Methods for Data Fitting and Model Parameter Estimation. Elsevier Science Publishers, Amsterdam 1987.

Tavassoli, Z., Carter, J .N., and King, P. R., 2004. Errors in history matching. SPE Journal (SPE86883-PA), 9(3), 352-361.

Torczon, V., 1997. On the convergence of pattern search algorithms. Siam J. Optimize., 7: 1-25. DOI: 10.1137/S1052623493250780.

Trani, M., Arts, R., Leeuwenburgh, O., and Brouwer, J., 2011. Estimation of changes in saturation and pressure from 4D seismic AVO and time-shift analysis. Geophysics; March-April 2011; v. 76; no. 2; p. C1-C17; DOI: 10.1190/1.3549756.

Traine, A., Donatella A., Marcelo B., 2002. Seismic applications throughout the life of the reservoir. Oilfield review 2002, 40-65.

Tron, Kristiansen,T., Barkved, O., Landrø, M., Lasse, A., 2009. Linking seismic response to geomechanics, Geoexpro, Issue 6, Volume 6.

Tsuji, T., and Iturrino, G., 2008. Velocity-porosity relationships in oceanic basalt from eastern flank of the Juan de Fuca Ridge: The effect of crack closure on seismic velocity, Explor. Geophys., 39, 41-51.

Tura, A., and Lumley, D., 1999. Estimating Pressure and Saturation Changes from Time-Lapse AVO Data. In SEG International Exposition and Annual Meeting, Houston, Texas.

Van Gestel, J., Best, K. D., Barkved, O. I., and Kommedal, J. H., 2009. Life-of-field seismic system adds value to reservoir simulation of Valhall field, Offshore, v. 69 no. 2, Feb.

Vargas-Guzmán J.A., and Al-Qassab H., 2006. Spatial conditional simulation of facies objects for modelling complex clastic reservoirs. Journal of Petroleum Science and Engineering 54 (2006) 1-9.

Vernik, L, 1994. Predicting lithology and transport properties from acoustic velocities based on petrophysical classification of siliciclastics: Geophysics, 59, 420-427.

Voigt, W., 1928. Lehrbuch der kristallphysik: Teubner.

de Waal, H., and Calvert, R., 2003. Overview of global 4D seismic implementation strategy. Petroleum Geoscience, 9, 1, 1-6.

Waggoner, J., Cominelli, A., and Seymour, R., 2002. Improved Reservoir Modelling with Time-Lapse Seismic in a Gulf of Mexico Gas Condensate Reservoir (SPE77514). In SPE Annual Technical Conference and Exhibition, San Antonio, Texas.

Walker, G., Allan, P., Trythall, R., Parr, R., Mash, M., Kjelstadli, R., Barkved, O., Johnson, D. and Lane, S., 2006. Three case studies of progress in quantitative seismic-engineering integration. The Leading Edge, 25(9), pp. 1161-1166.

Walker, G., and Scott, L., 2007. Assessing the accuracy of history matching predictions and the impact of time-lapse seismic data: A case study of the Harding

Reservoir. SPE 106019, Reservoir Simulation symposium, Houston, Texas, U.S.A., 26-28 February.

Walnut, F. D., 2003. An Introduction to Wavelet Analysis. ISBN: 978-0-8176-3962-4.

Wang, Z., and Nur, A., 1992. Dispersion analysis of acoustic velocities in rocks: J. Acoust. Soc. Am., 87, 2384-2395.

Wang, Z., 1997. Feasibility of time-lapse seismic surveys.

Wang, Z., and Nur, A., 2000. Velocity relationships in granular rocks, in Wang, Z. and Nur, A. Eds., Seismic and acoustic velocities in reservoir rocks, vol. 3: Recent development, published by Society of Exploration Geophysicists. micreservoir monitoring: The physical basis, The Leading Edge, 16, No.9, 1327-1329.

Wang, Z., 2001. Fundamentals of seismic rock physics. Y2K Tutorial, Geophysics, vol. 66, 398-412.

Wang G. G., 2003. Adaptive Response Surface Method Using Inherited Latin Hypercube Design Points. Journal of Mechanical Design, volume 125, 210-220.

Wang, Y., Li, G., and Reynolds, A., 2009. Estimation of Depths of Fluid Contacts by History Matching using Iterative Ensemble Kalman Smoothers. Paper SPE 119056, Reservoir Simulation Symposium, the Woodlands, Texas, 2-4 February. DOI: 10.21188/119056-MS.

Wathelet, M., 2008. An improved neighborhood algorithm: parameter conditions and dynamic scaling. Geophysical Research Letters, 35, L09301, doi:10.1029/2008GL033256.

Wen, X. H., and Chen, W. H., 2005. Real-time reservoir model updating using ensemble Kalman filter. SPE 92991. SPE Reservoir Simulation Symposium.

Watts, G. F., Jizba, D., Gawith, D. E., and Gutteridge, P., 1996. Reservoir monitoring of the Magnus Field through 4D time-lapse seismic analysis: Petroleum Geo science, 2, 361-372.

White, C.D. and Royer, S.A., 2003. Experimental design as a framework for reservoir study. SPE79676 Reservoir Simulation Symposium, Houston, Texas, U.S.A., February 3-5.

White, C. D., and Royer, A., 2003. Experimental Design as a Framework for Reservoir Studies. SPE 79676. Presented at the 17th SPE Reservoir Simulation Symposium, Houston, Texas, 2-5 February.

Williams, G. J. J., Mansfield, M., MacDonald, D. G., and Bush, M. D., 2004. Top-Down Reservoir Modelling. SPE89974, Annual Technical Conference and Exhibition, Houston, TX, 26-29 September.

Wolf, M., 2010. Probabilistic Subsurface Forecasting, SPE 132957.

Wu, Z., Reynolds, A.C., and Oliver, D.S., 1999. Conditioning Geostatistical Models to Two-Phase Production Data. SPEJ 4 (2): 142-155. SPE-56855-PA.

Yadav, S., Heim, R., Bryant, S., and Sinha, R., 2007. Optimal Region Delineation in a Reservoir for Efficient History Matching. SPE Annual Technical Conference and Exhibition, 11-14 November, Anaheim, California, U.S.A.

References

Yeh, W. G., 1986. Review of parameter estimation procedures in ground water hydrology: The inverse problem, Water Resour. Res., 22(2),95-108, 1986.

Yemen, B., Castellini, A., Guyaguler, B., and Chen, W.H., 2005. A Comparison Study on Experimental Design and Response Surface Methodologies, SPE93347, Reservoir Simulation Symposium, 31 January-2 February.

Yeten, B., 2007. Optimization of Field Development. Proceedings of 9th International Forum on Reservoir Simulation, Abu Dhabi, UAE, 9-13 December.

Yielding, G., Overland, J.A., and Byberg, G., 1999a. Characterisation of fault zones in the Gullfaks field for reservoir modelling. In: Fleet, A.J. & Boldy, S.A.R. (eds) Petroleum Geology of Northwest Europe: Proceedings of the 5th Conference. Geological Society, London, 1177–1185.

Yilmaz, O., 1987, 1991. Seismic Data Processing. SEG, Tulsa, U.S.A.

Yu, T., Wilkinson, D., and Castellini, A., 2008. Constructing Reservoir Flow Simulator Proxies Using Genetic Programming for History Matching and Production Forecast Uncertainty Analysis Journal of Artificial Evolution and Applications Volume 2008, Article ID 263108, 13 pagesdoi:10.1155/2008/263108.

Zabalza, I., Blanc, G., Collmobier, D., and Mezghani, M., 2000. Use of Experimental Design in Resolving Inverse Problems: Application to History Matching. ECMOR, European Conference on the Mathematics of Oil Recover, 7th, Baveno, September 5-8.

Zhang, K., Wu, Y.S., Ding, C. Pruess, K., and Elmroth, E., 2001. Parallel Computing Techniques for Large-Scale Reservoir Simulation of Multi-Component and Multiphase Fluid Flow. SPE Reservoir Simulation Symposium, 11-14 February 2001, Houston, Texas.

Zhang Y., and Oliver D. S., 2010. Improving the ensemble estimate of the Kalman gain by bootstrap sampling. Mathematical Geosciences 42: 327(345).

Zimmer, M., Prasad, M., Mavko, G. and Nur, A., 2007. Seismic velocities in unconsolidated sands: Part1-Pressure trends from 0.1 to 20 MPa: Geophysics,72, no. 6, E1-E13.

Zubarev, D.I., 2009. Pros and Cons of Applying Proxy-models as a Substitute for Full Reservoir Simulations. SPE Annual Technical Conference and Exhibition, 4-7 October, New Orleans, Louisiana. Doi:10.2118/124815-MS.